PROCEEDINGS OF THE AIR FORCE HIGH ENERGY DENSITY MATERIALS CONTRACTORS CONFERENCE

28 Feb - 2 Mar 1988

Newport Beach, CA

This report has been reviewed and is approved for publication.

Larry P. Davis

LARRY P. DAVIS, Maj, USAF
Project Manager

FOR THE COMMANDER

Donald L. Ball

DONALD L. BALL
Director, Chemical and
Atmospheric Sciences

UNCLASSIFIED
SECURITY CLASSIFICATION OF THIS PAGE

REPORT DOCUMENTATION PAGE

Form Approved OMB No. 0704-0188

1a. REPORT SECURITY CLASSIFICATION Unclassified	1b. RESTRICTIVE MARKINGS
2a. SECURITY CLASSIFICATION AUTHORITY	3. DISTRIBUTION/AVAILABILITY OF REPORT Approved for public release; distribution unlimited
2b. DECLASSIFICATION/DOWNGRADING SCHEDULE	
4. PERFORMING ORGANIZATION REPORT NUMBER(S)	5. MONITORING ORGANIZATION REPORT NUMBER(S)
6a. NAME OF PERFORMING ORGANIZATION Air Force Office of Scientific Research 6b. OFFICE SYMBOL (If applicable) NC	7a. NAME OF MONITORING ORGANIZATION Air Force Office of Scientific Research/NC
6c. ADDRESS (City, State, and ZIP Code) Building 410 Bolling AFB, DC 20332-6448	7b. ADDRESS (City, State, and ZIP Code) Building 410 Bolling AFB, DC 20332-6448
8a. NAME OF FUNDING/SPONSORING ORGANIZATION 8b. OFFICE SYMBOL (If applicable)	9. PROCUREMENT INSTRUMENT IDENTIFICATION NUMBER
8c. ADDRESS (City, State, and ZIP Code)	10. SOURCE OF FUNDING NUMBERS PROGRAM ELEMENT NO. 61102F; PROJECT NO. 2303; TASK NO. B1; WORK UNIT ACCESSION NO.

11. TITLE (Include Security Classification)

(U) Report on Second High Energy Density Materials Contractors Conference

12. PERSONAL AUTHOR(S)

Larry P. Davis and Francis J. Wodarczyk, Editors

13a. TYPE OF REPORT	13b. TIME COVERED	14. DATE OF REPORT (Year, Month, Day)	15. PAGE COUNT
FINAL	FROM 87/5 TO 88/3	88/5/27	

16. SUPPLEMENTARY NOTATION

Extended Abstracts from Second High Energy Density Contractors Conference

17. COSATI CODES			18. SUBJECT TERMS (Continue on reverse if necessary and identify by block number)
FIELD	GROUP	SUB-GROUP	Metastable Molecules, High Energy Materials

19. ABSTRACT (Continue on reverse if necessary and identify by block number)

This report documents presentations given by contractors and in-house researchers at the second High Energy Density Materials held at Newport Beach, California on 28 February - 2 March 1988. It consists of extended abstracts from each of the presentations.

20. DISTRIBUTION/AVAILABILITY OF ABSTRACT ☒ UNCLASSIFIED/UNLIMITED ☒ SAME AS RPT. ☐ DTIC USERS	21. ABSTRACT SECURITY CLASSIFICATION Unclassified
22a. NAME OF RESPONSIBLE INDIVIDUAL Larry P. Davis, Major, USAF	22b. TELEPHONE (Include Area Code) (202) 767-4963 22c. OFFICE SYMBOL NC

DD Form 1473, JUN 86 *Previous editions are obsolete.*

SECURITY CLASSIFICATION OF THIS PAGE

UNCLASSIFIED

TABLE OF CONTENTS

FOREWORD

The High Energy Density Materials Program is administered jointly by the Air Force Astronautics Laboratory (AFAL), the Aeropropulsion Laboratory of the Wright Aeronautical Laboratories (AFWAL/PO), and the Air Force Office of Scientific Research (AFOSR). The program is designed to search for new molecules and materials which have an energy content that could result in revolutionary improvements in rocket propulsion, yet have the stability required to be used as propellants. In scientific terms, it is a search for the "limits of metastability." The program plan includes periodic Contractors Conferences to share research results and evaluate the progress of the program.

The second High Energy Density Materials Contractors Conference was held on 28 February - 2 March 1988 in Newport Beach, California. The meeting was attended by approximately 150 people, and they heard 40 presentations of research results. These talks were given by both in-house researchers from the Air Force Astronautics Laboratory and the Aeropropulsion Laboratory of the Wright Aeronautical Laboratories, and contractors of AFAL, AFWAL/PO, and AFOSR.

This report represents the official documentation of the second conference. It includes extended abstracts of the material that was presented by the researchers at the scientific meetings. The detail presented in these extended abstracts should be sufficient to allow an in-depth review of the type of research being conducted in the program.

The third High Energy Density Contractors Conference is scheduled for New Orleans, Louisiana, on 12-16 March 1989.

Larry P. Davis

LARRY P. DAVIS, Major, USAF
Editor

Francis J. Wodarczyk

FRANCIS J. WODARCZYK
Editor

High Energy Density Materials Contractors Conference

Technical Program

Monday, 29 February 1988

Session Chairman - Larry P. Davis, AFOSR

8:00 - Administrative Announcements

8:05 - Welcome - Richard Weiss, Chief Scientist, AFAL

8:15 - "AFAL Perspective of HEDM Research," Stephen Rogers, AFAL

8:30 - "The AFOSR High Energy Density Materials Program," Larry P. Davis and Frank J. Wodarczyk, AFOSR

8:45 - "Dissociation and Stabilization Measurements of High-Energy Molecules" Peter Bletzinger and Michael Ruark, AFWAL/POOC

9:00 - "Synthesis of New Xe and Kr Compounds Involving Novel Bonding Situations," A.A.A. Emara and G.J. Schrobilgen, McMaster University

9:25 - "Experimental Studies on the Synthesis of New Noble Gas Fluorides and High Oxidation State Energetic Fluorine Compounds Involving Unusual Bonding Situations," W.W. Wilson and K.O. Christe, Rocketdyne

9:50 - Break

10:15 - "Synthesis of New Polynitropolyhedranes," Alan P. Marchand, North Texas State University

10:40 - "Highly Fluorinated Nitrogen-Containing Compounds," Jean'ne M. Shreeve, University of Idaho

11:05 - "Synthesis and Properties of Nitrocarbenes," William P. Dailey, University of Pennsylvania

11:30 - "New High Energy Density Small Ring Systems," Koop Lammertsma and Osman F. Guner, University of Alabama at Birmingham

12:00 - Lunch

Session Chairman - Stephen Rodgers, AFAL

1:30 - "Computational Studies of the Properties of Tetrahedrane, Triprismane, and Their Aza Analogs," Peter Politzer and Jorge Seminario, University of New Orleans

1:55 - "Energy Storage in Rare Gas Solids Via Charge Separation and Trapping," Ara V. Apkarian, University of California, Irvine

2:20 - "Energy Transfer Processes in Rare Gas Solids," Henry Helvajian, Aerospace Corporation

2:45 - "Theoretical Studies of Protons in a Rare Gas Matrix," Marcy E. Rosenkrantz, AFAL

3:10 - Break

3:35 - "High Energy Density Systems in Cryogenic Media: The Production and Reaction of Atoms and Radicals," Eric Weitz, Northwestern University

4:00 - "Photoinitiated Chain Reactions in Low Temperature Solids," Charles A. Wight, University of Utah

4:25 - "Photochemistry in Cryogenic Liquids," A.T. Pritt, Jr, N. Presser, and R.R. Herm, Aerospace Corporation

Tuesday, 1 March 1988

Session Chairman - Chester J. Dymek, Jr - FJSRL

8:00 - "Theoretical Investigation of Energy Storage in Atomic and Molecular Systems," H.H. Michels and J.A. Montgomery, Jr, United Technologies Research Center

8:25 - "Theoretical Studies of Oxygen Rings: Cyclotetraoxygen, O4," Edward T. Seidl and Henry F. Schaefer III, University of Georgia

8:50 - "Investigations of Hypervalent Compounds as High-Energy Materials," Paul Engelking and Tom Dyke, University of Oregon, and John Farley, University of Nevada at Las Vegas

9:15 - "Theoretical Studies of Novel Boron Compounds," George F. Adams, U.S. Army Ballistic Research Laboratory

9:40 - "Theoretical Study of Ion-Pair States," Roberta P. Saxon and Dahbia Talbi, SRI International

10:05 - Break

10:30 - "Multiresonant Spectroscopy and Dynamics of Molecular Superexcited States," Edward R. Grant, Purdue University

10:55 - "Laser and Fourier Transform Spectoscopy of Novel Propellant Molecules," Peter F. Bernath, University of Arizona

11:20 - "Theoretical Investigations of Metastable Molecular Systems," K.P. Kirby, Harvard-Smithsonian Center for Astrophysics

11:45 - "The Role of Long Range Interactions in the Stabilization of Highly Energetic Molecules," James E. Bohr, AFAL

12:15 - Lunch

Session Chairman - Frank J. Wodarczyk, AFOSR

1:30 - "Model Studies of CBES Decomposition," D.J. Benard and R.H. Cohn, Rockwell International Science Center

1:55 - "Theoretical Studies of Highly Energetic CBES Materials," N.E. Brener, J. Callaway, and N.R. Kestner, Louisiana State University

2:20 - "Collaborative Experimental and Theoretical Study of the Photodissociation and Reactions of the Azide Radical," Millard H. Alexander, University of Maryland, and Paul J. Dagdigian, Johns Hopkins University

2:45 - "Energy Flow and Decomposition of Energetic Molecules from Metastable Vibrational States," D.S. King, M.P. Casassa, and J.C. Stephenson, National Bureau of Standards

3:10 Break

3:35 - "Potential Energy Surfaces and Stability of High Energy Content Excited Bound Clusters" - C.A. Nicolaides, National Hellenic Research Institute

4:00 - "Photochemical Preparation and Spectroscopic Detection of H_4," A.H. Kung, Y.T. Lee, and C.B. Moore, University of California, Berkeley

4:25 - "Characterization of Tetrahydrogen Via State-Selected Excitation of $H_2(B)$," William J. Marinelli, Don W. Arnold, and Anne M. Woodward, PSI

4:50 - "Spectroscopy of Polyatomic Hydrogen Ions," Takeshi Oka, University of Chicago

Wednesday, 2 March 1988

Session Chairman - Walter J. Lauderdale, AFAL

8:00 - "Investigations of Metastable Hydrogen Molecules" - H. Helm and L.J. Lembo, SRI International

8:25 - "Ionic Solid Hydrogen Fuel: Production and Properties of Hydrogen Ion and Energetic Neutral Clusters," Young K. Bae and Philip C. Cosby, SRI International

8:50 - "Quantum Monte Carlo Study of Decomposition Pathways of Tetrahydrogen," William A. Lester, Jr, University of California, Berkeley

9:15 - "Theoretical Studies of the Lifetime of Metastable Trihydrogen," Aron Kuppermann, California Institute of Technology

9:40 - "Experimental Studies of the Properties of Trihydrogen," Aron Kuppermann, California Institute of Technology

10:05 - Break

10:30 - "Theoretical Study of the Radiative Lifetime for the Spin-Forbidden Transition X <- a in He_2 * Using Ab Initio State Averaged MCSCF + CI Methods," Cary F. Chabalowski, U.S. Army Ballistic Research Laboratory

10:55 - "The Static and Dynamic Influence of Condensed Phase on Metastability," P.K. Swaminathan, B.C. Garrett, C.S. Murthy, M.J. Redmon, and B.M. Rice, Chemical Dynamics Corporation

11:20 - "Theoretical Studies of Spin-Forbidden and Electronically Nonadiabatic Processes Relevant to the Structure and Stability of Potential High Energy Density Materials," David R. Yarkony, Johns Hopkins University

11:45 - Concluding Remarks

High Energy Density Materials Contractors Conference
The Newporter Hotel, Newport Beach, CA
February 28 - March 2, 1988

PARTICIPANTS LIST

Dr. George Adams
AMXBR-IBD
Aberdeen Proving Ground
Aberdeen, MD 21005-5006

Professor Millard H. Alexander
Dept. of Chemistry
Univ. of Maryland
College Park, MD 20742

Mr. E. L. Anderson
Chemical Sciences Division
United Technologies
PO Box 49028
San Jose, CA 95161-9028

Richard C. Anderson
Chemical Sciences Division
United Technologies
P.O. Box 49028
San Jose, CA 95161-9028

Mr. E. L. Andersen
United Technologies
Chemical Science Division
P.O. Box 49028
San Jose, CA 95161-9028

Dr. V. Ara Apkarian
Dept. of Chemistry
University of California
Irvine, CA

Dr. Young K. Bae
SRI International
333 Ravenswood Avenue
Menlo Park, CA 94025

Dr. Dave Benard
Rockwell International Science
Center
1049 Camino dos Rios
Thousand Oaks, CA 91360

Dr. Peter Bernath
Department of Chemistry
Univ. of Ariozona
Tucson, AZ 85721

Mr. R. L. Bickford
Aerojet Tech Systems Co
D/9990, B/2019A2
P.O. Box 13222
Sacramento, CA 95813

Dr. Mitat Birkan
AFOSR/NA
Bolling AFB, DC 20332-6448

Professor Charles Blahous
Dept. of Chemistry
University of Georgia
Athens, GA 30602

Dr. Randall Blair
Aerospace Corp.
2300 E. El Segundo Blvd
El Segundo, CA 90245

Dr. Peter Bletzinger
AFWAL/POOC
Wright Patterson AFB, OH 45433

Dr. James Bohr
AFAL/CX
Edwards AFB, CA 93523-5000

Dr. Patricia Bond
Lockheed Missiles and Space Co.
P.O. Box 3504
Sunnyvale, CA 94088-3504

Dr. Frank G. Borgardt
Lockheed Missiles and Space Co.
Org. 83-01, Bldg. 157
P.O. Box 3504
Sunnyvale, CA 94088-3504

Dr. Michael T. Bowers
Department of Chemistry
University of California
Santa Barbara, CA 93106

Dr. Nathan Brener
Department of Physics and Astronomy
Louisiana State University
Baton Rouge, LA 70803-4001

Lt. Col Larry W. Burggraf
AFOSR/NC
Bolling AFB, DC 20332-6448

Dr. J. Callaway
Department of Physics
Louisana State University
Baton, Rouge, LA 70803

Dr. Pat Carrick
Dept. of Physics
Mississippi State University
Mississippi State, MS 39762

Dr. Michael P. Cassasa
National Bureau of Standaards
Washington, DC 20234

Dr. Cary F. Chabalowski
U.S. Army Ballistic Research Laboratory
SLCBR-IB-I
Aberdeen Proving Ground, MD 21005-5066

Dr. Robert Chapman
AFAL/LKL
Edwards AFB, CA 93523

Dr. Karl Christe
Rockwell International
Rocketdyne Division
6633 Canoga Avenue
Canoga Park, CA 91304

Dr. Robert Coombe
Dept. of Chemistry
University of Denver
Denver, CO 80208-0179

Dr. Robert Corley
AFAL/CX
Edwards AFB, CA 93523

Dr. Paul J. Dagdigian
Johns Hopkins University
Department of Chemistry
Baltimore, MD 21218

Dr. William Dailey
Dept. of Chemistry
Univ. of Pennsylvania
Philadelphia, PA 19104-6323

Maj. Larry P. Davis
AFOSR/NC
Bolling AFB, DC 20332-6448

Dr. Ernest A. Dorko
Air Force Weapons Lab
Kirtland AFB, NM

Lt. Col. Chet Dymek
FJSRL/NC
United States Air Force Academy
Colorado Springs, CO 80540

Dr. John J. Eisch
Dept. of Chemistry
State University of New York
Binghamton, NY 13901

Dr. Paul Engelking
Chemical Physics Institute
Univeristy of Oregon
Eugene, OR 97403

Dr. Carl S. Ewing
Department of Chemistry
Vanderbilt University
Nashville, TN 37235

Dr. Ted Fay
McDonnell Douglas Astronautics Co.
5301 Bolsa Avenue
Huntington Beach, CA 92647

Dr. Francis Fendell
TRW

Professor Joseph Francisco
Department of Chemistry
Wayne State University
75 Chemistry Building
Detroit, MI 48202

Dr. Bryan Ferguson
93-50/Chemistry Dept.
Lockheed Missiles & Space Co.
Research and Development Division
3251 Hanover St. B/204
Palo Alto, CA 94304-1187

Dr. Scott Farley

Dr. Patrick Frye
Rocketdyne
6633 Canoga Ave
Dept. 631, FB25
Canoga Park, CA 91303

Dr. Thomas F. George
Dept. of Chemistry and Physics
239 Fronczak Hall
State Univ. of New York at Buffalo
Buffalo, NY 14620

Dr. Ira B. Goldberg
Rockwell International Science Ctr.
1049 Camino dos Rios
Thousand Oaks, CA 91360

Professor Mark Gordon
Dept. of Chemistry
North Dakota State University
Fargo, ND 58105

Dr. Edward R. Grant
Dept. of Chemistry
Purdue University
West Lafayette, IN 47907

Dr. Mark Grubelich
Johns Hopkins University
Applied Physics Lab
Johns Hopkins Road
Laurel, MD 20707-6009

Dr. Steven L. Guberman
Institute for Scientific Research
33 Bedford St., Suite 19A
Lexington, MA 02173

Dr. V. E. (Bill) Haloulakos
McDonnell Douglas Astronautics Company
5301 Bolsa Avenue,
Huntington Beach, CA 92647

Dr. Hanspeter Helm
SRI International
333 Ravenwood Avenue
Menlo Park, CA 94025

Dr. Henry Helvajian
Laser Kinetics and
Spectroscopy Dept.
Aerospace Corporation
El Segundo, CA 90245

Dr. Herbert W. Jones
Dept. of Physics
Florida A&M University
Tallahassee, FL 32307

Dr. Dan Katayama
AFGL/LIU
Hanscom AFB, MA 01731-5000

Professor Myron Kaufman
Department of Chemistry
Emory University
Atlanta, GA 30322

Dr. J. Daniel Kelley
McDonnell-Douglas Research Labs
Bldg. 110
PO Box 516
St. Louis, MO 63166

Dr. Neil R. Kestner
Dept. of Chemistry
Louisiana State University
Baton Rouge, LA 70303

Dr. David King
National Bureau of Standards
Molecular Spectroscopy Division
Gaithersburg, MD 20899

Dr. Scott Kinkead
Los Alamos National Lab
INC-4, C346
Los Alamos, NM 87544

Dr. Kate P. Kirby
Research Physicist
Harvard-Smithsonian Center
for Astrophysics
60 Garden Street
Cambridge, MA 02138

Dr. Robert L. Kirchmeier
Dept. of Chemistry
Univ. of Idaho
Livermore, CA 94550

Dr. Brooke Koffend
Aerospace Corp.
2300 E. El Segundo Blvd.
El Segundo, CA 90245

Dr. Charles E. Kolb
Aerodyne Research, Inc
45 Manning Road
Billerica, MA 01821-3976

Dr. Daniel Konowalow
AFAL/CX
Edwards AFB, CA 93523

Dr. Andrew H. Kung
Dept. of Chemistry
Univ. of Calif.
Berkeley, CA 94720

Dr. Aron Kuppermann
Div. of Chemistry and Chemical Engineering
California Inst. of Tech.
Pasadena, CA 91125

Dr. Koop Lammertsma
Dept. of Chem
Univ. of Alabama
Univ. Station 219 PHS
Birmingham, AL 35294

Dr. E. Miller Layton
AFAL
Lt. Walt Lauderdale
AFAL/CX
Edwards AFB, CA 93523-5000

Professor Edward Lee
Lawrence Livermore National Lab.
Livermore, CA 94550

Professor Byron H. Lengsfield
Lawrence Livermore National Lab.
Livermore, CA 94550

Dr. William Lester
Dept. of Chemistry
University of California
Berkeley, CA 94720

Dr. George Lo
Manager, Chemistry Dept. 0/93-50 B-204
Lockheed Missiles & Space Co. Inc.
Research and Development Division
3251 Hanover Street
Palo Alto, CA 94304-1187

Dr. Alan P. Marchand
Dept. of Chemistry
North Texas State University
Box 5068
Denton, TX 76203-5068

Dr. William Marinelli
Physical Science, INC.

Dr. Anthony J. Matuszko
AFOSR/NC
Bolling AFB, DC 20332-6448

Dr. Ted M. McKinney

Dr. Vincent McKoy
Dept. of Chemistry and Chemical Engineering
California Institute of Technology
Pasadena, CA 91125

Prof. Horia I. Metiu
University of California
Dept. of Chemistry
Santa Barbara, CA 93106

Dr. Harvey Michels
Applied Physics Dept.
United Technologies Research Center
400 Main Street
East Hartford, CT 06108

Mr. C.M. Mihlfeith
Hercules, Inc.
P.O. Box 98 MS ATR
Magna, UT 84044

Lt. Jeffrey Moler
AFWAL/POSF
Wright-Patterson, OH 45433-6563

Dr. John A. Montgomery, Jr.
Applied Physics Department
United Technologies Research Center
400 Main Street
East Hartford, CT 06108

Dr. C. Bradley Moore
Dept. of Chemistry
University of California
Berkeley, CA 94720

Dr. C. S. Murthy

Dr. C. A. Nicolaides
Theoretical and Physical
Chemistry Institute
National Hellenic Research Inst.
48 Vas Constantinou Ave
Athens 11635, Greece

Major Gerald Nordley
AFAL/CX
Edwards AFB, CA 93523-5000

Col. J. Ross Nunn
AFAL/CC
Edwards AFB, CA 93523-5000

Dr. Takeshi Oka
Department of Chemistry
The University of Chicago
5801 S. Ellis Avenue
Chicago, IL 60637

Professor S. V. O'Neil
JILA
University of Colorado
Mail Stop 440
Boulder, CO 80309-0440

Dr. Fred Peinemann
Program Development Manager
Rocketdyne Division
Rockwell International Corporation
6633 Canoga Avenue
Canoga Park, CA 91303

Dr. Peter Politzer
Dept. of Chemistry
University of New Orleans
New Orleans, LA 70148

Dr. Nathan Presser
Infrared Sciences Department
Chemistry and Physics Laboratory
Aerospace Corporation
El Segundo, CA 90245

Lt. Col. Homer M. Pressley
AFAL/DY
Edwards AFB, CA 93523-5000

Dr. A. T. Pritt
Infrared Sciences Department
Chemistry and Physics Laboratory
Aerospace Corporation
El Segundo, CA 90245

Dr. Herschel Rabitz
Dept. of Chemistry
Princeton University
Princeton, NJ 08540

Dr. Steven Robbins

Dr. Stephen L. Rodgers
AFAL/LKLR
Edwards AFB, CA 93523-5000

Dr. Wayne E. Roe
Astronautics Laboratory
Edwards AFB, CA 93523-5000

Dr. Raymond N. Rogers
University of California
Los Alamos National Laboratory
Box 1663, MS P917
Los Alamos, NM 87545

Dr. Marcy Rosenkrantz
AFAL/CX
Edwards AFB, CA 93523

Dr. David Ross
SRI International
PSL69
Menlo Park, CA 94025

Professor John Ross
Department of Chemistry
Stanford University
Stanford, CA 94305

Dr. Michel Rossi
Physical Sciences Division
SRI International
Menlo Park, CA 94025

Dr. Roberta Saxon
SRI International
Menlo Park, CA 94025

Dr. Steve Scheffee
Atlantic Research Corporation
5390 Cherokee Ave
Alexandria, VA 22312

Dr. Robert J. Schmitt
Chemistry Laboratory
SRI International
Menlo Park, CA 94025

Dr. Gary Schrobilgen
Dept. of Chemistry
McMaster University
Hamilton, Ontario L8S 4MI

Dr. Tom Seder

Dr. John Sherohman
Lawrence Livermore National Laboratory
PO Box 808, MC L-389
Livermore, CA 94550

Dr. James Shogi
Rocketdyne
6633 Canoga Ave
Dept. 631, FB25
Canoga Park, CA 91303

Dr. Jeanne M. Shreeve
Dept. of Chemistry
Univ. of Idaho
Moscow, ID 83843

Dr. Wayne C. Solomon
Univ. of Illinois
Aeronautical and Astronautical
Engineering Dept.
104 S. Matthews
Urbana, IL 61801

Dr. Jeffrey I. Steinfeld
Dept. of Chemistry
Massachusetts Institute of
Technology
Cambridge, MA 02139

Dr. Richard H. Stolpe
Los Alamos National Labs
Mail Stop F632
PO Box 1663
Los Alamos, New Mexico 87545

Dr. Suresh Suri
Air Force Atmospheric Research Lab
Edwards AFB, CA 93523-5000

Dr. Pazhayannur K. Swaminathan
Chemical Dynamics Corporation
9560 Pennsylvania Avenue #106
Upper Marlboro, MD 20772

Dr. Donald L. Thompson
Dept. of Chemistry
Oklahoma State University
Stillwater, OK 74078

Mr. Steve Thompson

Dr. Julian Tishkoff
AFOSR/NA
Bolling AFB, DC 20332-6448

Dr. James Travis
P915
Los Alamos National Lab
P.O. Box 1663
Los Alamos, NM 87545

Dr. William C. Trogler
Department of Chemistry
University of California
LaJolla, CA 92093

Lt. Monte D. Turner
AFAL/CX
Edwards AFB, CA 93523-5000

Major Dennis Vincent
HQ AFSC/XTSS
Andrews AFB, DC 20334-5000

Dr. Joseph Wander
HQ AFESC/RDVS
Tydall AFB, FL 32403-6001

Dr. Richard Weiss
AFAL/CA
Edwards AFB, CA 93523-5000

Professor Eric Weitz
Northwestern University
Dept. of Chemistry
2145 Sheridan Road
Evanston, IL 60201

Dr. Charles Wight
Dept. of Chemistry
University of Utah
Salt Lake City, UT 84112

Dr. R. L. Wilkins
P.O. Box 92957
MS: M5-747
Los Angeles, CA 90009

Dr. William W. Wilson
Rocketdyne, BA26
6633 Canoga Avenue
Canoga Park, CA 91303

Dr. Francis J. Wodarczyk
AFOSR/NC
Bolling AFB, DC 20332-6448

Dr. David R. Yarkony
Dept. of Chemistry
Johns Hopkins University
Baltimore, MD 21218

Dissociation and Stabilization Experiments of High Energy Molecules

P. Bletzinger and M.E. Ruark

In the study of high energy radicals of interest as storable high energy compounds the radicals are commonly produced by photolytical dissociation of the molecular beam during deposition or of the deposited material in the matrix. Another way of production is collisional dissociation using metastable gas atoms. This method has the advantage of using a simple discharge system and, if helium ions are used, can provide energies up to 24.6 eV. Disadvantages are the limited and discrete range of energies and the possible deposition of the metastable source gas. Also one foregoes the possibility of reaching higher energies using multiphoton excitation. Available metastables, their energies and radiative lifetimes are listed in Table 1 [1].

TABLE 1

RADIATIVE LIFETIMES AND DECAY MECHANISMS FOR A NUMBER OF METASTABLE ATOMS

SPECIES	METASTABLE STATE	EXCITATION ENERGY (eV)	τ(sec)	PRINCIPAL DECAY MECHANISM
He	$1s2s\ ^3S_1$	19.82	7.9×10^3	M1
	$^1S_0$	20.61	2.0×10^{-2}	2-PHOTON
Ne	$2p^5 3s\ ^3P_2^0$	16.62	2.4×10^1	M2
	$^3P_0^0$	16.71	4.3×10^2 $(> 8 \times 10^{-1})^{(a)}$	M1
Ar	$3p^5 4s\ ^3P_2^0$	11.55	5.6×10^1	M2
	$^3P_0^0$	11.72	4.5×10^1 $(> 1.3)^{(a)}$	M1
Kr	$4p^5 5s\ ^3P_2^0$	9.913	8.5×10^1	M2
	$^3P_0^0$	10.56	4.9×10^{-1} $(> 1.0)^{(a)}$	M1
Xe	$5p^5 6s\ ^3P_2^0$	8.314	1.5×10^2	M2
	$^3P_0^0$	9.446	7.8×10^{-2}	M1

We previously have conducted several experiments investigating collisional energy transfer from metastable nitrogen and helium in pulsed and flowing afterglows using diagnostic methods such as tracer gases and LIF. The present experiment (Figure 1) uses a flowing afterglow with flow speeds of about 30 m/sec at up to 1 Torr pressure pumped by a roots blower. The gas to be dissociated can be injected 8 cm upstream of an orifice which leads into the high vacuum chamber pumped by a cryopump or, at much lower pressures, into the sampled gas stream after the orifice. Initial experiments will analyze the composition of the gas jet coming through the nozzle with a residual gas analyzer. In later experiments the gas jet will be directed towards the coldfinger of a helium cryostat and the deposit will be analyzed by emission or absorption spectroscopy or LIF. Initial

gases to be investigated will include CH_4 and C_2H_2, the dissociation products being CH radicals.

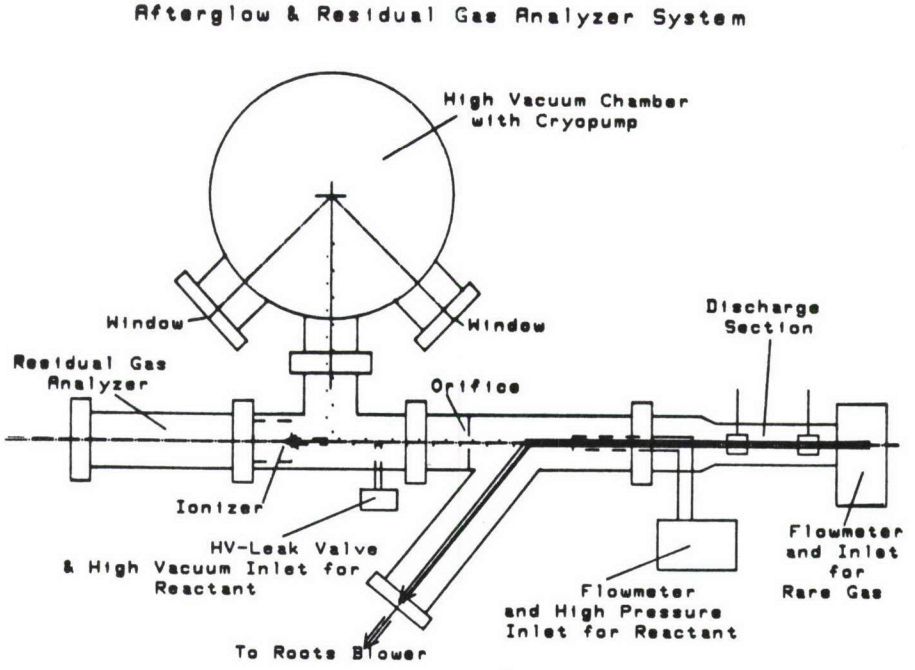

Figure 1

The CH radical has been the subject of many investigations, starting with its production in the oxyacetylene flame, where its A - X band emission is a very prominent feature of the flame spectrum. Other methods of production include dissociation of CH_4 using very powerful (kJ) flashlamps [2], VUV irradiation of C_2H_2 in the gaseous state or in a matrix [3], IR or UV multiphoton dissociation of compounds such as $CHBr_3$ [4], pulsed radiolysis [5], pulsed rf [6] and production of the ion in an ion cyclotron resonance trap [7]. All of these methods produce either only a very small amount of CH or do it in a pulsed fashion, both not very suitable for depositing larger amounts in a matrix. Chang, Setser and Taylor [8] have used a helium flowing afterglow to investigate metastable energy transfer to, among other gases, C_2H_2. Their energy diagram of the helium 2^3S metastable state and the exit channels of N_2, CO and C_2H_2 are shown in Figure 2. Energy levels of metastable neon and argon have been added. In their spectral measurements they observed that while CH_4 produced the largest spectral intensity in the CH A-X band, its quenching rate for the helium metastable was only a fraction of that of C_2H_2 (Table 2), suggesting that C_2H_2 is the optimum choice for this method of producing CH.

It is well known that CH is a very reactive radical; reaction rates with selected gases are shown in Table 3 [9]. It is therefore essential that the reaction system be carefully designed and the flow lengths between metastable generation, injection point of the gas to be dissociated and the mass analyzer sampling orifice or cold finger be held to a minimum. This has been successfully accomplished for optical analysis for example in Yamaguchi's et al experiment [10]. They where able to investigate the interaction of C_2H_2 with helium ions. One of their optical spectra is shown in Figure 3; it is typical of excitation spectra produced with metastable energy transfer.

Relative Intensities of Observed Spectra from Hydrocarbons.

(Chang, Setser & Taylor, Chem.Phys.25,201(1978))

	CH_4	C_2H_4	C_2H_2
CH(A-X)	0.67	0.46	0.33
CH(B-X)	0.28	0.11	0.06
CH(C-X)	0.05	0.04	<0.01
C_2(e-b) -		<0.01	<0.01
C_2(d-x) -		<0.01	0.01
C_2(c-b) -		0.02	0.07
C_2(B-X)-		0.05	0.07
C_2(A-X)-		0.28	0.33

Excitation rate constants for quenching He(2^3S) (10^{-12} cm^3 $molec^{-1}$ s^{-1})

0.6	2.9	10.1

Table 2

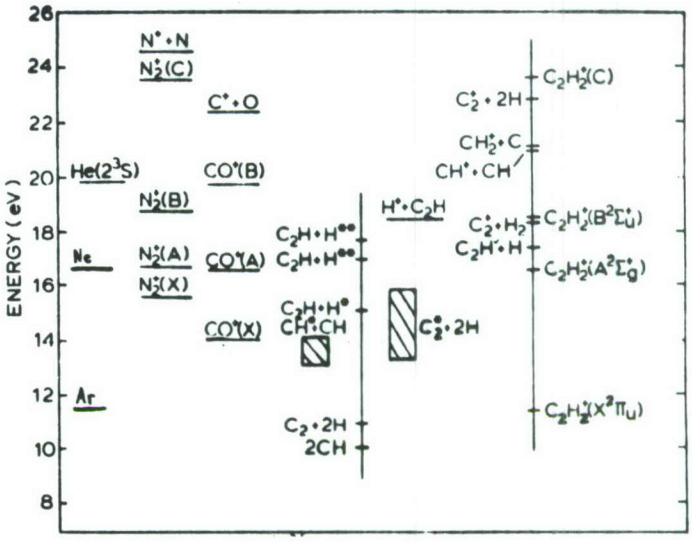

Figure 2

Rate Data for $CH(X^2\Pi)$ at 300 K
(Nokes & Donovan, Chem.Phys. 90,167(1984))

Reactant	k(cm^3 $molecule^{-1}$ s^{-1})
H_2	$(1.4 \pm 0.3)X10^{-11}$
O_2	$(5.1 \pm 05)X10^{-11}$
NO	$(2.0 \pm 02)X10^{-10}$
CO	$(2.6 \pm 02)X10^{-11}$
N_2O	$(7.8 \pm 1.4)X10^{-11}$
CH_4	$(1.02 \pm 0.04)X10^{-10}$
C_2H_6	$(2.7 \pm 0.2)X10^{-10}$
C_2H_4	$(4.2 \pm 0.3)X10^{-10}$
C_2H_2	$(4.2 \pm 0.2)X10^{-10}$

Table 3

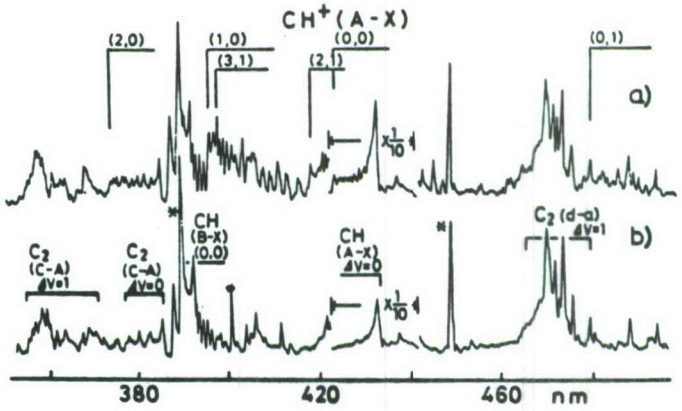

FIG. 2. Emission spectra obtained from the reactions of (a) He^+, He_2^+, and He^* and (b) He^* with C_2H_2. Lines marked * are stray HeI lines.

Figure 3

Initial attempts to measure CH radicals in our flow system have not been successful. This may be due to excessive metastable or radical losses in the flow system or to the requirement for pressures in the 10^{-5} Torr range for the RGA and cold finger operation which reduces the metastable density at the injection point to too low a level. We are presently improving the flow system and analyzing its operation. Also we mesured the yield of CH produced by the RGA ionizer at 5% of the dissociation products of C_2H_2. This yield should make it possible to produce a CH ion beam with reasonable efficiency. However, it will be necessary to neutralize the ion beam and reduce its energy before deposition.

[1] R. C. Slater et al., "Research on sources of gas phase metastable atoms and molecules", AFWAL/TR-82-2029, May 1982
[2] W. Braun et al., J. Chem. Phys. 46,2071 (1967)
[3] E. E. Milligan, M. E. Jacox and L. Abouf-Marguin, J. Chem. Phys. 46,4562 (1967)
[4] J. E. Butler et al., Chem. Phys. Lett. 63,104 (1979)
[5] M. W. Bosnali and D. Perner, Zschr. Naturfschg. 26a, 1768 (1971)
[6] R. A. Anderson et al., J. Chem. Phys. 63, 5287 (1975)
[7] M. Gerard et al., Chem. Phys. 30, 75 (1978)
[8] R. S. F. Chang et al., Chem. Phys. 25, 201 (1978)
[9] C. J. Nokes and R. J. Donovan, Chem. Phys. 90, 167 (1984)
[10] S. Yamaguchi et al., J. Chem. Phys. 86, 4952 (1987)

SYNTHESIS OF NEW XENON AND KRYPTON COMPOUNDS INVOLVING NOVEL BONDING SITUATIONS

A.A.A. Emara and G.J. Schrobilgen

Department of Chemistry, McMaster University, Hamilton, Ontario L8S 4M1, Canada

The chemistry of the noble gases is presently limited to that of Kr, Xe and Rn. While only the chemistry of Kr and Xe can be dealt with by conventional physical methods of structural determination, the chemistries of both gases have been severely limited by the field of suitable ligating groups. Initially only fluorine and oxygen were found capable of stabilizing the +2, +4 and +6 oxidation states of xenon while the only the +2 oxidation state is known for krypton and was only stabilized by fluorine. Subsequently, a number of highly electronegative inorganic ligands bonded through oxygen were shown to be capable of stabilizing xenon(II) and, in fewer instances, xenon(IV) and xenon(VI). Until the present work, only two ligands in which xenon is bonded to nitrogen, namely $-N(SO_2F)_2$ and $-N(SO_2CF_3)_2$, were known. In order to extend the range of noble-gas compounds in which Xe is bonded to ligating atoms other O and F, and Kr is bonded to an atom other than F, we have undertaken the investigation of the interactions of the Lewis acid noble-gas fluorocations with neutral Lewis bases. The majority of the bases selected for study are oxidatively resistant perfluoro-organic nitrogen bases with first adiabatic ionization potentials exceeding 10-11 eV. As a result of these studies it has been possible to (1) significantly extend the range of known Xe-N bonded species, (2) demonstrate that a large range of fluoro-organic ligands are capable of stabilizing Xe(II), (3) produce several examples of the first componds in which a noble-gas atom serves as an aromatic substituent; (4) provide new series of model compounds which may aid in developing synthetic approaches to the formation of the first xenon-carbon bond, the "holy grail" of the noble-gas chemist; (5) provide preliminary evidence for the first Kr-N bonded species.

Several of these points are illustrated by the syntheses of the novel Xe-N bonded cations: $RC{\equiv}N\text{-}XeF^+$ (1,2), $C_5F_5N\text{-}XeF^+$ (1,3), $4\text{-}CF_3C_5F_4N\text{-}XeF^+$ (1,3), $C_3F_3N_2N\text{-}XeF^+$ (1), $(CF_3)_3C_3N_2N\text{-}XeF^+$ where AsF_6^- is the counter ion; R = H, CH_3, C_2H_5, C_3F_7, $(CH_3)_3C$, C_6F_5; R' = C_5F_5N (pentafluoropyridine), $4\text{-}CF_3C_5F_4N$ (4-trifluoromethyltetrafluoro-pyridine); R" = $C_3F_3N_3$ (trifluoro-s-triazine), $(CF_3)_3C_3F_3N_3$ (tris(trifluoromethyl)-s-triazine.

The nitrile cations were prepared in HF solvent according to equation (1)

$$RC{\equiv}N + XeF^+ (\text{or } Xe_2F_3^+)AsF_6^- \longrightarrow RC{\equiv}N\text{-}XeF^+AsF_6^- (+ XeF_2) \qquad (1)$$

Owing to the higher basicities of the perfluoropyridines, the pyridine cations were prepared from the pyridinium salts in the aprotic solvent BrF5 according to equation (2)

$$4\text{-}R'\text{-}C_5F_5NH^+AsF_6^- + XeF_2 \longrightarrow 4\text{-}R'\text{-}C_5F_5N\text{-}XeF^+AsF_6^- + HF \quad (2)$$

The triazine cations were prepared by the interaction of the neat liquid triazines with $XeF^+AsF_6^-$ at room temperature (equation (3)) and were found to be the most stable species encountered thus far in the present series of studies.

$$R''_3C_3N_3 + XeF^+AsF_6^- \longrightarrow R''_3C_3N_2N\text{-}XeF^+AsF_6^- \quad (3)$$

The cations have been characterized by both multinuclear magnetic resonance spectroscopy (^{129}Xe, ^{19}F, ^1H, ^{13}C and ^{14}N NMR) and low-temperature Raman spectroscopy. A particularly novel feature of the the NMR characterization of these species has been the observation of the diagnostically important spin-spin coupling $^1J(^{129}Xe\text{-}^{14}N)$, despite the asymmetry of the electric field gradient about the quadrupolar ^{14}N nuclei in these cations. The low degree of quadrupole relaxation is attributed to the low viscosity of HF solvent in which these couplings were observed, the strong axial symmetries these cations possess as well as the small quadrupole moment of ^{14}N.

The first example of Kr bonded to an element other than F has been provided by our synthesis and characterization of the fluoro(hydrocyano)krypton(II) cation, $HC{\equiv}N\text{-}KrF^+$, as the AsF_6^- salt (1,4). The compound was synthesized in both HF and BrF_5 solvents at low temperature according to equation (4)

$$KrF_2 + HC{\equiv}NH^+AsF_6^- \longrightarrow HC{\equiv}N\text{-}KrF^+AsF_6^- + HF \quad (4)$$

The solid compound, precipitated from HF solvent, is thermally unstable above -50 °C. It has, however, been possible to obtain a vibrational (Raman) spectrum of the solid under frozen HF at -196 °C. The salt has also proven soluble in BrF_5 at -55 to -58 °C with only slow decomposition permitting the a full characterization of the $HC{\equiv}N\text{-}KrF^+$ cation by ^1H, ^{13}C (99.2% enrichment), ^{15}N (99.5% enrichment) and ^{19}F NMR spectroscopy. The observation of the spin-spin couplings $^1J(^{13}C\text{-}^1H)$, $^2J(^{15}N\text{-}^1H)$, $^2J(^{19}F\text{-}^{15}N)$, $^3J(^{19}F\text{-}^{13}C)$ and $^4J(^{19}F\text{-}^1H)$ as well as the ^{82}Kr, ^{84}Kr and ^{86}Kr isotopic shifts in the ^{19}F NMR spectrum provide definitive proof for the cation's Kr-N bonded structure.

REFERENCES:

1. Chem. and Eng. News, 1988, 66, 16.

2. A.A.A. Emara and G.J. Schrobilgen, J.C.S. Chem. Commun. 1987, 1644.

3. A.A.A. Emara and G.J. Schrobilgen, J.C.S. Chem. Commun. 1988, 257.

4. G.J. Schrobilgen, J.C.S. Chem. Commun., in press.

EXPERIMENTAL STUDIES ON THE SYNTHESIS OF NEW NOBLE GAS FLUORIDES AND HIGH OXIDATION STATE ENERGETIC FLUORINE COMPOUNDS INVOLVING UNUSUAL BONDING SITUATIONS

W.W. WILSON AND K.O. CHRISTE

ROCKETDYNE DIVISION OF ROCKWELL INTERNATIONAL
CANOGA PARK, CALIFORNIA 91303

The primary objective of this program is the synthesis of new "super oxidizers" based on hypervalent, high oxidation state fluorides of nitrogen, oxygen, chlorine and the noble gases. The target compounds include NF_5, ClF_5O, ClF_6^-, ClF_7 and ArF^+ which are among the most challenging synthetic problems encountered in high energy chemistry.

A concerted effort to obtain experimental evidence for the existence of NF_5 failed. This effort included numerous experiments involving UV-photolysis of either NF_3-F_2 mixtures in different matrices at 10°K or NF_3 solutions in liquid F_2 at 77°K, and reaction of NF_3 with microwave generated F atoms in an argon matrix at 10°K. The efficiency of the F atom generating system was demonstrated for the $O_2 + \dot{F} \longrightarrow \dot{O}_2F$ reaction and therefore could not be blamed for the failure of NF_5 formation. This raised the question whether the failure of NF_5 formation might be due to nitrogen not being able to coordinate five fluorine ligands.

A conclusive answer to this question was obtained by an ^{18}F radiotracer experiment carried out in collaboration with Drs. Schrobilgen and Chirakal of McMaster University. ^{18}F labeled NF_4HF_2 was prepared by the following reactions:

$$^{20}Ne(d,\delta) \longrightarrow \overset{*}{F}_2$$

$$\overset{*}{F}_2 + H_2 \longrightarrow 2\,H\overset{*}{F}$$

$$CsF + H\overset{*}{F} \longrightarrow Cs\overset{*}{HF}_2$$

$$NF_4PF_6 + Cs\overset{*}{HF}_2 \xrightarrow{H\overset{*}{F}} Cs\overset{*}{PF}_6 + NF_4\overset{*}{HF}_2$$

The thermal decomposition of $NF_4N\overset{*}{HF}_2$ involves an attack of the $\overset{*}{HF}_2^-$ anion on NF_4^+. If nitrogen (+V) can coordinate five fluorine ligands, the ^{18}F should be distributed statistically over the NF_3, F_2 and HF products, but if the maximum coordination number of nitrogen towards fluorine is only four, the ^{18}F should be retained exclusively by F_2 and HF.

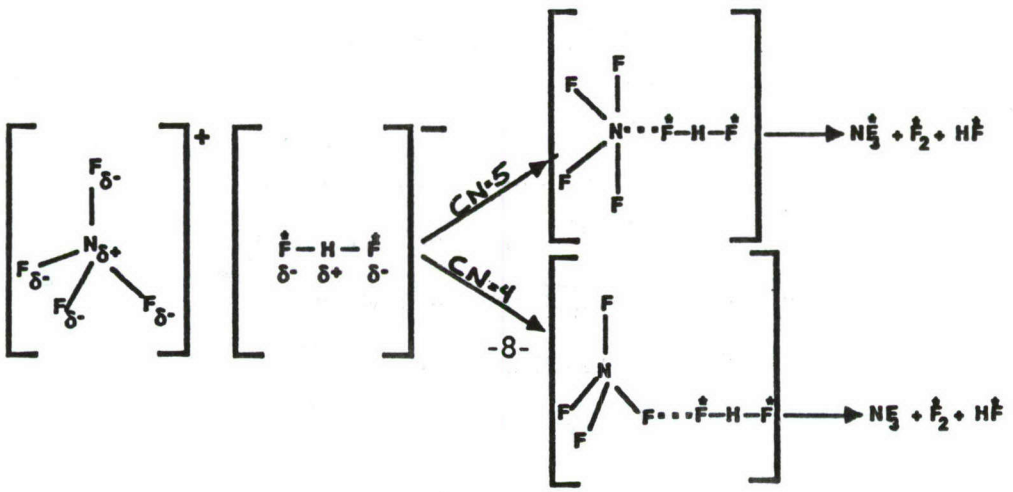

The observed results, i.e. no ^{18}F activity in the NF_3, conclusively prove that (i) the attack of $\overset{*}{F}$ occurs on the fluorine ligand of NF_4^+, (ii) the maximum coordination number of nitrogen (+V) toward fluorine is 4, and (iii) covalent NF_5 cannot exist for steric reasons. A remaining point of interest in the synthesis of $NF_4^+AsF_6^-$ is which radical, i.e. $\dot{N}F_4$ or $\dot{A}sF_6$, is the key intermediate.

The second target compound pursued was ClF_5O. This unknown molecule is predicted to be stable and to deliver a specific impulse which is about ten seconds higher than that of ClF_5, the best presently known earth storable liquid oxidizer. The following approaches and reaction systems were studied:

(i) Low temperature glowdischarge in a sapphire reactor

$$ClF_5 + O_2 \xrightarrow[-186°C]{-196°C} O_3$$

$$\xrightarrow[-126°C]{-142°C} ClF_3 + F_2$$

$$ClF_3O + F_2 \xrightarrow[-142°C]{-186°C} ClF_5 + O_2$$

$$\xrightarrow{-126°C} ClF_3 + O_2$$

$$ClF_5 + OF_2 \xrightarrow[-186°C]{-196°C} \text{NO REACTION}$$

$$\xrightarrow{-142°C} ClF_3 + F_2$$

$$FClO_3 + F_2 \xrightarrow[-142°C]{-186°C} \text{NO REACTION}$$

(ii) Low temperature UV-photolyses

$$ClF_3O + F_2 \xrightarrow{-186°C} ClF_5 + ClF_3 + FClO_2$$

$$\xrightarrow{-45°C} ClF_5 + FClO_3 + FClO_2$$

$$ClF_5 + OF_2 \xrightarrow[-186°C]{-196°C} \text{NO REACTION}$$

$$\xrightarrow{-142°C} ClF_3 + F_2$$

$$ClF_3 + OF_2 \xrightarrow[-186°C]{-196°C} ClF_5$$

$$Cl_2 + F_2 + O_2 \xrightarrow{-196°C} ClF_5$$

$$FClO_3 + F_2 \xrightarrow{-196°C} \text{NO REACTION}$$

$$ClF_3O + Kr + F_2 \xrightarrow{-186°C} ClF_5 + KrF_2$$

(iii) High temperature fluorination reactions

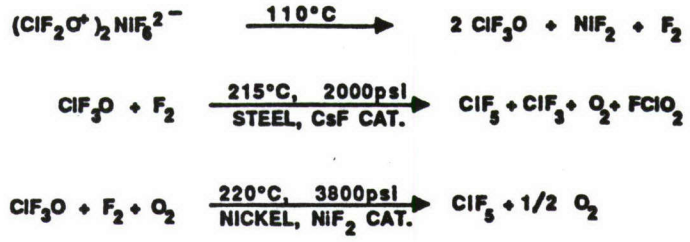

(iv) UV-photolysis in matrix at 10°K

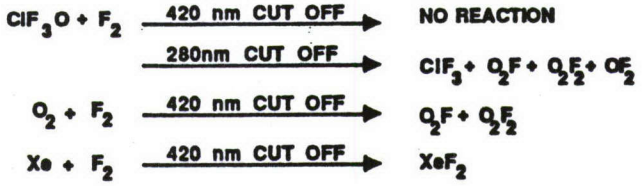

(v) Fluorination Reactions of ClF_3O with

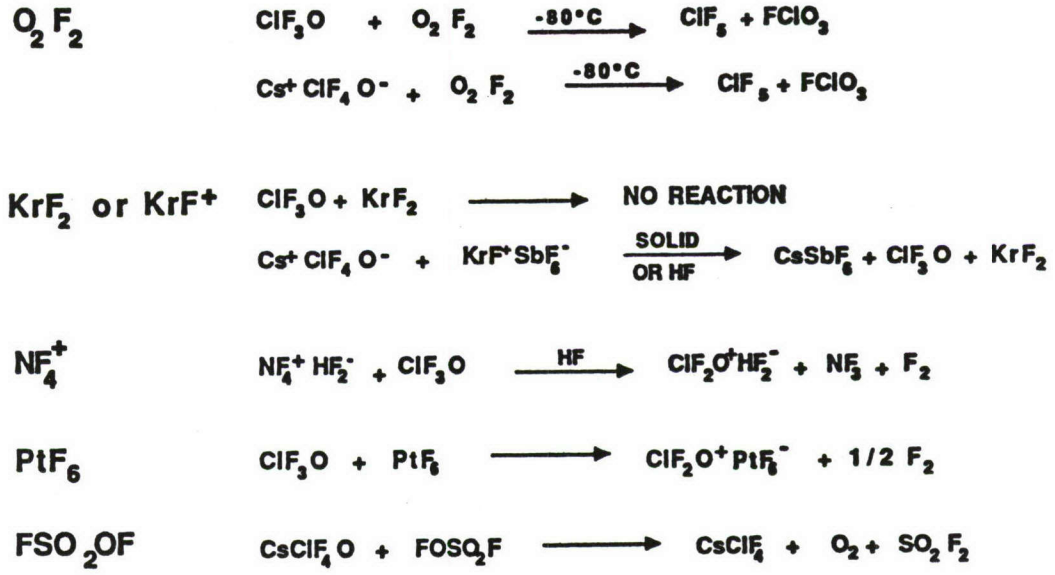

Although so far none of these reactions has yielded detectable amounts of ClF_5O, the synthesis of ClF_5O will be further pursued.

In collaboration with Drs. Schrobilgen and Chirakal of McMaster Unviersity, a ^{18}F radiotracer study was carried out to determine the maximum coordination number of Cl(+V and +VI) towards fluorine. A displacement reaction between $ClF_6^+AsF_6^-$ and FNO was carried out and gave the following result:

$$ClF_6^+AsF_6^- + \overset{*}{F}NO \longrightarrow NO^+AsF_6^- + Cl\overset{*}{F}_5 + \overset{*}{F}_2$$

77.0% 23.0%

Since the observed ^{18}F activity was higher than those predicted for either one of the following two mechanisms,

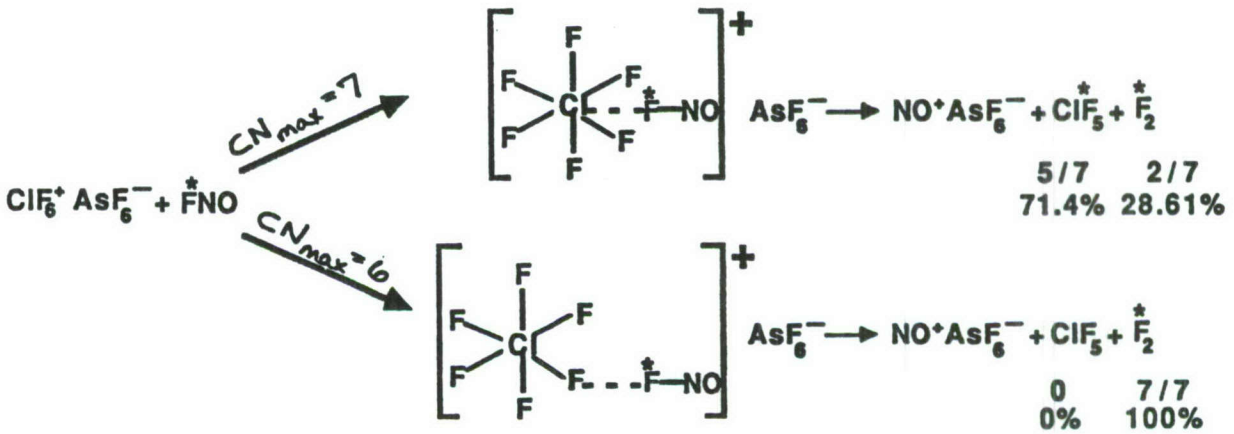

a third possibility, namely scrambling between ClF_5 and $\overset{*}{F}NO$ was suspected to contribute to the above reactions:

$$ClF_5 + \overset{*}{F}NO \longrightarrow Cl\overset{*}{F}_5 + \overset{*}{F}NO$$

83.3% 16.7%

The correctness of this assumption was experimentally verified by studying the ClF_5 + $\overset{*}{F}NO$ system. The observed values, i.e. $Cl\overset{*}{F}_5$ (85%), $\overset{*}{F}NO$ (15%), are in reasonable agreement with the predictions and suggest the existence of an unstable intermediate ClF_6^- anion. The structure of the ClF_6^- anion, i.e. the steric activity of the free valence electron pair on the chlorine central atom presents an interesting problem which will be further pursued by NMR studies at McMaster University.

AFOSR-84-0085: SYNTHESIS OF NEW POLYNITROPOLYHEDRANES

Principal Investigator: Dr. Alan P. Marchand

Department of Chemistry. North Texas State University, Box 5068, Denton, TX 76203

LONG ABSTRACT

I. As part of a program that is involved with the synthesis and chemistry of polynitropolycyclic systems,[1] we recently completed the syntheses of di-, tri- and tetranitro-2,3,4,8-tetraphenyl-1,3-bishomocubanes, (route shown below).[2]

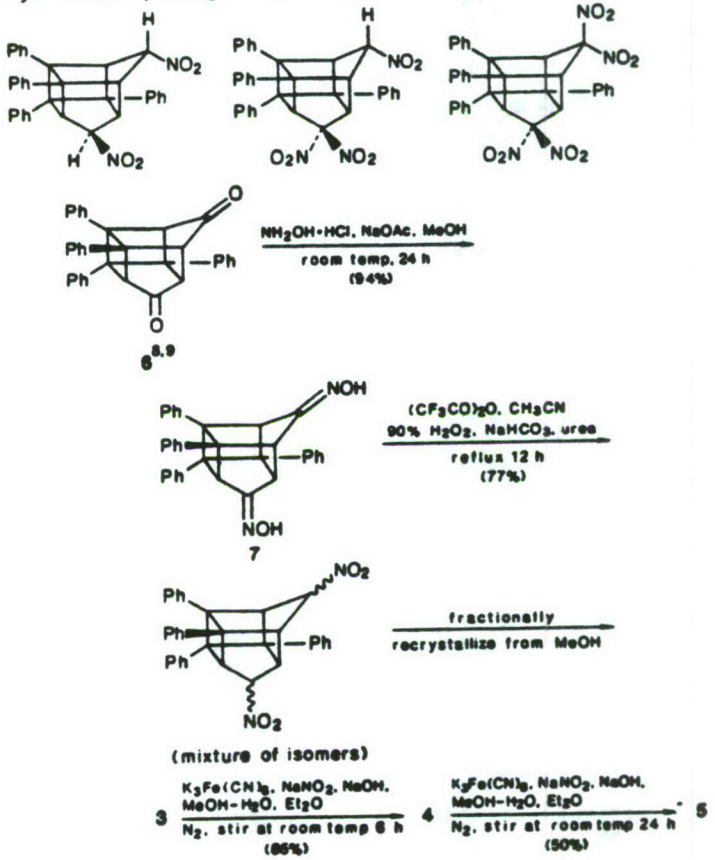

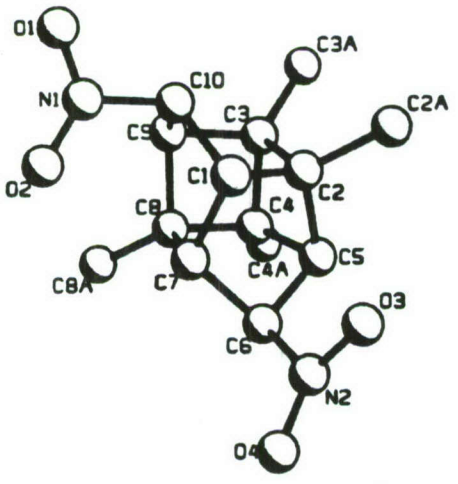

igure 1. Results of the X-ray study on 3. For clarity, the phenyl roups on C-2, C-3, C-4, and C-8 are represented as single atoms -2a, C-3a, C-4a, and C-8a).

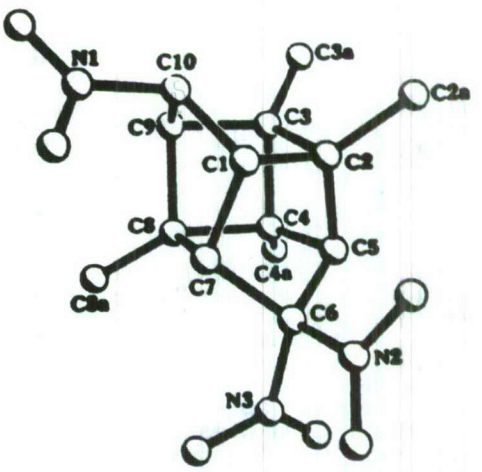

Figure 2. Results of the X-ray study on 4. For clarity, the phenyl groups on C-2, C-3, C-4, and C-8 are represented as single atoms (C-2a, C-3a, C-4a, and C-8a).

In addition, we have also completed the synthesis of D_3-hexanitrotrishomocubane via the route shown below:[3]

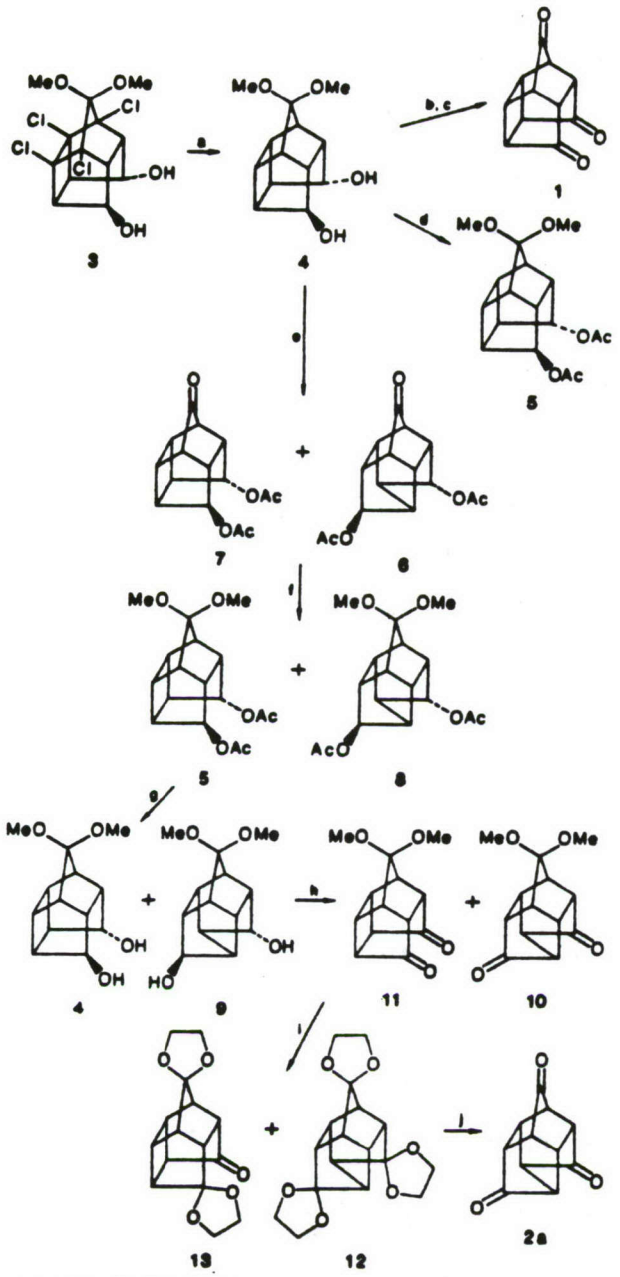

[a] (a) Li, *t*-BuOH, THF, liquid NH_3, -33 °C (92%); (b) excess 10% aqueous HCl, reflux 4 h (100%); (c) PCC, CH_2Cl_2 (100%); (d) Ac_2O, pyridine, room temperature, 10 h (87%); (e) glacial HOAc, concentrated H_2SO_4, 150 °C (sealed tube), 42 h (55%); (f) $HC(OMe)_3$, TsOH (catalytic amount), overnight at room temperature (91%); (g) $LiAlH_4$, THF-Et_2O, room temperature, 6 h (95%); (h) PDC, CH_2Cl_2, room temperature, 4 days (90%); (i) $HOCH_2CH_2OH$, TsOH (catalytic amount), benzene, reflux 48 h [12 (29%) + 13 (27%)]; (j) concentrated H_2SO_4, CH_2Cl_2, room temperature, 2 days (69%). [b] Stereochemical assignments for, e.g., 6, 8, and 9 were made on the basis of (i) simple mechanistic considerations and (ii) analysis of the ^1H and ^{13}C NMR spectra of these compounds.

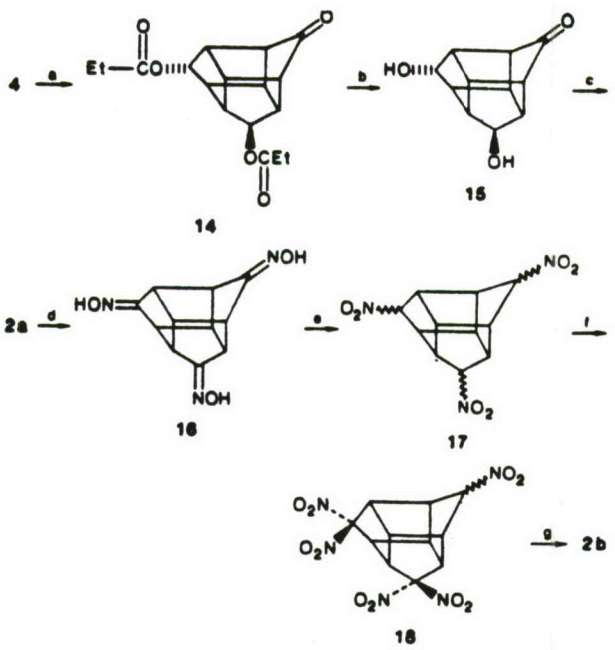

[a] (a) $EtCO_2H$, concentrated H_2SO_4, 150 °C, 72 h, N_2 (51%); (b) Na, dry MeOH, room temperature, 1 h (100%); (c) PCC, CH_2Cl_2, room temperature, 2 h (46%); (d) NH_2OH·HCl, NaOAc, aqueous MeOH, 0 °C → room temperature, overnight (70%); (e) $(CF_3CO)_2O$, 90% H_2O_2, $NaHCO_3$, urea, CH_3CN, 70–75 °C, overnight (35%); (f) NaOH, aqueous MeOH, 3 h; then $K_4Fe(CN)_6$, aqueous $NaNO_2$, Et_2O, 1 h (65%); (g) NaOH, aqueous MeOH, 24 h; then $K_3Fe(CN)_6$, aqueous $NaNO_2$, Et_2O, 12 h (62%). [b] Stereochemical assignments for 14 and 15 were made on the basis of (i) simple mechanistic considerations and (ii) analysis of the ^1H and ^{13}C NMR spectra of these compounds.

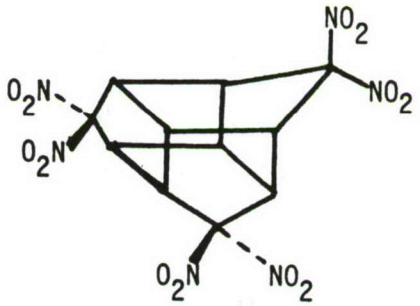

D_3-Hexanitrotrishomocubane (2b)

A study of the shock sensitivity of D_3-hexanitrotrishomocubanes reveals that it is both less shock-sensitive and a substantially more powerful explosive than is TNT. Pertinent thermodynamic data are given below:[4]

DSC Thermogram (heating rate 10 $^{o}C\text{-}min^{-1}$): Exotherm onset occurred at 272 ^{o}C: exotherm maximum occurred at 308 ^{o}C, and the exothermic process ended when the temperature reached 331 ^{o}C. A second smaller exotherm set in at 331 ^{o}C, reached a maximum at 338 ^{o}C, and subsided at 355 ^{o}C.

II. Thermal reaction of 2-phenyl-3-carboethoxynorbornadiene with iron pentacarbonyl affords a single dimer ketone and a single cage dimer (a substituted heptacyclotetradecane) in low yields along with a mixture of diastereoisomeric substituted ferrocenes:

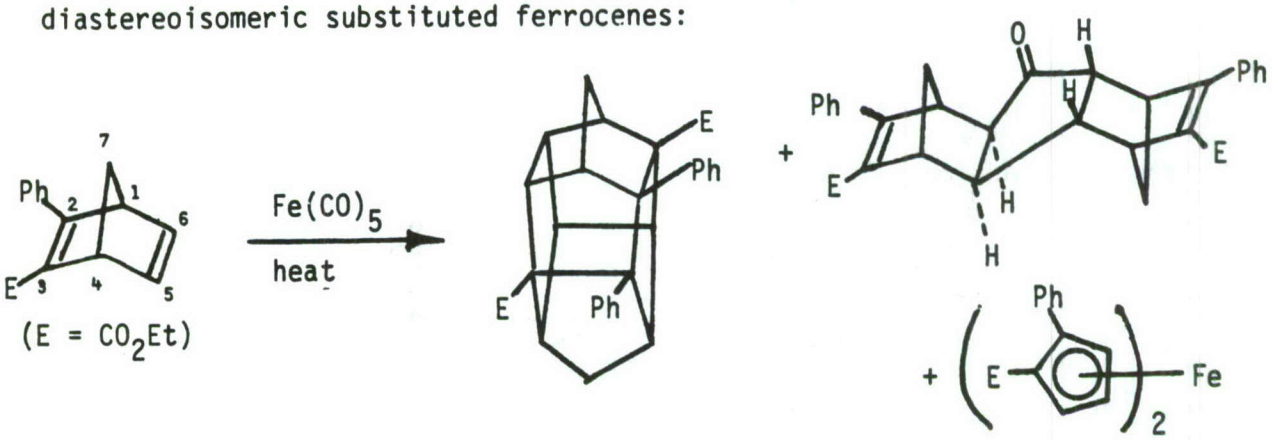

The structures of the cage dimer and the product of hydrogenation of the dimer ketone, above, have been verified via single crystal X-ray structural analysis. These compounds appear to have been formed via enantioselective (or possibly enantiospecific) reactions of 2-phenyl-3-carboethoxynorbornadiene with Fe(0). The results of INDO calculations (MM2-optimized geometry) suggest that enantiomeric recognition in this reaction is governed by substituent effects upon the relative magnitudes of the atomic orbital coefficients in the LUMO of the reacting double bond [C(5)-C(6)] in the substrate.[5]

III. Ring expansion of pentacyclo[5.4.0.$0^{2,6}$.$0^{3,10}$.$0^{5,9}$]undecane-8,11-dione (PCUD-8,11-dione, **1**) was performed via reaction of **1** with ethyl diazoacetate (2 equivalents) in the presence of boron trifluoride etherate. The reaction occurred regiospecifically to afford a new ring system, (i.e., a substituted pentacyclo[6.5.0.0^{4,12}.$0^{5,10}$.$0^{9,13}$]tridecane, **3a**, below):[6]

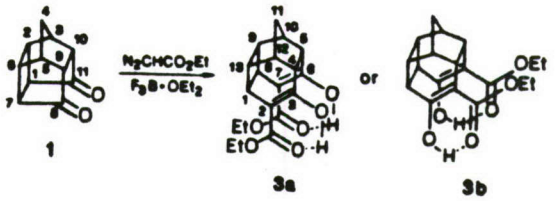

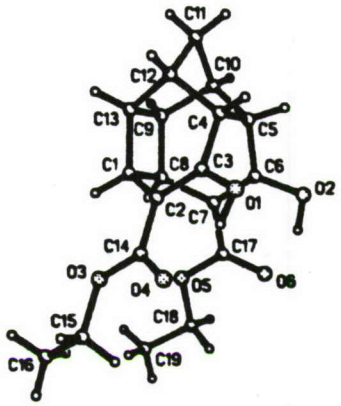

Figure 1. Diagram of 3a as determined by X-ray diffraction. Only one of the two molecules in the asymmetric unit is shown.

Some reactions of **3a** are summarized below:

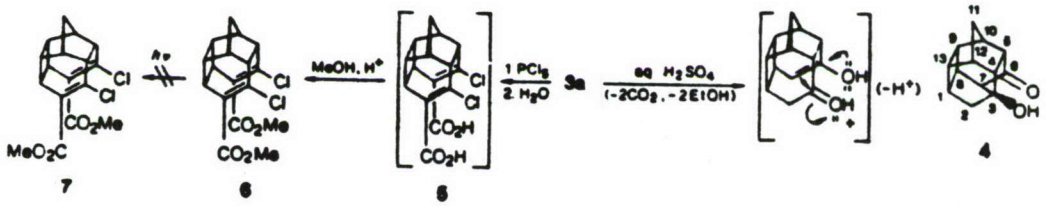

1-Substituted PCUD-8,11-diones also have been found to undergo ring expansion when treated with N_2CHCO_2Et (1 equivalent) in the presence of $F_3B{:}OEt_2$. However, these reactions proceed regiospecifically but <u>opposite</u> to the manner in which the parent PCUD-8,11-dione reacts under these conditions:

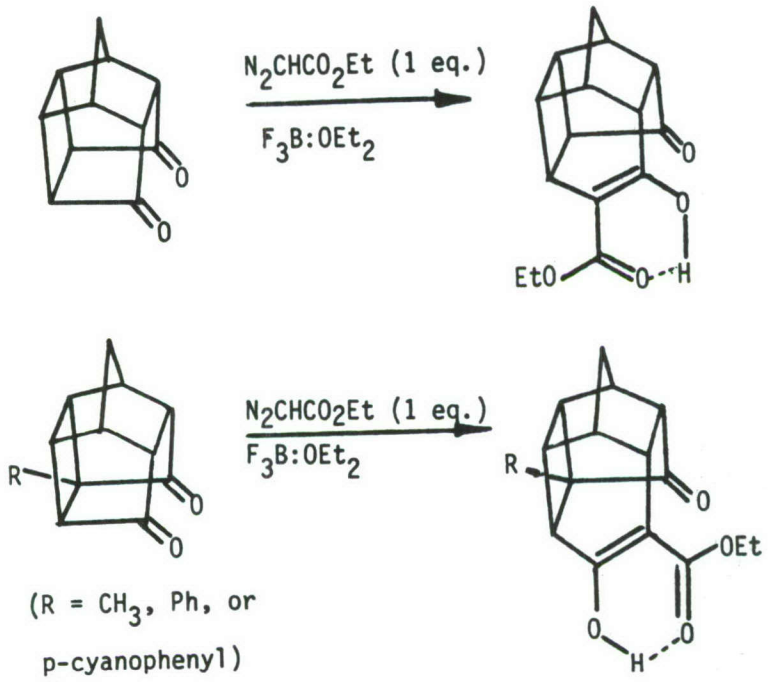

(R = CH_3, Ph, or p-cyanophenyl)

The detailed mechanism of this ring expansion process is currently under investigation.[7]

REFERENCES

1. A. P. Marchand. "Synthesis and Chemistry of Novel Polynitropolycyclic Cage Molecules", Tetrahedron. in press.

2. A. P. Marchand. G. S. Annapurna. V. Vidyasagar, J. L. Flippen-Anderson, R. Gilardi. C. George. and H. L. Ammon J. Org. Chem.. **52**. 4781 (1987).

3. A. P. Marchand. G. V. M. Sharma. G. S. Annapurna, and P. R. Pednekar. J. Org. Chem.. **52**. 4784 (1987)

4. R. W. Velicky. S. Iyer. C. Campbell. O. Sandus. J. Alster. A. P. Marchand. G. V. Madhav Sharma. and G. S. Annapurna. J. Energetic Materials. in press.

5. A. P Marchand, P R. Dave. J. L. Flippen-Anderson. R. Gilardi, C. George. and M. D. Johnston Jr. unpublished results.

6. A. P Marchand B. E. Arney, Jr., R. Gilardi. and J. L. Flippen-Anderson, J. Org. Chem. **52**. 3455 (1987).

7 A P. Marchand and Pendri Annapurna unpublished results.

Highly Fluorinated Nitrogen-Containing Compounds

AFOSR 87-0067

Jean'ne M. Shreeve

University of Idaho

Earlier we had reported the reactions of NF_2CF_2CN (1) with chlorine fluoride and the subsequent dimerization of the resulting N,N-dichloroamines. More recently our studies have led to an examination of condensation and cyclization reactions of 1. In addition, we have examined the reactions of (difluoroamino)difluoroacetamidoxime, $F_2NCF_2(C{=}NOH)NH_2$, with perfluoroacyl chlorides to form 1,2,4-oxidiazoles.

i) Reaction of F_2NCF_2CN with NH_3.

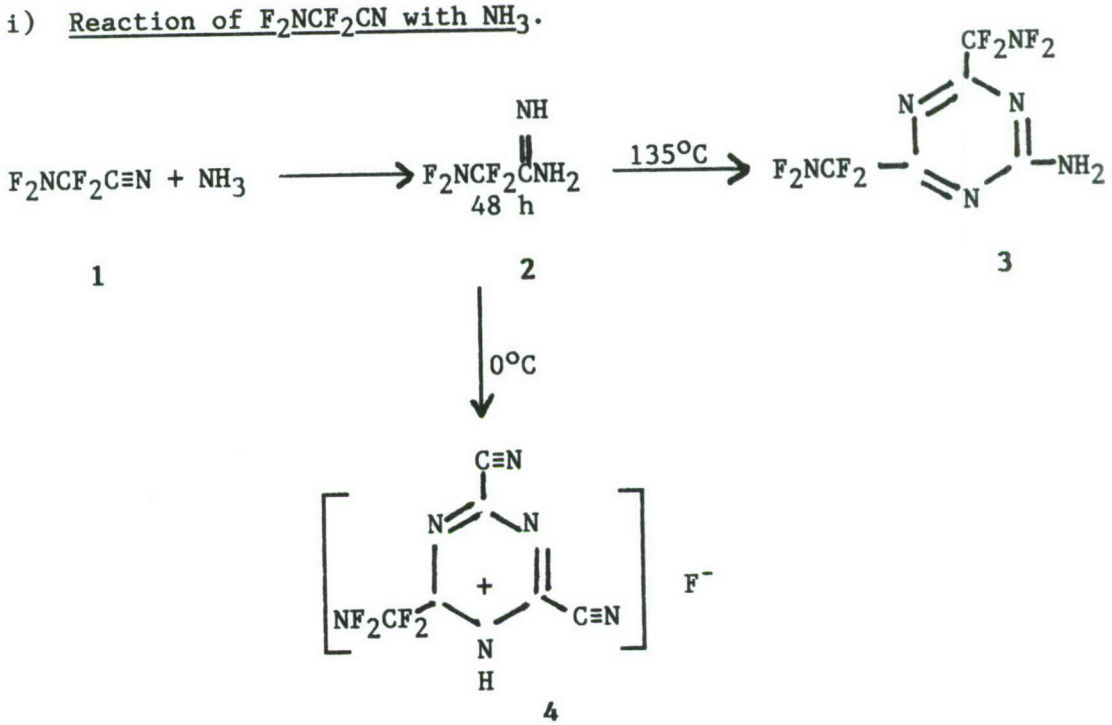

1 2 3

4

Ammonia with 1 gives the volatile, viscous compound (difluoro-amino)difluoro-

acetamidine, **2**. On heating **2** was converted to 1-amino-3,5-bis[(difluoroamino)difluoromethyl] triazine (**3**), which is a white, sublimable solid. At low temperature a compound, 1,3-dicyano-5-(difluoroamino)difluoro-methyltriazonium fluoride, **4**, could be isolated.

ii) <u>Reaction of **1** with hydrazine</u>

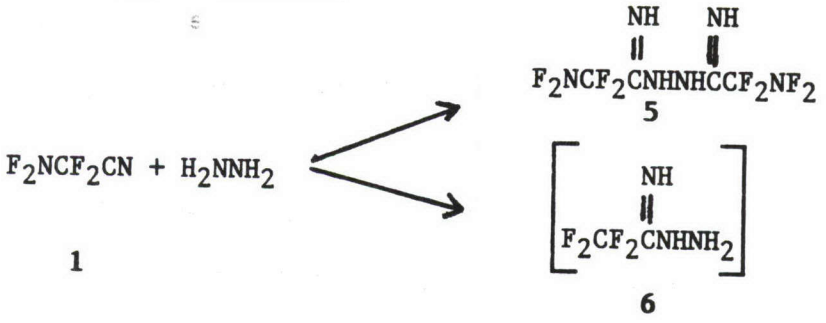

(Difluoroamino)difluoromonoacetamidine hydrazine, **6** is stable only in solution with explosive decomposition accompanying removal of the solvent. However, N,N'-bis(fluoroamino)difluoroacetamidine hydrazine **5** is a stable, sublimable crystalline solid. The instability of **6** may be attributed to the closing of the five-membered ring with concomitant loss of two hydrogen fluoride molecules followed by loss of N_2.

iii) <u>Reaction of **1** with polyfluorinated alcohols</u>.

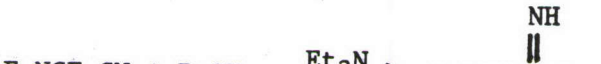

$R_f = CF_3CH_2$ (**7**), $(CF_3)_2CH$ (**8**)

2,2,2-Trifluoroethanol and 1,1,1,3,3,3-hexafluoro-2-propanol were reacted with **1** in the presence of triethylamine. Any unconsumed Et_3N is removed by reaction with HCl at reduced temperature. Both **7** and **8** were confirmed by the usual spectroscopic methods and **7** also was characterized by elemental analysis.

iv) Reaction of 1 with NH_2OH.

$$F_2NCF_2CN + NH_2OH\cdot HCl \xrightarrow[THF/H_2O/Et_2O]{K_2CO_3} \underset{\mathbf{9}}{F_2NCF_2C(=NOH)NH_2}$$

(Difluoroamino)difluoroacetamidoxine, **9**, was prepared by modifying the earlier methods. Using the latter method, in which hydroxylamine was generated *in situ* by the reaction of sodium methoxide with hydroxylamine hydrogen chloride in CH_3OH, only a very low yield of **9** was obtained. Therefore, a two-phase method was developed in which the NH_2OH was freed from the hydrogen chloride salt in the aqueous phase by the addition of an equivalent amount of K_2CO_3. The free NH_2OH transferred to the organic phase (diethyl ether and tetrahydrofuran) where it was reacted with **1**. Although it is possible for **9** to exist in two tautomeric forms, the simplicity of the infrared spectrum supports the existence of only one form, $F_2NCF_2C(=NOH)NH_2$.

v) Reaction of **9** with perfluoroacyl chlorides.

Further support for the above tautomer is obtained when **9** is reacted with $R_fC(O)Cl$ (R_f = CF_3, C_2F_5, C_3F_7) to form the respective difluoroaminodifluoroethylamidoximes that undergo ready cyclization to 3-(difluoroamino)difluoroethyl-5-perfluoroalkyl-1,2,4-oxadiazoles. Compound **9** was reacted with $R_fC(O)Cl$ as follows:

$$\underset{\mathbf{9}}{F_2NCF_2C(=NOH)NH_2} + R_fC(O)Cl \xrightarrow[-HCl]{Et_2O} \underset{\mathbf{10,\ 11,\ 12}}{F_2NCF_2C(=N-C(=O)-CR_f)NH_2}$$

$$\xrightarrow[-H_2O]{P_4O_{10}} \underset{\mathbf{13,\ 14,\ 15}}{F_2NCF_2C\text{(oxadiazole)}CR_f} \qquad R_f = CF_3\ (\mathbf{10,\ 13}),\ C_2F_5\ (\mathbf{11,\ 14})\ C_3F_7\ (\mathbf{12,\ 15})$$

Each of these O-acyldifluoroacetamidoximes is a stable sublimable solid, but each is highly susceptible to hydrolysis. However, **10** begins to decompose even at room temperature which made elemental analysis difficult.

3-(Difluoroamino)difluoroethyl-5-perfluoroalkyl-1,2,4-oxadiazoles **13,14,15,** are colorless, volatile, stable liquids that have characteristic infrared absorption bands at 1590-1615 and 1530-1510 cm^{-1} due to the stretching vibrations of the two distinct $\rangle C{=}N{=}$ moieties of the 1,2,4-oxadiazole ring.

When **9** was heated at 160°C with perfluorosuccinic acid over P_4O_{10} a novel bis(1,2,4-oxadiazole) resulted. It is likely that the reaction proceeds via the initial formation of perfluorosuccinic acid anhydride that is then acylated and subsequently dehydrated to the bis(1,2,4-oxadiazole), i.e.,

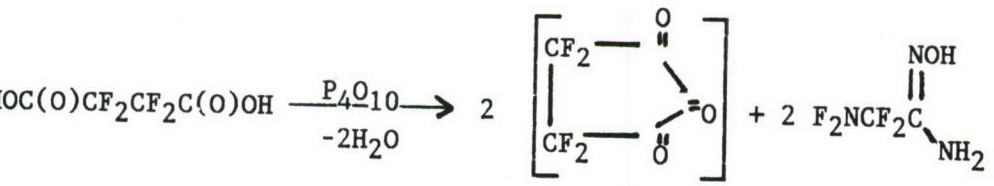

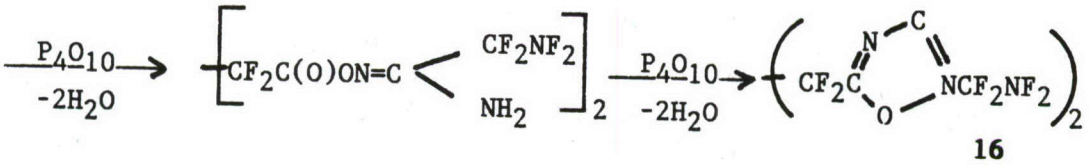

16

Phosgene in large excess was also used successfully as an O-acylating agent to give O-chloroformyl(difluoroamino)difluoroacctamidoxime, **17**, in essentially quantitative yield.

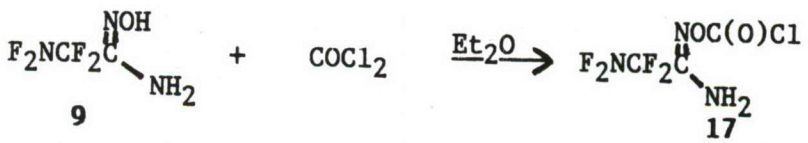

9 **17**

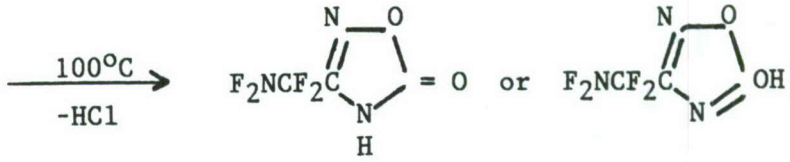

18 d e

The structure of **17** was confirmed by infrared, chemical ionization mass, and NMR spectra, and elemental analysis. On heating **17**, HCl gradually evolved giving rise to **18**. Infrared spectra of **18** supported the lactone structure d rather than the alcohol structure e.

Reactions of $Na^+[NF_2CF_2\overline{CNNNN}]^-$ and $Na^+[CF_3\overline{CNNNN}]^-$

Sodium azide reacts easily with NF_2CF_2CN, **1**, to form sodium 5-difluoro-aminodifluoromethyltetrazoate, **19**. Not unexpectedly the reaction of NaN_3 with CF_3CN proceeds in an analogous manner.*

*Norris, W.P.; J. Org. Chem. **1962**, 27 3248.

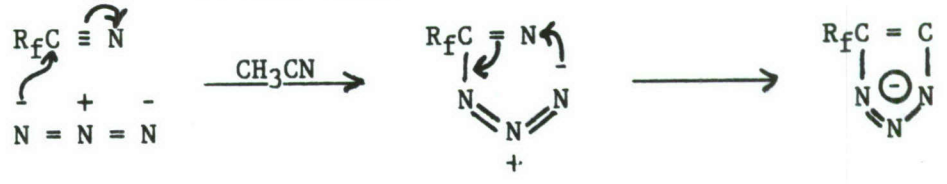

$R_f = NF_2CF_2$ **(19)**, CF_3 **(20)**

Just as for the previously prepared compound, **20**, the new compound **19** is a highly hygroscopic crystalline compound that is highly soluble in THF, CH_3CN, C_2H_5OH, DMF and H_2O.

Each of the four nitrogen atoms of the tetrazole ring is, in principal, capable of acting as a coordination site. Variable kinds of coordination for tetrazoles have been observed - monodentate, e.g., $Cu_2(CF_3CN_4)_2\{[CH_2P(C_6H_5)_2]_2\}_3$ at N-2 or N-4; and 2,3 and 3,4 bidentate, e.g., $Ag_2(P\Phi_3)_4(CF_3CN_4)_2$. There is no evidence that suggests any type of bonding other than by donation from one or two nitrogen atoms in the tetrazole ring to the acceptor moiety.

SYNTHESIS AND PROPERTIES OF NITROCARBENES

William P. Dailey
Department of Chemistry
University of Pennsylvania
Philadelphia, PA 19104-6323

There has been a recent interest in the synthesis of strained ring nitro compounds as high energy density materials.[1] Several methods are described in the literature for the preparation of nitro substituted cyclopropanes,[2] but the successful addition of nitrocarbene to alkenes has not been reported. An ideal precursor, nitrodiazomethane (1), was prepared by Schollkopf and Markusch[3], but they found that it failed to add nitrocarbene to olefins under either thermal or photochemical conditions. Instead they found evidence that nitrocarbene fragments to formyl radical and nitric oxide. Possible pathways for this reaction are shown below.

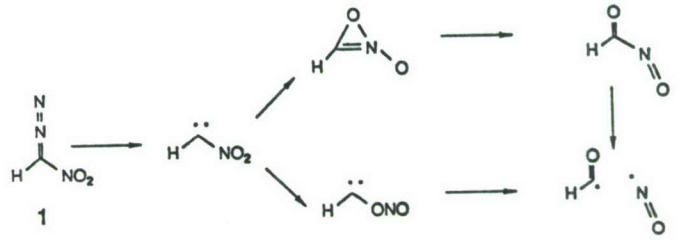

Transition metal mediated cyclopropanation of olefins using diazo compounds is a valuable synthetic reaction.[4] For instance, formylcarbene undergoes Wolff rearrangement to ketene rather than addition to olefins, but the copper catalyzed decomposition of formyldiazomethane in the presence of olefins yields cyclopropanes.[5] We wish to report that nitrodiazomethane in the presence of rhodium(II) acetate will form nitrocyclopropanes with electron rich olefins. As an example, the dropwise addition of an ether solution of nitrodiazomethane to a solution of 2,3-dimethyl-2-butene containing 1 mole % of rhodium(II) acetate cleanly produced 1-nitro-2,2,3,3-tetramethylcyclopropane (2), m.p. 48-

-49°, in 15% yield after preparative glc. Ir ($CDCl_3$): 1535, 1360, 1110 cm^{-1}; ^1H nmr ($CDCl_3$): 3.77 (s, 1H), 1.34 (s, 6H), 1.20 ppm (s, 6H); ^{13}C nmr : 74.3, 32.8, 22.3, 16.0 ppm.

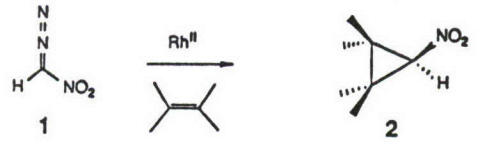

1 2

Likewise, the use of isobutylene as the trapping olefin produced the known 1,1-dimethyl-2-nitrocyclopropane[3] (3) in 4% yield while the use of cyclohexene produced a 2:1 mixture of isomeric nitrocyclopropanes 4 in 14% combined yield. The use of a more electron rich olefin, vinyl acetate, produced a 60:40 mixture of isomeric 1-acetoxy-2-nitrocyclopropanes 5 in low yield. The use of an electron poor olefin, e.g. vinylidene chloride or ethyl acrylate, produced no trace of cyclopropane. Similar results have been observed in other transition metal catalyzed cyclopropanations.[4]

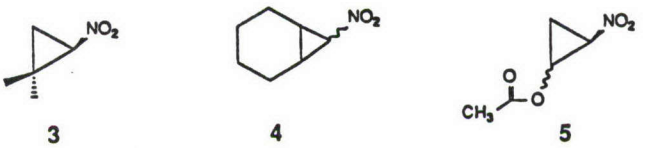

3 4 5

While the yields of nitrocyclopropanes are generally low with the present method, it offers the advantage of a simple one-step synthesis of novel nitrocyclopropanes. We attempted to extend the scope of this reaction to include other nitrodiazomethanes.[6] However we have found no evidence for the formation of any cyclopropanes using the corresponding trifluoromethyl or carboethoxy diazomethanes. This result is rather surprising since both ethyl diazoacetate and diethyl diazomalonate both give good yields of cyclopropanes using a transition metal catalyst.

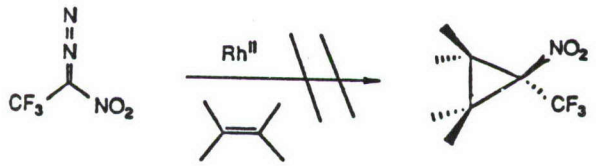

We desired to learn why nitrocarbene should be so unstable. Therefore we have carried out ab initio calculations[7] on nitrocarbene and some of its isomers using the 3-21G basis set with complete geometry optimization using the Gaussian 82 program.[8] Single point energy calculations partially corrected for electron correlation were performed using third order Moller-Plesset perturbation theory (MP3) and the 6-31G* basis set. The total and relative energies are shown below for singlet nitrocarbene, singlet nitritocarbene, nitrosocarbaldehyde, and free nitric oxide and formyl radical.

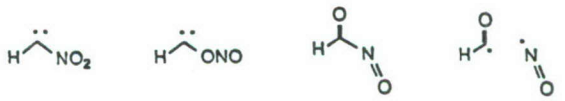

-E	242.98024	243.03113	243.14164	242.98523 hartrees
rel. E	101.3	69.3	0.0	98.1 kcal/mol

We were unable to find a local minimum corresponding to oxazirine-N-oxide (6) but we did locate a transition structure (see below) in this area of the potential surface.

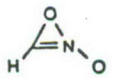

6

The calculations reveal that the rearrangement of singlet nitrocarbene is highly favored on thermodynamic grounds. However there may still be a substantial barrier to the rearrangement. Further calculations using the 6-31G* basis set and complete geometry optimization were performed on singlet nitrocarbene and the transition structure for oxygen migration. The nature of both of these stationary points (minimum and transition structure) was confirmed by analytical frequency calculations. These were followed by single point energy calculations at the MP3

level in addition to multiconfigurational SCF (MCSCF) calculations using three configurations. Partial geometries and the HF, MP3, and MCHF total energies for the singlet ground state of nitrocarbene and the transition structure for oxygen migration are shown below.

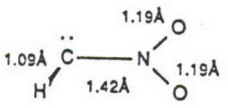

minimum

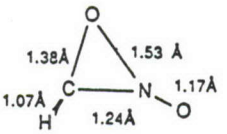

transition structure

-E (HF)	242.35404	242.33370 hartrees
(MP3)	242.98024	242.99360 hartrees
(MCHF)	242.37453	242.37396 hartrees

If one takes zero-point energies into account, then the barrier to rearrangement at the HF/6-31G* level is calculated to be 12.4 kcal/mol while at the MP3/6-31G* level, the barrier is calculated to be much less than zero (-16.8 kcal/mol). The MP3 method, a non-variational procedure, appears to greatly overestimate the stability of the transition structure relative to the ground state. On the other hand, the MCSCF method, a variational procedure, predicts that the barrier is very close to zero. Further calculations at the HF/3-21G level reveal that this transition structure leads to nitrosocarbaldehyde. These results agree with the experimental observation that nitrocarbene is a very labile species.

Acyl nitroso compounds are well known in organic synthesis and have been used as dienophiles in hetero Diels-Alder reactions.[9] Thermolysis of nitrodiazomethane in the presence of several different 1,3-dienes produced no detectable amount of Diels-Alder adduct. However, we have also been unable to prepare and trap authentic nitrosocarbaldehyde from the corresponding hydroxylamine.

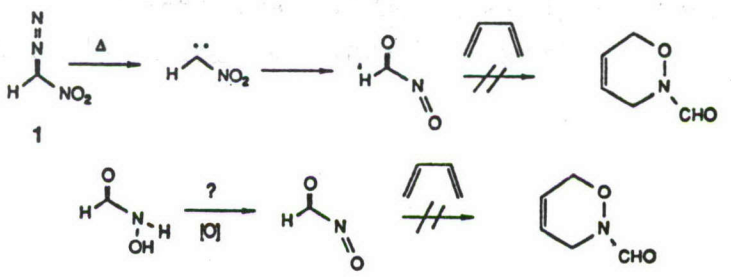

1

We are attempting to prepare and spectroscopically characterize these novel acyl nitroso compounds using the dimethylanthracene Diels-Alder adducts shown below. The adducts will be treated under flash vacuum pyrolysis conditions and the volatiles will be deposited onto a cold window.

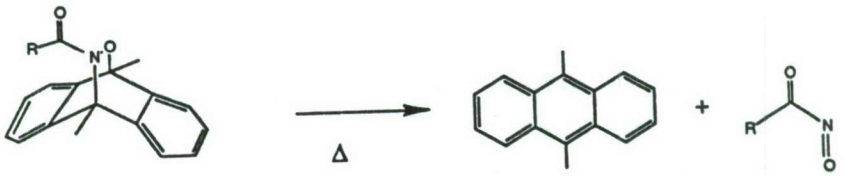

R = H, CH_3 , CF_3

REFERENCES

1. (a) Wade, P. A.; Dailey, W. P.; Carroll, P. J. J. Am. Chem.-Soc. 1987, 109, 5452. (b) Eaton, P. E.; Ravi Shankar, B. K.; Price, G. D.; Pluth, J. J.; Gilbert, E. E.; Alster, J.; Sandus, O. J. Org. Chem. 1984, 49, 185. (c) Paquette, L. A.; Fischer, J. W.; Engel, P. J. Org. Chem. 1985, 50, 2524. (d) Marchand, A. P.; Suri, S. C. J. Org. Chem. 1984, 49, 2041. (e) Marchand, A. P.; Reddy, D. S. J. Org. Chem. 1984, 49, 4078.

2. (a) Asorskis, J.; Shechter, H. J. Org. Chem. 1968, 33, 1164.
(b) Parham, W. E.; Braxton, H. G.; Serres, C J. Org. Chem. 1961, 26, 1831. (c) Kuwajima, I.; Ryochi, A.; Tomso, S. Tetrahedron Lett. 1983, 24, 4429. (d) Valades, L., Siminez, M.; Rodreguez-Hahn, L. Rev. Latinaom. Quim 1975, 6, 152.

3. Schollkopf, U.; Markusch, P. Ann. Chem. 1971, 753, 143.

4. (a) Doyle, M. P.; Griffin, J. H.; Bugheri, V.; Dorow, R. L. Organometallics 1984, 3, 53. (b) Doyle, M. P.; Dorrow, R. L.; Tamblyn, W. H.; Buhro, W. E. Tetrahedron Lett. 1982, 23, 2261. (c) Doyle, M. P.; Van Lensen, D.; Tamblyn, W. H. Synthesis 1981, 10, 787.
(d) Anciaux, A. J.; Hubert, A. J.; Noels, A. F.; Petinot, N.; Teyssie', P. J. Org. Chem. 1980, 45, 695.

5. Arnold, Z. J. Chem Soc., Chem. Comm. 1967, 299.

6. Schollkopf, U.; Tonne, P.; Schafer, H.; Markusch, P. Ann.-Chem. 1968, 722, 45.

7. For an excellent review on ab initio molecular orbital calculations using the Gaussian series of programs, see: Hehre, W. J.; Radom, L.; Schleyer, P. v. R.; Pople, J. A. "Ab Initio Molecular Orbital Theory", Wiley, New York, 1986.

8. Binkley, J. S.; Frisch, M. J.; DeFrees, D. J.; Raghavachari, K; Whiteside, R. A.; Schlegel, H. B.; Fluder, E. M.; Pople, J. A. Department of Chemistry, Carnegie-Mellon University, 1983.

9. (a) Kirby, G. W.; McGuigan, H.; Mackinnon, J. W. M.; McLean, D.; Sharma, R. P. J. Chem. Soc., Perkin Trans. I, 1985, 1437. (b) Kirby, G. W.; Sweeny, S. G. J. Chem. Soc., Perkin Trans. I, 1981, 3250.

2nd HIGH ENERGY DENSITY MATERIALS CONFERENCE

28 February - 2 March 1988 — Newport Beach, CA

NEW HIGH ENERGY DENSITY SMALL RING SYSTEMS*

Koop Lammertsma and Osman F. Güner

Department of Chemistry, University of Alabama at Birmingham
Birmingham, Alabama 35294

Theoretical ab initio MO calculations have been performed on small molecular clusters to identify candidates for advanced chemical propulsion systems. In the search for high energy density systems we concentrate on new classes of tetraatomic compounds. In our studies the planar rhombic structure has a central place. These rhombic molecules are highly strained, have no hydrogens, and consequently are of high energy. Because of their structural properties these binary or ternary systems may result in densely packed solid materials.

Our calculations concern isolated tetraatomic systems consisting of the "light" elements of the periodic table. An evaluation of 53 tetraatomic dicarbides and diborides, with ligands ranging from the first row element Li to the second row Si, shows 47 rhombic structures as minima on the HF/6-31G* potential energy surface.

The rhombic structure appears to be common to most tetraatomics. Even geometrical parameters seem similar for different molecules. Illustrative is the average C–C distance in 26 dicarbides of 1.449 Å(SD 0.060) and the average B–B distance in 27 diborides of 1.763 Å(SD 0.111). These bridgehead C–C and B–B separations are remarkably short. Despite the apparent geometrical similarity, these structures have very different bonding modes. For example, rhombic C4 is considered a 2π aromatic species with two inverted tricoordinate carbons whereas rhombic C_2Be_2 is viewed as highly ionic.

To establish the scope and limitations of rhombic structures and to evaluate the general bonding principles and in particular the high energies of these high density tetraatomic clusters, we have performed full singlet and triplet potential

* Supported under Contract F04611-86-K-0073

energy surface surveys of C_2Si_2, B_2Be_2, and B_2Li_2, with vibrational analysis of all stationary points. These calculations show a high energetic sensitivity to the effect of electron correlations and a delicate balance between the dense tetrahedral and rhomboidal structures for the lightest compounds.

The ab initio molecular orbital calculations were carried out by utilizing the GAUSSIAN-82 and -86 series of programs with geometry optimizations and characterizations performed at both HF/3-21G and HF/6- 31G*. Final energy comparisons between isomers include the effects of valence electron correlation at the full fourth order with Møller-Plesset perturbation theory, donated as MP4(SDTQ)/6-31G*.

To test the applicablity of inverted tricoordinated atoms to other systems, we first explored extensively the singlet and triplet potential energy surface of the binary disilicon dicarbide C_2Si_2. Fourteen species were investigated. There are similarities with the well studied C4. The global C_2Si_2 energy minimum is the rhombic structure **1**. Interestingly, rhomboidal structure **2**, which contains an inverted tricoordinate carbon as well as an inverted tricoordinate silicon, is only slightly less stable. Both are favored over the triplet linear isomer **3**. The relative energies of these three equilibrium structures are listed in Table 1. Whereas the relative energies are very sensitive to electron correlation effects, addition of diffuse functions at the Hartree-Fock level (HF/6-31+G*) has little influence on the geometries and relative energies. The HF/3-21G level is inadequate for this system.

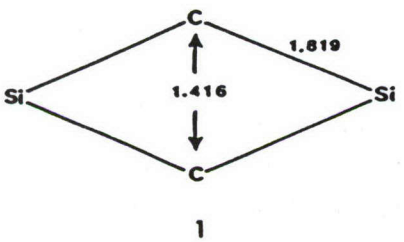

1

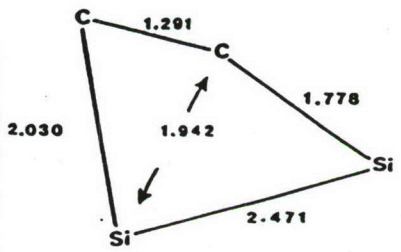

2

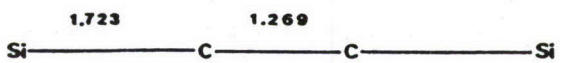

3

Subsequently we focussed our attention to tetraatomics of lower molecular weight and studied the singlet and triplet potential energy surface of diberyllium diboride, Be_2B_2. For comparison, the rhombic diberyllium dicarbide C_2Be_2 is a high energy isomer with the linear triplet form as global energy minimum. We

emphasize that of the many binary beryllium-boron solid state materials there is currently no molecular composition known with a Be:B ratio of 1:1. Investigation of thirteen Be_2B_2 species showed the singlet tetrahedral **4** as global minimum which has an energy difference with structural isomers of 30 kcal/mol and more. This tetrahedral species **4** has a barrier of 19 kcal/mol for a through-plane inversion (**5**) and an energy difference with the rhombic structure **6** of 61 kcal/mol. Structure **4** is favored at all theoretical levels employed. Some triplet isomeric structures proved of high energy after elimination of spin contamination. A tetrahedral structure is of course also a good candidate for a densely packed high energy material. Cluster calculations on the Be_2B_2 tetrahedron are currently conducted by Brenner, Callaway, and Kestner at Louisiana State University to evaluate solid state packing arrangements.

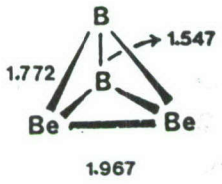

4

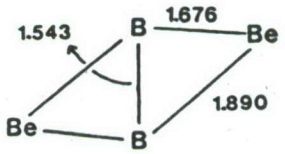

5

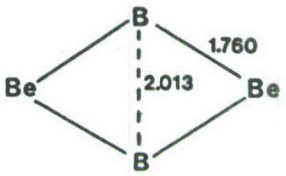

6

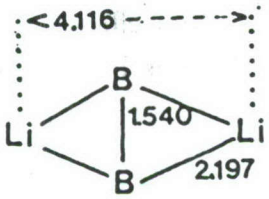

7

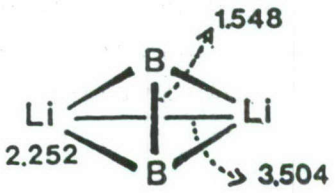

8

Concurrently, we investigated the singlet and triplet potential energy surface of dilithium diboride, B_2Li_2. For comparison, the dilithium dicarbide C_2Li_2 has a singlet rhombic and linear structure of nearly the same energy. In contrast, B_2Li_2 strongly favors the singlet rhombic **7** and tetrahedral **8** forms, with the rhombic isomer as global minimum at MP4/6- 31G* (see Table 1). The small energy difference between the two densely packed rhombic and tetrahedral structures may suggest fluctional behavior. The relative energies between the 10 studied species are very dependent on the calculational levels and in particular on correlation effects. This is illustrated in Table 1 and Figure 1.

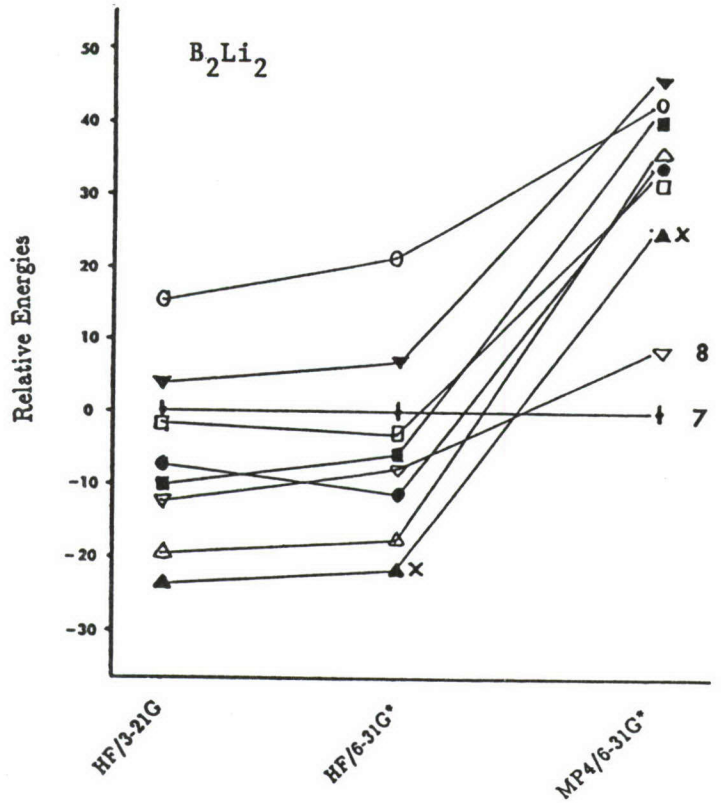

Table 1. Relative Energies of C_2Si_2, Be_2B_2, and B_2Li_2 Isomers.

Structure		HF/3-21G	HF/6-31G*	MP4/6-31G*
C_2Si_2	**1**	0	0	0
	2	−3	9	9
	3	−31	0	11
Be_2B_2	**4**	0	0	0
	5	11	14	19
	6	17	27	61
B_2Li_2	**7**	0	0	0
	8	−11	−9	9

COMPUTATIONAL STUDIES OF THE PROPERTIES OF TETRAHEDRANE, TRIPRISMANE AND THEIR AZA ANALOGS.

Peter Politzer and Jorge Seminario
Department of Chemistry
University of New Orleans
New Orleans, Louisiana, 70148

INTRODUCTION

The work being reported is the initial phase of a computational study and evaluation of a group of strained nitro and nitro/methyl derivatives of tetrahedrane (I), triprismane (II), and their aza analogs (III - X), in which one or more C-H units have been replaced by nitrogens. The estimated detonation velocities, detonation pressures and specific impulses of some of these derivatives show them to be potentially important high-energy systems. Our study shall assess the anticipated chemical, thermal and shock/impact sensitivities of these compounds, the difficulties involved in their syntheses, and the combinations of substituents that are likely to provide optimum overall performance. The general objective is to identify the most promising candidates for designation as high-energy target systems in a program of synthesis and testing. The primary focus of this project will be on the nitro and nitro/methyl derivatives shown below. The present report, however, deals with the first phase of the project, which is an analysis of the parent molecules, I - X.

I II III IV V VI VII VIII IX X

Molecules related to tetrahedrane:

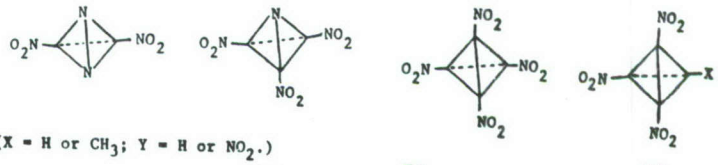

Molecules related to triprismane: (X = H or CH_3; Y = H or NO_2.)

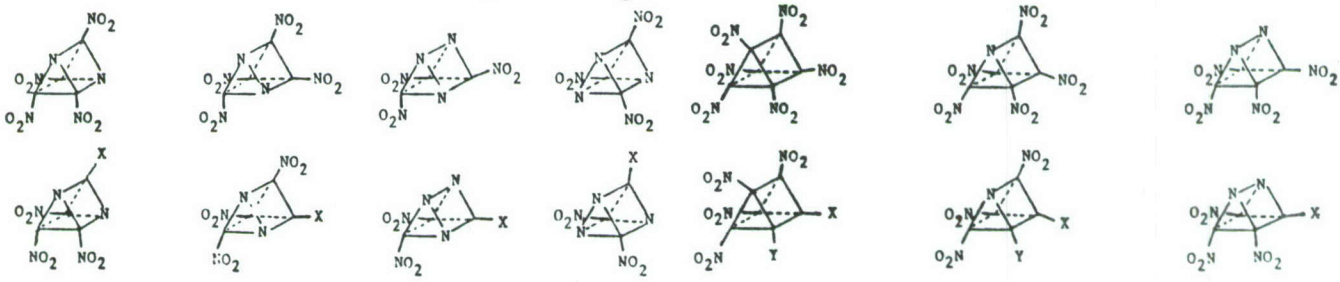

COMPUTATIONAL APPROACH

We use an ab initio self-consistent-field molecular orbital procedure (GAUSSIAN 82) to compute optimized structures and key properties for the molecules of interest. The structures are optimized at the 3-21G level, which we have found to be satisfactorily close to the results obtained with larger basis sets, including 6-31G*. These geometries are then used to calculate the molecular electrostatic potentials and bond deviation indices at minimum basis set levels, which past experience has shown to give good results for these properties.

The electrostatic potential $V(\vec{r})$ that is created in the space around a molecule by its nuclei and electrons is given rigorously by eq. (1):

$$V(\vec{r}) = \sum_A \frac{Z_A}{|\vec{R}_A - \vec{r}|} - \int \frac{\rho(\vec{r}')d\vec{r}'}{|\vec{r}' - \vec{r}|} \qquad (1)$$

Z_A is the charge on nucleus A, located at $\vec{R}_A$, and $\rho(\vec{r})$ is the electronic density function. $V(\vec{r})$ is well-established as an effective tool for interpreting and predicting molecular reactivity [1-3]; for example, an approaching electrophile tends to go to those regions in which $V(\vec{r})$ is negative, where the effects of the molecule's electrons predominate. The electrostatic potential is a real physical property, which can be determined experimentally as well as computationally [3].

We have introduced the bond deviation index as a quantitative means for characterizing chemical bonds and measuring their degrees of strain. It represents the extent to which the actual path of maximum electronic density in a bond deviates from a reference path defined in terms of the superposed electronic densities of the undistorted free atoms placed at the same positions as they occupy in the molecule. We defined the bond deviation index, λ, by eq. (2):

$$\lambda = \frac{\left[\frac{1}{N}\sum_{i=1}^{N} r_i^2\right]^{1/2}}{R} \qquad (2)$$

The r_i are the lengths of N equally-spaced lines drawn between the actual and the reference bond paths. N is taken to be 320, which is well beyond the point at which further increases in N would change λ. We divide by the bond length R in order to be able to compare bonds of different lengths.

RESULTS AND DISCUSSION

1. Structures:

The calculated C-C bond lengths in tetrahedrane are 1.489 A, which is shorter than both the typical C-C single bond (1.54 A) and also that in cyclopropane (1.512 A). The introduction of nitrogens, in going to III and IV, shortens the C-C bonds yet further, to 1.452 and 1.410 A. The C-N bonds in III, on the other hand, are longer, at 1.540 A, than the typical 1.47 A; they decrease to 1.503 A in IV. The N-N bond in IV is remarkably long, 1.589 A, approximately 0.14 A longer than in hydrazine.

Triprismane has two different types of C-C bonds; both are longer than those in tetrahedrane. The ones in the three-sided faces are found to be 1.534 A in length, while the others are 1.570 A. The introduction of nitrogens decreases these values by 0.02 to 0.04 A. The C-N distances follow the same pattern as in the azatetrahedranes, generally being in the neighborhood of 1.54 A but decreasing to approximately 1.50 A in VII, IX and X. Finally, the N-N bonds are again long, roughly 1.58 A.

2. Bond Deviation Indices:

The C-C bond deviation index in tetrahedrane is 0.113, which is greater than we have found for any other molecule. For comparison, the C-C λ values in cyclopropane and cubane are 0.080 and 0.029, respectively [4,5]. Upon proceeding to III and IV, the C-C λ diminishes to 0.101 and 0.087. For the C-N bonds, λ also decreases with the introduction of nitrogens, from 0.105 in III to 0.091 in IV. Thus, the effect of the nitrogens is clearly to diminish the strain in the molecule. For the N-N bond in IV, $\lambda = 0.109$.

In triprismane, the bond deviation indices for the two types of C-C bonds are 0.077 (three-sided faces) and 0.032. This suggests that these bonds are similar, in their strain, to those in cyclopropane and cubane (see above). In the azatriprismanes, these values are again smaller, e.g. 0.069 and 0.026 in IX. The C-N bonds are considerably less strained than in the azatetrahedranes; thus $\lambda = 0.064$ (three-sided face) and 0.016 in V, and decreases to 0.052 - 0.066 (three-sided faces) and 0.012 in IX. For the N-N bonds, λ is 0.6 - 0.7 in the three-sided faces, and approximately 0.10 in the others.

3. Electrostatic Potentials:

The electrostatic potentials of tetrahedrane and triprismane (Figure 1) show the interesting and important features of negative regions near the midpoints of the C-C bonds. While this is not typical of bonds in general, we have found it to be characteristic of the C-C bonds in strained hydrocarbons [4-6]. These bonds can accordingly serve as initial sites for electrophilic attack, as has indeed been observed in the cases of cyclopropane [4] and cubane [5]. It is notable that the most negative values for the two types of C-C bonds in triprismane, -4.9 and -13.2 kcal/mole, are very similar to those found for cubane, -4.6 [5], and cyclopropane, -13.0 [4]. This supports the earlier suggestion, based upon the calculated bond deviation indices, that there should be similarities between these respective bonds.

Due to the presence of the electron-withdrawing nitrogen, the negative C-C bond potentials are eliminated in III and greatly weakened in V. However there are now strong and extensive negative regions associated with the nitrogens, which can be attributed to their lone pairs (Figure 2). These negative potentials become weaker as the number of nitrogens in the molecule increases, since they are competing for the same polarizable electronic charge; thus the most negative values change from -87 to -75 to -66 kcal/mole in going from V to VI to X. The nitrogens are consistently more negative in the azatriprismanes than in the corresponding azatetrahedranes.

SUMMARY AND CONCLUSIONS

(1) In both the tetrahedrane and the triprismane systems, there is a relaxation of bond strain as the number of nitrogens is increased.
(2) The negative electrostatic potentials associated with strained C-C bonds are greatly weakened or eliminated as nitrogens are introduced, making these bonds less susceptible to electrophilic attack.
(3) The nitrogens in the azatriprismanes are more negative and accordingly more basic than those in the azatetrahedranes. In both types of systems, these basicities decrease as the number of nitrogens increases.
(4) In the triprismanes, the bonds can be separated into cyclopropane-like and cubane-like.
(5) The N-N bonds in both the azatetrahedranes and the azatriprismanes are abnormally long.

ACKNOWLEDGEMENT

We greatly appreciate the support of this work by the Air Force Office of Scientific Research, Grant No. AFOSR-88-0068.

REFERENCES

[1] E. Scrocco and J. Tomasi, Adv. Quantum Chem. 11, 115 (1978).

[2] P. Politzer and K. C. Daiker, in: The Force Concept in Chemistry, B. M. Deb, ed., Van Nostrand-Reinhold, New York, 1981, ch. 6.

[3] P. Politzer and D. G. Truhlar, eds., Chemical Applications of Atomic and Molecular Electrostatic Potentials, Plenum Press, New York, 1981.

[4] P. Politzer, L. N. Domelsmith, P. Sjoberg and J. Alster, Chem. Phys. Letters 92, 366 (1982).

[5] P. Politzer, L. N. Domelsmith and L. Abrahmsen, J. Phys. Chem. 88, 1752 (1984).

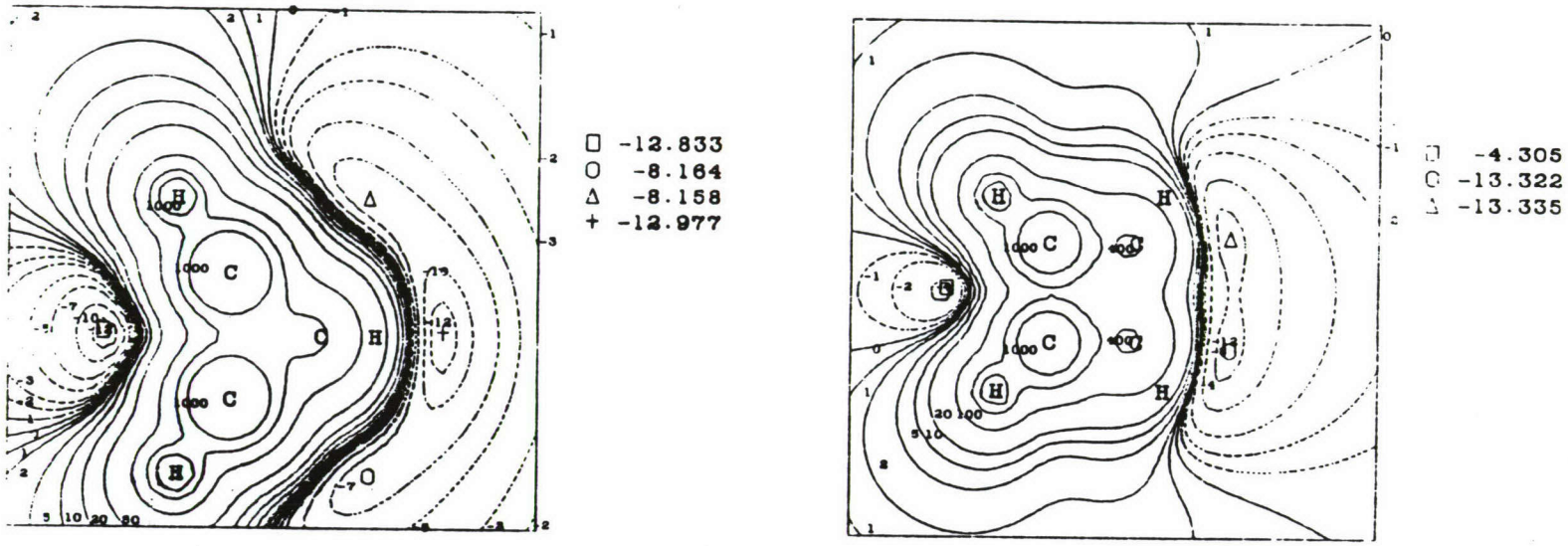

Figure 1. Electrostatic potential of tetrahedrane (left), in plane through one C-C bond and bisecting the opposite one, and of triprismane (right), in plane through C-C bond connecting the three-sided faces and bisecting these faces. Dashed contours correspond to negative potentials. The most negative points are indicated, and the corresponding values, in kcal/mole, are given at the side.

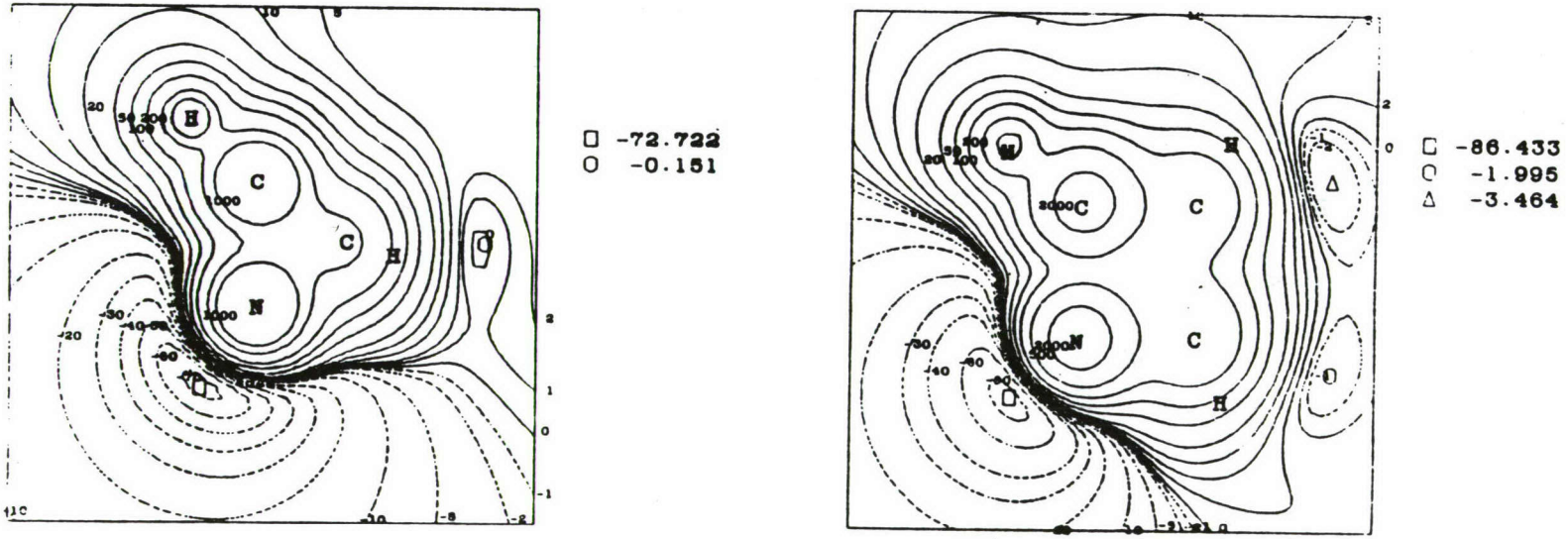

Figure 2. Electrostatic potential of monoazatetrahedrane (left) and monoazatriprismane (right) in same planes as in Figure 1. See caption to Figure 1 for further details.

Energy Storage in Rare Gas Solids via Charge Separation and Trapping

V.A. Apkarian

Department of Chemistry

University of California,

Irvine, California 92717

Paper presented at:

U.S. Air Force

High Energy Density Materials

Contractors Conference

February 29 - March 2, 1988

Solid xenon doped with atomic halogens, X, where X = (F, Cl, Br, I) have been used as prototypical media for optical energy storage via charge separation and self-trapping. The principles and experimental results are summarized in this report.

A. Preparation of Atomic Solids:

A prerequisite to these studies is the preparation of the atomic solids -- atomic rare gases doped with atomic halogens. This is achieved by the in situ photoproduction of halogen atoms in solids originally doped with hydrogen halides or molecular halogens. The permanent photodissociation of molecular dopants in rare gas solids is in general an inefficient process due to a strong cage effect. This effect is less severe in the case of hydrogen halides which at finite temperatures have finite cross sections for permanent dissociation. As an example, a permanent cage exit probability of ~10% is observed for H atoms produced by photodissociation of HI in crystalline xenon at 17 K -- 90% will geminately recombine within the cage. The H atoms that exit the cage are trapped at neighboring interstitial sites and cause large lattice deformations. The details can be found in recent reports of the photodissociation dynamics of HI in crystalline xenon which has been studied both theoretically[1] and experimentally[2]. Molecular halogens are known to be prevented from photodissociation by a nearly perfect cage effect when the molecular repulsive surfaces are accessed optically. This can be verified by monitoring the recombinant emissions which remain constant with irradiation time. As an example, when Cl_2 is promoted to its dissociative $^1\Pi$, $^3\Pi$ surfaces by excitation at 308 nm, emission is observed from the recombinant Cl_2 ($A' \rightarrow X$) transition:

$$Cl_2\,(X) + h\nu\,(308) \rightarrow Cl_2\,(^1\Pi, {}^3\Pi) \rightarrow [Cl(P_{3/2}) + Cl\,(P_{3/2})]$$

followed by in-cage recombination

$$[Cl\,(P_{3/2}) + Cl(P_{3/2})] \rightarrow Cl_2\,(X)$$

$$\rightarrow Cl_2\,(A')$$

and monitored by the radiative relaxation of the A' state

$$Cl_2\,(A') \rightarrow Cl_2\,(X) + h\nu$$

an example is shown from a Cl_2/Kr sample in figure 1. The constancy of the observed $A' \rightarrow X$ emission intensity with irradiation time verifies the absence of any permanent dissociation. A permanent dissociation quantum yield of less than 10^{-5} can be verified.

Molecular halogens dissociate with great efficiency in solids by the photoinduced harpoon reaction vis:

$$X_2 + Rg + 2h\nu \rightarrow (Rg^+X_2^-) \rightarrow Rg^+X^- + X$$

the diatomic exciplex will further react to form the most stable molecular charge transfer complex, namely the triatomic exciplex

$$Rg^+X^- + Rg \rightarrow Rg_2^+X^-$$

and the process can be followed by monitoring the radiative dissociation of the exciplex

$$Rg_2^+X^- \rightarrow 2Rg + X + h\nu.$$

The emission spectra of all triatomic xenon halides are illustrated in figure 2. The growth of exciplexic emission with irradiation time is shown in figure 3. The principles of this process were first established in Cl_2 and HCl doped solid xenon.[3] The generalization of the principles to all halogens in solid and liquid rare gases has been demonstrated and recently reported.[4,5] The inordinate efficiency of the harpoon reaction in producing permanent dissociation, has lead to the concept of a "negative" cage effect: the polarizable cage intimately participates in ejecting the neutral halogen atom by collapsing around the ionic charge transfer complex.[4,5]

In short, rare gas solids (RGS) doped with atomic halogens can be prepared by photodissociation via ionic potentials. The description of the charge transfer states of such solids which is essential for the understanding of the principles of energy storage is taken up in the next section.

B. Charge Transfer States of X/RGS

It has been well established that the emission spectra from the charge transfer (CT) states of X/RGS correspond to vibrationally relaxed triatomic molecular exciplexes. This was first demonstrated by spectral simulations[3] and subsequently by following the

exciplexic emission continuously as a function of density of the medium, and across phase transitions: gas-liquid-solid.[6] Therefore the relaxed charge transfer states of halogen doped rare gas solids are the lowest energy localized molecular CT complexes -- the triatomic exciplexes. Note that relaxation in this case implies a severe lattice contraction. The nearest neighbor distance in solid xenon is 4.34 Å, while the inter-xenon distance in $Xe_2^+X^-$ is ~3.2 Å. This is the key to the stability of localized CT states.

The localized description is inadequate for the vertically accessed CT states of X/Xe solids. An electron transfer from xenon to an atomic halogen creates a hole in the valence band of the solid and an electron localized on the halogen atom due to the large electron affinity of the latter. The ion-hole pair are coupled via a screened Coulombic potential, therefore the hole is not a truly free valence band state, but more appropriately described as a mobile polaron. The pair form eigenstates of the extended solid and therefore an excitonic CT state. Based on the mobility and extent of delocalization of the hole several limiting behaviors and therefore descriptions are possible.

In the case of strong localization, a molecular approach is possible. The formalism of Diatomics in Ionic Systems (DIIS) is appropriate in this limit.[7] In this approach the impurity atom and its nearest neighbors (12 in substitutional site and 6 in interstitital site) are considered explicitly. The charge transfer states of the cluster $Xe_{12}^+X^-$ (or $Xe_6^+X^-$) are then treated as linear combinations of the valence atomic orbitals and the effect of the extended solid as a perturbation -- a dielectric continuum that solvates the dipole of the cluster. The Franck-Condon accessed charge transfer states of the complex are found to be delocalized -- a halide ion with a positive charge delocalized over the nearest neighbors as illustrated in fig 4. The minimum energy configuration of the system closely resembles the gas phase triatomic $Xe_2^+X^-$ geometry, therefore the model correctly predicts the relaxation to the localized molecular configuration.[8]

It is worth considering the limit of fully delocalized mobile holes. This limit is appropriate for the case of solids with large valence bands. As before, the electron is

assumed to be strongly localized in the halogen atom and therefore of infinite effective mass. The CT exciton in this limit would correspond to the Wannier description, electron-hole pairs separated by many lattice sites, and a Rydbergian series of states in which the hole orbits around the negative ion is to be expected (illustrated in fig 4). The valence bands of rare gas solids under normal conditions are narrow, and the effective mass of holes is large; $m_h \sim 10\, m_e$. Further localization due to the Coulombic field of the negative ion is to be expected to produce even heavier holes and therefore localization on the lattice points of the solid. An intermediate description between the molecular and fully delocalized excitonic limits is necessary.

The intermediate excitonic description is achieved by treating the hole wavefunction as a packet created by integration over Bloch states of the solid

$$\psi_h (r-r_j) = \int_{k_L}^{k_o} e^{-ik \cdot r}\ \Phi_k (r-r_j)\, dk$$

In which Φ_k represent the tight-binding Bloch functions. The resulting wavefunctions have extended spatial extent however are centered on individual xenon atoms, as illustrated in figure 4. Therefore ion-hole pairs separated by several lattice sites are possible to create by optical excitations. In the resultant excitonic state the hole has limited mobility. The optically accessed charge transfer states of such a system are dictated by: the ground state configuration of the solid; the extent of overlap between electron and hole wavefunctions; and the screened Coulombic potential between the charge pair. The optical transition probability can be cast into a modified reflection approximation:

$$P(\omega) = \frac{4\pi}{h} \mid \mu_o \mid^2 \int dr\, e^{-\lambda r}\, g_{12}(r)\, r^2\, \delta (h\omega - V_{HT}(r))$$

in which $g_{12}(r)$ is the halogen-xenon radial distribution function, a transition dipole which decays exponentially with the separation between electron and hole is assumed and V_{HT} is the hole transport potential -- a screened Coulomb potential, adiabatic with respect to nuclear coordinates and fully diabatic with respect to electronic coordinates.

Excitation spectra of Cl, Br and I doped solid xenon at two different temperatures is collected in fig 5. The theoretically predicted spectra are also shown. The coarse agreement between the two is taken as justification of the intermediate excitonic treatment. We note that F atoms are bound to xenon in the ground state, and in contrast with the heavier halogens, which isolate as atoms, the spectra are treated as that of XeF isolated in solid Xe. Since the XeF internuclear distance is shorter in the ground state than in the ionic Xe^+F^- state, the excitation spectra only sample the repulsive wall of the ionic upper state. Therefore the excitation spectra can be adequately treated as that of the gas phase X $\rightarrow$B and X $\rightarrow$ D absorptions, and little can be learned in this case about long range interactions. The spectra and theoretical fits are shown in fig 6.

In short, the optically accessed CT states of X/Xe are excitonic in nature. However these states are unstable with respect to localization, or equivalently self-trapping, to form the molecular exciplexic states. Emission is exclusively observed from the localized states.

C. Charge Separation and Energy Storage:

An alternate channel for the relaxation of the excitonic CT state is the self-trapping of the hole at a lattice site well separated from the negative ion. This expectation is based on the fact that valence band holes are known to self-trap in all RGS. Given the fact that the holes in the excitonic state are even heavier than those in the valence band of the pure solid, self-trapping of the hole by coupling to phonons and local lattice deformation is to be expected. The result is a pair of oppositely charged polarons separated by a lattice deformation barrier that cannot be overcome at low temperatures. The most likely structure for the self-trapped hole is that of Rg_3^+.[9] This process is schematically illustrated in fig 7.

This indeed is observed and monitored by phosphorescence and thermoluminescence spectroscopy.[10] UV irradiated X/RGS show a persistent afterglow and thermo-luminescence. The afterglow has been followed over ten decades in time (see fig 8). Its decay is temperature independent and hyperbolic in time. This is the expected behavior for tunneling recombination between ion-STH pairs with a uniform distribution of separations.

Thermoluminescence in these solids has been induced as long as 35 hrs after the initial irradiation. The emission spectra in the three modes of radiation, fluorescence, afterglow (phosphorescence) and thermoluminescence are identical: all assigned to the radiative relaxation of the exciplex $Xe_2^+X^-$. It is then clear that the optical energy is stored in these solids via charge separation and that thermoluminescence corresponds to thermally activated detrapping of the self-trapped hole. Thermoluminescence curves, intensity versus temperature plots, have been obtained from Cl, Br and I doped xenon (see fig 9). In all cases a main peak at 48 K can be seen which can be assigned to the intrinsic hole trap. Kinetic analysis of these curves yields 800 ± 200 cm^{-1} as the depth of the STH. Finally, comparison of fluorescence and thermoluminescence intensities indicate that charge densities of ~10^{17} cm^{-3} are stored routinely in these systems. The storage density limits are not yet known.

The main ingredients that lead to energy storage in these solids are: the coexistence of both delocalized and localized CT states, the unstable nature of delocalized states, and large lattice deformation barriers associated with self-trapped states. A general prescription that leads to these conditions is: a dielectric solid of large band-gap, doped with an impurity of large electron affinity (to create localized in-gap electrons), a valence band broad enough to create ion-hole pairs at large separation, yet narrow enough such that the lattice relaxation energy for self-trapping of the hole is larger than the excitonic band and hence localization by the creation of a pair of oppositely charged polarons is efficient.

References:

1. R. Alimi, R.B. Gerber and V.A. Apkarian, "Dynamics of Molecular Reactions in Solids: Photodissociation of HI in Crystalline Xenon", J. Chem. Phys., in press, 1988.
2. F. Okada, W. Lawrence and V.A. Apkarian, manuscript in preparation.
3. M.E. Fajardo and V.A. Apkarian, J. Chem. Phys., 85, 5660 (1986).
4. M.E. Fajardo and V.A. Apkarian, "Charge Transfer Photodynamics in Halogen Doped Xenon Matrices II: Photoinduced Harpooning and the Delocalized Charge Transfer States of Solid Xenon Halides (F,Cl,Br,I)", submitted for publication, J. Chem. Phys.
5. M.E. Fajardo, R. Withnall, J. Feld, F. Okada, W. Lawrence, L. Wiedeman and V.A. Apkarian, scheduled to appear in: Laser Chemistry, vol. 8 (July, 1988).
6. L. Wiedeman, M.E. Fajardo, and V.A. Apkarian, J. Phys. Chem., 92, 342 (1988).
7. I. Last and T.F. George, J. Chem. Phys., 87, 1183 (1987).
8. I. Last, T.F. George, M.E. Fajardo, and V.A. Apkarian, J. Chem. Phys., 87, 5917 (1987).
9. M. Umehara, Phys. Rev. B, 33, 4237 (1986), 33, 4245 (1986).
10. M.E. Fajardo and V.A. Apkarian, "Energy Storage and Thermoluminescence in Halogen Doped Solid Xenon III: Photodynamics of Charge Separation, Self-Trapping, and Ion-Hole Recombination",submitted for publication, J. Chem. Phys.

Figure Captions:

Fig. 1. Emission spectrum of Cl_2 isolated in solid Kr. The excitation is to the repulsive $^1\Pi$, $^3\Pi$, molecular potentials. The observed progression is due to the recombinant $A' \rightarrow X$ emission.

Fig. 2. Emission spectra of the triatomic xenon halides in solid xenon.

Fig. 3. Emission spectrum of $Kr_2^+Cl^-$ in solid Kr. In the inset the growth of the emission with irradiation time is shown. Excitation at 225 nm.

Fig. 4. Schematic representation of the excitonic charge transfer states of Cl doped solid xenon. In the molecular limit, an electron transfer from xenon to Cl corresponds to the creation of Cl^-Xe^+. Linear combination of the p-holes on xenon atoms, summed over nearest neighbors yeilds a positive charge delocalized over the cage surrounding the negatively charged halogen. If fully delocalized, the hole would orbit the negative ion producing a Rydberg series of states. However, holes are heavy and more appropriately described as polaronic functions, centered on xenon atoms yet with a large spatial extent.

Fig. 5. Charge transfer excitation spectra of X/Xe and their simulations by the reflection approximation. The spectra are for I (a,b), B(c,d) and Cl (e,f) doped solid xenon. In each pair of spectra, the lower trace is recorded at 12 K while the upper at 50 K.

Fig. 6. Excitation spectrum of XeF/Xe. The top trace is experimental. The stick spectrum is obtained by numerical evaluation of Franck-Condon factors for XeF ($B \leftarrow X$) and ($D \leftarrow X$) transitions. The envelop fit is obtained by reflection of the ground state diatomic wavefunction from the repulsive wall of the upper state. All parameters are taken from the known gas phase potentials.

Fig. 7. Schematic representation of self-trapping of the hole and charge separation. An ion-hole pair separated by several lattice sites is created by the optical excitation. The hole may self-trap as Xe_3^+ and lose all mobility. The trapped polaron may recombine with the negative ion by trapping, tunneling or thermally activated detrapping.

Fig. 8. Radiation subsequent to photo-induced charge transfer in Cl/Xe. The phosphorescence and afterglow are hyperbolic.

Fig. 9. Thermoluminescence curves, intensity versus temperature, for solid xenon doped with halogen atoms. In all cases a well defined peak at 48 K is observed and assigned to the detrapping of the hole. First order kinetic analysis of the curves yields frequency factors and activation energies for detrapping.

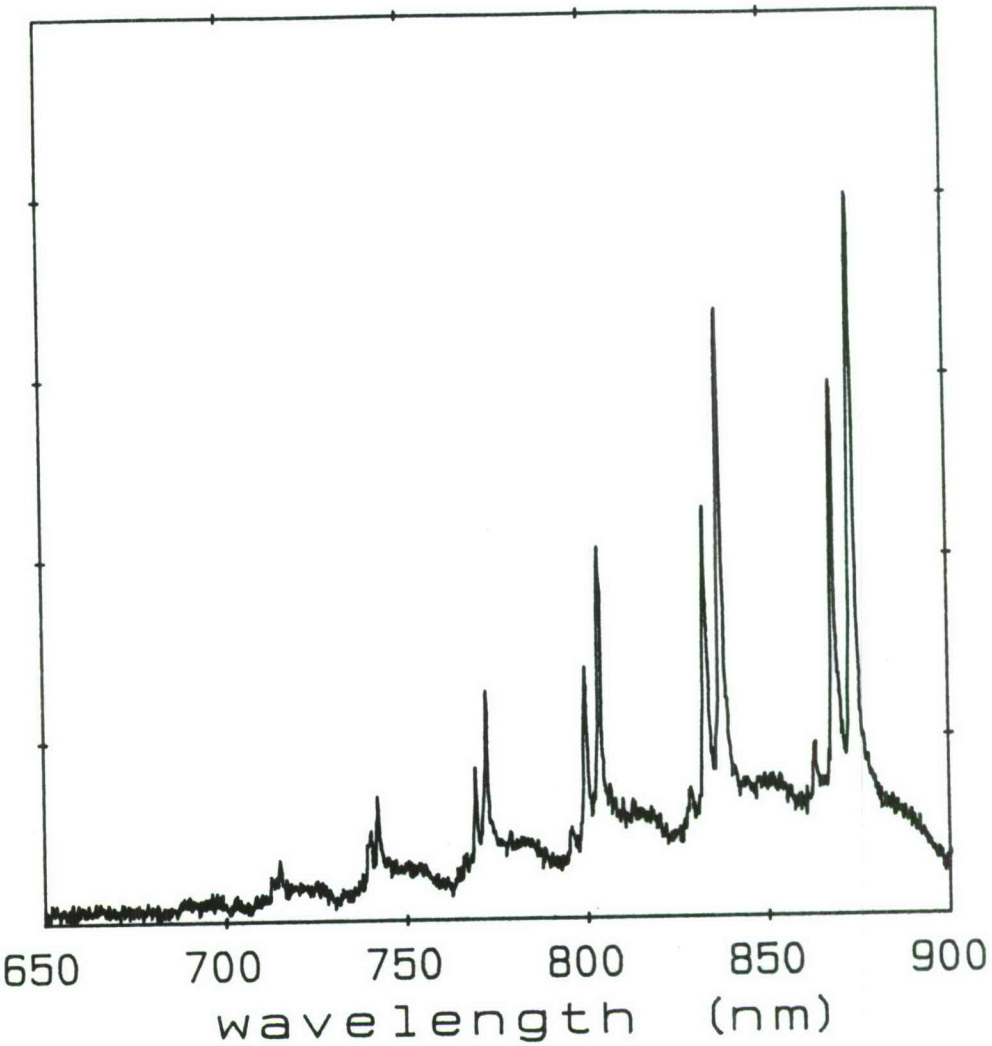
650
700
750
800
850
900
wavelength (nm)

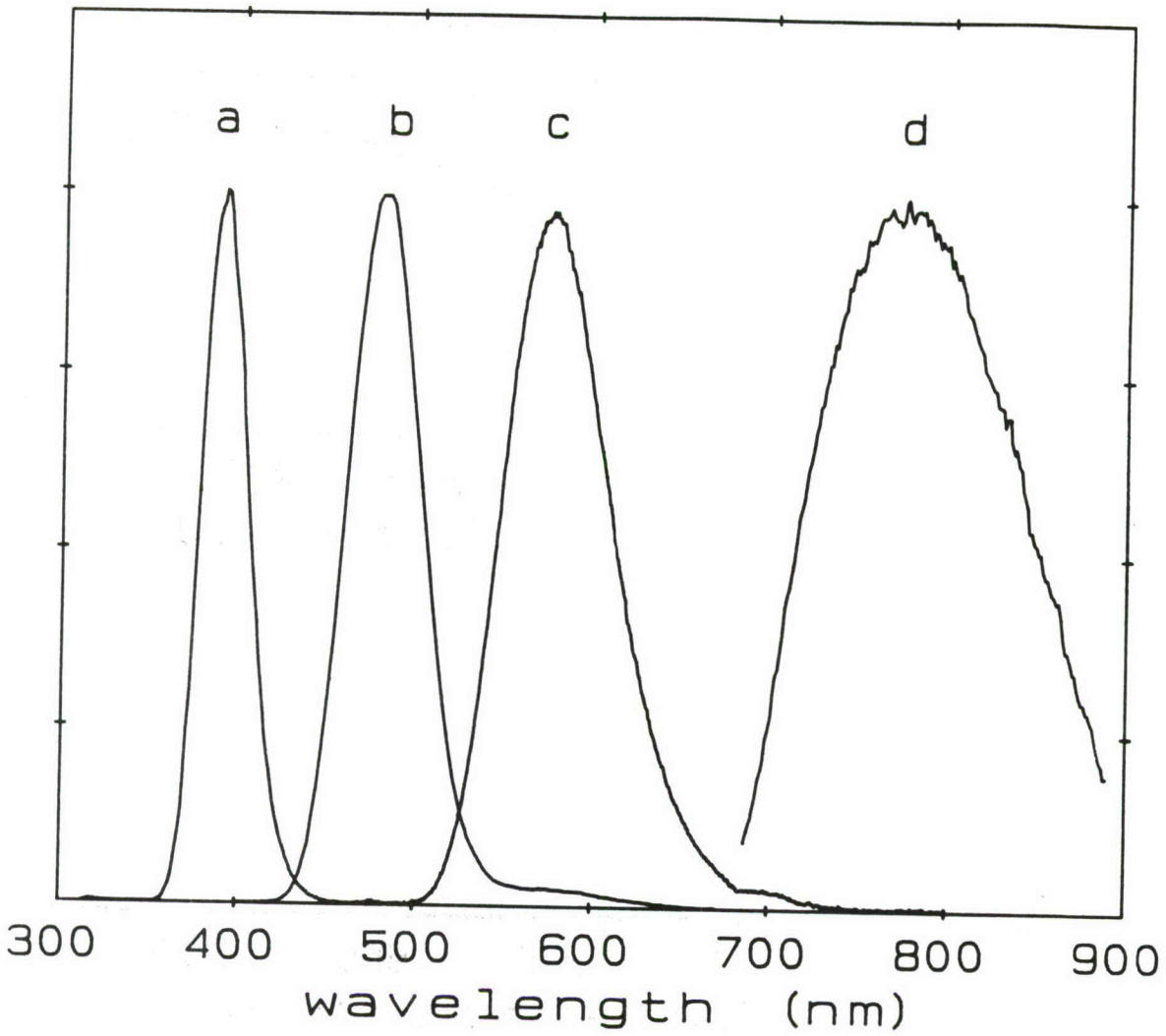
a
b
c
d
300
400
500
600
700
800
900
wavelength (nm)

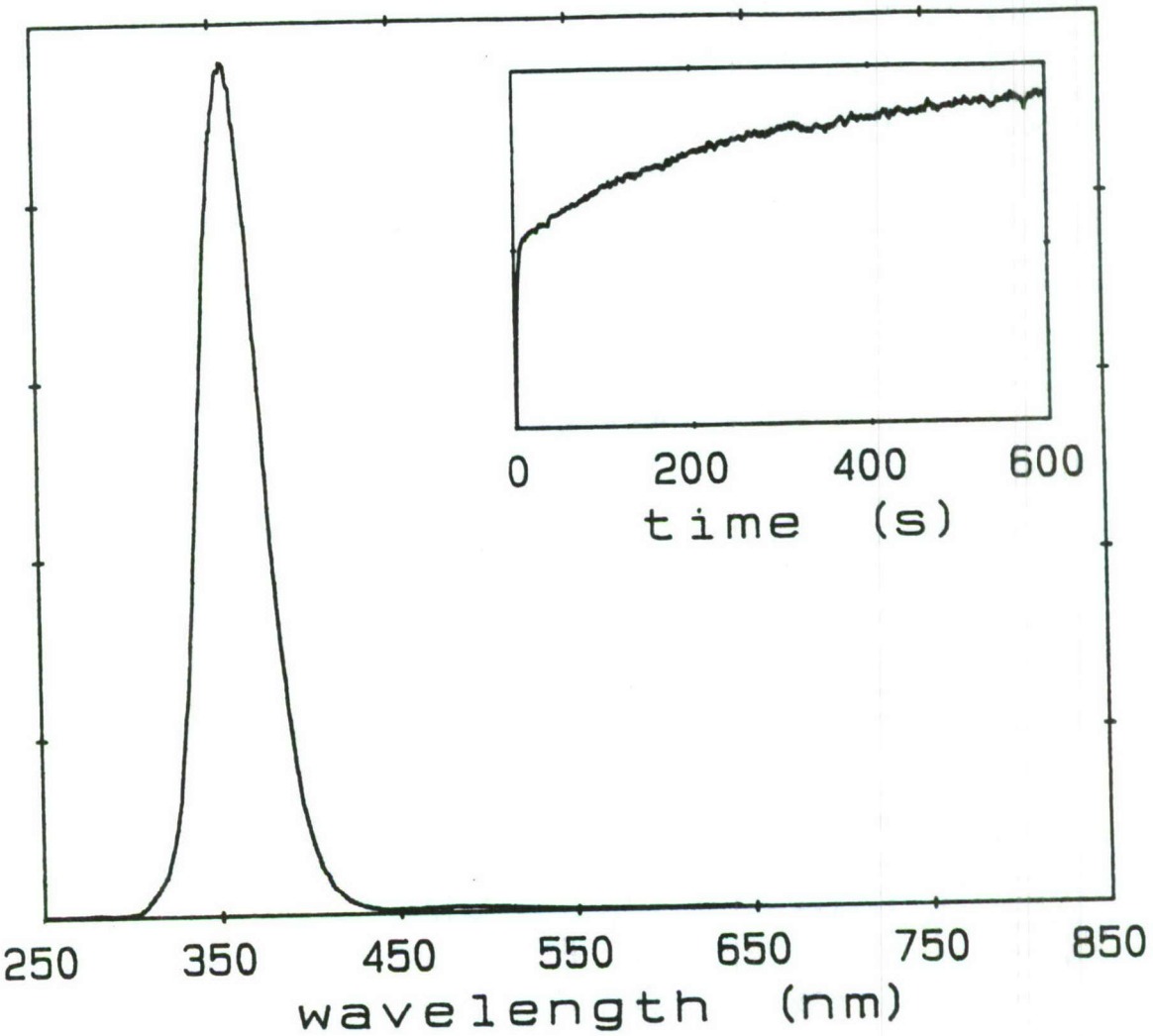
0
200
400
600
time (s)
250
350
450
550
650
750
850
wavelength (nm)

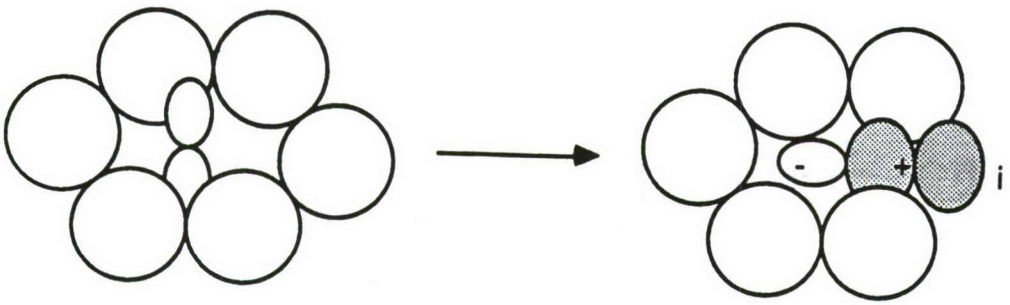

Cl/Xe

$Xe^{+}\,\bar{C}l/Xe$

$$\Phi = \sum_{i}\sum_{m} c_{im}\Psi_{im}$$

DIS

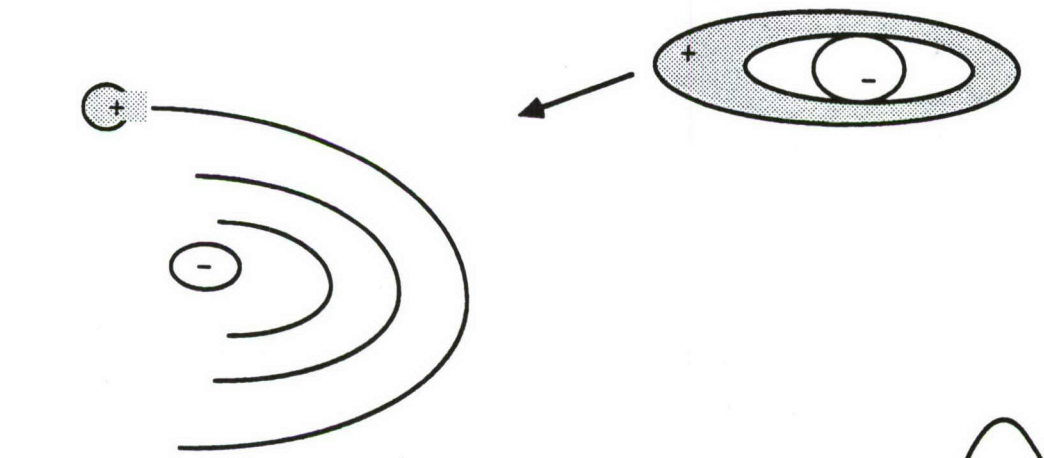

Wannier Exciton

$$\Phi = \int_{k_I}^{k_0} e^{-ik\cdot r}\,\Psi_{Bloch}$$

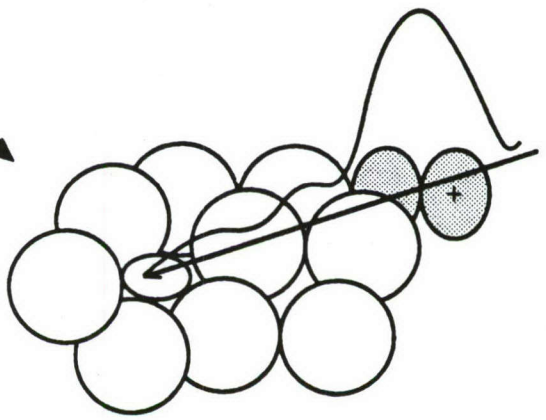

"heavy" ion-hole pair

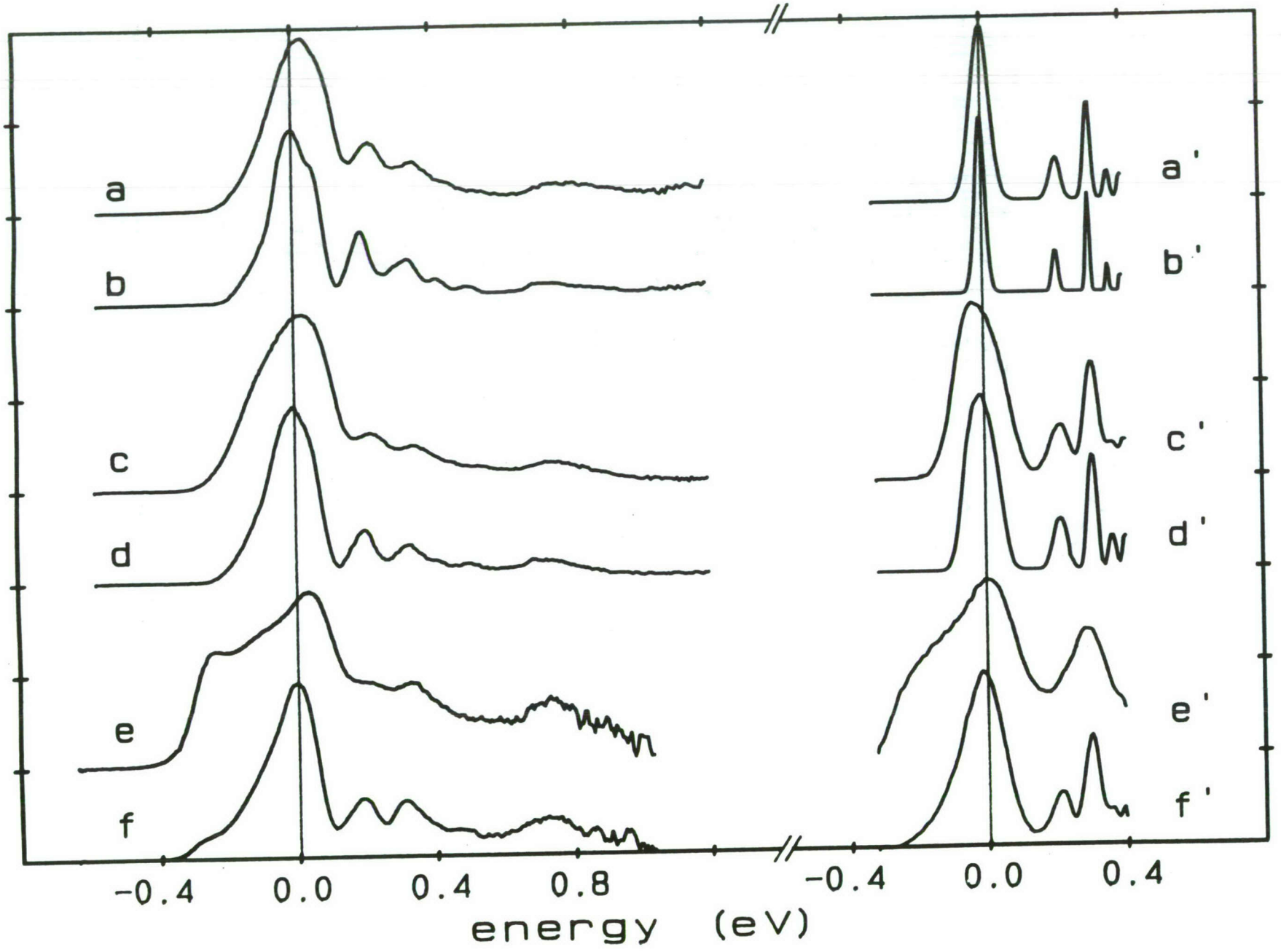
a
b
c
d
e
f
a'
b'
c'
d'
e'
f'
-0.4
0.0
0.4
0.8
-0.4
0.0
0.4
energy (eV)

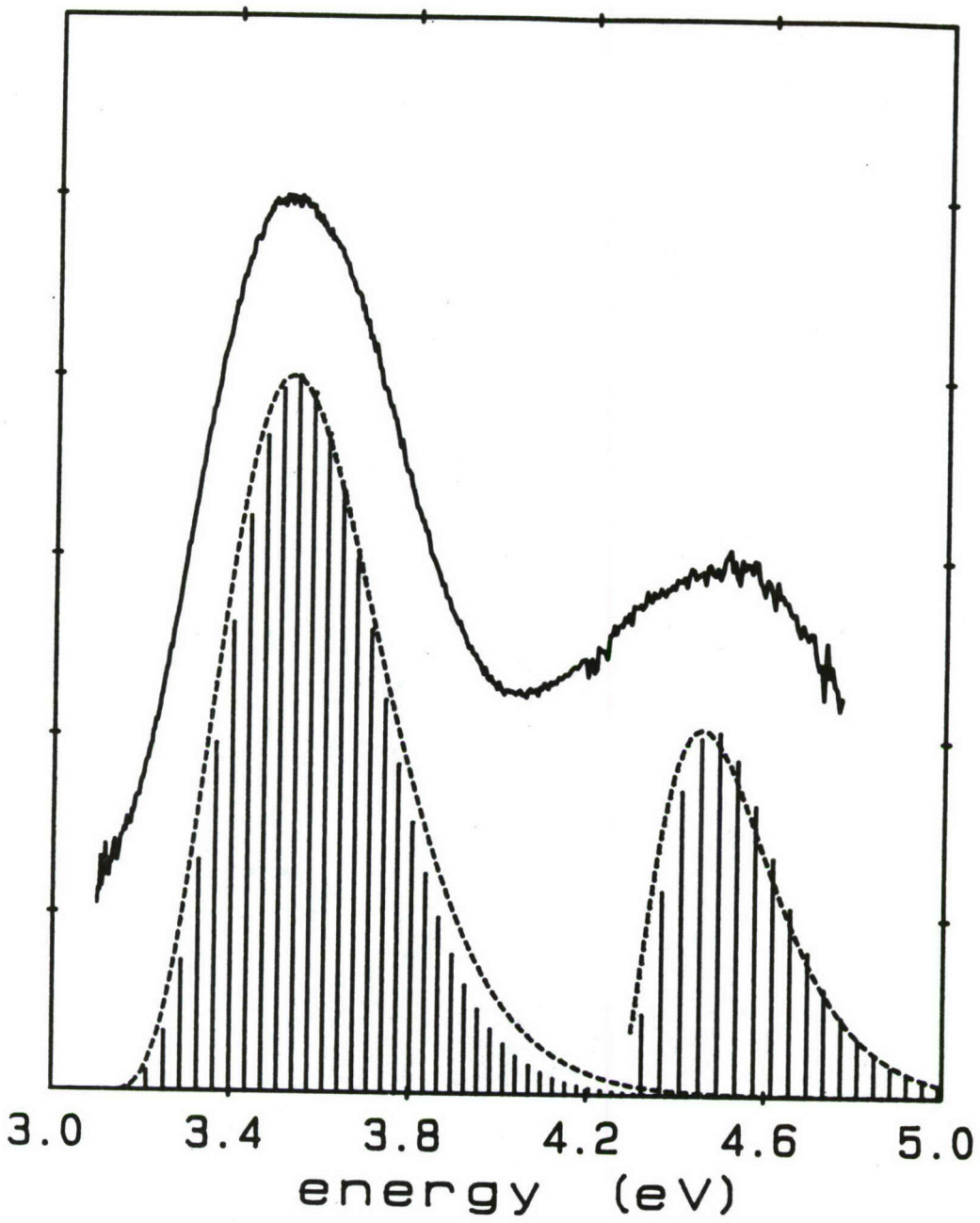
3.0
3.4
3.8
4.2
4.6
5.0
energy (eV)

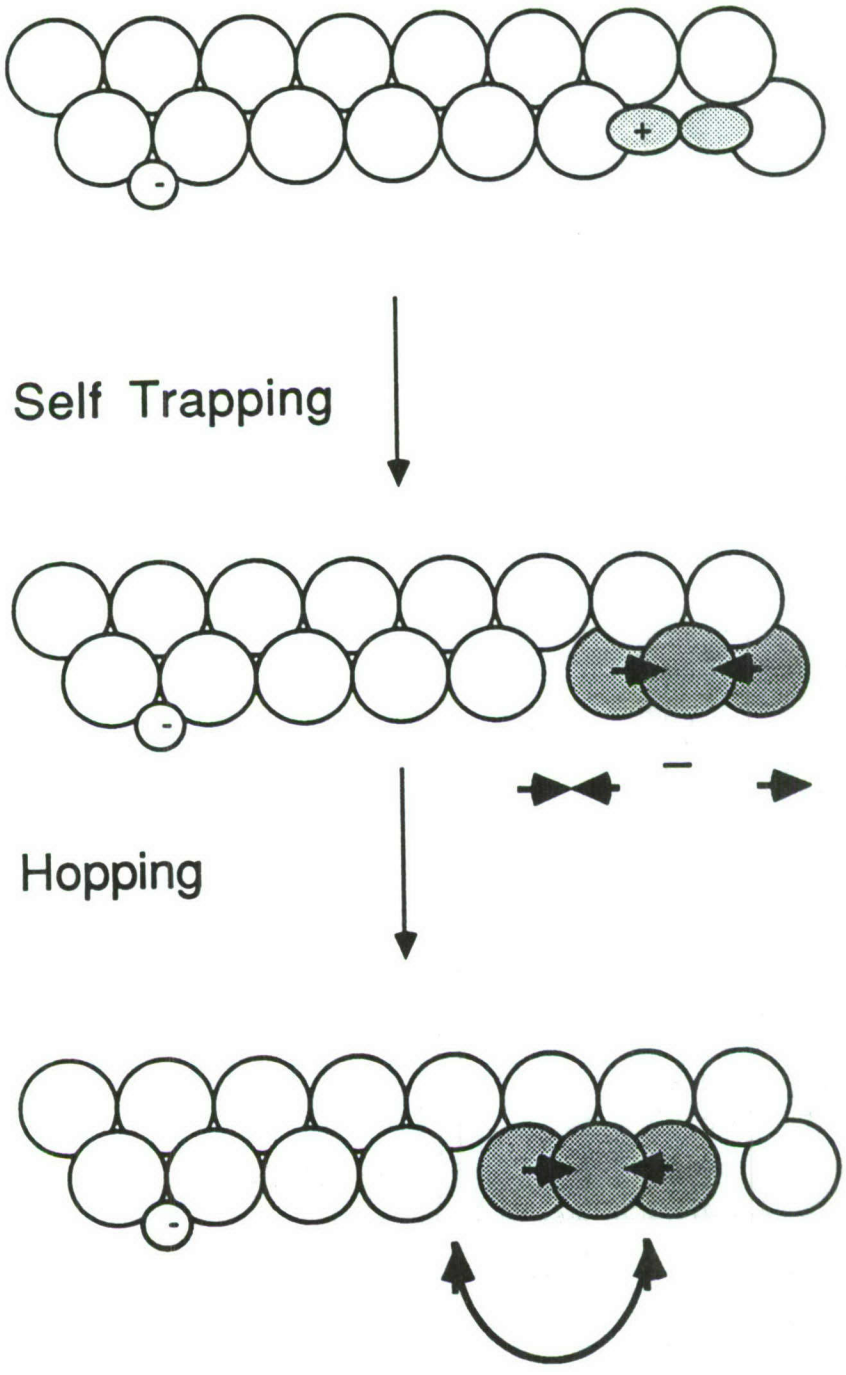
+
-
Self Trapping
-
Hopping
-

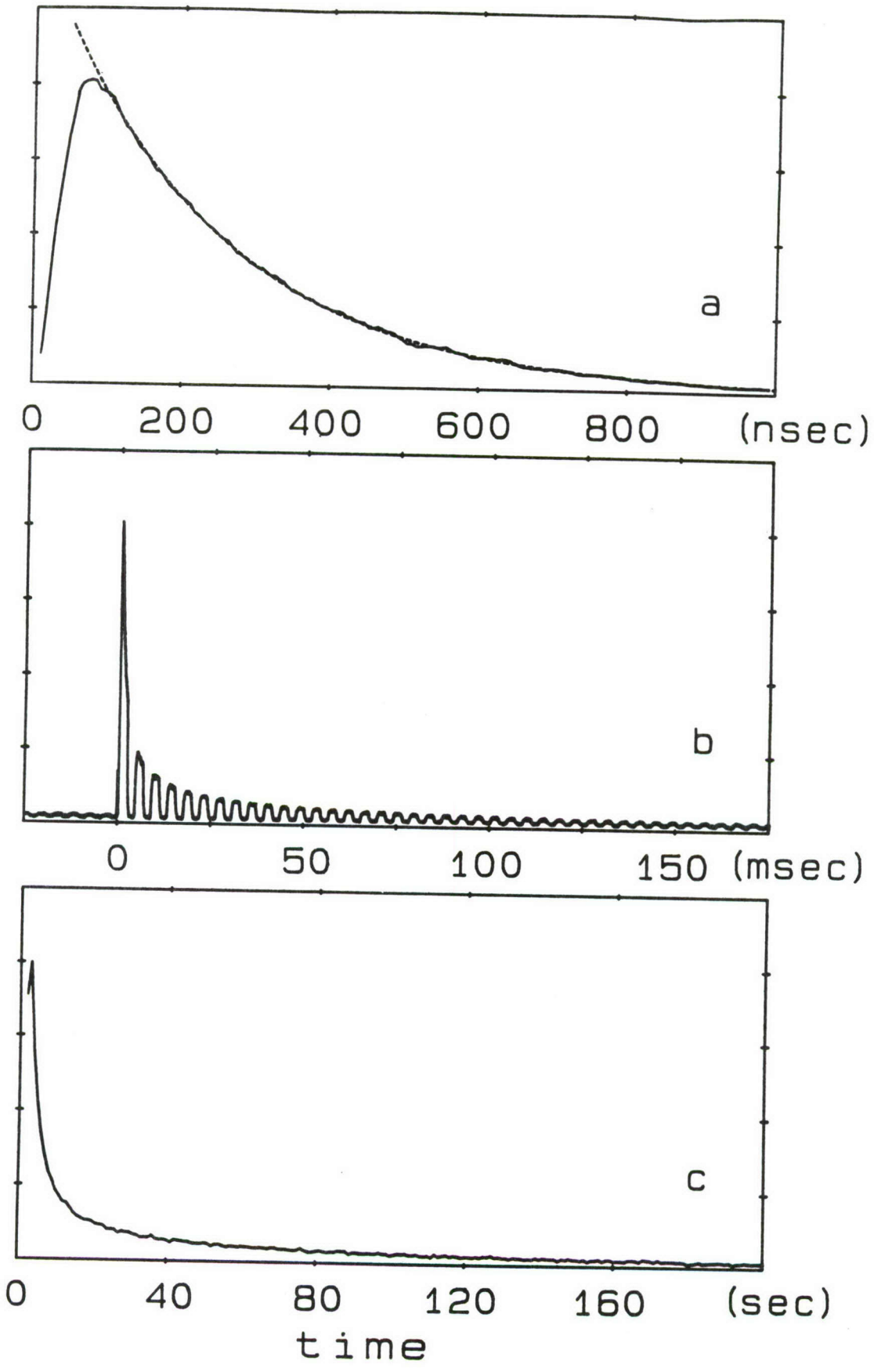
a
0
200
400
600
800
(nsec)
b
0
50
100
150 (msec)
c
0
40
80
120
160
(sec)
time

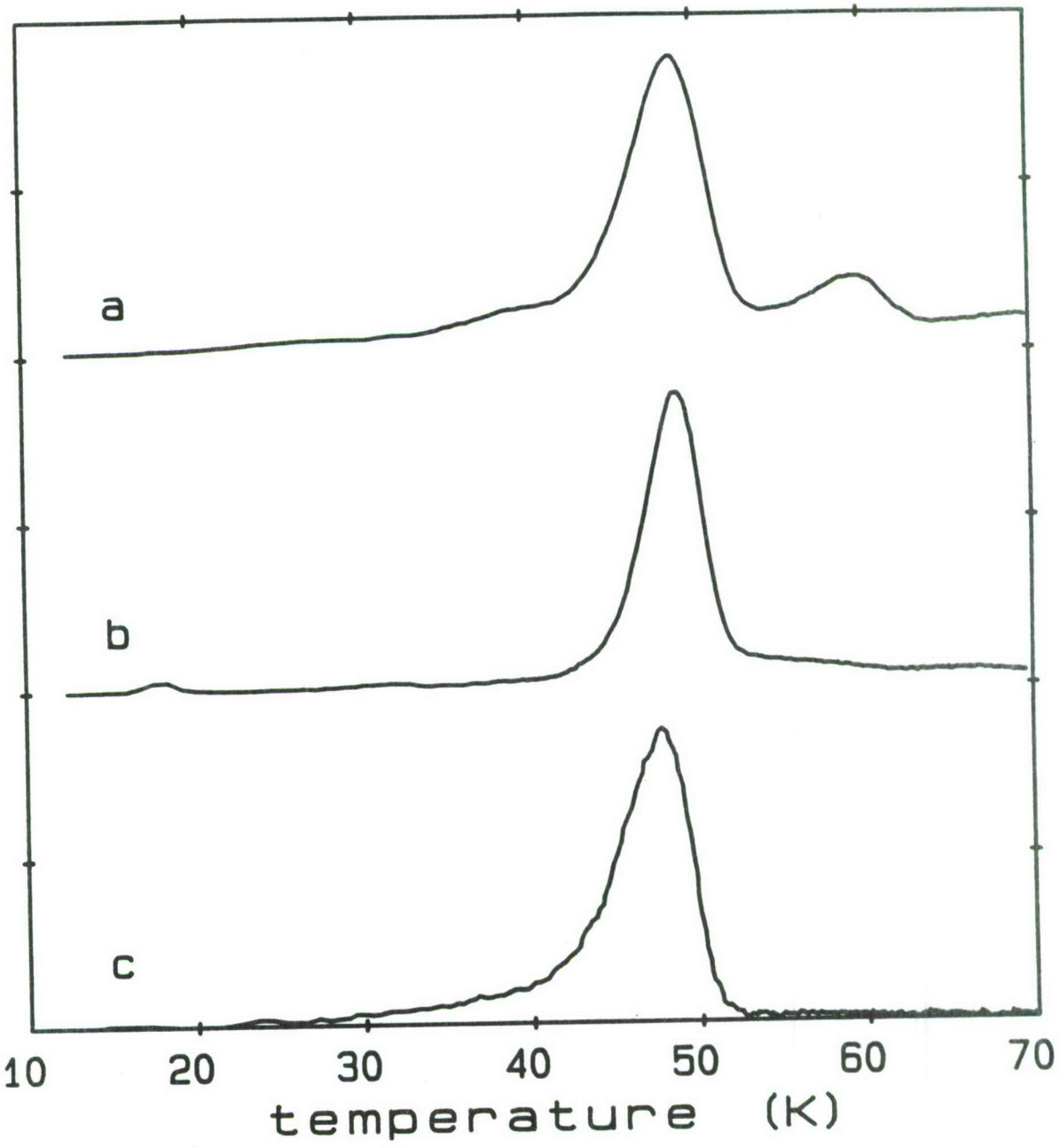
a
b
c
10
20
30
40
50
60
70
temperature (K)

ENERGY TRANSFER PROCESSES IN RARE GAS SOLIDS[*]

H. HELVAJIAN, J. B. KOFFEND, AND L. WIEDEMAN
AEROSPACE CORPORATION
LASER KINETICS & SPECTROSCOPY DEPARTMENT
LOS ANGELES, CA. 90009

ABSTRACT

We are preparing an experiment which will measure product energy disposal following pulsed electron charge neutralization within a rare gas solid (RGS).

Our experiment is designed to trap protons (H^+) in a RGS via formation of stable Ar_nH^+ species. The trapped rare gas hydride ions have the potential for releasing large energies (>8 eV/molecule) following charge neutralization. In our experiment the molecular ions will be trapped either by co-condensing a mass selected ion beam with the matrix host (Ar), or prepared in situ by VUV photolysis of a suitable precursor. The "charged" RGS is neutralized by a laser initiated pulsed electron gun (20 nsec). For monitoring product state distributions, our diagnostics include both emission and LIF spectroscopy, and resonant MPI time-of-flight (TOF) mass spectroscopy.

We have designed and built an experimental chamber which incorporates an ion source with mass selector, a multichannel quadrupole mass detector, a rotatable cryogenic surface (10K), pulsed electron gun, and various optical ports and extensions for monitoring deposited impurity levels (FTIR), thickness (HeNe interferometry), and means for laser VUV generation.

[*] Project Funded by AFAL (Project Order # AFAL 70018)

INTRODUCTION

There is a need to make advanced propellants for rocket propulsion. The new propellants must achieve a specific impulse (I_{sp}) which is greater than that provided by current fuel-oxidizer combinations. To achieve the necessary increase in I_{sp}, research in new propulsion concepts must be done. In the interim, the use additives with existing propellants may increase the I_{sp} above what is available today. In this framework, our proposal considers the concept where the stored "fuel" or additive is pre-energized prior to lift-off. A number of chemical reactions, ion/molecule, Rydberg atom/molecule, and high energy metastable/molecule which when conducted in a laboratory produce very large I_{sp} species. However means for storing large densities of energized reactants is currently limited.

In the past half century, there have been significant advances in understanding rare gas solids (RGS)[1]. A neon RGS can be grown to macroscopic size and will exist at the cryogenic temperatures found in the liquid O_2/H_2 propellant tanks. Experiments have shown that RGS can trap and store both cations/anions, and radicals. Furthermore, these condensed rare gases will self trap localized excitation (excitons; 99% of excitation to form diatomic excimers). Excitons can have excitation energies in excess of 10 eV, and depending on the exciton, binding energies of 1 eV or more. They also have been prepared with molar concentration fractions in excess of 0.1 (10^{21} energized species/cm^3). In the case of cation/anion trapping, experiments show that charge separation can be maintained as long as the RGS is kept at cryogenic temperatures[2]. Upon "warm-up", charge neutralization can release for a reaction such as $ArH^+ + e^- \rightarrow Ar + H + \Delta E > 10eV$/reaction.

The rare gas hydride ions (XH^+, where X = He, Ne, Ar, Kr, and Xe) offer some of the features necessary for building an "energized" RGS. The neutral diatomic species are bound only by van der Walls forces (30 - 60 meV), while the ions in the ground state are strongly bound (2 - 4 eV)[3-5]. Earlier studies with electron impact ionization observed the following reactions.

$$H_2^+ + He \rightarrow HeH^+ + H \qquad (1)$$

$$H_2^+ + Ne \text{ ---> } NeH^+ + H \qquad (2)$$

$$H_2^+ + Ar \text{ ---> } ArH^+ + H \qquad (3)$$

$$Ar^+ + H_2 \text{ ---> } ArH^+ + H \qquad (4)$$

Reactions (1) and (2) are exothermic if there is vibrational excitation in H_2^+ (v= 2 or 3). However reactions (3) and (4) are exothermic and do not have an energy barrier. The rate constant for reaction (3)+(4) has been measured and is 1.6 x 10^{-9} cm^3 $molecule^{-1}$ sec^{-1} (k(3)/k(4) = 0.2) [5,6]. This rate is greater than the gas kinetic rate and reflects the very large cross sections which are typically observed in ion/molecule reactions. We will use either reaction (3) or (4) to prepare rare gas hydride ions. The prepared ions will be mass selected and co-deposited with Ar on a substrate held at 10 K. The Coulombic repulsion will limit the density of positive ions deposited, unless co-deposited are negatively charged ions. If the ions can be trapped in the rare gas matrix, then 13.6 eV minus the proton binding energy can be released <u>on demand</u> by charge neutralizing the trapped H^+ proton(Ar_nH^+). Of interest to propulsion is the channel for dissociative energy release in Ar_nH^* converting the energy to relative translational motion.

The results of two earlier experiments provide the foundation necessary to this proposal. First, experiments on the gas phase dissociative charge exchange of HeH^+ have shown that the majority of the dissociated species have 8-9 eV of translational kinetic energy[7], and second, experiments have spectroscopically identified protons trapped in the RGS (Ar_2H^+ at 905 cm^{-1})[8]. Our proposal is to study the "energized RGS" concept as a possible rocket "fuel" additive or source. Our experiment is to measure the energy release to products following prompt "de-energizing" of trapped $(Ar^n)H^+$ species in the RGS.

EXPERIMENTAL

Our experimental chamber schematically shown in Figure 1, is designed whereby both the preparation cycle ("building" the RGS) and the experiment are done in situ and under carefully controlled conditions. The reactive agents are introduced either via laser photochemical process or by an ion source which can deliver to the experiment a mass selected (magnetic sector) ion beam with near uniform energy. The experimental chamber is designed to house two ion sources to allow the future possibility of "sandwiching" in alternate layers species having opposite charges. The chamber also contains a rotatable target which is kept at cryogenic temperatures (10K). Two types of diagnostics are available for monitoring. In the "RGS building" stage, continuous monitoring (FTIR) of the "sample" is done to insure "sample" purity. During the experiment, the energy disposition will be measured simultaneously by emission spectroscopy (electronically excited species), laser spectroscopy (ground state species), quadrupole/ time-of-flight mass spectrometry (ejected mass and velocity distributions). The energy stored in the "pre-energized" RGS will be released either by pulsed laser heating, or in the case of trapped ions, pulsed electron gun neutralization.

The experiment is conducted by first depositing on a 10 K target either the proton precursor species or cocondensing ArH^+ species with the Ar buffer gas. The sample thickness is measured by monitoring the HeNe laser multiple reflection interference fringes generated from the thin RGS. Simultaneously with the deposition phase, an FTIR will be used to monitor both the deposited impurities and the expected 905 cm^{-1}n absorption in Ar_2H^+. Following deposition, the sample is rotated to face the quadrupole mass spectrometer. A laser initiated pulsed electron gun delivers a dose of moderate energy electrons (50 -150 eV) to the surface. Two photomultipliers are used to monitor any emission (visible and VUV) following charge neutralization. A pulsed laser, delayed relative to the electron gun, and tuned to H Lyman-α is used to multiphoton ionize hydrogen atoms ejected from the sample target. The quadrupole detects ions generated by the MPI laser or by turning on its ion source, all other species. By using this technique we can measure the velocity of selected ejected species (laser MPI/quadrupole detection), or its mass composition (quadrupole ionization and detection).

REFERENCES

[1] M. L. Klein, and J. A. Venables, "Rare Gas Solids" Vols 1 & 2, (Academic Press, NY) 1976, 1977.

[2] M. E. Fajardo, and V. A. Apkarian, J. Chem. Phys., **85**, 5660 (1986).

[3] G. Das, A. F. Wagner, and A. C. Wahl, J. Chem. Phys., **68**, 4917 (1978).

[4] W. A. Chupka, M. E. Russell, and K. Refaey, J. Chem. Phys., **48**, 1518 (1968).

[5] W. A. Chupka, and M. E. Russell, J. Chem. Phys., **49**, 5426 (1968).

[6] D. P. Stevenson, and D. O. Schissler, J. Chem. Phys., **29**, 282 (1958).

[7] W. J. van der Zande, W. Koot, and D. P. de Bruijn, Phys. Rev. Lett., **57**, 1219 (1986).

[8] D. E. Milligan, and M. E. Jacox, J. Mol. Spectrosc., **46**, 460 (1973).

RPL Argon Matrix Chamber
Experimental Plane

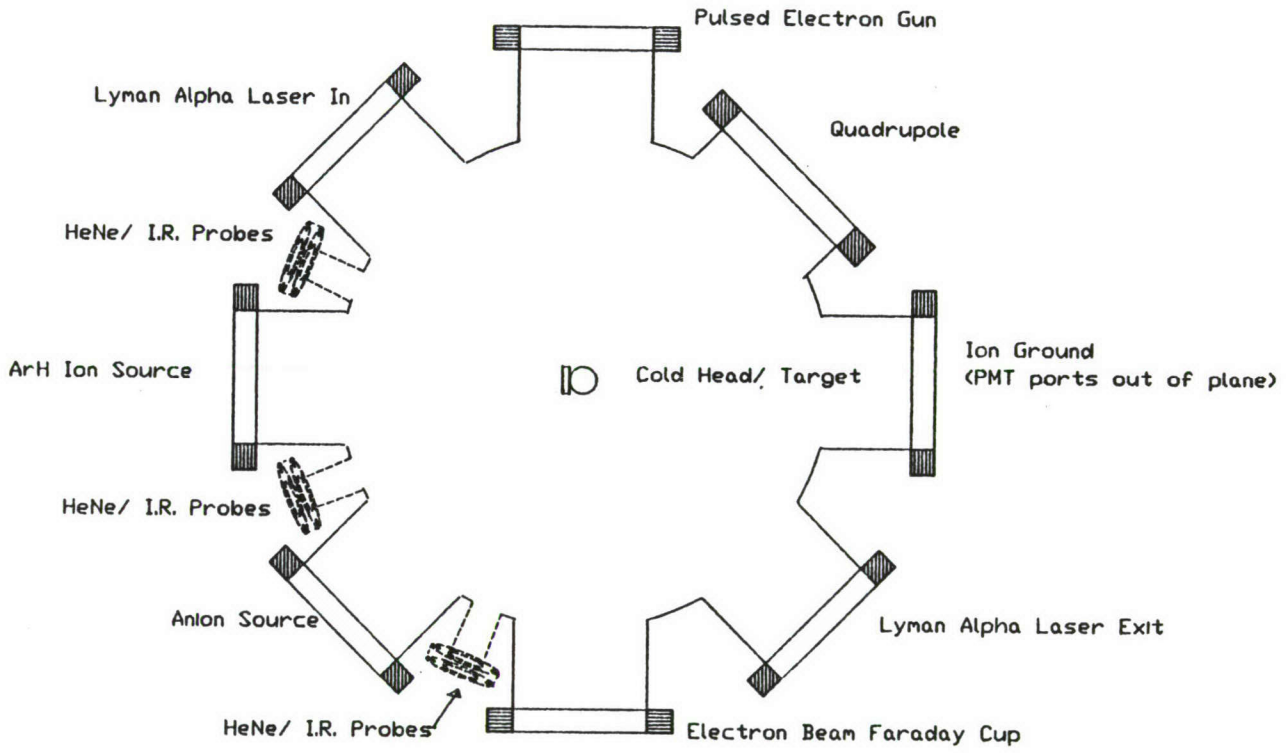

THEORETICAL STUDIES OF PROTONS IN A RARE GAS MATRIX

Marcy E. Rosenkrantz, Air Force Astronautics Laboratory

If protons are to be stored in a rare gas matrix[1], it is necessary to determine mechanisms which could cause ArH^+ to capture an electron prematurely. It is also vitally important to know if protons can indeed be stored in a rare gas matrix for an appreciable amount of time. There has been some discussion in the literature concerning this point [2,3].

Milligan and Jacox[2] (MJ) and Bondybey and Pimentel[3] (BP) have investigated the photolysis of hydrogen and deuterium containing molecules in argon matrices at 14K. Both groups observed absorptions at 905 cm^{-1} for hydrogen containing systems and at 644 cm^{-1}. Milligan and Jacox attribute these absorptions to the presence of Ar_nH^+ and Ar_nD^+ species, with n equal to 2,4,.... Bondybey and Pimentel attribute the peaks to the presence of a neutral H (or D) atom in a octahedral site of argon atoms. The crux of the argument by BP against the absorber being ArH is that this is too unstable. Furthermore, since no counter ions were observed, the absorbing specie cannot be an ion. They conclude that because of the magnitude of the D-H isotope shift the absorber must find itself in an octahedral site. MJ argued that there is a large body of evidence indicating that molecular ions can indeed be trapped in argon matrices. Furthermore, the peaks at 905 cm^{-1} and 644 cm^{-1} are especially prominent in systems with known electron acceptors, and that coulombic stabilization of ion pairs in Ar lattices is appreciable. There is also mass spectrometric evidence, by Chupka and Russell [4] that Ar_2H^+ is stable. More recent work by Jacox[5] on $HCCl_3$ in Ar and Kr substantiates her arguments in favor of the presence of Ar_2H^+

There have been several theoretical investigations of ArH[6-10] and ArH^+ [6,11]. However, to our knowledge, there has been no recent single study of the ground and low-lying excited states of ArH and the ground state of ArH^+. If we are to understand the electron attachment mechanisms and possible dissociative recombination channels of ArH^+ we must be able to investigate all of the states at the same level of approximation. The MESA[12] codes with their ability to do complete active space self consistent field (CASSCF) and multireference determinant configuration interaction calculations (MRDCI) based on the CASSCF wavefunctions are uniquely suited to such a study.

We have performed some preliminary investigations of the ground states of ArH and ArH^+. These calculations have indicated what basis sets for Ar and H are necessary to obtain reasonable results. Our first calculations employed a very large basis for Ar, developed by Stark and Peyerimhoff[13] and a very small basis for H, developed by Huzinaga[14]. Our results, which are included in tables 1 for ArH and 2 for ArH^+ are unsatisfactory for ArH. This is probably due to a very large amount of basis set superposition error since the basis set for hydrogen is so much smaller than that for argon. We also investigated the efficacy of the use of the compact effective core potential and shared exponent basis sets for argon developed by Stevens, Basch, and Krauss[15]. The latter basis sets will have to be augmented with

several polarization functions in order to give us a nearly correct binding energy of ArH.

The key in choosing the best basis set is to have sufficient polarization functions on argon and hydrogen to give the best description of the van der Waals interaction which governs the existence of the long range potential well in ArH. These interactions are a direct result of the induced dipole-induced dipole interactions in argon and hydrogen and higher order dispersion interactions like the induced quadrupole-induced quadrupole, etc.

We have investigated a third basis set which seems to meet our criteria of being small enough to be tractable but large enough to include polarization functions necessary for a correct description of the interactions. That basis set is given in table 3 and employs basis sets by McLean and Chandler,[16] and by Meyer[17].

Our results thus far are quite rudimentary. We have performed first order configuration interaction calculations of ArH and ArH^+ using a wavefunction obtained from a Hartree-Fock single configuration self consistent field calculation. Our results employing the third basis set are in quite good agreement with results from other calculations and from experiment[17]. The earliest calculations[6,7] were performed at a rather high level of approximation with relatively small basis sets. Those results are subject to basis set superposition errors which may offset the opposite effects of the high level of approximations made; thus the rather excellent agreement between those results and experiment. It is however clear from our results that the specie whose absorption was observed in the argon matrix studies is neither ArH nor ArH^+.

REFERENCES

1. Helvajian, H., see previous abstract.

2. Milligan, D.E. and Jacox, M.E., J. Mol. Spect., 46, 460 (1973).

3. Bondybey, V.E. and Pimentel, G.C., J. Chem. Phys., 56, 3832 (1972).

4. Chupka, W.A., and Russell, M.E., J. Chem. Phys., 49, 5426 (1968).

5. Jacox, M.E., Chem. Phys., 12, 51 (1976).

6. Das, G., Wagner, A.F. and Wahl, A.C., J. Chem. Phys., 68, 4917 (1978).

7. Matcha, R.L. and Milleur, M.B., J. Chem. Phys., 69, 3016 (1978).

8. Theodorakopoulos, G. Farantos, S.C., Buenker, R.J., and Peyerimhoff, S.D., J. Phys. B, 17, 1453 (1984).

9. Chambaud, G., Levy, B., and Pernot, P., Chem. Phys.,96, 299 (1985).

10. Van Hemert, M.C., Dohmann, H., and Peyerimhoff, S.D., Chem. Phys.,110, 55 (1986.

11. Pyykko, P. and Laaksonen, L., Chem. Phys. Lett.,141, 535 (1987).

12. MESA, Byron H. Lengsfield, III, U.S. Army Ballistic Research Laboratory, and Paul Saxe, Los Alamos Scientific Laboratory, 1988.

13. Stark, D. and Peyerimhoff, S.D., J. Mol. Struct. (Theochem),150, 203 (1987).

14. Huzinaga, S., J. Chem. Phys.,42, 1293 (1965).

15. Stevens, W.J., Basch, H., and Krauss, M., J. Chem. Phys.,81, 6026 (1984).

16. McLean, A.D., and Chandler, G.S., J. Chem. Phys.,72, 5639 (1980).

17. Meyer, W., Chem. Phys.,17, 27 (1976).

18. Johns, J.W.C., J. Mol. Spectrosc.36, 488 (1970).

19. Stevens, W.J., unpublished results.

20. Simandiras, E.D., Gaw, J.F., and Handy, N.C., Chem. Phys. Lett.,141, 166 (1987).

ACKNOWLEDGMENTS

I wish to thank Dr. Paul Saxe and Dr. Byron H. Lengsfield, III for generously allowing me to use the MESA programs in advance of their general availability, and for their help in getting them to work on the Cray-2 at AFWL.

Table 1. Characteristic constants of ArH.

Source	$R_e(a_o)$	$D_e(cm^{-1})$	$w_e(cm^{-1})$	$w_ex_e(cm^{-1})$
Present[1]	6.94	216.5	107.5	13.3
Present[2]	7.75	4.8	--	--
Present[3]	6.77	67.9	--	--
Das, et al[4]	6.59	38.7	--	--
Welz[5]	6.82	33.1	--	--

1 The basis set of ref. 13 for Ar; H basis the double zeta polarization basis of ref. 14.
2 The basis set of ref. 15 for Ar; H basis the double zeta plus polarization basis of ref. 14.
3 The basis set of ref. 16 for Ar with polarization functions of ref. 20. The H basis is from ref. 17.
4 ref. 6.
5 Welz, W., Ph.D. Dissertation, Max-Planck-Institute fur Stromungsforschung, Gottingen, Federal Republic of Germany, 1976.

Table 2. Characteristic constants of ArH^+.

Source	$R_e(a_o)$	$D_e(cm^{-1})$	$w_e(cm^{-1})$	$w_ex_e(cm^{-1})$
Present[1]	2.44	32 828	2736	57.0
Present[2]	2.51	29 925	2736	62.5
Present[3]	2.44	33 216	2728	56.0
Matcha and Milleur[4]	2.57	21 940	2771	--
Chupka and Russell[5]	2.53	33 635	--	--

1 The basis set of ref. 13 for Ar; H basis the double zeta polarization basis of ref. 14.
2 The basis set of ref. 15 for Ar; H basis the double zeta plus polarization basis of ref. 14.
3 The basis set of ref. 16 for Ar with polarization functions of ref. 20. The H basis is from ref. 17.
4 Ref. 7.
5 Ref. 4.

Table 3. The "best" combination of basis sets for Ar and H we have used thus far. see refs. 17 and 20 for a discussion.

Argon			Hydrogen		
Type	Zeta	Contraction Coefficient	Type	Zeta	Contraction Coefficient
s	118022.4	0.000747	s	68.1600	0.00255
	17683.5	0.005790		10.2465	0.01938
	4027.8	0.029919		2.34648	0.09280
	1145.40	0.119196			
	377.16	0.369096		0.673320	1.00000
	138.160	0.576399			
				0.224660	1.00000
	138.160	0.283926			
	54.989	0.622980		0.082217	1.00000
	23.171	0.283926			
			p	0.70000	1.00000
	7.3779	1.000000			
				0.20000	1.00000
	2.9237	1.000000			
				0.07000	1.00000
	0.6504	1.000000			
			d	0.20000	1.00000
	0.2328	1.000000			
				0.07000	1.00000
	0.08	1.000000			
p	663.06	0.003042			
	157.09	0.023949			
	50.231	0.107088			
	18.635	0.291873			
	7.4465	0.452621			
	3.0957	0.308483			
	1.1065	1.000000			
	0.4156	1.000000			
	0.1454	1.000000			
	0.0500	1.000000			
d	1.000000	1.000000			
	0.3	1.000000			
	0.1	1.000000			

High Energy Density Systems in Cryogenic Media: The Production and Reaction of Atoms and Radicals

Eric Weitz
Department of Chemistry
Northwestern University
Evanston, IL 60208

The major areas of investigation in our AFOSR supported work will center on:

- The effect of low temperature condensed phase media on the rates and pathways of chemical reactions.
- Measurements of diffusion coefficients in low temperature condensed phase media.
- Investigations of the influence of low temperature condensed phase media on dynamical processes including photodissociation and energy transfer.

This report will present results in the latter two areas.

Diffusion

We have devised an experimental procedure to measure diffusion coefficients of species in low temperature condensed phase systems. The procedure involves the photolytic production of the species of interest and the measurement of the diffusion coefficient of the species by monitoring the rate of a diffusion controlled reaction of the species under study. One of the first systems we are exploring is the diffusion of H atoms. This is particularly interesting since H atoms become quantum mechanical particles at low temperatures in rare gas matrices: The de Broglie wavelength becomes larger than the interstitial spacing between the rare gas atoms. As this occurs diffusion would be expected to be dominated by tunneling. Thus a change in the diffusive behavior and the diffusion coefficient of H atoms would be expected as a function of temperature.

We are generating H atoms via photolysis of HI. The reaction we are monitoring involves the reaction of H atoms with O_2 to form HO_2. This reaction is reported to have a negative activation energy[1] and thus would be expected to be diffusion controlled in a low temperature condensed phase system. That HO_2 has been produced via KrF laser irradiation of a matrix of composition $HI:O_2:Kr$ in ratios of 1:2:150 can be seen in figure 1. The bands shown in this figure correlate well with the absorptions assigned by Milligan and Jacox to HO_2[2].

We have been able to monitor the formation of HO_2 with a diode laser tuned to 1386 cm^{-1} but consider the date on the resulting diffusion coefficient too preliminary to report without further study.

Energy Transfer

We have been able to produce vibrationally excited species in condensed media via any of the following three processes. They are:

1) Photodissociation and recombination of a diatomic. This has been applied with success to HCl photolyzed by ArF radiation.[3]

2) Direct excitation of the desired species with a pulsed tunable infrared laser. This has also been applied with success to HCl.[4]

3) Photoelimination of a vibrationally excited species from an appropriate precursor. This has also been successfully applied to HCl[5] and will be the method of choice for the subsequent discussion.

HF^* (vibrationally excited HF) can be produced via ArF photolysis of C_2HF_3. We have measured the vibrational relaxation of HF (v=1) in the gas phase with Kr or Xe collision partners and in liquid Kr and liquid Xe. Comparisons of the gas phase rate and the liquid phase rate, both measured at the same temperature, are made in the context of an isolated binary collision (IBC) model of vibrational relaxation to determine the effect of the liquid rare gas environment of the dynamics of vibrational relaxation. Vibrational relaxation is monitored by following the infrared emission of HF (v=1) with an InSb detector. The HF(v=1) emission is isolated from emission from higher vibrational states using an interference filter which primarily views the R branch of the v=1 → v=0 transition. The signal from the InSb detector is digitized and averaged with a LeCroy digital oscilloscope. The averaged signal is fed to a computer for analysis. Data for the relaxation of HF by Kr at 193 K in both the gas phase and in liquid Kr are shown in figures 2 & 3. Similar data has been taken for HF relaxation by Xe at 204 K in both the gas phase and in liquid Xe.

An expectation for the rate of relaxation of a molecule in the liquid phase can be obtained from an IBC model for relaxation. In the context of this model, it is assumed that vibrational energy relaxation is due to binary interactions which are separated in time (time between encounters that leads to energy transfer >> vibrational period) and the probability of relaxation per encounter (P) is independent of phase and τ is the lifetime of the excited species. Then,

$$\frac{1}{\tau} = \frac{1}{\tau_o} \cdot P \qquad (1)$$

where P can be determined from the gas phase rate constant.

A variety of approaches have been used to calculate $1/\tau_c$. The simplest is the cell model[6] where

$$\frac{1}{\tau_c} = \frac{\bar{v}}{(\rho^{-1/3} - \sigma)} \qquad (2)$$

where $\bar{v}$, ρ and σ have their usual meaning. Current treatments generally employ radial pair distribution functions and derive formulas of the type

$$\frac{1}{\tau_\ell} = \frac{1}{\tau_g} \frac{\rho_\ell}{\rho_g} \frac{g_\ell(R^*)}{g_g(R^*)} \qquad (3)$$

where various methods are used to obtain $g_\ell(R^*)$, the radial distribution function at R^*, the effective distance for vibrational energy transfer. We have used a treatment by Chesnoy.[7] For HF in liquid Xe and liquid Kr this predicts that,

$$\frac{1}{\tau_\ell} \simeq \frac{1}{\tau_g} \frac{\rho_\ell}{\rho_g} \qquad (4)$$

We measure that the ratio for the rate of relaxation of HF in liquid Xe ,scaled for the density of liquid Xe, versus gas phase Xe at 204 K

$$\frac{\tau_g \rho_g}{\tau_g \rho_g} \qquad (5)$$

is 0.1 rather than 1 which would be predicted by equation (4). Similarly, the rate of relation of HF by liquid Kr, scaled for the density of liquid Kr, versus gas phase Kr at 193 K is .15 rather than the predicted 1.0! Thus HF relaxes significantly more slowly in liquid Kr or liquid Xe than expected based on gas phase relaxation probabilities.

Two possible related explanations for this behavior involve: 1) formation of a transient HF-M complex which increases the effective moment of inertia of the HF which would lead to a decrease in the rotational velocity in an HF - rare gas collision and thus a decrease in the probability of vibration-rotation energy transfer; the process by which HF is known to relax in the gas phase or; 2) formation of a transient HF-M complex which may be a multicentered complex where the complexed rare gas atoms shield the HF from impulsive collisions with the remainder of the rare gas atoms thus also decreasing the probability of vibration-rotation energy transfer.

Both the measurement of transport properties in condensed phase and an understanding of the change in the dynamics of energy transfer processes will affect the conceptualization and design of energy storage schemes in condensed phase.

References

1) Rate Constants of Gas Phase Reactions by V.N. Kondratiev , N.B.S. (1972).

2) D.E. Milligan and M. Jacox, J. Chem. Phys. 38, 2627 (1963).

3) J.T. Knudtson and Eric Weitz, Chem. Phys. Letters 104, 71 (1984).

4) Y.P. Vlahoyannis, H. Krueger and E. Weitz, J. Chem. Phys. 86, 3311 (1987).

5) J.T. Knudtson, Y.P. Vlahoyannis, H. Krueger and E. Weitz, J. Chem. Phys. 82, 4381 (1985).

6) W. M. Madigosky and T. A. Litovitz, J. Chem. Phys. 34, 489 (1961).

7) J. Chesnoy, Chem. Phys. 83, 283 (1984).

Figure Captions

Figure 1. FTIR spectrum of HO_2 absorptions in the region around 1387 cm^{-1}. Details regarding matrix composition and method of preparation are in the text.

Figure 2. Plot of the rate of relaxation of HF (v=1) as a function of Kr pressure at 193 K. The slope yields a rate constant for the rate of relaxation of HF (v=1) of 8.8×10^{-17} cc/molec/s.

Figure 3. Plot of the rate of relaxation of HF(v=1) versus C_2HF_3 (parent) pressure in liquid Kr at 193 K. The intercept is the rate of relaxation of HF(v=1) by liquid Kr.

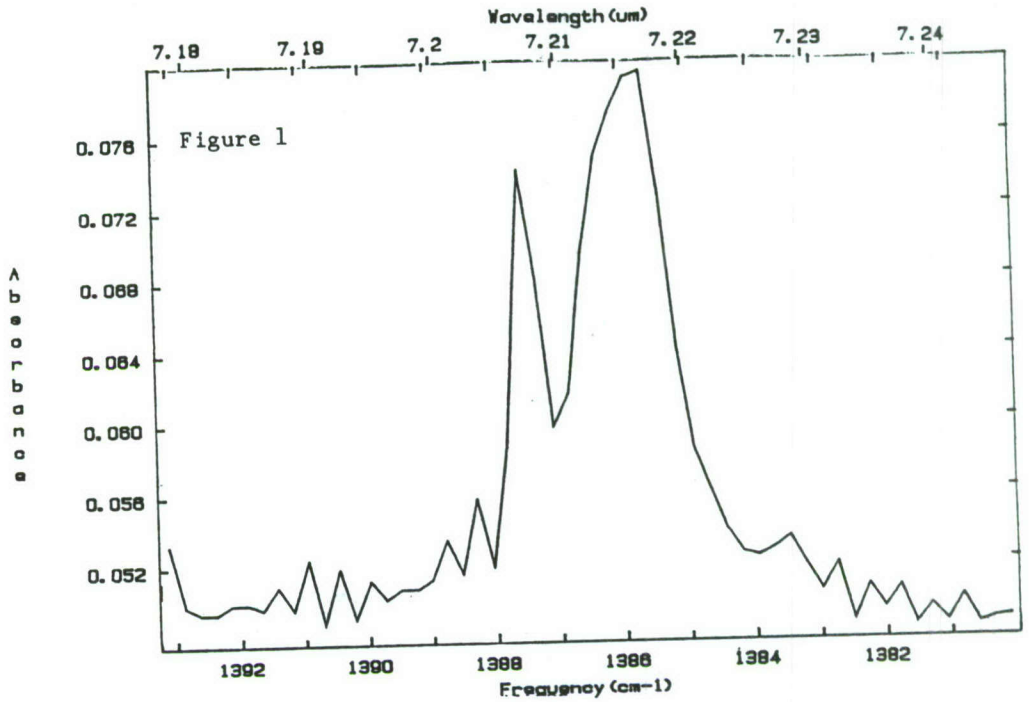
Wavelength (um)
7.18
7.19
7.2
7.21
7.22
7.23
7.24
Figure 1
0.076
0.072
0.068
0.064
0.060
0.056
0.052
Absorbance
1392
1390
1388
1386
1384
1382
Frequency (cm-1)

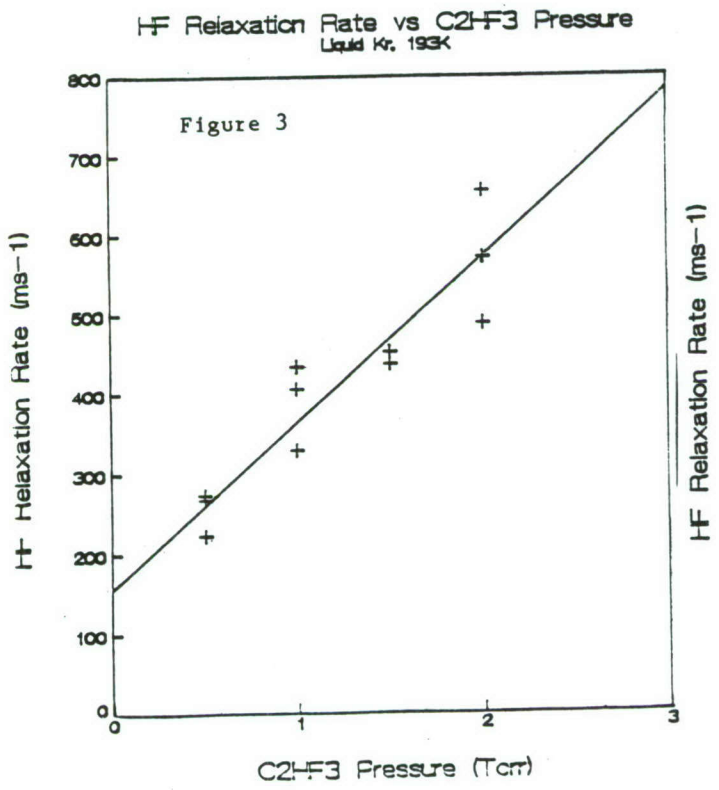
HF Relaxation Rate vs C2HF3 Pressure
Liquid Kr, 193K
Figure 3
HF Relaxation Rate (ms-1)
800
700
600
500
400
300
200
100
0
0
1
2
3
C2HF3 Pressure (Torr)

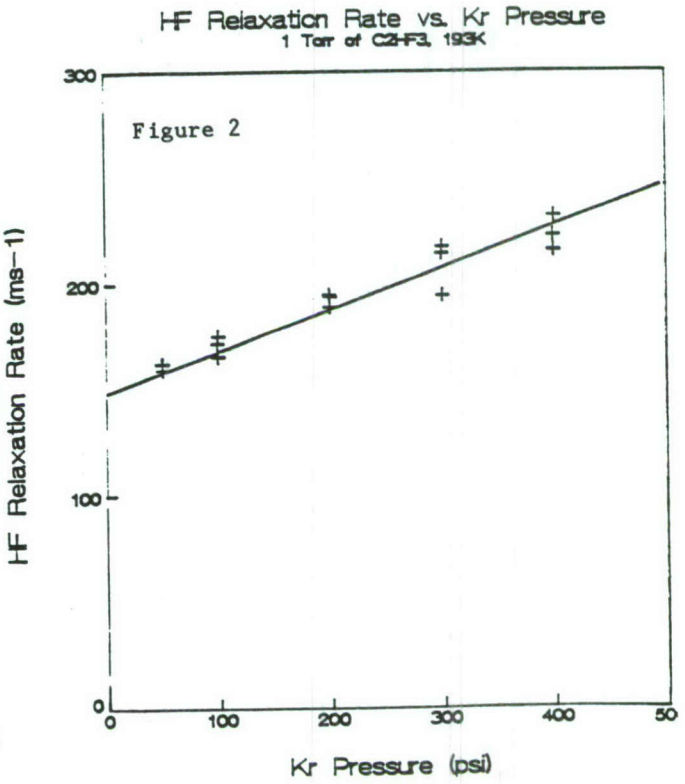
HF Relaxation Rate vs. Kr Pressure
1 Torr of C2HF3, 193K
Figure 2
HF Relaxation Rate (ms-1)
300
200
100
0
0
100
200
300
400
50
Kr Pressure (psi)

2nd Annual HEDM Conference Proceedings
Newport Beach, CA
February 28 - March 2, 1988

PHOTOINITIATED CHAIN REACTIONS IN LOW TEMPERATURE SOLIDS

Charles A. Wight

Department of Chemistry
University of Utah
Salt Lake City, UT 84112

ABSTRACT

A fundamental understanding of free radical chemistry in low temperature solids is desirable from the standpoint of stabilizing and storing high energy density materials. We have been investigating a series of halogen/hydrocarbon free radical chain reactions with chlorine in thin amorphous films as model systems to characterize reaction mechanisms under these conditions. The radicals are generated by UV laser photolysis of the films. Straight chain hydrocarbons studied thus far appear to react via a simple radical recombination mechanism. However, cyclopropane and cyclobutane react by chain mechanisms which generate up to 30 product molecules per UV photon absorbed by the sample.

EXPERIMENTAL DETAILS

The experiments are conducted by depositing a binary mixture of chlorine and a small hydrocarbon onto a CsI optical window at 10-77 K. The window is mounted at the cold tip of a liquid nitrogen dewar vessel or a closed cycle helium refrigerator. Typical sample thickness is 2-10 μm. Reactions within the thin films are initiated by irradiation with a nitrogen laser (337 nm) or excimer laser (308 nm) to dissociate some of the chlorine molecules into Cl atoms. Reaction product quantum yields and branching ratios are determined by obtaining transmission infrared or Raman spectra of the films before and after irradiation.

The quantum yields are determined by a series of measurements. The absorbance of the samples at 308 and 337 nm is measured directly with a Cary 17 spectrometer, and the incident laser fluence is measured with an absorbing disc calorimeter. The integrated intensities of several IR absorption bands are measured before and after irradiation. Separate yields are calculated for disappearance of reactants and appearance of products to check the consistency of the results.

Work sponsored by AFAL Contract # F04611-87-K-0023

RESULTS AND DISCUSSION

Photochlorination of straight chain hydrocarbons occurs via initial H atom abstraction to form HCl and an alkyl radical. In the gas phase and in solution, the alkyl radical may then react with Cl_2 to form the corresponding alkyl chloride, regenerating another Cl atom in the process. This general type of chain propagation mechanism is illustrated by Reactions (1) and (2).

$$Cl\bullet + RH \rightarrow HCl + R\bullet \quad (1)$$
$$R\bullet + Cl_2 \rightarrow RCl + Cl\bullet \quad (2)$$

In our solid state experiments, we observe the formation of HCl and alkyl halides, but the quantum yields for product formation are too low to be attributable to a chain reaction mechanism. The yield in the propane system, for example is 0.12 ± 0.01 for formation of 1-chloropropane and 2-chloropropane from an equimolar mixture of propane and chlorine. Although the participation of chain reaction processes cannot be definitively ruled out, the low quantum yield strongly suggests that radical recombination processes dominate the reaction mechanism. One way to visualize this is depicted in the upper panel of Figure 1.

Proposed reaction mechanism for low product yields: $Cl_2 + C_3H_8$

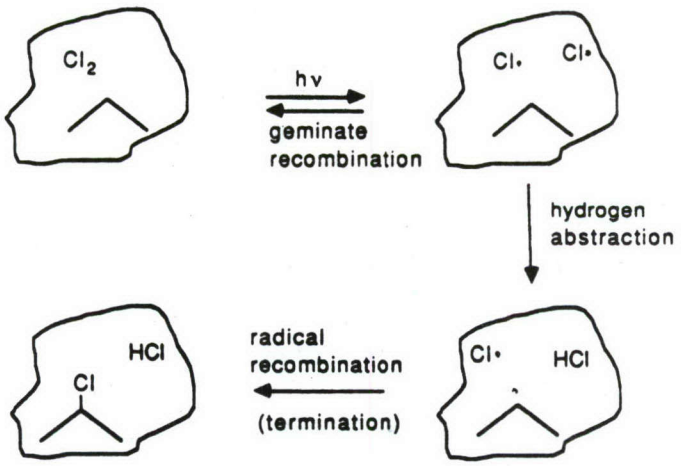

Proposed reaction mechanism for high product yields: Cl_2 + cyclo-C_3H_6

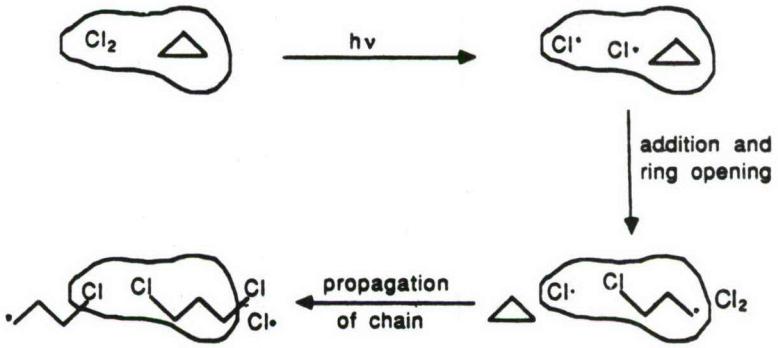

Reaction is initiated by photodissociation of molecular chlorine to two Cl atoms. The solid environment confines the atoms to a local cage which allows them to recombine to molecular chlorine. In a small fraction of these events, one of the Cl atoms may abstract an H atom from a nearby propane molecule forming HCl. The propyl radical generated by this reaction may then recombine with the partner chlorine atom (which was trapped in the same cage) to form 1-chloropropane or 2-chloropropane, depending on whether the initial H atom abstraction occurred at a primary or secondary position on the hydrocarbon. The two chloropropanes and HCl are observed in the infrared spectra of irradiated samples of chlorine and propane and are the only reaction products observed.

An interesting aspect of the propane reaction system involves the selectivity of H atom abstraction by a chlorine atom at secondary vs. primary positions on the hydrocarbon. At 77 K, we observed that the product branching ratio (2-chloropropane:1-chloropropane) is 5.6:1. When corrected for the fact that propane contains only one third as many secondary H atoms as primary, the relative reactivity is 17:1. The selectivity presumably arises from the lower activation energy for abstraction at the secondary site (in turn, reflecting the greater stability of the secondary radical). Interestingly, this ratio of products is exactly that which one would expect at 77 K based on the gas phase Arrhenius parameters determined by Knox and Nelson.[1] The agreement may be fortuitous, but the Cl atoms nevertheless exhibit a remarkable degree of selectivity for attack at the secondary position of propane.

When experiments are conducted at lower temperatures, the selectivity for formation of the lower energy product actually decreases. Below about 50 K, the relative reactivity is approximately 2.5:1. The Arrhenius parameters predict the relative reactivity to be 2.3:1 in the limit of high temperature. We have therefore interpreted this observation in terms of reaction of <u>hyperthermal</u> Cl atoms with propane molecules. The energy of each 308 nm photon exceeds the bond dissociation energy of Cl_2 by about 150 kJ/mole, so each Cl atom is born with a significant amount of excess translational energy. To the extent that this energy can be used to surmount the barrier to H atom abstraction, the selectivity for formation of 2-chloropropane should be diminished. Although the exact reasons for the onset of hot atom reactions below 50-70 K are unclear, we note that propane has a relatively low melting point (85 K). It is possible that thermalization of Cl atoms is more efficient in the slushy environment near the melting point compared to the more rigid solid below 50 K.

Recent experiments conducted with n-butane and isobutane show similar behavior to propane. In each case the quantum yields are less than unity, making the participation of chain reaction steps unlikely. Also, the butane reactions exhibit a marked preference for formation of the lower energy reaction product when the sample is near its melting point. As in the case of propane, reducing the photolysis temperature reduces this selectivity, consistent with the onset of hot Cl atom reactions.

In contrast to straight chain hydrocarbons, photochlorination of cyclopropane occurs by an addition mechanism forming chloropropyl radical, which subsequently reacts with Cl_2 to form 1,3-dichloropropane.

$$Cl\bullet + c\text{-}C_3H_6 \rightarrow ClCH_2CH_2CH_2\bullet \quad (3)$$

$$ClCH_2CH_2CH_2\bullet + Cl_2 \rightarrow ClCH_2CH_2CH_2Cl + Cl\bullet \quad (4)$$

The best evidence that the reaction proceeds via a true chain reaction mechanism is the observation of quantum yields greater than unity. In fact,

the yield for an equimolar mixture of chlorine and cyclopropane is measured to be 30 ± 6 for consumption of cyclopropane and 26 ± 6 for production of 1,3-dichloropropane. Two important observations have been made from these experiments. The first is that although the yields are much greater than 1.0, they are small in comparison with typical chain lengths measured in the gas phase and in solution (10^4-10^7). The second observation is that the largest yields are obtained for samples in which the relative concentrations of the two reagents are equal. Yields drop monotonically to zero as the samples are made progressively richer or leaner in the hydrocarbon component.

For the purposes of comparison, Figure 1 also depicts a proposed mechanism for the chain reaction of chlorine with cyclopropane. In this case, the ring opening step forms a chloropropyl radical in which the unpaired electron is spatially removed from the partner chlorine atom. We believe that the ring opening is therefore crucial to the separation of radical pairs and is largely responsible for the observation of chain reactions in the cyclopropane system. The infrared spectra of the products show conclusively that only the anti-anti conformer of 1,3-dichloropropane is formed in the chain reaction. This provides detailed information about the spatial relationships of the molecules during the course of reaction, as previously discussed.[2] Although the role of radical recombination in the cyclopropane system cannot be ruled out, chain reactions obviously play a major role in the reaction mechanism as this is the only reasonable way in which quantum yields greater than 1.0 can be rationalized.

Termination of the reaction likely occurs by trapping of free radicals in unreactive sites within the solid. In the absence of diffusion, each radical may react only with neighboring molecules. A Cl atom, for instance, may be generated by Reaction (4) in a site where it is completely surrounded by Cl_2 molecules. This would represent a trapped configuration. Similarly, the chloropropyl radical produced by Reaction (3) may be surrounded by hydrocarbon. The trapping probabilities may be easily predicted on the basis of a simple statistical model which is quantitatively consistent with the concentration dependence of the photochemical quantum yield measurements.[2]

Similar experiments involving photochlorination of cyclobutane also offer interesting observations concerning the reaction mechanism in the solid state. This reaction occurs exclusively by an H atom abstraction mechanism depicted by Reactions (1) and (2). The only observed products are cyclobutyl chloride and HCl.

A somewhat curious observation in the cyclobutane system is that the quantum yield for formation of the chlorocyclobutane product is a maximum in samples which are rich in the hydrocarbon component. For chlorine/cyclobutane experiments in which the chlorine mole fraction is 0.08, the probability that any cyclobutyl radical formed in Reaction (8) has a chlorine molecule as one of its six nearest neighbors is only 0.34. The quantum yield predicted using a statistical model of this sort[2] is only 0.52 and should increase with increasing chlorine concentration. The experimentally determined quantum yield is 7.4 ± 0.8 and has the opposite concentration dependence.[3] Even if each radical could interact with 12 of its nearest neighbors (a practical upper limit), the predicted quantum yield is only 1.7.

The high yields and concentration dependence therefore suggest that cyclobutyl radicals are able to migrate over substantial distances in the solid in order to seek out molecular chlorine with which to react. Physical diffusion is out of the question since the temperature of the experiments (77 K) is far below the melting point of cyclobutane (223 K). A more likely

explanation involves symmetric H atom transfer reactions between cyclobutane and cyclobutyl radicals, Reaction (5).

(5)

The idea that the mobility of a radical in solids involves, in some cases, the successive transfer (hopping) of a hydrogen atom was proposed by Dole and co-workers[4] who observed the elimination of vinylidene groups in polyethylene following gamma irradiation. Additional evidence for a hydrogen hopping mechanism has recently been provided by Clough[5] who observed H/D exchange in gamma irradiated tetracosane (h_{50}/d_{50}) crystals. A drawback of the studies involving gamma radiolysis is that details of the initiation process are often not well understood. In our studies, photolysis at low fluence in the near ultraviolet virtually eliminates the possibility of forming ions or other high energy species in the solid which might complicate the analysis.

CONCLUSIONS

Our investigations of free radical chain reactions have provided insight to mechanistic details of chemistry which occurs in amorphous solids. We have noted that in many cases, the classical cage effect results in efficient recombination of radical pairs produced by laser photolysis. However, this is not always the case. For example, ring opening of cyclopropane provides a mechanism for separating radicals. This inhibits recombination and promotes the onset of true free radical reactions in the solid.

Reactions of chlorine with acyclic hydrocarbons provides the opportunity to study the selectivity of H atom abstraction from primary, secondary, and tertiary sites. In all cases studied so far, we have observed that near the melting point of the solid, selectivity of attack can be very high and is generally in agreement with the predictions of gas phase Arrhenius parameters. The clear implication is that under these conditions, Cl atoms are thermalized to the characteristic temperature of the environment on a time scale which is fast compared with reaction. At lower temperatures, this selectivity decreases and the results are consistent with reactions of hot Cl atoms generated by photolysis of Cl_2. There is still much that we do not understand about the dynamics of energy transfer and chemical reactions in amorphous solids, and the field remains ripe for new investigations.

REFERENCES

1. J. H. Knox and R. L Nelson, Trans. Faraday Soc. 55, 937 (1959).
2. A. J. Sedlacek, E. S. Mansueto and C. A. Wight, J. Am. Chem. Soc. 109, 6223 (1987).
3. A. J. Sedlacek and C. A. Wight, J. Chem. Phys. 88, 2847 (1988).
4. M. Dole and C. D. Kneeling, J. Am. Chem. Soc. 75, 6082 (1953).
5. R. Clough, J. Chem. Phys. 87, 1588 (1987).

Photochemistry in Cryogenic Liquids

A. T. Pritt, Jr, N. Presser, R. Blair and R.R. Herm
Infrared Sciences Department
The Aerospace Corporation
El Segundo, CA 92797

Introduction

Chemical reactions in rare gas liquids are very much like those which take place in high pressure gas cells but at much lower temperatures. Collision frequencies in liquids approach those of molecular vibrations, and, therefore, reactant intermediates can be energetically stabilized. These intermediates can represent high energy density materials. Three-body encounters are nearly as prevalent as bimolecular ones, enabling efficient atom and radical recombination. At room temperature small energy barriers are easily crossed, but at low temperatures these barriers can have significant effects. Reactions with small activation barriers become far less probable, and species trapped in shallow energy potential wells have much longer lifetimes. Although many of these features are present in solid rare gas matrices, mobilities of atoms and radicals are significantly constrained. One of the objectives of this experimental program is to exploit the unique features of the rare gas cryogenic liquid environment for the synthesis of new chemical species.

Our AFAL proposal to investigate light mass atom and atom clusters in cryogenic solutions was reported on last year. The AFAL apparatus is nearly completed and experiments are scheduled to begin soon. The work reported here is based on a program sponsored by the Aerospace Corporation. During the past year the apparatus to investigate cryogenic liquids was assembled, and a survey study of several systems with potentially interesting photochemical products was begun. Reported here are our preliminary results on laser UV photolysis of N_2O, diborane , and HNCO, each dissolved in liquid Ar at ~86K.

Experimental Details

The cryogenic cell, FTIR spectrometer, and photolysis source are shown in figure 1. The cell fashioned from a copper cube, coated internally with teflon, and gold-plated externally sits on the cold stem of a cryocooler inside a gold-plated shroud (77K). The entire assembly is inserted into the vacuum chamber. The cell admits an IR beam at right angles to UV photolysis pulses from an excimer laser. Along the UV path all the windows are MgF_2, and along the infrared path the windows on the cell are CsI and those on the vacuum chamber were KCl. A temperature controller regulates the temperature of the cell. An FTIR spectrometer comprised of an IR source, a Michelson interferometer, and a HgCdTe detector is used to obtain infrared absorption spectra of the cryogenic solutions. The overall spectrometer resolution is 2 cm^{-1}.

The gases used in this study were as follows: Ar (Spectra Gas, Inc., 99.9995%); N_2O (Spectra Gas, Inc., 99.998%); and diborane (Scientific Gas Products, 4.97% in Ar). HNCO was prepared from the reaction of steric acid and potassium isocyanate under vacuum conditions. HNCO was isolated via trap-to-trap distillation and purified by freeze-pump-thaw cycles.

The experimental procedure was to dilute the photolysis species (30-500 ppm) in argon, condense the gases into the cryogenic cell, and obtain a reference infrared absorption spectrum. An excimer laser was used to photolyze the liquid mixture, and infrared spectra were again taken.

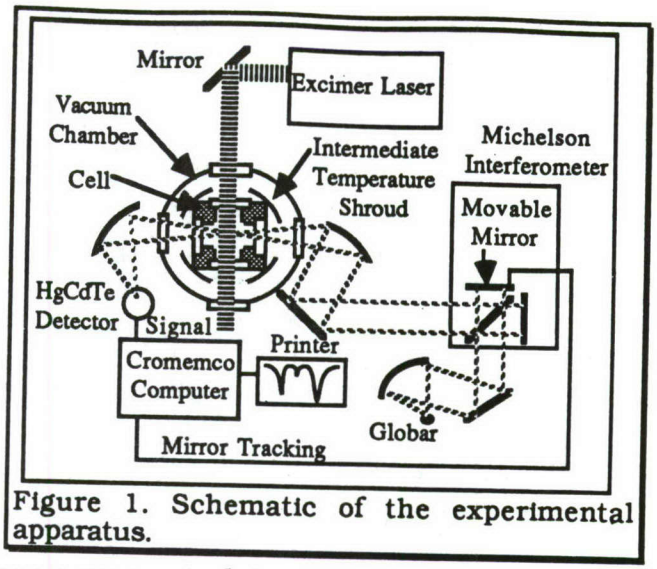

Figure 1. Schematic of the experimental apparatus.

Photolysis of N_2O in Liquid Argon

Room temperature, gas phase, UV photolysis of N_2O is well understood: photofragmentation of N_2O near 200 nm results in the unit yield production of $O^*(^1D_2)$;[1] reaction of O^* with the parent molecule N_2O produces either N_2 and O_2 or two NO molecules at approximately one third gas kinetic rates. The probability of these two reactive routes are equal.[2] *Ab initio* calculations by H. H. Michels and J. A. Montgomery[3] show that along the $O^*(^1D_2)$+ N_2O reaction path leading to the formation of N_2 and O_2, a potential well is positioned near the entrance channel, having depth of ~10 kcal/mole. The configuration of the resulting a-N_2O_2 intermediate is asymmetric, having Cs symmetry similar to isoelectronic FN_3 which is "stable." At low pressure passage across this well on the O^*+N_2O surface is rapid with no stabilization. Stabilization of this reaction intermediate in a cryogenic liquid, however, is possible since the collision frequency is approaching typical vibrational frequencies of 10^{13} s^{-1}.

Samples of N_2O, ranging from 120-1000 ppm, were dissolved in liquid argon. Infrared absorption spectra of these mixtures after photolysis at 193 nm showed the presence of ozone but no characteristic features of a-N_2O_2. Based on the *ab initio* calculations,[3] infrared active vibrational frequencies of a-N_2O_2 should appear at 1206 cm and 2501 cm^{-1}, regions which are free from absorption interferences by N_2O. Any a-N_2O_2 generated may have been photodissociated. A large absorption cross-section of FN_3 at 193 nm has

1 G. Paraskevopoulos and G. G. Cvetanovic, J. Chem. Phys. **50**, 590 (1969).

2 L. Law, D. R. Hastie, B. A. Ridley, and H. I. Schiff, J. Photochem. **15**, 119 (1981).

3 H. H. Michels and J. A. Montgomery, Proceedings from the first High Energy Density Materials Conference and also to appear in J. Chem. Phys. (June 1,1988).

been measured.[4] A mixture of N_2O and O_3 was prepared by photolyzing at 193 nm 500 ppm of N_2O in liquid argon. The mixture was photolyzed again but at 248 nm. At this wavelength N_2O does not absorb, but O_3 strongly absorbs and photofragments to O* and $O_2(a^1\Delta_g)$. The infrared spectrum after photolysis did not show any evidence for a-N_2O_2, but small quantities of NO, $(NO)_2$, NO_2, N_2O_4 and the symmetric form of N_2O_3 were produced. The presence of NO demonstrates that O* lives sufficiently long to react with N_2O. In conclusion, either a-N_2O_2 is not made under these conditions, or any a-N_2O_2 generated is chemically removed or is photolytically removed in a subsequent photolysis pulse. Plans call for modifying the apparatus to monitor transient species in selected IR regions.

Photolysis of Diborane

Diborane (B_2H_6) is the lowest molecular weight, stable boron hydride. Lower order boron hydride species, e.g., B_2H_4 and B_2H_2, have not been observed. Recent calculations show that B_2H_2 is a stable species.[5] Kompa and co-workers[6,7] have shown that the gas phase photolysis of diborane at 193 nm fragments only to borane (BH_3) and at higher fluences inferred that BH_3 is further fragmented to BH_2 + H. In a cryogenic liquid some of the BH_2 species may recombine to form B_2H_4. Furthermore, it is conceivable that continued photolysis will also produce BH, which could recombine to B_2H_2.

In figure 3 the solid line shows the infrared spectrum of the dissolved diborane. The absorption features at 1600 cm^{-1} and at 1800-1900 cm^{-1}, the ν_{17} and ν_{13} bands, respectively, correspond to normal modes involving only boron atoms and bridging hydrogens. The strong absorption features at

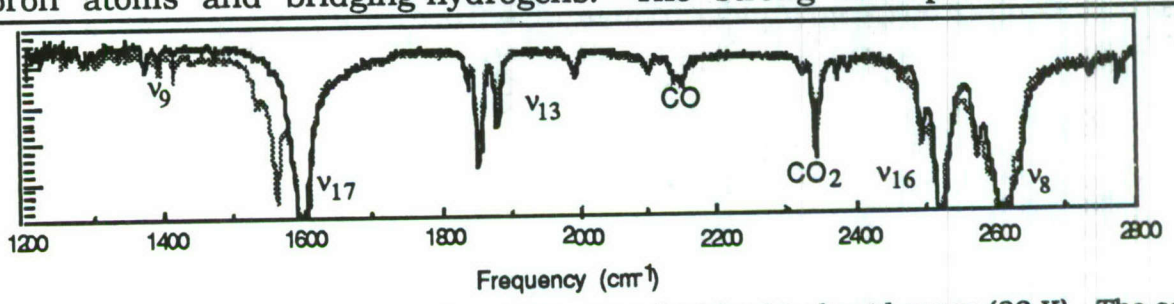

Figure 1. Infrared absorption spectra of diborane dissolved in liquid argon (86 K). The solid curve represents ~100 ppm of diborane in liquid argon and the dashed line shows the absorption spectrum after photolysis at 193 nm. During the photolysis, ~ 24 Joules of radiation was deposited.

2550 cm^{-1} and 2600 cm^{-1}, the ν_{16} and ν_8 bands, involve motions of the end BH_2 groups only and not bridging hydrogens. The dashed line in figure 3 shows the spectrum obtained after depositing ~24 Joules of 193 nm radia-

4 D. Patel, A. T. Pritt, Jr., and D. J. Benard, J. Phys. Chem. **90**, 1931 (1986).
5 C. Jouany, J. C. Barthelat, and J. P. Daudey, Chem. Phys. Letts. **136**, 52 (1987).
6 M. P. Irion and K. L. Kompa, J. Photochem. **32**, 139 (1986).
7 **ibid.**, J. Chem. Phys. **76**, 2338 (1982).

tion into this mixture. The shape of the ν_{16} and ν_8 bands changed, implying that new chemical environments were established for the BH_2 motions. The ν_{13} bands uniformly decreased indicating that diborane was partially removed from the solution. The new strong features to the red of the strongly absorbing ν_{17} band suggest, however, that new chemical species involving bridging hydrogens may have been produced. These features, however, do not correspond to known absorptions for B_4H_{10} or B_5H_9 which are the next higher order boron hydride compounds.

Photolysis of HNCO

Trans-diimide (HNNH) has been unequivocally identified in a matrix by Bondybey and Nibler.[8] The cis form, which is ~6 kcal/mole greater in energy, is less well characterized. Rosengren and Pimentel[9] have reported on the infrared absorption spectrum of cis-diimide, but these results have never been reproduced. Several methods of generating cis-HNNH can be envisioned. Here we have selected to photolyzed HNCO. Gas phase photolysis of HNCO at 193 nm is known to produce predominantly NH(a) and CO(X).[10] Should NH(a) rapidly quench in these cryogenic solutions, the resulting NH(X) could recombine to a statistical distributions of both the cis and trans forms. A ~50 kcal/mole energy barrier between these two forms has been calculated,[11] thus preserving the nascent distributions. In addition, the infrared active vibrational modes of cis and trans forms are on the order of 10-20 cm^{-1} apart,[12] making their identification straight forward in cryogenic liquids.

After condensing 100 ppm HNCO in liquid argon, the characteristic absorptions of HNCO were found at 770, 2280, and 3225 cm^{-1}. Several of the features, however, appeared broad and diffuse, suggesting that HNCO clusters were present. After photolysis at 193 nm, CO absorption was readily evident at 2140 cm^{-1}, but no new absorption features for N-H stretches were observed. Since it is unclear that HNCO was properly dissolved in the solution, experiments are planned to dissolve HNCO in liquid Kr. Liquid Kr has greater solvation powers and the equilibrium vapor pressure of HNCO at 120 K is greater.

---

8 V. E. Bondybey and J. W. Nibler, J. Chem. Phys. **58**, 2125 (1973).

9 K. Rosengren and G. C. Pimentel, J. Chem. Phys. **32**, 133 (1960).

10 T. A. Spiglanin, R. A. Perry, and D. W. Chandler, J. Phys. Chem. **90**, 6184 (1986).

11 J. A. Pople, K. Raghavachari, M. J. Frisch, J. S. Binkley, and P. v. R. Schleyer, J. Am. Chem. Soc.. **105**, 6389 (1983).

12 N. C. Craig and I. W. Levin, J. Chem. Phys. **71**, 400 (1979).

Dynamic Constraints on Stochastic Behavior in the Chemistry of Highly Excited Molecules

Barry K. Carpenter and John R. Wiesenfeld
Department of Chemistry, Baker Laboratory, Cornell University
Ithaca, New York 14853-1301.

AFOSR-87-0165

Earlier evidence for the important role of dynamic effects in the retro-vinylcyclopropane rearrangement of phenyl-substitued bicyclo[2.1.1]hexenes-5-*d* (**1** and **2**) has now been followed by similar evidence for the forward vinylcyclopropane rearrangement of optically active *trans*-2-methyl-1-(*trans*-2-phenylvinyl)cyclopropane (**3**).

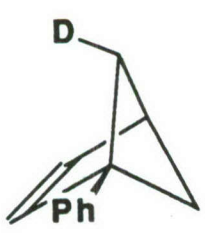

1

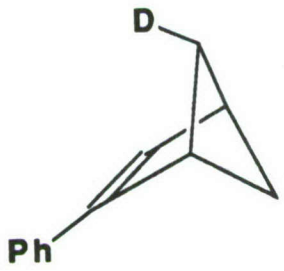

2

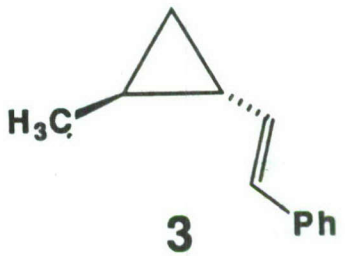

3

This is particularly significant because the vinylcyclopropane rearrangement is one of the most thoroughly studied of unimolecular rearrangements in all of organic chemistry. If dynamic effects can play an important but hitherto unrecognized role for this reaction, then there is the real possibility that such effects are widespread and that many reaction mechanisms will have to be reevaluated.

The data leading to the invocation of dynamic effects for **1** and **2** consisted of the observation of a strong preference for inversion of configuration in their thermal rearrangement, combined with a temperature independent inversion:retention ratio. These two observations cannot be reconciled within the confines of the classical statistical theories (RRKM theory or transition state theory) unless one claims highly implausible coincidences of activation enthalpy for competitive mechanistic pathways.

The new data on **3** reveal that racemization and diene formation occur with activation enthalpies that are identical within experimental error. This is expected since the racemization and *trans* to *cis* isomerization of **3** (the latter being a prerequisite to diene formation) are expected to occur *via* the same pair of biradicals, **4** and **5** (see Figure 1). The more signifcant result is that the two enantiomers of *trans*-4-methyl-3-phenylcyclopentene are also formed with activation enthalpies that are identical within experimental error (see Figure 2). This, too, would be expected if they came from the biradical **5** (biradical **4** cannot be involved in this branch of the reaction because it would yield a cyclopentene with a *trans* double bond). *However, biradical **5** is achiral and yet the enantiomeric products are formed in a 7:1 ratio.* Again, then, there is a fundamental inconsistency between the thermochemistry and stereochemistry, just as was seen for the bicyclo[2.1.1] hexenes. The only rationale that seems plausible is that the biradicals are involved in all branches of this reaction but that their stereochemistry of reaction is dynamically influenced.

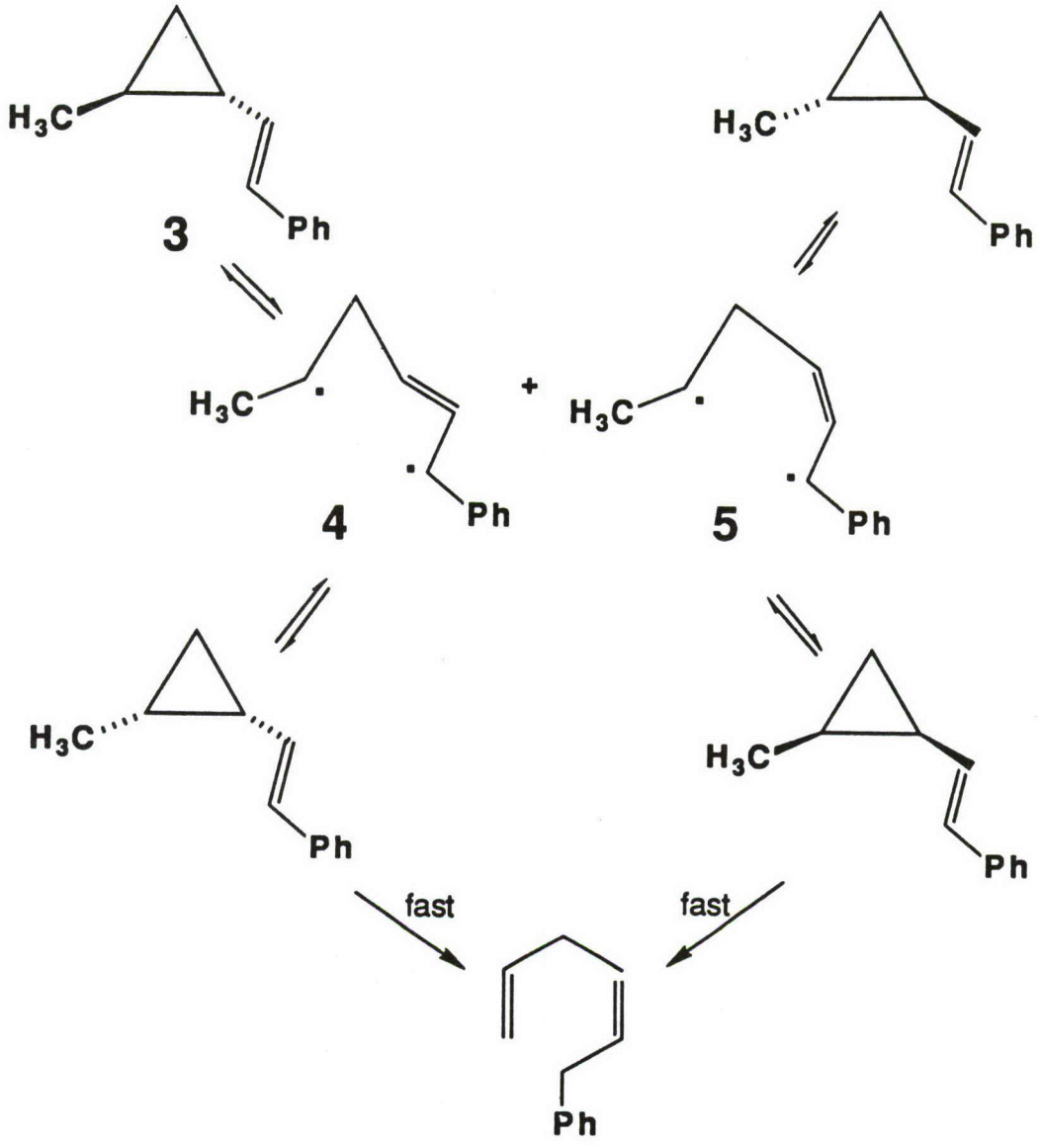

Figure 1

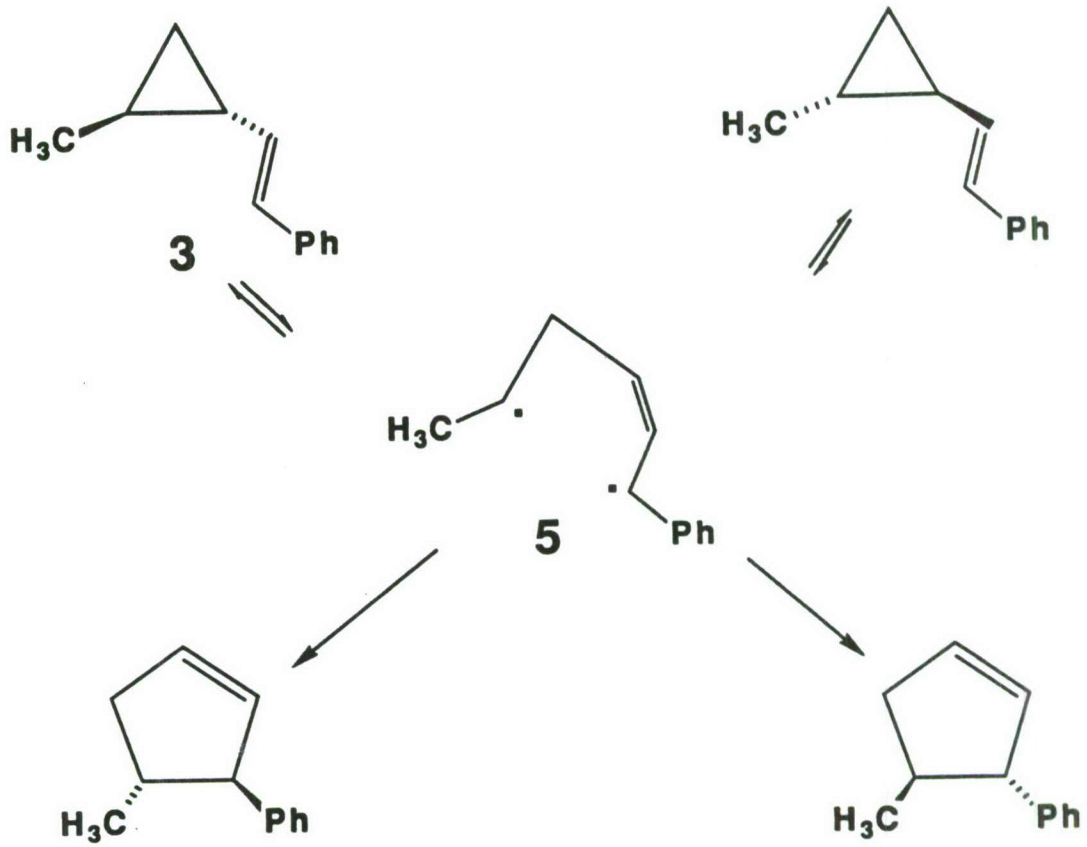

Figure 2

The second part of this collaborative effort to elucidate dynamic constraints upon chemical reactivity has involved an examination of the unimolecular dissociation of highly excited, chemically activated molecules prepared by the reaction of electronically excited oxygen atoms, $O(^1D_2)$, with hydrogen containing substrates. The insertion process

$$O(^1D_2) + RH \rightarrow ROH^{\ddagger} \quad (1)$$

competes with direct abstraction

$$O(^1D_2) + \dot{R}H \rightarrow R + OH. \quad (2)$$

The chemically activated intermediate, $ROH^{\ddagger}$, can itself undergo cleavage at either the C-O bond

$$ROH^{\ddagger} \rightarrow R + OH \quad (3)$$

or at one of the C-C bonds

$$ROH^{\ddagger} \rightarrow R' + R''OH \quad (4).$$

Note that process (1) followed by (3) results in the production of OH; it is that combination of insertion/dissociation that governs the reaction of $O(^1D_2)$ with H_2. Here we ask to what extent abstraction competed with insertion and whether C-O bond scission can occur before energy is distributed into the $ROH^{\ddagger}$ complex where C-C bond scission becomes energetically favored.

The following table provides an summary of both the energetics and results of the pulsed photolysis/laser induced fluorescence experiments carried out in our lab.

Substrate	E_{avail}	P(v"=1)/P(v"=0)	f(OH)
CH_4	48.9 kcal	1.0	0.80
C_2H_6	56.1	0.58	0.03
C_3H_8	56.4	0.21	0.02
neo-C_5H_{12}	61.1	0.11	0.03
CH_3F	56.0	≈ 0.8	0.03
cyclo-C_3H_6	49.3*	0.25	0.03

* Does not include ring strain energy

Here, E_{avail} includes the center-of-mass collision energy, P(v"=1)/P(v"=0) represents the ratio of OH product formed in the two lowest vibrational levels, and f(OH) is the fraction of $O(^1D_2)$ converted to OH product in all states. This last quantity is corrected for the effect of electronic quenching.

The degree of vibrational excitation depends almost exclusively upon the size of the substrate. Reaction of $O(^1D_2)$ with heavier hydrocarbons leads to less product vibrational excitation. That observation coincides with a similar one concerning rotational excitation which also decreases for the heavier substrates. Indeed, clear evidence is observed (in the form of highly nonlinear surprisals) for the presence of two mechanisms for production of OH following attack of excited oxygen atoms upon the larger substrate molecules. Presumably this can be associated with abstraction in process (1) becoming relatively important, the presence of multiple C-C bonds enhancing the probability that an $ROH^{\ddagger}$ complex will dissociate there rather than at the C-O bond.

To test for the importance of direct abstraction in the lighter substrates, we used CH_3F, for which the insertion product may also dissociate to form HF,

$$O(^1D_2) + CH_3F \rightarrow HOCH_2F^{\ddagger}$$

$$HOCH_2F^{\ddagger} \rightarrow H_2CO + HF,$$

a process known to yield vibrationally excited HF. In fact, our results suggest that ≈97% of the reactive encounters proceed in this way, only 3% yielding OH directly. Interestingly, the rotational distribution of that OH is virtually identical to that observed following the reaction of $O(^1D_2)$ with CH_4! Thus one cannot simply assign that product to the direct abstraction pathway.

Finally, the experimental observation of similar OH product energetics following attack on *cyclo*-propane and *n*-propane seems very interesting. Apparently, the ring strain energy is not released following attack of the $O(^1D_2)$ upon the *cyclo*-C_3H_6. That once again suggests that the OH product may all arise from direct abstraction and not insertion/elimination. However, if anything, the orientation preference of these radicals suggest that they are formed following an elimination. Further investigation of these phenomena is currently in progress.

Theoretical Investigation of Energy Storage in Atomic and Molecular Systems*

H. H. Michels and J. A. Montgomery, Jr.
United Technologies Research Center
East Hartford, CT 06108

ABSTRACT

Theoretical electronic structure calculations are being carried out for several high energy species that are attractive candidates for advanced chemical propulsion systems. Using deliverable specific impulse and storability as the major criteria for the goodness of new oxidizers or fuels, primary consideration is being given to ground state molecular structures, of low molecular weight, which exhibit a high positive heat of formation. Calculations to date have been carried out on: 1) light element C_{3v} structures (H_4, Li_3H, LiH_3, Li_4); 2) azide-like structures (FN_3, a-N_2O_2, FNCO, CO_3, FNBF); 3) cyclic boron structures (B_3H_3, B_2H_2NH); and 4) hypervalent structures (NF_5).

We find that the ground states of H_4 (tetrahydrogen), LiH_3 and Li_4, as C_{3v} structures, are unstable toward dissociation into diatomic fragments. These molecules do not look promising as storable, high energy chemical species. Li_3H appears to be vibrationally stable as a C_{3v} structure but preliminary studies indicate a low energy content.

All of the azide-like structures are vibrationally stable with high (400-500 kJ/mol) positive heats of formation. The best candidate appears to be asymmetric dinitrogen dioxide, a-N_2O_2, which exhibits a heat of formation of +500 kJ/mol and can deliver 450 seconds I_{sp} as a hybrid propellant with hydrogen.

None of the cyclic boron structures examined to date are highly energetic. Their chemistry is further complicated by condensation reactions which cause conversion to higher molecular weight structures.

The hypervalent NF_5 molecule has been studied as a D_{3h} structure, as the ionic $NF_4^+F^-$ form and as a C_{3v} structure. Preliminary calculations indicate stability for NF_5 both as a D_{3h} and C_{3v} structure. Detailed correlated energy calculations are in progress for NF_5 and for several azide structures.

A discussion of our theoretical calculations of the four types of compounds that we have studied to date is given below.

---

* Supported in part under AFAL Contract F04611-86-C-0071

DISCUSSION

1. Light Element C_{3v} Structures

H_4

Detailed calculations of H_4 in C_{3v}, and lower symmetry, were carried out using two different Gaussian basis sets and several different levels of theory. The first basis set examined was that reported by Nicolaides, et al.[1] in their earlier studies of H_4. A larger, more flexible basis set was also developed that included more diffuse functions and more flexibility to describe polarization effects. In addition to optimized structure calculations, both a frequency analysis and stability analysis were carried out on H_4, starting from C_{3v} symmetry. These calculations indicate that the potential energy minimum found in C_{3v} symmetry corresponds to a saddle region rather than a stable bound state and that distortion (via vibrational or rotational modes) leads monotonically to dissociation into two H_2 molecules. Details of this study are given in reference 2.

Li_3H

The C_{3v} structure of Li_3H, which is the analog of tetrahydrogen with a Li_3^+ base, was examined using several basis sets and at the SCF and MP2 levels of theory. Calculations at both the SCF and MP2 level of theory, using several basis sets including diffuse orbitals, indicate that this species is stable in all approximations that were examined. A diffuse basis (6-31++G*) was examined at the SCF level to insure that Li^- and H^- were accurately represented. The results for this basis, however, were essentially the same as those with the double-zeta plus polarization basis sets. The optimized structure for Li_3H has a short pyramid height (~ 1.1 Å) for the H^- anion above the Li_3^+ base. The structure thus somewhat resembles the NH_3 molecule. The basic reason that Li_3H is stable, while H_4 is a saddle geometry, is that the back charge transfer of an electron from H^- into the Li_3^+ base does not create an instability. Li_3 as a neutral species has stability relative to $Li + Li_2$ whereas H_3 is unstable relative to $H + H_2$. Further studies of Li_3H in C_s symmetry are indicated.

LiH_3, Li_4

Our previous argument concerning the stability of Li_3H would predict that the LiH_3 molecule should be unstable since back charge transfer into the H_3 base would create an instability. We find that this indeed is the case for LiH_3, where two separate basis sets both yielded a structure with imaginary frequency

---

[1] C.A.Nicolaides, G.Theodorakopoulos, I.D.Petsalakis, J.Chem.Phys,80,1705(1984).
[2] J. A. Montgomery, Jr. and H. H. Michels, J. Chem. Phys., 86, 5882 (1987).

components, i.e. a saddle geometry. Surprisingly, the Li_4 structure also has an imaginary frequency for the e-mode (triangle distortion), even with a diffuse (6-31+G*) basis set. The optimized geometry for Li_4 in C_{3v} yields bond lengths which suggest that a lower order symmetry is the true ground state. A search through the Carnegie-Mellon University archive verifies this idea, where the rhombus structure (D_{2h}) of Li_4 is found to be lower in energy. This D_{2h} structure is stable, relative to 2 Li_2, by approximately 0.6 eV. Li_4 is thus probably less energetic as a fuel than Li(s) or LiH(s).

2. Azide-Like Structures

Calculations of hydroazoic acid (HN_3), fluorine azide (FN_3), fluorine isocyanate (FNCO), asymmetric dinitrogen dioxide (a-N_2O_2) and difluoroaminoborane (FNBF) were carried out at several levels of theory to determine the most stable geometries of these azides and azide-like compounds. The results are summarized in Table 1 which indicates that a stable C_s structure exists for each of these compounds. A vibrational frequency analysis has also been carried out on each of these compounds. The results indicate a stable structure in $^1A'$ symmetry.

A comparison with experimental structures is shown in Table 1 for HN_3 and FN_3. It is clear that very good agreement has already been achieved at the MP2 level of theory. Further studies are in progress at higher levels of theory, and with basis sets larger than the 6-31G* sets used in these initial studies.

The most significant result of our studies of azide-like structures is the prediction of a stable, asymmetric C_s structure of dinitrogen dioxide with a characteristic IR frequency of 1206 cm^{-1}, corresponding to the N-O stretch. This frequency has previously been reported by Milligan and Jacox[3] in argon matrix studies of irradiated N_2O in the presence of alkali atoms and assigned to a possible N_2O_2 anion. It is not characteristic of other known nitrogen oxides. The calculated geometry for a-N_2O_2 is very similar to the structures of the isoelectronic species FN_3 and FNCO, which have recently been characterized both theoretically and experimentally.[4,5]

The reaction of O [^1D] atoms with CO_2 is believed to yield the cyclic C_{2v} CO_3 structure (dioxirane), which has been found by Pople et al. to be more stable than the C_s structure.[6] Therefore, calculations were also performed on the analogous C_{2v} structure of N_2O_2. Although it is a saddle point at the HF/3-21G level of theory, our HF/6-31G* calculations indicate that there is a vibrationally stable C_{2v} structure of N_2O_2 about 160 kJ/mol above the C_s structure. An optimized HF/6-31G* transition state for the C_{2v} to C_s rearrangement was found only 2 kJ/mol above the C_{2v} structure. Preliminary studies at the CISD level suggest that this barrier becomes even smaller when electron correlation effects are included. Therefore, it seems unlikely that the C_{2v} N_2O_2 structure will be formed in the O [^1D] + N_2O reaction.

---

[3] D. E. Milligan and M. E. Jacox, J. Chem. Phys. 55, 3404 (1971).
[4] D. Christen, H.G. Mack, G. Schatte, H. Willner, J.Am.Chem. Soc.,110,707(1988).
[5] K. Gholivand, H. Willner, D. Bielefeldt, A. Haas, Z.Naturforsch 39b,1211(1984).
[6] J. A. Pople, U. Seeger, R. Seeger, P.V.R. Schleyer, J. Comp.Chem. 1,199(1980).

There are also low-lying triplet states of N_2O_2, arising from O [^3P] + N_2O and O_2 [$^3\Sigma_g^-$] + N_2, and it is necessary to know their location to assess the stability of the singlet. A CISD/6-31G* energy calculation on the lowest $^3A''$ state, performed at the optimized geometry of the singlet, shows that the triplet lies 67 kJ/mol higher than the singlet. Since asymptotically the triplet surface lies lower than the singlet, further calculations are underway to characterize the crossing region and its effect on the stability of singlet a-N_2O_2.

A thermodynamic analysis of a-N_2O_2 at the CISD/6-31G* level of theory (including size-consistency corrections) yields a predicted heat of formation of approximately +500 kJ/mol, similar to the +565 kJ/mol recently reported for FN_3.[7] a-N_2O_2 may be highly unstable and potentially explosive, as are other azide-like molecules. The barrier to decomposition into N_2 + singlet O_2 is about 65 kJ/mol, similar to that found for FN_3; decomposition to O [^1D] + N_2O [$X^1\Sigma^+$] is predicted to be endothermic by 40 kJ/mol. Additional calculations of the N_2O_2 potential surfaces are in progress.

Our results to date on a-N_2O_2 are summarized in Table 2. Based on our calculated heat of formation for a-N_2O_2, the vacuum specific impulse obtainable with a H_2/a-N_2O_2 propellant combination is 455 sec. Metal loading (hybrid configuration) would improve this performance. As a direct replacement for ammonium perchlorate (AP) in a typical composite propellant, we find a specific impulse improvement of 1 sec/% replacement of AP by a-N_2O_2. Using typical binder loading, a 10 second improvement should be realizable with current mixes.

3. Cyclic Boron Structures

Calculations were carried out on cyclotriborane (B_3H_3) and iminodiborane (B_2H_2NH) at the SCF level of theory using a 6-31G* basis set. The C_{3v} structure for B_3H_3 is found to be unstable but further studies indicate a vibrationally stable state in C_{2v} symmetry. The anion $B_3H_3^-$ is found to be stable as predicted by Lipscomb's rules. Iminodiborane (B_2H_2NH) is a stable structure in C_{2v} symmetry. The optimized geometries and calculated frequencies are shown in Fig. 1. Further studies of B_2H_2NH are indicated but our calculated energetics to date indicate that this is not a high-energy structure. A further negative view is that most iminoboranes eventually form borazine ($B_3N_3H_6$), which is not a high energy fuel. Further studies of boron hydrides, however, may prove useful.

4. Hypervalent Compounds

An analysis of NF_5 structures has been carried out at the HF/6-31G* level of theory. Ionic $NH_4^+F^-$, D_{3h} and C_{3v} structures of NF_5 are being studied. The ionic $NF_4^+F^-$ structure appears to have no minimum relative to decomposition to NF_3 + F_2. However, covalent NF_5 is stable, at the HF level, both as a D_{3h} structure (trigonal bipyramid) and as a C_{3v} structure. The geometry and vibrational analysis are given in Table 3. Further studies at higher levels of theory are in progress for this system.

---

[7] D. Patel, A. T. Pritt, Jr. and D. J. Benard, J. Phys. Chem. 90, 1931 (1986).

TABLE 1

Optimized Geometries
Of Azides

Compound	Theory	R_1 (Å)	R_2 (Å)	R_3 (Å)	α (deg)	β (deg)
HN_3	SCF	1.0055	1.2381	1.0987	108.181	173.815
	MP2	1.0182	1.2502	1.1583	109.946	171.209
	EXP.[1]	1.012	1.240	1.134	112.65	(180.0)
FN_3	SCF	1.3820	1.2536	1.0995	104.315	174.108
	MP2	1.4309	1.2799	1.1521	103.765	171.803
	EXP.[2]	1.444	1.253	1.132	103.8	170.9
FNCO	SCF	1.3737	1.2387	1.1354	109.846	173.235
	MP2	1.4185	1.2622	1.1765	110.717	168.914
a-N_2O_2	SCF	1.7574	1.2024	1.0844	103.966	179.506
	[MP2	1.5305	1.2272	1.1548	103.591	179.488]
	CISD	1.5817	1.2240	1.1072	102.867	179.344
FNBF	SCF	1.2993	1.2068	1.2871	180.000	180.000
	MP2	1.3394	1.2491	1.3069	154.650	169.291

( ) Assumed
[ ] ψ_o not stable relative to rotation to complex form

[1] Tables of Interatomic Distances and Configuration in Molecules and Ions, L. E. Sutton, ed., Chemical Society, London (1985)

[2] D. Christen, H. G. Mack, G. Schatte and H. Willner, J. Am. Chem. Soc., 110, 707 (1988).

TABLE 2

N_2O_2 Theoretical Predictions

C_s Structure [$^1A'$]				C_{2v} Structure [$^1A_1$]	
Level	HF/6-31G*	CISD/6-31G*	HF/6-311G*		HF/6-31G*
Energy	-258.348 838	-258.932 499	-258.417 315		-258.287 006
Geometry					
R(O-O)	1.7574	1.5817	1.8014	R(O-O)	1.4787
R(N-O)	1.2024	1.2240	1.1901	R(N-O)	1.3519
R(N-N)	1.0844	1.1072	1.0787	R(N-N)	1.1268
α	103.97	102.87	106.20		
β	179.51	179.34	179.62		
Vibrational Frequencies[a]					
a' N-N stretch	2677 (8.46)	2501	2656	a_1 N-N stretch	2203
a' O-N stretch	1262 (4.53)	1206	1282	a_1 symmetric stretch	1178
a' O-O stretch	697 (0.90)	648	707	a_1 O-N-O scissor	900
a' O-N-N bend	291 (2.08)	526	271	b_2 O-N-O rock	670
a' O-O-N bend	188 (0.05)	227	169	b_2 asymmetric stretch	449
a" out-of-plane	648 (0.38)	580	655	b_1 out-of-plane	515

[a]HF/6-31G* IR intensities (in $D^2amu^{-1}{}^{\circ}A^{-2}$) for the C_s structure are given in parenthesis following the corresponding frequencies.

Bond lengths are in angstroms, bond angles are in degrees, energies are in hartrees, and vibrational frequencies are in wavenumbers.

TABLE 3

Geometry and Vibrational Analysis of NF_5

HF/6-31G*

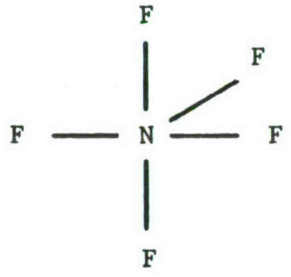

R_p = 1.3267 Å E = -551.1038565 a.u.

R_h = 1.5312 Å $E_{NF_3 + F_2}$ = -551.2178132 a.u.

Frequencies (cm^{-1})

e'		a_1'		e"		a_2"	
276	1352	509	857	656	663	459	828

Ionic structure $[NF_4^+F^-]$ has no minimum relative to decomposition to $NF_3 + F_2$. The C_{3v} structure appears to be stable.

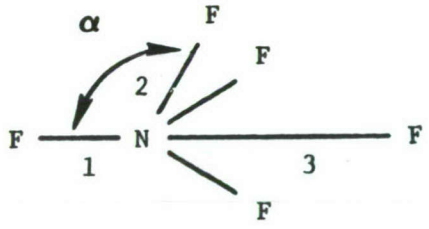

NF_1 = 1.3474 Å α = 100.8°

NF_2 = 1.2834 Å

NF_3 = 2.0336 Å

E = -551.0990132 a.u.

Frequencies (cm^{-1})

a_1				e			
126	672	921	1110	290	524	694	1474

Cyclotriborane (B_3H_3)

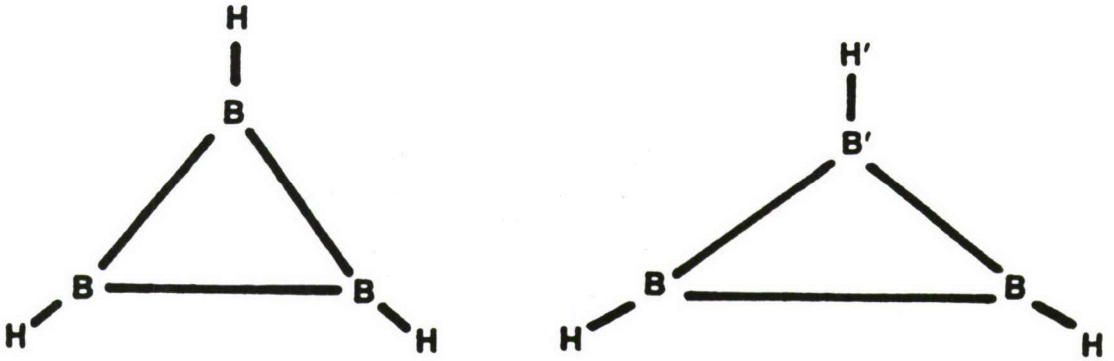

$R_{BB} = 1.734$ Å
$R_{BH} = 1.178$ Å
E = −75.174458, unstable (2)

$R_{B'H'} = 1.180$ Å
$R_{BH} = 1.174$ Å
$R_{B'B} = 1.536$ Å
$R_{BB} = 2.032$ Å
E = −75.647600, stable

Iminodiborane (B_2H_2NH)

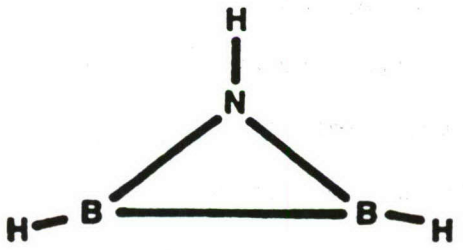

$R_{BB} = 1.621$ Å
$R_{BH} = 1.174$ Å
$R_{NH} = 0.989$ Å
$R_{BN} = 1.423$ Å

∠ HBN = 136.2°
∠ BNH = 145.3°
E = −104.981636

Frequencies (cm^{-1})

B_1	A_1	A_2	B_2	B_2	B_1	A_1	B_2	A_1	B_2	A_1	A_1
700	818	921	923	989	1000	1110	1268	1423	2878	2916	3965

Fig. 1 CYCLIC BORON COMPOUNDS

A New Hypothesis for New High Energy Density Molecular Systems

Henry F. Schaefer III
Center for Computational Quantum Chemistry
School of Chemical Sciences
University of Georgia
Athens, GA 30602

Abstract

An analogy is constructed between the known composition of elemental sulfur (principally S_8 rings) and the unknown oxygen rings. Due to the weakness of O-O simple bonds, as in hydrogen peroxide, it is hypothesized that oxygen rings are potential high energy density materials. A particularly attractive candidate is the O_4 molecule, for which ring strain is expected to provide further destabilization relative to two separated O_2 molecules. To pursue these qualitative suggestions, ab initio molecular quantum mechanics has been employed. Both self-consistent-field (SCF) and configuration interaction including single and double excitations (CISD) methods have been employed in conjunction with double zeta plus polarization basis sets. At the highest level of theory the nonplanar (D_{2d} point group, O-O-O-O torsional angle 25°) equilibrium structure is predicted to lie 2.9 kcal below the planar D_{4h} structure, which is a transition state. The infrared spectrum is predicted at the DZ+P CISD level, as well as lower levels of theory. The O_4 minimum is predicted to lie ~100 kcal/mole above the asymptotic limit of two O_2 molecules.

The Hypothesis

The development of efficient and safe conventional (i.e., non-nuclear) propellants and/or fuels is a goal of obvious technological significance. A desirable quality of such a propellant is clearly a high ratio of energy release to mass. The present hypothesis rests on a simple, but previously unrecognized, analogy between oxygen and sulfur. Preliminary studies showed that the proposed oxygen ring systems are sufficiently promising to warrant the detailed, high-level theoretical research reported here.

Our idea begins with the observation[1] that elemental sulfur exists as sulfur rings, S_n. The stability of these sulfur rings is attested by the fact that the single most important commercial source of sulfur is elemental sulfur in the caprock salt domes in the United States and Mexico.[2] The most common allotrope of sulfur is the yellow, orthorhombic α-form, to which all other modifications eventually revert at room temperature. As long ago as 1935 the crown structure of cyclo-S_8 was established by x-ray crystallography.[3] The D_{4d} point group experimental structure[4] of S_8 is depicted in Figure 1.

The essence of our proposal is to make an analogy between sulfur rings and oxygen rings. Given the remarkable stability of sulfur rings, should it not be possible to prepare oxygen rings? Oxygen lies directly above sulfur in the periodic table, and the analogy is an appealing one. Before pressing on further with this analogy, let us say a bit more about cyclic forms of sulfur other than S_8.

Although S_8 dominates elemental sulfur, more than a dozen additional sulfur rings S_n have been synthesized in the past 20 years.[2,5] Long before this, in 1891, a rhombohedral form, ε-sulfur, was prepared by Engel.[6] By 1961 ε-sulfur was clearly established to be cyclo-S_6, the molecular structure of which is given[4] in Figure 2. Note that for both S_6 and S_8 all sulfur atoms

are equivalent. S_7 is also known to exist as a C_s ring structure, with four distinct S-S distances,[7] ranging from 1.99 A to 2.18 A. S_9, S_{11}, and S_{13} have been synthesized and appear from spectroscopic studies to be cyclic, although no crystal structures have been reported.[2,8]

S_{10} belongs to the rarely observed point group D_2 and has experimental bond distances[9] in the relatively narrow range 2.03-2.08A. The twelve membered sulfur ring was predicted in 1949 in a classic paper by Pauling[10] to be unstable. Nevertheless, S_{12} was synthesized in 1966 and turns out to be second only to S_8 in stability.[2] S_{12} is monocyclic, with S-S bond distances in the very narrow range 2.05-2.06 A. S_{18} is also monocyclic, as is S_{20} and experimental crystal structures[11,12] exist for both molecules.

The reason for this relatively detailed description of the cyclic S_n isomers is that there should be a one-to-one correspondence with cyclic O_n isomers, a principal topic of this research. However, unlike the S_n rings, the analogous O_n rings will be high energy density molecular systems.

Before going on further, let us attempt to make some plausible guesses as to the energy content of the metastable O_n rings. First one notes that the valence-isoelectronic cyclic S_8 contains <u>no</u> energy in this sense. Specifically, crystalline S_8 lies 15.4 ± 0.1 kcal per mole of sulfur atoms below four gas phase diatomic S_2 molecules.[13] Can one guess this result using the dissociation energy of S_2 (D_o = 4.37 eV = 100.8 kcal/mole)[14] and some reasonably standard S-S single-bond dissociation energy,[15] say 54 kcal/mole? The answer to this question is a qualified "yes". Using this simple model, one predicts S_8 to lie (54-50.4) = 3.6 kcal/mole below four S_2 molecules on a per atom basis. By increasing the S-S bond energy from the standard 54 kcal to 66 kcal, the known experimental energy difference for

$$S_8 \text{ (crystalline)} \rightarrow 4\, S_2 \qquad (1)$$

is precisely reproduced. This adjustment reflects the fact that the S-S bonds in S_8 are stronger than those in organosulfur compounds such as CH_3SSCH_3.

The comparable oxygen thermodynamic data make it immediately obvious why oxygen rings should be high energy density materials. First the standard O-O bond dissociation strength[15] is 35 kcal/mole, much weaker than the 54 kcal for S-S bonds. Secondly, the dissociation energy[14] of diatomic O_2 is D_o = 5.12 eV = 118.0 kcal/mole, much stronger than the 100.8 kcal for S_2. Thus the estimate for the energy stored in the "generic" oxygen ring is (35-59) = -24 kcal per mole of oxygen atoms. That is, the dissociation process

$$O_n \text{ (n even)} \rightarrow \frac{n}{2}\, O_2 \text{ (g)} \qquad (2)$$

is estimated to be exothermic by 24 kcal per mole of oxygen atoms. Alternately 48 kcal of energy is released per mole of O_2 molecules. A larger energy release might be expected for the smaller rings, specifically O_4 and O_6, which presumably have smaller average O-O bond energies due to ring strain.

A similar estimate is readily made for the isoelectronic cyclic system $(NH)_n$, which will also be metastable and dissociate (directly or indirectly) via

$$(NH)_n \text{ (n even)} \rightarrow \frac{n}{2}\, N_2(g) + \frac{n}{2}\, H_2(g) \qquad (3)$$

This proposal, of course, takes advantage of the tremendous strength (D_o = 9.76 eV = 225.1 kcal/mole)[14] of the N≡N triple bond. Using in addition $D_o(H_2)$ = 4.48 eV = 103.3 kcal and the average N-N single bond strength (39 kcal) and

N-H bond strength (93 kcal),[15] one estimates ΔH for (3) to be

$$39 + 93 - 112.5 - 51.6 = 32.1 \text{ kcal}$$

per mole of N (or H) atoms. Alternately, reaction (3) is suggested to be exothermic by 64.2 kcal/mole of N_2 molecules released. It is apparent that within the limits of the simple estimates made here, systems like $(NH)_8$ may be even more effective than the above-discussed oxygen rings as high energy density molecular systems. It is ultimately intended to theoretically investigate both O_n and $(NH)_n$. The order of the discussion presented above was mandated by the analogy (with the sulfur rings) by which this idea came to us.

A traditional measure of the effectiveness of a propellant is the specific impulse I_{sp}. I_{sp} is given in seconds from the relationship

$$I_{sp} = (\text{constant}) \frac{\Delta H(\text{kcal/mole})}{\text{Molecular Weight (grams/mole)}}$$

The traditional standard of comparison is the exothermic reaction

$$H_2 + \tfrac{1}{2} O_2 \rightarrow H_2O \qquad (4)$$

for which I_{sp} is of the order of 400 seconds. Substitution of unstrained (e.g., O_8) oxygen rings for O_2 will increase the specific impulse by ~100 seconds. Use of the smaller oxygen rings O_4, O_5, or O_6 would presumably result in a significantly larger I_{sp}.

It should be emphasized of course that high energy density is a necessary but certainly not sufficient condition for the development of an effective

propellant. The material also must have a significant range of metastability - it should not explode when a match is unintentionally lit 100 meters away. The great stability of elemental sulfur, in the form of sulfur rings, gives some encouragement that the band of metastability for oxygen and NH rings might be rather broad. Precisely this point, of course, may be investigated in the theoretical studies of the type reported here.

Literature Citations

1. B. Meyer Sulfur, Energy, and Environment (Elsevier, Amsterdam, 1977).
2. N. N. Greenwood and A. Earnshaw, Chemistry of the Elements (Pergamon, Oxford, 1984); see especially pages 757-781, which contain an excellent review of the structures of elemental sulfur.
3. B. E. Warren and J. T. Burwell, J. Chem. Phys. 3, 6 (1935).
4. J. Donohue, The Structures of the Elements (Wiley, New York, 1974).
5. M. Schmidt, pages 1-12 of New Uses of Sulfur, Volume II, Editor D. J. Bourne, Advances in Chemistry, Series No. 165 (American Chemical Society, Washington, D.C., 1978).
6. M. R. Engel, Compt. Rend. Acad. Sci. Paris 112, 866 (1891).
7. R. Steudel, R. Reinhardt, and F. Schuster, Angew. Chem. Int. Ed. Engl. 16, 715 (1977); J. Donohue, J. Crystal Molec. Struc. 8, 141 (1978).
8. T. Sandow, J. Steidel, and R. Steudel, Angew. Chem. Int. Ed. Engl. 21, 794 (1982).
9. R. Reinhardt, R. Steudel, and F. Schuster, Angew. Chem. Int. Ed. Engl. 17, 57 (1978).
10. L. Pauling, Proc. Natl. Acad. Sci. USA 35, 495 (1949).
11. T. Debaerdemaeker and A. Kutoglu, Naturwissenschaften 60, 49 (1973).
12. T. Debaerdemaeker, E. Hellner, A. Kutoglu, M. Schmidt, and E. Wilhelm, Naturwissenschaften 60, 300 (1973).
13. D. R. Stull and H. Prophet, JANAF Thermochemical Tables, Second Edition, NSRDS-NBS 37 (Superintendent of Documents, Washington, D.C., 1971).
14. K. Huber and G. Herzberg, Constants of Diatomic Molecules (Van Nostrand Reinhold, New York, 1979).

15. See Table on page 85 of S. H. Pine, J. B. Hendrikson, D. J. Cram, and G. S. Hammond, Organic Chemistry, Fourth Edition (McGraw-Hill), New York, 1980).

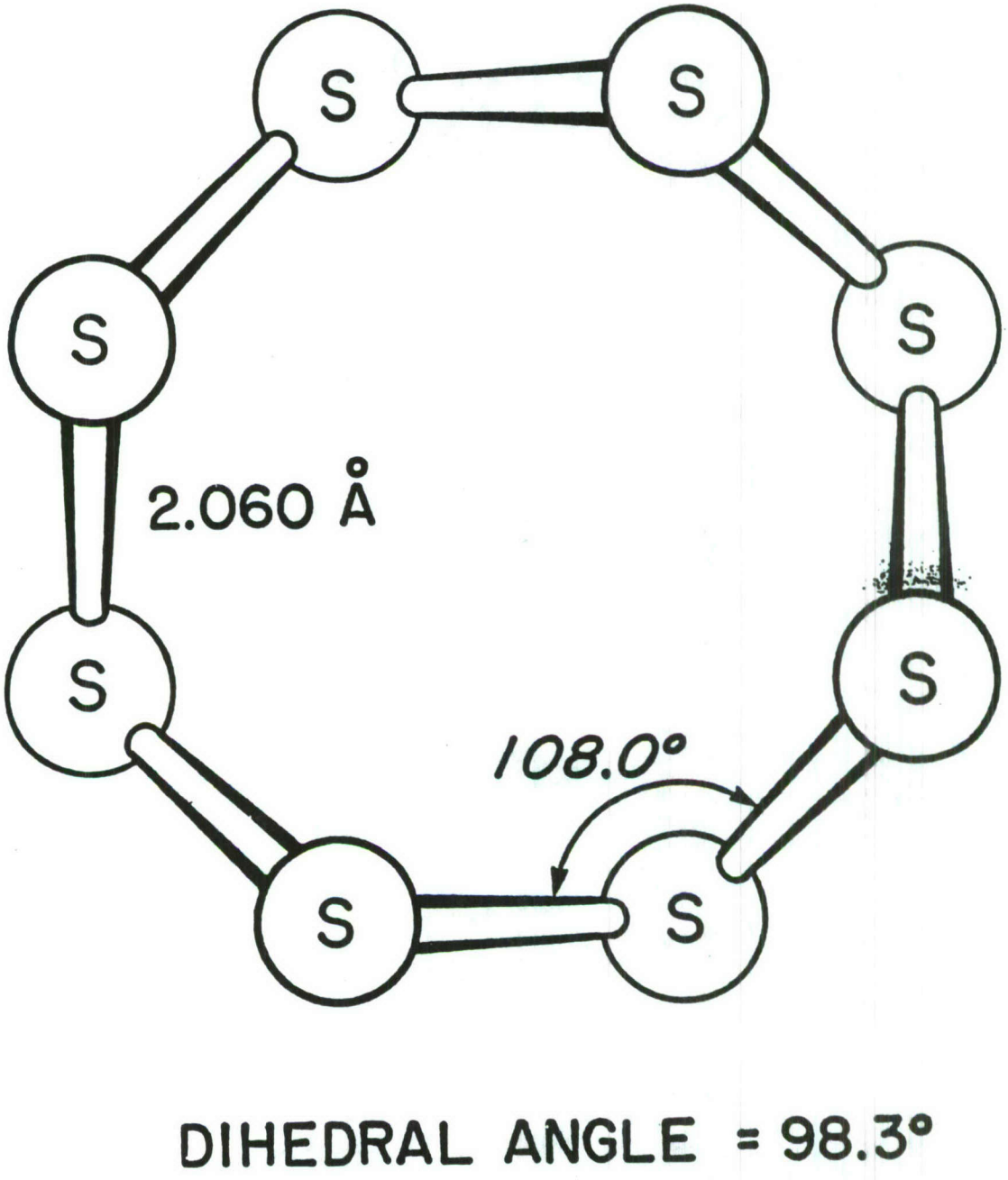

Figure 1. Experimental (reference 4) crystal structure for the most common form of elemental sulfur, S_8.

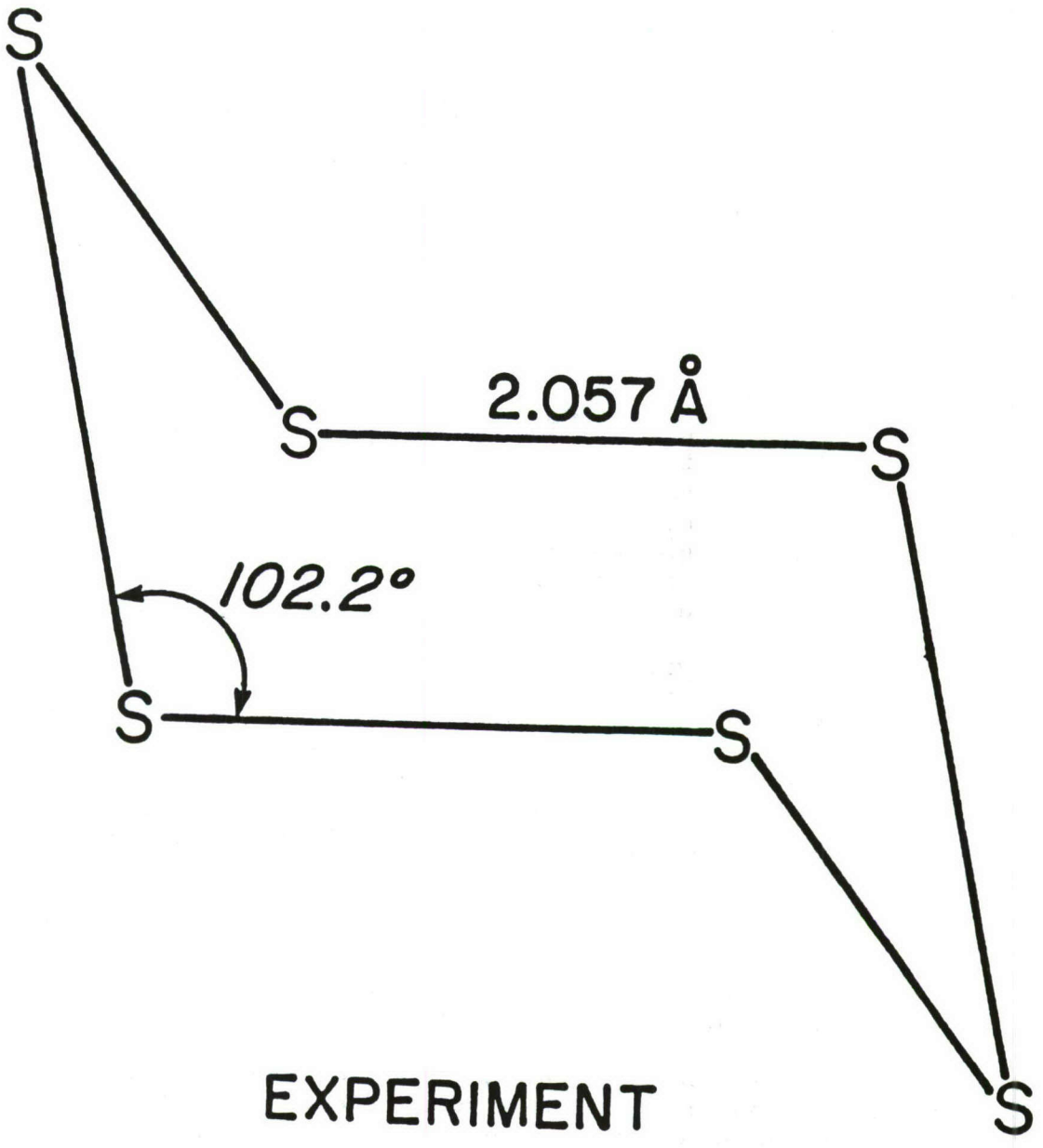

Figure 2. Experimental (reference 4) crystal structure for the rhombohedral form of sulfur, ε-sulfur, S_6.

ABSTRACT FOR "HIGH ENERGY DENSITY MATERIALS CONTRACTORS MEETING"
28 February 1988 - 2 March 1988

"INVESTIGATIONS OF HYPERVALENT COMPOUNDS AS HIGH-ENERGY MATERIALS"

Paul Engelking & Tom Dyke
Department of Chemistry
University of Oregon
Eugene, OR 97403

John Farley
Department of Physics
University of Nevada, Los Vegas
Los Vegas, Nevada

Two classes of experiments are being performed to investigate hypervalent ions. These unusual species have more bonds about a central atom than "normal" chemistry would allow.

The major target ions in this class are the anions SiH_5^-, NH_4^-, and CH_5^- The silane-hydride ion is believed [1-6] to have a trigonal bipyramidal structure, forming spontaneously from H^- and SiH_4. It is metastable to elimination [1] of H_2. It has been observed to exchange more than one hydrogen for deuterium in sequential flowing afterglow reactions, giving evidence that at least two hydrogens are equivalent. [7] No spectroscopic structural information is yet available.

The ammonia-hydride has been calculated to have two configurations: either a $H^-..HNH_2$ ion-dipole cluster geometry, [8-11] or a higher energy tetrahedral geometry, [8,9,12] 4-25 kJ/mol above NH_3 + H−, and metastable to rearrangement with a 70-80 kJ/mol barrier. [8] The ion has been observed in mass spectrometry, [13] and has been studied through photoelectron spectrometry. [14] The experimental evidence for the high energy T_d form is equivocal, consisting of only a sole, weak "blip" on the low electron affinity end of the photoelectron spectrum. [9,14] No experimental spectroscopic or structural data is yet available. The ammonia hydride ion has an interesting first cousin, a high energy rydberg molecule, the NH_4 "ammonium radical," which has been observed in high pressure discharges in ammonia. [15,16] This suggests that the higher energy ammonia-hydride species would best be prepared at high pressures under high excitation conditions.

These hypervalent ions are to be formed in a corona-excited supersonic-expansion ion-source. When this source operates with NH_3/H_2 mixtures, mass spectra of ions evidence NH_4^- species, while emission spectra evidence the high energy NH_4 neutral rydberg species. Thus, this source produces ions of the right mass and definitely produces high energy species.

Spectroscopic studies will be performed with two different apparatus, both detecting the absorption of laser radiation by the disappearance of the target ions and the appearance of photodetachment or photodissociation products. These two methods of investigation complement one another.

An existing fast-ion beam is combined with a coaxially propagating F-center ion laser beam to explore the high-frequency (2800-4000 cm^{-1}) vibrational motions. This apparatus has the advantages of high resolution and "doppler" tuning, making operation with even fixed frequency lasers possible. The production of fast (2-5 keV) neutral products allows sensitive neutral detection.

The second method of investigation is a slow, molecular ion beam with coaxial laser excitation and time-of-flight mass spectrometric detection. This apparatus, which is nearing completion, will have greater ion/laser interaction times, permitting the use of both lower power CW lasers (such as IR diode lasers in the 700-2500 cm^{-1} range) and pulsed lasers.

For proof of method, ions that could be formed in a more conventional, low pressure source, were used in the fast beam apparatus. In the last year, the ion HNO^- has been detected, measured and analyzed. The results of this study show a bent (117°) triatomic with an anomalously long NO bond (1.32 A). While the ion can be formed in the approach of H^- to NO, the geometry of the resulting ion reflects more of an $HN..O^-$ structure. The NH bond is very tight. The method that NO uses to tightly bind H^---delocalizing the charge out of the NH bond--is expected to be the same mechanism that a truely hypervalent species will use to stablize its bonding arrangement.

As demonstrated in HNO^-, the predissociating spectra also contain information about ion stability and lifetime, through the measurement of line widths.

The novel hypervalent anions are expected to be readily formed during the next year in a corona excited supersonic expansion source pioneered at Oregon for molecular spectroscopy. Analysis of the HNO- spectra within 6-months of the collection of the data, including writing of the 38 parameter fitting routines for the upper and lower state asymmetric-tops with spin-rotation interactions, suggests the usefulness of the experimental data.

---

[1] U. Brandemark and P.E. Siegbahn, Th. Chem. Acta 66, 233 (1984).

[2] P. Baybutt, Mol. Phys. 29, 389 (1975).

[3] N.M. Vitkovskaya, V.B. Mantsivoda, T.E. Moskovskaya, and M.G. Voronkov, Int. J. Quantum Chem. 17, 299 (1980).

[4] M.S. Gordon, L.P. Davis, L.W. Burggraf, and R. Damrauer, J. Am. Chem. Soc. 108, 7889 (1986).

[5] F. Keil and R. Ahlrichs, Chem. Phys. 8, 384 (1975).

[6] D.L. Wilhite and L. Spialter, J. Am. Chem. Soc. 95, 2100 (1973).

[7] D.J. Hadjasz and R.R. Squires, J. Am. Chem. Soc. 108, 3139 (1986).

[8] H. Cardy, C. Larrieu, and A. Dargelos, Chem. Phys. Lett. 131, 507 (1986).

[9] J.V. Ortiz, J. Chem. Phys. 87, 3557 (1987).

[10] C.D. Ritchie and H.F. King, J. Am. Chem. Soc. 90, 838 (1968).

[11] J. Kalcher, P. Rosmus, and M. Quack, Can. J. Phys. 62, 1323 (1984).

[12] D. Cremer and E. Kraka, J. Phys. Chem. 90, 33 (1986).

[13] W. DeLange and N.M. Nibberling, Int. J. Mass Spectr. Ion Phys. 80, 201 (1987).

[14] J.V. Coe, J.T. Snodgrass, C.B. Freidhoff, K.N. McHugh, and K.H. Bowen, J. Chem. Phys. 83, 3169 (1985).

[15] K.P. Huber and T.J. Sears, Chem. Phys. Lett. 113, 129 (1985).

[16] M.N. Ashfold, C.L. Bennell, R.N. Dixon, P. Fielden, H. Rieley, and R.J. Stickland, J. Mol. Spectr. 117, 216 (1986).

[17] G. Herzberg, "Molecular Spectra and Molecular Structure III. Electronic Structure of Polytatomic Molecules" (Van Nostrand, New York, 1966).

Fig. 1. Observed transitions in HNO^-

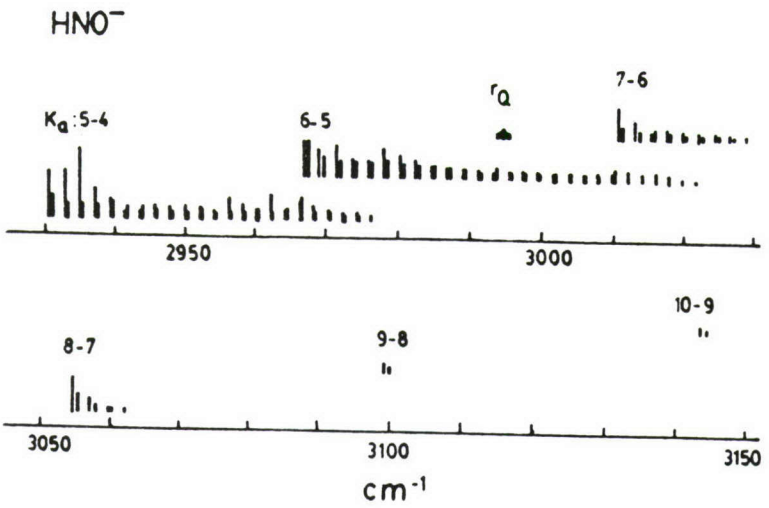

Fig. 2. Comparative geometries. Neutral data from Herzberg, (17) Polyatomics; ion geometry is still preliminary.

	ν_1	A	B	C	R_{NH}	R_{NO}	α
		cm^{-1}			Å	Å	deg.
$\tilde{A}$ HNO	2854	22.2	1.33	1.24	1.04	1.24	116.3
$\tilde{X}$ HNO	3596	18.5	1.41	1.31	1.06	1.21	108.6
$\tilde{X}$ HNO^-	2736	20.0	1.17	1.08	(1.05)	1.32	117

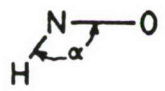

Quantum Chemical Studies of Small Boranes

George F. Adams
Byron H. Lengsfield III*
US Army Ballistic Research Laboratory

Mary Gallo
The Johns Hopkins University

Introduction.

Efforts to increase specific impulse of propellant materials have often focused on the use of low molecular weight compounds, especially the boron hydrides. As recently as two years ago, a joint service workshop reviewed the efforts made to develop conventional propellants that included borane and carborane salts. One concern of the workshop participants was the lack of a history of the research that occured. The areas of molecular structure and thermochemistry are two areas requiring a significant review.

The present research effort focuses on materials that might provide remarkable increases in specific impulse. As part of the Ballistic Research Laboratories participation in this effort, we have used the quantum chemical tools available to us to address the bonding of a unique class of low molecular weight compounds, the boranes. This abstract summarizes the results we have recently obtained on the structures of several diborane abd triborane compounds. In addition, we present the results of a series of calculations we have performed on sigma-bonded systems that may have a significant impact on the overall Air Force initiative in High Energy Density Materials. We first outline the facilities used to perform this research.

THEORETICAL TOOLS

The facilities for quantum chemical research available at the Ballistic research Laboratory are among the finest in the world. The laboratory has two modern supercomputers, a Cray X/MP-48 with SSD and a Cray 2. In addition, the quantum chemistry team has a dedicated Alliant FX8 minisupercomputer. Two major quantum chemistry computational suites are available on these machines. The Cambridge Analytic Derivatives Package (CADPAC) is used for studies of the structures and properties of molecules. This package has been used for much of our production studies on large molecules. The MESA system of codes has been developed over the past five years by current and former members of the BRL quantum chemistry team, in collaboration with the group at Johns Hopkins. MESA provides the ability to search a potential energy surface using SCF, CI, and MCSCF wavefunctions. In addition, we have code that permits the study of many properties of molecular excited states, although most of this code has yet to be ported to the Crays. These codes provide computation of spin-orbit interactions, mixed second and third derivatives for molecular properties, and first and second derivative nonadiabatic coupling

matrix elements (NACMEs). These codes are needed to accurately compute the lifetime of excited states when the decay channel involves spin-forbidden processes and when derivative and/or rotational coupling between different states are large enough that nonradiative decay channels must be considered. As coded, the methods provide automated searching for stationary points on potential energy surfaces and incorporate the effects of electron correlation. Correlation effects are also included in the properties evaluation. These attributes are often essential when attempting to locate equilibrium structures of metastable species or when characterizing a second(excited) state in a symmetry. Our discussion of the small boranes demonstrates the neccesity for these capabilities.

Di- and Triboranes

There are many di- and triborane compounds. Adams and Page have investigated the structures and thermochemistry of most of the diboranes1. We did not consider the nonclassical isomer of diborane(2); that species will be dealt with in this note. We also consider the structures of several of the triboranes, with emphasis on two isomers of triborane(3).

Diborane(2). The structure of the linear diborane(2) compound was computed using a double zeta plus polarization basis set. There were no surprises. The structure posesses seven non-zero positive frequencies, as required for a stable point. We have not yet looked at this molecule using the correlated wavefunction methods available with MESA. The MESA and CADPAC codes give precisely the same results. We have also located a symmetric bridged structure for this molecule. The second derivative computation indicates that this is not a stable point. Recently, Lengsfield has found a symmetry-broken bridged structure. Clearly, an MCSCF study is needed to determine whether a closed shell bridged structure occurs. Those calcu;ations are underway.

Triborane(3). Michaels has noted that triborane(3) does not have a D3h minimum2. We had noted that a C2v structure did have a zero gradient. In checking the results of MESA calcualtions with CADPAC results, we found that the two codes predicted different structures for triborane(3). We were able to reproduce the MESA result with CADPAC. Thus, we had two stable C2v structures, each with twelve nonzero positive frequencies. The figure shows the structures, which we will refer to as "tight" and "loose", describing thereby the B-B-B bond angle. The loose isomers SCF energy is 3 millihatrees lower than the tight isomer's energy. Both isomers have multiple low energy virtual orbitals. Efforts to perform CAS-MC calculations using SCF orbitals as starting orbitals for a 4-in-4 calculation failed. The MCSCF calculations did not converge. Therefore, we performed a modest double excitation CI calculation to obtain a set of natural orbitals to use as starting orbitals for the MCSCF calculation. The results of the natural orbital calculation convinced us that more orbitals needed to be included in the active space. We optimized the structure for each of the isomers using a 4-in-8 CAS. The

structures differed little from the structures predicted by the SCF calculations. These calculations were followed by computing the sacond derivatives for the two isomers with a 4-in-8 calculation. The loose structure still has twelve positive second derivatives. The tight structure has one small negative second derivative. This seems to indicate that the tight structure is not a true minimum on the hypersurface, but the small magnitude of the imaginary frequency (88 wavenumbers) suggests that a more elaborate calculation might be required. We are performing more thorough studies of these isomers.

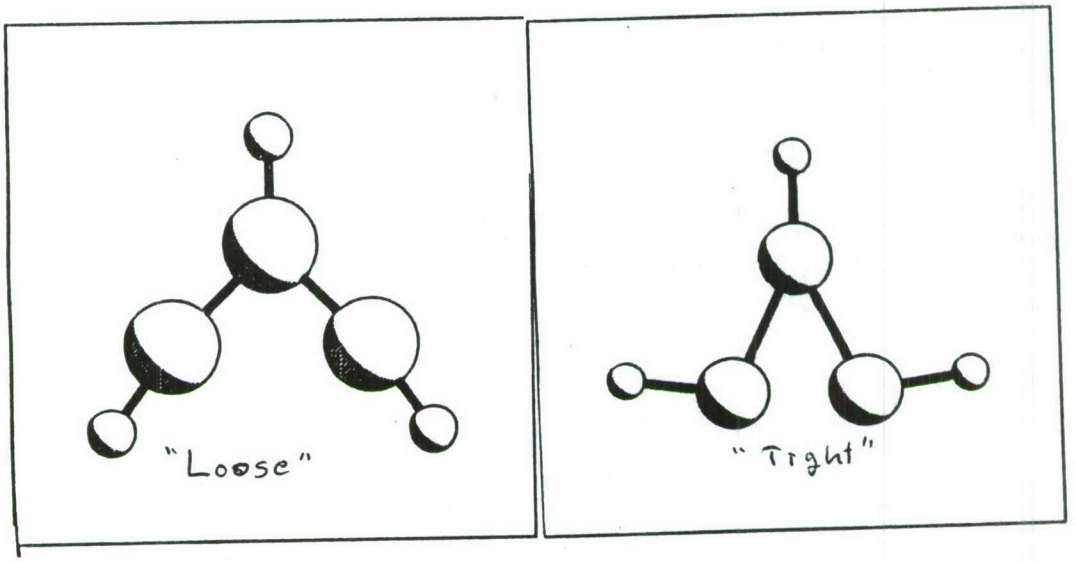

Triborane(5). We have completed SCF studies on two isomers of triborane(5), a classically bonded isomer and a bridged structure. We are currently working on small MCSCF calculations for both isomers. This work should be completed reasonably soon.

PERTURBATION THEORY

In the course of thermochemical studies of various molecules over the past several years, it has become 'gospel' that accurate results require enormous basis sets and full fourth-order perturbation theory calculations. We would like to note that, for some classes of compounds, excellent results can be obtained with third-order calculations, provided an enormous basis set is used. The basis sets used in the large calculations extend the 6-311G basis. To each atoms basis we add one set of s and p diffuse functions, three sets of first polarization functions and one set of second polarization functions. Since we restrict ourselves to third-order, we recognize that thermochemistry of compounds with multiple bonds is not realistic. The table lists comparisons of atomization energies for a numder of first row hydrides. The fourth-order results were obtained either by Page and Adams, or are from Pople group publications. All results are for closed shell states.

Molecule	MP3	MP4-SDTQ
BH	83.1 kcal/m	83.7 kcal/m
BH2	170.4	169.8
BH3	280.4	280.3
H2O	236.1	230.9
NH3	296.8	296.2
CH4	421.1	419.9
B_2H_6	576.6	577.4

We believe that there may be an error in the published number for the water molecule. Note, the technique will, in general, fail when applied to molecules with multiple bonds. The fourth order triple excitation effects are important in those cases. In the case of the BO molecule, the MP3 result was ~10 kcal/m too low.
* Dr. Lengsfield is now at LLNL.

1. G.F. Adams and M. Page, BRL Technical Report, 1988.
2. H. Michaels, comment at May, 1987 AFAL/AFOSR Contractors Meeting.

THEORETICAL STUDY OF ION-PAIR STATES†

Roberta P. Saxon and Dahbia Talbi
Chemical Physics Laboratory, SRI International
Menlo Park, California 94025

Metastable molecular fuels, high-energy long-lived molecular species that do not decay by radiation, tunneling, or other means, when isolated in vacuum, have been proposed as the basis for possible new propulsion schemes. This theoretical project is devoted to examination of ion-pair species, bound by the Coulomb attraction between a stable positive and stable negative ion, as possible candidate fuels. Work, thus far, has concentrated on the H_3O molecule. The goal of our study of H_3O has been two-fold: (1) to characterize as completely as possible the low-lying states of this interesting candidate system, and (2) to develop and validate theoretical methods that can be used in the future to efficiently investigate other systems.

A standard double zeta plus polarization basis set (DZP) augmented by diffuse s and p functions on O to describe the anion or Rydberg character was used for all of our calculations. Most of the results presented here were obtained at the First Order CI (FOCI) level using MCSCF orbitals determined for the $1^2A'$ state. Additional calculations designed to verify the validity of the theoretical model and to establish error limits are reported below.

Consistent with our expectations that an ion-pair state of H_3O will have H_3^+ in its equilateral triangle equilibrium geometry with O^- above the center, our original survey calculations were restricted to C_{3v} geometries. (Calculations were performed, however, in C_s symmetry.) FOCI results for the first and second $^2A'$ states at fixed H-H distances are plotted in Figs. 1 and 2, respectively, as a function of the vertical oxygen distance. There is a local minimum on the $1^2A'$ surface in C_{3v} geometries, which may be characterized as an H_3O^+ ion surrounded by an oxygen 3s Rydberg electron, and which is not stable with respect to dissociation to H_2O + H, in agreement with previous work[1]. There are two local minima on the $2^2A'$ surface in C_{3v} geometries, the higher of which has the H-H separation of the H_3^+ equilibrium geometry and is due to ion-pair bonding. There is no binding in states of quartet multiplicity.

The correlation diagram linking these three local minima to the asymptotes, namely H_2O + H, OH + H_2, and O + H_2 + H is illustrated in Fig. 3 in $^2A'$ symmetry and in Fig. 4 in $^2A''$ symmetry. The higher minimum on the $^2A'$ surface is indicated by a dashed line in Fig. 3. The $1^2A'$ state correlates with the ground state of OH + H_2 and of H_2O + H and is higher in energy than either of these limits. The lowest minimum on the $2^2A'$ surface is bound with respect to the excited states of OH and of H_2O with which it correlates. However, the higher (ion-pair) minimum on the $2^2A'$ surface lies above H_2 + H + O and $OH(A^2\Sigma^+)$ + H_2. The $2^2A'$ state is one component of the doubly degenerate E state in C_{3v} symmetry. The other component, the $1^2A''$, correlates to $OH(X^2\Pi)$ + H_2, which is considerably lower in energy. Because we must assume Jahn-Teller type coupling will link the $2^2A'$ and the $1^2A''$ states at

their C_{3v} geometries, the stability of the $2^2A'$ state hinges on whether there is a barrier to the dissociation of the $1^2A''$ state to OH + H_2.

The local minima discussed thus far have been determined in restricted C_{3v} geometries. Optimized geometries in lower symmetry are summarized in Table I. The C_{3v} minimum previously identified is the true minimum on the $1^2A'$ surface. Relaxing the symmetry results in a lowering of 4.9 kcal/m for the lowest minimum on the $2^2A'$ surface and of 20.8 kcal/m on the $1^2A''$ surface. On breaking the C_{3v} symmetry, the ion-pair minimum on the $2^2A'$ surface dissociates to O + H_2 + H without a barrier as illustrated in Fig. 5.

The dissociation pathways linking $1^2A'$ to OH + H_2 and to H_2O + H, and linking $1^2A''$ to OH + H_2 are under active investigation using MCSCF analytic gradient techniques. A negligible barrier (<2kcal/m) has beeen found for dissociation of $1^2A'$ to H_2O + H, as reported previously.[1] An interesting double transition state, characterized by two imaginary frequencies, leading to both OH + H_2 and to H_2O + H, has been identified approximately 15 kcal/m above $1^2A'$. Finally, quite preliminary results indicate a barrier of appoximately 30 kcal/m in the dissociation of $1^2A''$ to OH + H_2.

Calculations probing the methodology may be summarized as follows: (1) Energy differences calculated with the economical first order CI (FOCI) expansion have been compared to those obtained with the far more costly second order CI (SOCI) method. An uncertainty of 7 kcal/m due to use of the smaller CI expansion has been obtained. (2) The ability of the basis set used for oxygen to describe the electron affinity of the oxygen atom has been probed. A qualitatively correct result is obtained. (3) The reliability of the FOCI description of the excited state wavefunction using ground state MCSCF molecular orbitals in regions where the first and second states are very different in character has been verified by comparison with calculations in which the MCSCF orbitals were optimized for the second state and in which a larger MCSCF active space was used.

In this study we have found the MCSCF/FOCI procedure provides an economical reliable approach for characterizing previously unknown potential surfaces. Construction of the correlation diagram at an early stage guides investigation of the important dissociation pathways. In the H_3O system, two local minima (C_{3v}) on the excited potential surface have been identified. The higher (ion-pair) minimum decays without a barrier to O + H_2 + H. The $2^2A'$ state, 98.8 kcal/m above H_2O + H, is predicted to be stable with respect to dissociation. It, however, is Jahn-Teller coupled to $1^2A''$ state which correlates to OH(X) + H_2. Preliminary results give a barrier of 30 kcal/m in this dissociation path. A more accurate determination of this barrier will conclude our study of H_3O.

1. K. S. E. Niblaeus, B. O. Roos, and P. E. M. Siegbahn, Chem. Phys. 25, 207 (1977).

†Work supported by AFAL under contract F04611-86-C-0070.

Table I. Optimized geometries (a_o)

State	Distances[a]		Symmetry	Energy above H_2O+H (kcal/m)
$1^2A'$	O-H	1.986	C_{3v}	28.9
	H-H	3.052		
$2^2A'$ }	O-H	2.177	C_{3v}	103.7
$1^2A''$ }	H-H	3.350		
$2^2A'$	O-H1	2.227	C_{2v}	98.8
	O-H2	2.074		
	H1-H2	3.350		
	H2-H3	3.040		
$1^2A''$	O-H1	1.851	C_s	82.9
	O-H2	2.513		
	H1-H2	3.319		
	H2-H3	3.509		
$2^2A'$ }	O-H	3.627	C_{3v}	143.9
$1^2A''$ }	H-H	1.650		
upper minimum (ion-pair)				

[a] H2 and H3 are symmetric in all cases. C_s plane bisects ∠H2H1H3.

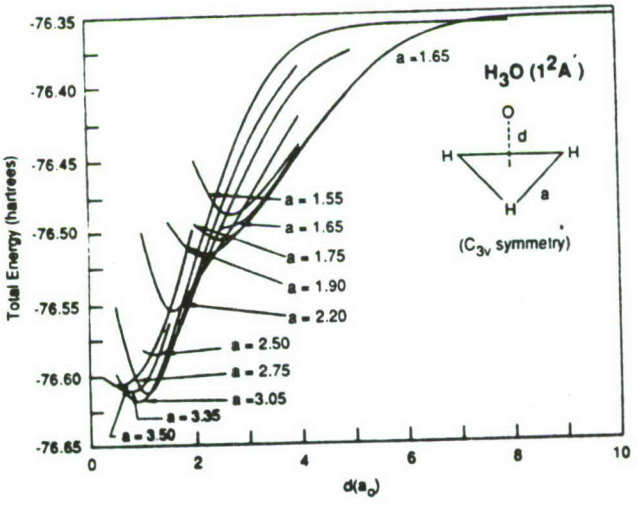

Fig. 1. Cuts through $1^2A'$ potential surface at fixed H-H distance as function of vertical distance.

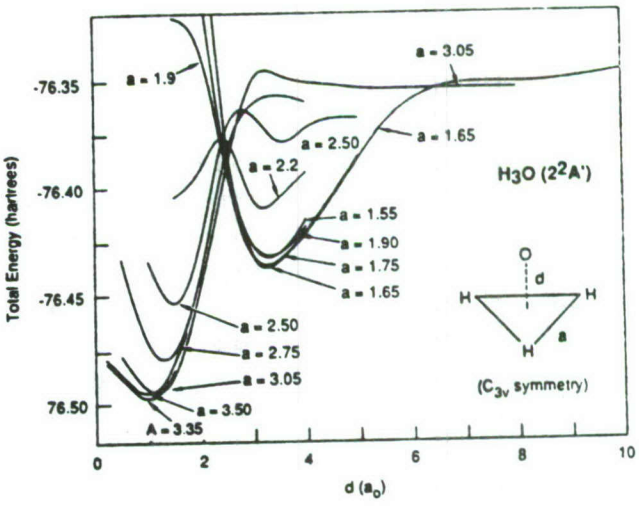

Fig. 2. Cuts through $2^2A'$ potential surface at fixed H-H distance as function of vertical distance.

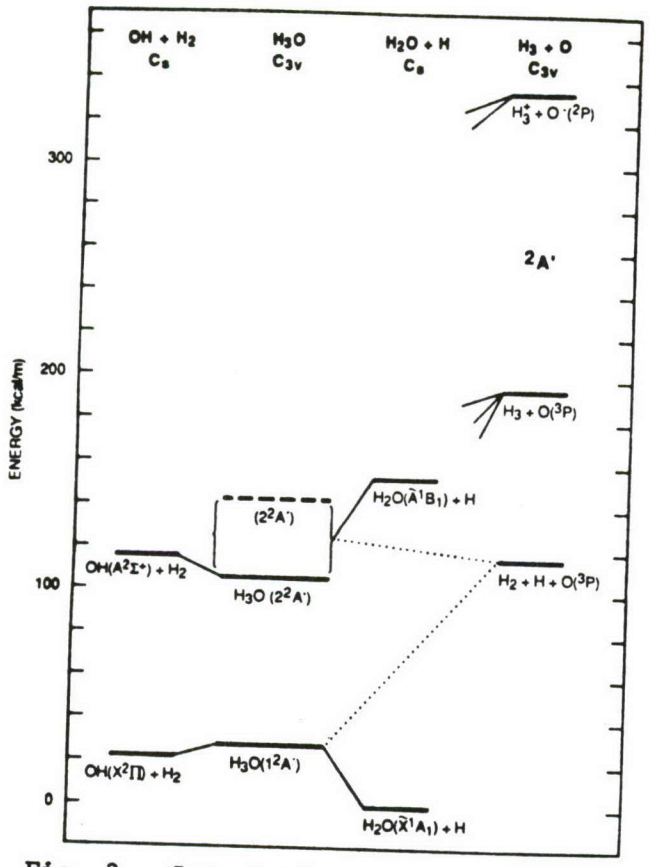

Fig. 3. Correlation diagram for H_3O $^2A'$ states. H_3O energies are minima in C_{3v} (equilateral triangle) geometries.

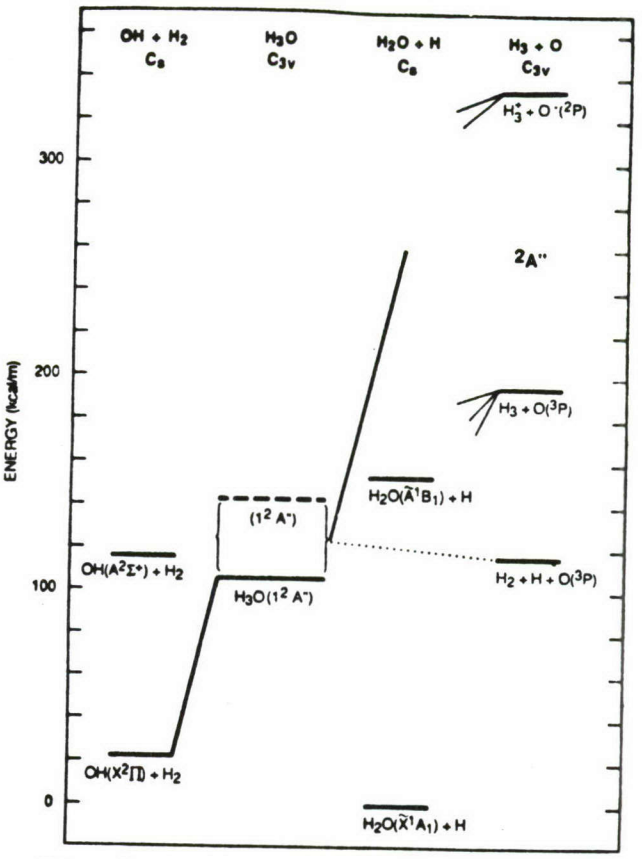

Fig. 4. Correlation diagram for H_3O $^2A''$ states. H_3O energies are minima in C_{3v} (equilateral triangle) geometries.

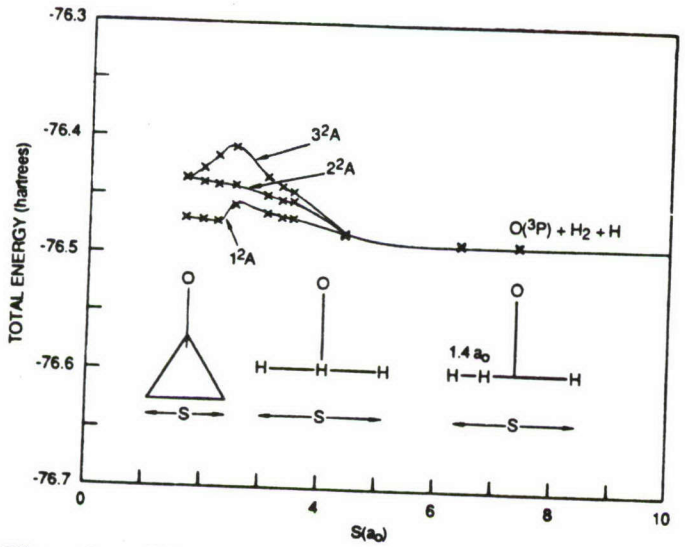

Fig. 5. Dissociation of H_3O upper minimum in C_{3v} $^2A'$ surface (a = 1.65 a_o, d = 3.5 a_o) to $O(^3P)$ + H_2 + H as a function of pseudo-reaction coordinate. DZP/FOCI calculations in C_1 symmetry.

Multiresonant Spectroscopy and the Dynamics of Molecular Superexcited States

Edward R. Grant
Department of Chemistry
Purdue University
West Lafayette, IN 47907

With internal energies near and above first ionization potentials, corresponding to 2-3 times the energy of a typical chemical bond, molecular superexcited states characteristically exhibit a rich dynamics of competing pathways for unimolecular decay. At the same time, the formal description of states at such energies is characteristically simplified by the applicability of appropriate zeroth order separations. Among the most successful of these is the Rydberg approximation, in which a state prepared near a first ionization threshold is assembled from a cation in a well defined internal state together with an electron in a diffuse, weakly interacting hydrogenic orbital. This is a convenient separation with particularly important implications for spectroscopy. In an ideal Rydberg limit, vibration rotation fine structure observed in an electronic transition is simply that of the cation core shifted down by the binding energy of the electron. Transitions to Rydberg states from neutral ground states exhibit Franck-Condon factors that match corresponding transitions from ground states to vibrational levels of corresponding ions, as observed for example in photoelectron spectra. Franck-Condon factors for Rydberg-Rydberg and Rydberg-continuum transitions are perfectly vertical in this limit.

A great deal of recent experimental evidence, in the form of absorption spectroscopy to Rydberg levels from neutral ground states, from lower Rydberg states, and from Rydberg states to the continuum, has secured this description for ion cores whose geometries lie in Franck-Condon corridors for transitions from accessible levels of the ground state. Deviations, then, which may take the form of perturbations in spectral positions and short lifetimes with respect to various accessible fragmentation routes (eq. predissociation, autoionization or ion pair production) can be cast in terms of electron core inelastic and reactive scattering. Formal constructs exist within which it is readily possible to approach such dynamics from this point of view. More generally the study of superexcited intramolecular dynamics is an area in which a rapid growth can be expected, propelled in particular by concerns with the storage of energy in chemically bound excited states, as well as the fundamental potential of this field as a common ground in which well established

theories of radiationless processes combine with those of coloumb scattering to address the problem of high-energy intramolecular relaxation in a universal class of systematically related electronic states.

Our work in the first five months of AFOSR support has focussed on the development of multiresonant multiphoton methods for the isolation of and dynamical characterization of individual rovibronic states at 9 eV in a prototypical polyatomic molecule, NO_2. Our story begins with a characterization of the low lying (55,000 cm^{-1}), long-lived 3pσ Rydberg state of NO_2 by conventional two-photon spectroscopy. At photon energies required for this process, a real intermediate state exists which is dissociative. The presence of this intermediate system has the effect of opening the Franck-Condon envelope thus facilitating the overall bent-to-linear transition. Rotational structure characteristic of the long-lived linear excited state is resolved but its congestion, even under beam conditions, together with the low yield associated with pumping through a dissociative intermediate state limits the utility of one-color two-photon photopreparation as a step which is effective for subsequently reaching higher Rydbergs. Much higher yield and greater selectivity is achieved by using two-colors, in which the first frequency excites the system to a discreet level of the bound visible excited state system. The celebrated highly mixed nature of these states is as effective as the dissociative continuum in bridging the Franck-Condon gap, and, additionally, discreet double resonance affords the opportunity to select a small subset of rotational transitions, from which it is readily possible to isolate an individual rotational level for promotion by absorption of a third tunable photon to high Rydberg and autoionizing states. The spectrum of this subsequent absorption also serves an immediate function of confirming rotational assignments (by exhibiting identical structure following each of a pair of separate transitions assigned to terminate on the same 3pσ Rydberg rotational state.)

Having confirmed rotational assignments for various vibrational levels of the 3pσ Rydberg state, we focus on the dynamical information content of spectra from specific rotational levels of vibrationally excited 3pσ Rydbergs, to autoionizing levels above the adiabatic ionization threshold.

Figure 1 shows a succession of such spectra taken from the two-color two-photon photoselected N=1 (R=0) level of the (110) vibrational band of the 3pσ Rydberg state.

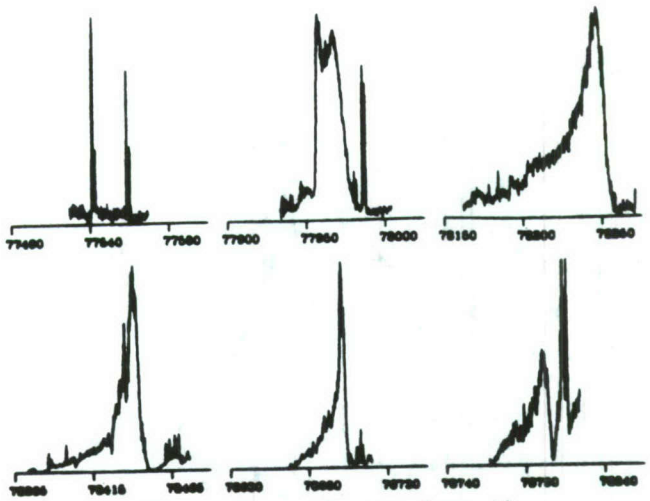

These transitions can be assigned to series of the same combination-band vibrational level in successive Rydberg electronic states of principal quantum number n = 8, 9, 10, 11, 12 and 13.. All of these states lie above the adiabatic ionization threshold of NO_2 (77320 cm^{-1}). Below 77970 cm^{-1}, excited NO_2 can autoionize by transferring the core vibrational energy associated with excited quanta of both ν_1 and ν_2 to the Rydberg electron. This process is evidently slow as evidenced by the sharp structure of the band at 77550 cm^{-1}. Energies above 77970 are sufficient to produce an ion excited with one quantum of ν_2, and so autoionization by a $\Delta v = -1$ transition in symmetric stretch, ν_1, is possible. This clearly broadens the linewidths associated with one of the rotationally selected Rydberg bands, but not the other, at least to a measurable degree.

To higher energy, the distinction between pairs of Rydberg states becomes less clear, and the distorted lineshape seen at the n = 9 threshold gives way to a well developed Fano profile. These proceed to narrow with quantum number increasing from n = 13. Beyond n = 12 the threshold for production of an ion in vibrational state (1,0,0) is exceeded (thus permitting autoionization of photo-prepared Rydberg states by a $\Delta v = -1$ transition in bending, ν_2). No increase in linewidth is seen for n = 13, suggesting that bend is less effectively coupled than stretch to the Rydberg electronic degree of freedom. Figure 2 shows a sequence of scans of (110) states below and above the $\Delta v_1 = -1$ autoionization threshold for successive rotational states of ion rotational quantum number R = 1, 5 and 8. The sharp low-frequency onset is seen to recede indicating that rotational energy is effective in promoting autoionization.

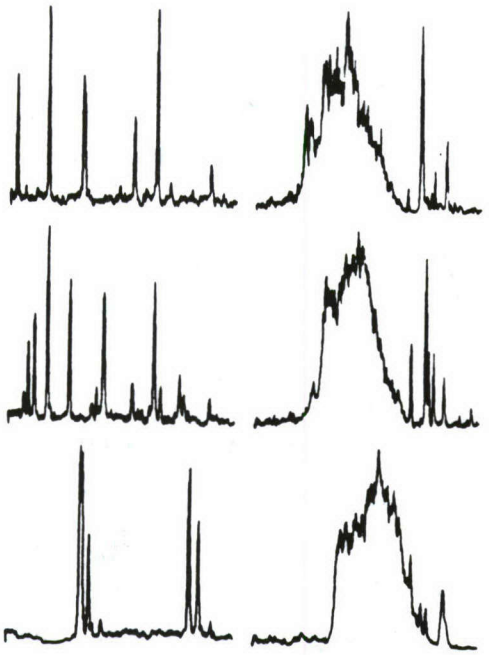

Three Laser Energy (cm−1)

Finally, Figure 3 shows a scan from 3pσ (1,1,0) R = O up to the vertical ionization threshold. The spectrum shows clearly the coalescence of series into single sets of rotational bands at successive principal quantum numbers evolving ultimately to regular convergent series as ℓ-uncoupling commences.

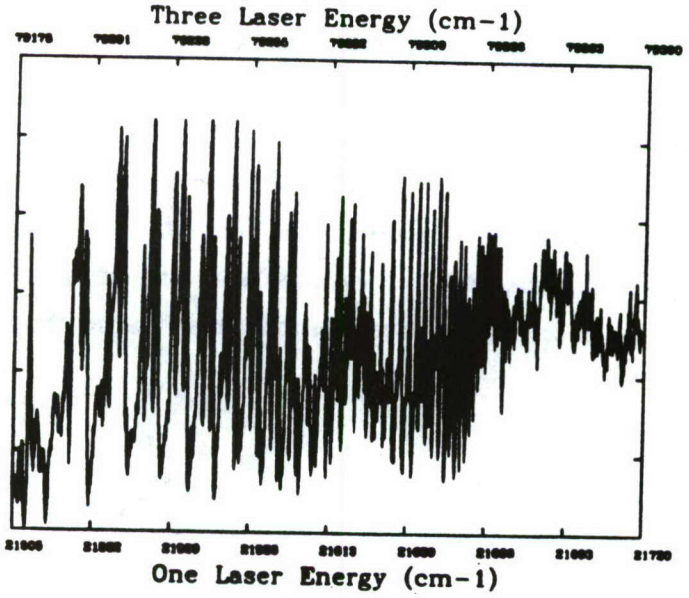

In summary, multiresonant excitation exploits the distinct Franck-Condon character of transitions from various intermediate states to resolve the spectroscopy and dynamics of NO_2 Rydberg states. Mixed optical states bridge bent-to-linear transitions $^2A_1 \rightarrow {}^2\Sigma_u^+$, and in double resonant transitions, select individual rotational states. Vertical Rydberg-Rydberg transitions isolate high series in various core vibrational states. Near the origin, $3p\sigma$ $^2\Sigma_u^+$ states are sharp and relatively long lived. Direct picosecond pump-probe experiments confirm long lifetimes for low Rydbergs, yielding $\tau \approx 150$ ps for (1,0,0). In the high Rydbergs, autoionization ($\Delta v \geq 1$) suggested by the prominence of series above the adiabatic IP, but lifetimes are long for all but $\Delta v = -1$ in ν_1 (symmetric stretch). Bands are broadest just above threshold. Linewidths are not dramatically affected by core rotational quantum state, but some evidence exists that rotational energy contributes to promote autoionization. Very high Rydberg series in selected vibrational and rotational states show manifestations of ℓ-uncoupling.

Research sponsored by the Air Force Office of Scientific Research under Contract F49620-87-C-0092.

Laser and Fourier Transform Spectroscopy of Novel Propellant Molecules

F 04611-87-K-2000

P. F. Bernath
Department of Chemistry
University of Arizona
Tucson, AZ 85721

We are exploring the spectroscopy of Rydberg molecules such as XeH and He_2. The ground state potential curves of Rydberg molecules have only shallow van der Waals minima. The strongly bound Rydberg excited states have ionic cores, XeH^+ and He_2^+, with a single weakly bound Rydberg electron.

A. He_2

The Fourier transform spectrometer of the National Solar Observatory at Kitt Peak was used to record infrared electronic emission spectra of XeH and He_2. For He_2 0-0 and 1-1 bands of the $b^3\Pi_g - a^3\Sigma_u^+$ transition was observed near 4700 cm^{-1} at 0.01 cm^{-1} resolution. The spectrum of He_2 was excited in a Ni hollow cathode operated at 280mA. A flow of He gas at 4 torr pressure was maintained through the cathode. The precision of our measurements was ±0.001 cm^{-1}.

Our measurements on He_2 fully resolve the triplet splittings of the $b^3\Pi_g - a^3\Sigma_u^+$ transition. These high-

resolution observations provide a very precise set of molecular constants for He_2, including Λ-doubling constants for the $b^3\Pi_g$ state. Interpretation of the fine structure and Λ-doubling constants provide some insight into the electronic structure. For example, the $b^3\Pi_g$ state is in accidental pure precession with the nearby $c^3\Sigma_g^+$ state. The observed line positions, spectroscopic constants and other details are available in a paper to be published in *Molecular Physics*.

B. XeH

The XeH Rydberg molecule was observed with the same techniques used for He_2. Instead of He, a slow continuous flow of 2.2 torr of H_2 and 100 mtorr of Xe was maintained through the Ni hollow cathode lamp. The resolution of the Fourier transform spectrometer was 0.02 cm^{-1}.

The 0-0 vibrational bands of two new infrared electronic transitions were observed: The $D^2\Sigma^+ - C^2\Pi$ transition near 4420 cm^{-1} and the $C^2\Pi - B^2\Sigma^+$ transition near 3250 cm^{-1}. A rotational analysis provided spectroscopic constants for the states connected by these transitions. A paper on these observations is in press in *Molecular Physics*.

C. BH

The vibration-rotation emission spectrum of the BH $X^1\Sigma^+$ state was observed with the McMath Fourier transform spectrometer at Kitt Peak. The 1-0, 2-1 and 3-2 bands were observed in a microwave discharge of 1 torr of B_2H_6 in 0.016 torr of He. Although there are previous measurements of

electronic spectra of BH, this work represents the first observation of the vibration-rotation spectrum. Spectroscopic constants of the individual vibrational levels and equilibrium molecular constants were determined. An RKR potential curve was calculated from the equilibrium constants. More details are available in a paper to be published in the *Journal of Molecular Spectroscopy*.

D. N_3

The antisymmetric stretching vibration, ν_3, of N_3 was measured in absorption near 1645 cm^{-1}. No previous high-resolution infrared measurements for this very energetic free radical are available. The spectrum of N_3 was recorded in absorption with the unique fast flow White cell of C. Howard of NOAA in Boulder, Colorado, with a BOMEM Fourier transform spectrometer. The N_3 radical was made by the reaction of Cl radicals and HN_3.

Molecular constants for the 000 and 001 vibrational levels of the ground $\tilde{X}^2\Pi_g$ state were determined. The vibrational frequency of 1645 cm^{-1} for the asymmetric stretch of N_3 was lower than expected by analogy with similar molecules. A complete report will be submitted to the *Journal of Chemical Physics* in the near future.

E. $CaBH_4$ and $SrBH_4$

The first gas-phase metal borohydrides were discovered by reaction of Ca and Sr vapors with diborane. The low-resolution laser spectra of $CaBH_4$ and $SrBH_4$ were recorded and a high-

resolution analysis is in progress. The low-resolution analysis is consistent with C_{3v} symmetry and the high-resolution analysis will provide a definitive molecular geometry.

F. SiC

The SiC molecule was discovered by observaticn of the $d^1\Sigma^+ - b^1\Pi$ electronic transition near 6100 cm^{-1} by Fourier transform emission spectroscopy (*Phys. Rev. Lett.* **60**, 197 (1988)). The SiC molecule was generated by sputtering in a composite-wall hollow cathode made by pressing Cu and SiC powders. *Ab initio* quantum chemical calculations confirm the identity of the carrier of the spectrum as SiC.

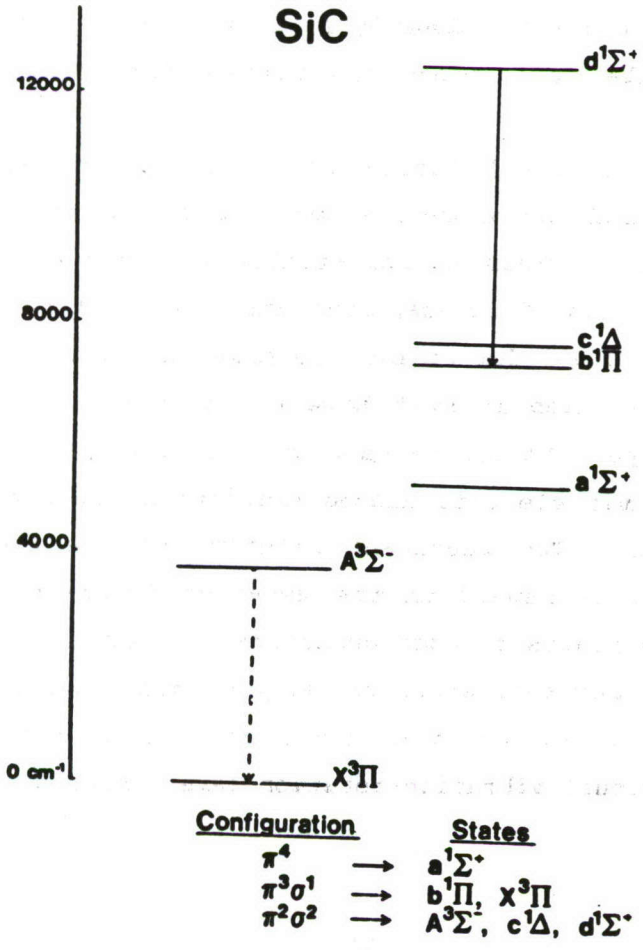

Theoretical Investigations of Metastable Molecular Systems

K. Kirby
Harvard-Smithsonian Center for Astrophysics

Air Force interest in the development of new rocket propulsion technology offers a particularly challenging opportunity to explore a class of energetic molecular systems about which little is known. Their potential utility as storable energy sources depends on their stability with respect to decay via radiation, ionization and dissociation. The quantity of interest in the evaluation of such materials is "specific impulse" which is proportional to the square root of the energy available for release divided by the mass. In order to increase specific impulse, one must maximize the energy available for the system while simultaneously minimizing the mass. These considerations lead one to identify small first-row diatomic and triatomic molecules as strong candidates for metastability studies.

Exploration of small first-row molecules as metastable systems using *ab initio* theoretical methods can be particularly advantageous. It provides an opportunity to explore molecular states and the details of interactions which have not before been investigated. In order for an excited molecular state to be of interest in our studies it must have a potential well (energy mimimum) with respect to separated atoms and the state must not be able to decay via electric dipole transitions to lower-lying electronic states. The resultant lifetime of the electronic state will therefore depend on the detailed interactions with other lower-lying states through operators such as spin-orbit or d/dR which cause predissociation or decay to radiative channels. The influence of nuclear motion on the coupling and therefore the lifetime of individual vibration-rotation levels must be explored

to see if particular vibrational energy levels may be very long-lived due to unfavorable Franck-Condon overlaps or the variation in magnitude of the coupling matrix element with internuclear separation.

High-spin multiplicity molecular states arising from ground state atoms may be a fruitful class of systems to investigate for a number of reasons. Recent advances in studies of spin-polarized hydrogen have spawned interest in other spin-polarized systems such as nitrogen. Predissociation, as a decay route, can be eliminated by considering metastable states which dissociate to ground state atoms. States of high-spin multiplicity (quintets, sextets, septets) are virtually unknown. Two familiar molecules which have high-spin states are: CO with quintet states arising from $C(^3P) + O(^3P)$, and CN with sextet states arising from $c(^3P) + N(^4S)$. In minimal basis set studies[1,2] made many years ago, there appeared to be at least .3eV of binding for the lowest $^5\Sigma^+$ and $^6\Sigma^+$ states in CO and CN, respectively. However, recent work of Konowalow and Rosenkrantz[3] showed that for CO, this potential well was due to basis set superposition error, and that the binding was more likely $\sim 700 cm^{-1}$. This well-depth does support at least seven vibrational levels. We are preparing to investigate the $^6\Sigma^+$ and $^6\Pi$ states of CN. This work will also include obtaining the quartet states of CN and determining the possible decay rate through spin-orbit interaction.

Doubly-charged molecular ions represent another very interesting class of energetic species which is largely unexplored. In practical terms, ions may be controlled much more easily than neutral molecules. The CH^{+2} molecule came to our attention due to recent studies, both experimental and theoretical, which both confirm and deny its existence. In charge-stripping experiments on methane in 1981, Ast, Porter, Proctor and Beynon[4] claim to have observed CH^{+2} with a lifetime of at least 3-4 μsec. In 1983 Butler, Guberman and Dalgarno[5], in

studying the charge-transfer of C^{++} with H, calculated the relevant $^2\Sigma^+$ potential curve which appeared unusually flat. However, due to the sparsity of calculated points at small internuclear separations, the existence of a potential minimum could not be confirmed or ruled out. In 1984, Wetmore, Boyd and LeRoy[6] specifically constructed a large basis set configuration interaction (CI) calculation to look for a potential minimum in CH^{+2}. They found a slight dip of ~.01eV, but their uncertainties were estimated at ~±.3eV. With an even larger basis set, they found the dip disappeared. In 1986 and 1987, Mathur *et al.*[7,8] reported using translational energy loss spectrometry to observe CH^{+2} produced by charge-stripping collisions of CH^+ with Kr. Also in 1987, Friedman, Preston and Dalgarno[9] constructed an empirical modification of the calculated potential curve of Butler, Guberman and Dalgarno[5] which contained a minimum with well-depth of ~1eV, which was necessary in order for the state to have a lifetime of 3 μsec. At the end of 1987 Koch *et al.*[10], in a combined experimental and theoretical paper, concluded that CH^{+2} did not exist and claimed that new charge-stripping mass spectrometry experiments showed no CH^{+2}. This was supported by *ab initio* calculations on the three lowest $^2\Sigma^+$ states of CH^{+2}, using a large basis set and complete single- plus double-excitation CI from the full valence space. Finally, in 1988 Hamdan *et al.*[11] claim evidence for an excited metastable state of CH^{+2} lying 12.3 eV above the disputed ground electronic state.

Of the three lowest-lying separated atom states: $C^+(^2P) + H^+$, $C^+(^2D) + H^+$ and $C^{++}(^1S) + H(^2S)$, only the last one is expected to exhibit any kind of attractive well, due to the polarization of H by C^{++}. The others will be dominated by the repulsive coulomb interaction of C^+ and H^+. However, it is important to look carefully at the details, particularly because of the controversy. Using MCSCF and CI methods, we will identify the binding in the $^2\Sigma^+$ channel and examine the dipole transition

moment between the bound state and lower-lying $^2\Sigma^+$ states. In addition we will locate the $^4\Sigma^+$ and $^4\Pi$ states arising from $C^{++}(^3P) + H(^2S)$ as well as lower-lying quartets dissociating to $C^+(^4P) + H^+$, to see if any quartet states might be metastable. This five electron system offers the theorist a particularly favorable opportunity to decide the issue of the existence of CH^{+2} definitively.

References

1. S. V. O'Neil and H.F. Schaefer, J. Chem. Phys. **53**, 3994 (1970).
2. H.F. Schaefer and T.G. Heil, J. Chem. Phys. **54**, 2573 (1971).
3. D. Konowalow and M. Rosenkrantz, private communication.
4. T. Ast, C. J. Porter, C. J. Proctor and J. H. Beynon, Chem. Phys. Lett. **78**, 439 (1981).
5. S. E. Butler, S. L. Guberman and A. Dalgarno, Phys. Rev. A **16**, 500 (1977); T. G. Heil, S.E. Butler and A. Dalgarno, Phys. Rev. A **27**, 2365 (1983).
6. R. Wetmore, R. K. Boyd, and R. J. LeRoy, Chem. Phys. **89**, 329 (1984).
7. D. Mathur, C. Badrinathan, F.A. Rajgara, and U.T. Raheja, Chem. Phys. **103**, 447 (1986).
8. D. Mathur and C. Badrinathan, J. Phys. B. **20**, 1517 (1987).
9. R. Friedman, S. Preston, and A. Dalgarno, Chem. Phys. Lett. **141**, 469 (1987).
10. W. Koch, B. Liu, T. Weiske, C. B. Lebrilla, T. Drewello, and H. Schwarz, Chem. Phys. Lett. **142**, 147 (1987).
11. M. Hamdan, A. G. Brenton and D. Mathur, Chem. Phys. Lett. **144**, 387 (1988).

HIGH ENERGY DENSITY MATERIALS CONTRACTORS MEETING

28 February - 2 March 1988

The Role of Long Range Interactions in the Stabilization of Highly Energetic Molecules

James E. Bohr

NRC Research Associate

Air Force Astronautics Laboratory/YSX

Edwards AFB, CA 93523-5000

Some molecules in excited states may have potential use in energy storage and delivery. The excited molecule must be weakly bound, yet highly stabilizable. If both the excited state and the ground state correspond to the same asymptotic dissociation fragments, a transition induced between them will deliver essentially the entire binding energy of the ground state to the surroundings. However, in order for this type of molecular system to store energy, the probability of spontaneous transitions between the two states must be very low. It is likely that a sample made up entirely of excited state molecules will undergo rapid decay to ground state molecules. One possible method of stabilizing the excited state and reducing the probability of spontaneous decay to the ground state is to surround it with rare gas atoms or molecular hydrogen, either in a liquid or solid matrix.

The energy of interaction between the excited molecule and the stabilizing species must be calculated to determine whether such a system is viable, and what its optimum characteristics should be. This will undoubtedly be a weakly interacting van der Waals system, requiring computational accuracy to many significant figures. Thus, configuration interaction (CI) studies would prove to be prohibitively expensive except for very small systems. To

overcome this problem a hybrid variation-perturbation scheme can be used. A self-consistent field (SCF) calculation is carried out on the supermolecule (excited state molecule plus stabilizing species), to which is added the long range dispersion interaction energy between the two, to give the total interaction energy:

$$\Delta E^{AB} = \Delta E^{AB}_{SCF} + \Delta E^{AB}_{disp} . \qquad (1)$$

The SCF energy contains electrostatic and induction interactions plus some exchange effects, while the dispersion energy approximates the effects of electron correlation.

How is the dispersion energy computed? Typically, overlap of the charge distributions of the interacting species is ignored, and the dispersion energy is written as an inverse power series in the separation R:

$$\Delta E^{AB}_{disp} = \Sigma_n C_n R^{-n} , \qquad (2)$$

where the summation runs from n = 6 to infinity. The van der Waals coefficients C_n are independent of R and are related to the polarizabilities of the individual species involved in the interaction. These are measurable properties, so the C_n can be easily determined.

However, this series is divergent for any finite value of the separation R! This is because some overlap of charge distributions does occur for all but infinite separations. The charge overlap tends to reduce or damp the energy of interaction. Thus Eq. (2) overestimates the dispersion energy, especially at small separations where overlap is greatest. If overlap effects cannot be ignored, and Eq. (2) is divergent, why use it at all? In practice the divergence can be avoided by truncating the series after a few terms. Also, the physical interpretation that this equation allows is very appealing. One way to incorporate the effects of charge overlap while retaining the form of Eq. (2) is to introduce damping functions χ_n, and writing the damped dispersion energy as:

$$\Delta E^{AB}_{dd} = \Sigma_n C_n R^{-n} \chi_n(R) . \qquad (3)$$

The $\varkappa_n$ have the following limiting behavior:

$$\lim_{R\to\infty} \varkappa_n = 1 , \tag{4}$$

and

$$\lim_{R\to 0} R^{-n} \varkappa_n = 0 . \tag{5}$$

Thus at infinite separation the usual dispersion series of Eq. (2) is recovered, while at finite distances the series is convergent.

Several semi-empirical damping functions have been developed. However these depend on the availability of reliable experimental data and so have little predictive value. Following the method of Koide [1], Krauss and coworkers derived from first principles expressions for the damped dispersion energies for atom-atom systems [2]. Rosenkrantz has extended the method to the interaction of atoms with diatomic molecules [3]. The theory begins with the second-order perturbation expression for the dispersion energy:

$$\Delta E^{AB}_{disp} = - \sum_{\substack{a\neq 0 \\ b\neq 0}}^{z} \frac{|\langle \psi^o(A)\ \psi^o(B)|V^{AB}|\psi^a(A)\ \psi^b(B)\rangle|^2}{(E^A_o - E^A_a) + (E^B_o - E^B_b)} \tag{6}$$

where V^{AB} is the interaction potential between the species A and B, given by

$$V^{AB} = \sum_{a,b}^{z} \frac{1}{|\underline{R} - \underline{r}_a + \underline{r}_b|} \tag{7}$$

In this equation $\underline{R}$ is the vector from an origin in A to an origin in B, $\underline{r}_a$ is the vector from the origin of species A to one of its electrons a, and $\underline{r}_b$ is the vector from the origin in B to one of its electrons b. Thus the denominator of Eq. (7) is simply the distance separating electron a of fragment A and electron b of fragment B. The summation runs over all the electrons in each species A and B.

Taking the Fourier transform of Eq. (7), inserting it into Eq. (6), and identifying appropriate multipole operators and polarizabilities leads ultimately to expressions for the

dispersion energy which incorporate the damping effects of overlap automatically. The damping functions do not have an easily definable form; in practice they are found numerically by dividing the damped energy term by its corresponding undamped energy term at each interfragment separation. The numerical damping functions are found to have the correct limiting behavior.

The expression derived by Rosenkrantz for the atom-diatom damped dispersion energy is limited to the induced dipole-induced dipole interaction. We are extending her work to include higher order effects, including induced dipole-induced quadrupole, induced dipole-induced octopole, and induced quadrupole-induced quadrupole interactions. The method is also being used to formulate equations for the damped dispersion interaction energy of two diatomic molecules.

REFERENCES

[1] A. Koide, J. Phys. B9, 3173 (1976).

[2] M. Krauss, D.B. Neumann, and W.J. Stevens, Chem. Phys. Lett. 66, 29 (1979); M. Krauss, W.J. Stevens, and D.B. Neumann, ibid. 71, 500 (1980); M. Krauss and W.J. Stevens, ibid. 85, 423 (1982).

[3] M.E. Rosenkrantz, Ph.D. Dissertation; M.E. Rosenkrantz and M. Krauss, Phys. Rev. A32, 1402 (1985).

MODEL STUDIES OF CBES DECOMPOSITION

D.J. Benard, T.A. Seder, B.K. Winker and R.H. Cohn
Rockwell International Science Center
Thousand Oaks, CA 91360

ABSTRACT

The molecule fluorine azide (FN_3) can be thought of as a bound and stabilized complex of the singlet metastable NF^* radical and a ground state N_2 molecule. The molecule is highly energetic ($\Delta H_f \approx 120 - 130$ kcal/mole) and highly unstable. Other speakers (H. Michels and N. Brenner) will discuss the potential surface of this species in greater detail. Last year, we described methodology to safely generate small quantities of FN_3 in the laboratory via reaction of HN_3 with F_2 in the gas phase. We have recently published the details of the apparatus which are available from the AFAL upon request. Our work with FN_3 is funded by the AFAL and the AFWL as well as company IR&D and has the goals of (1) investigating the detonation physics of FN_3 with an eye towards stabilization, (2) enhancing the performance of existing propellant systems and (3) using FN_3 as a chemical source of electronic energy to drive a short wavelength laser system. In this presentation we shall concentrate primarily on the detonation physics but will touch briefly on the other activities, as well.

Thin films of FN_3 are produced by spraying the FN_3 gas (diluted in He) onto a CaF_2 substrate that has been cooled to 77°K in a vacuum chamber. Growth of the film is monitored by absorption of 420 nm

radiation. The films are typically 5 to 10 microns in thickness which corresponds to an energy density of 5 to 10 joules/cm^2. The films are detonated by application of a 1 mj/1 ns pulse of 337 nm radiation from a nitrogen laser, and a gated OMA is used to collect the corresponding emission spectra. The most intense emissions occur in the blue-green and near ultraviolet regions of the spectrum. In early experiments we found that intense CN(B - X) emission at 385 nm was obtained which we attribute to hydrocarbon impurities. Comparison of the detonation spectra to flame spectra in the F + CH_3 + HN_3/FN_3 flames showed a much higher ratio of CN(B) to CN(A) in the flame systems suggesting a more selective mechanism for excitation in the detonation. We postulate that this effect may be due to the generation of a "dark state" at or above 3.2 eV excitation which pumps the CN(B) state by energy transfer as opposed to the reactive pumping which occurs in the flames. By carefully cleaning our system the hydrocarbon impurities were significantly reduced, revealing two new bands in the 410-440 and 440-470 nm range which we have not been able to assign at the present time. Comparison of these features with different aperture times on the OMA reveals that the 410-440 nm feature is short lived, while the 440-470 nm feature grows in at longer times and is therefore definitely the result of secondary reactions. By collecting data for specific chemiluminescence features as a function of aperture time, approximate time profiles can then be obtained by differentiation. Since the radiative rate of the CN(B) state is fast compared to the characteristic time scale for its rise and fall, the precursor of the CN(B-X) emission is also shown to be a secondary reaction product since a rising and falling double exponential is observed, rather than a simple

exponential decay. In the visible region we also observe a strong band at 490 nm due to secondary reactions that is not assigned. This band is independent of hydrocarbon impurities and we have seen it in F + H_2 + FN_3 flames in a flowtube reactor. The expected NF(b - X) emission at 528 nm is smeared out to the blue, which can be attributed to high levels of vibrational excitation accompanying the detonation reaction. In contrast to the detonation [1] of PbN_3 there was no detectable N_2(B - A) emission.

The observed features have the appearance of diatomic emission spectra but do not fit any of the known bands of N_2 or F_2. The spectroscopy of NF is extremely limited; the a, b → X transitions are well known and the c → b transition has only recently been reported.[2] Calculations of the NF potential curves by Harvey Michels suggest that transitions from higher states to the a, b states would fall in the correct wavelength range to account for some of the emissions that we have observed, however, these calculations also show considerable deplacement of the potential energy curves which would result in broader and more complex emission spectra than we were obtained. Since our goal in studying the spectral and temporal properties of the detonation chemiluminescence is to gain an understanding of the underlying mechanism we would benefit greatly from theoretical support because the existing data base is too weak to support an interpretation based on prior experimental results.

When Haller first synthesized FN_3 in 1942, he discovered that it could be stabilized by adsorption on KF at room temperature.[3] The possibility therefore exists that similar stabilization may occur on highly polar propellants such as ammonium perchlorate (AP). Since FN_3 is

more energetic than AP a stabilized FN_3:AP oxidant could form the basis for an enhanced impulse propulsion system. Experiments are underway to determine if FN_3 is adsorbed on AP and whether the adsorbed FN_3 is sufficiently stable in this state to be used in propellant systems.

Since the central bond in FN_3 is the weakest, transfer of vibrational energy (from molecules such as HF or DF) to FN_3 may cause dissociation to metastable NF fragments that can be used to drive a laser.[4] We are investigating a laser concept which utilizes this principal with the advantage of in-situ release of the electronically excited species (no transport loss) and optical initiation (no mixing limitation on kinetics or disturbance of optical homogeniety in the laser cavity).

In summary, FN_3 continues to be an interesting high energy molecule with a variety of applications. In each case, however, there are aspects of the problem which require theoretical support with respect to barriers to thermal and vibrational dissociation, yields of fragment species and their emission spectra, and stabilizing interactions of FN_3 with polar substrates.

REFERENCES

1. S. Rosenwaks, Beer-Sheva University, Israel, private communication.
2. H. Obase, M. Tsuji and Y. Nishimura, Chem. Phys. Letters 126 (1986) 134.
3. J.F. Haller, Ph.D. Dissertation, Cornell University, 1942.
4. D. Patel, A.T. Pritt and D.J. Benard, J. Phys. Chem. 90 (1986) 1931.

THEORETICAL STUDIES OF HIGHLY ENERGETIC CBES MATERIALS

Contract No. F04611-87-K-0026

QUARTERLY PROGRESS REPORT

December 1, 1987 - February 29, 1988

Work during the past three months of this project has concentrated on FN_3, Be_2B_2, and O_4. Substantial progress has been made in all three of these areas. In particular, surface studies have commenced to determine why FN_3 sticks to KF surfaces but not to similar materials such as LiF and NaF. Preliminary calculations have already shown binding for FN_3 on KF, in agreement with experiment. More extensive calculations are currently under way, with results expected soon. These investigations will reveal the mechanism by which FN_3 adheres to surfaces and thereby enable one to predict the materials that can serve as substrates for the deposition of FN_3 layers. An understanding of this process will enable the production of energetically enhanced materials, with the FN_3 layers providing the additional energy. In addition, preliminary results have been obtained for the FN_3 triplet curve, in particular the point at which it crosses the singlet curve. The location of this triplet-singlet crossing is important in determining the FN_3 decomposition mechanism. In the case of the Be_2B_2 studies, cluster calculations have provided a strong indication that this material will form a stable solid. Cluster calculations on O_4 have also suggested that this material can be stabilized in the condensed phase. All of the above results are described in detail below.

I. FN_3

Recent experimental results, which have been reported to us by Walt Lauderdale and Dave Bernard, have shown that FN_3 sticks to KF surfaces but not to surfaces of LiF, NaF, $LiClO_4$, $KClO_4$, $NaBH_4$, or NH_4ClO_4 (AP). These results are quite interesting, particularly since LiF and NaF are very similar to KF. What is needed at this point is a detailed understanding of the mechanism by which FN_3 sticks to surfaces.

In order to investigate this mechanism, we have begun cluster calculations for FN_3 molecules on KF, NaF and LiF surfaces. Initial studies have focused on the (100) surface of these materials since this is the typical orientation of alkali halide surfaces. The (100) surfaces of KF, NaF and LiF are face centered cubic structures with lattice constants of 5.347, 4.620, and 4.0173 Å, respectively. Fig. 1 shows the (100) surface of KF. Also shown in Fig. 1 is an FN_3 molecule in the gas phase geometry (Fig. 2) which is parallel to the surface, with the F in FN_3 being directly above a K atom. Currently various distances from the surface and orientations of the FN_3 molecule are being considered in the cluster calculations in order to determine the configuration that is preferred energetically. Preliminary calculations have already shown binding for the configuration of Fig. 1 with a surface-FN_3 distance of 2.646 Å (which is close to the K-F distance on the surface). More extensive calculations are currently in progress. These calculations will yield the binding energy of FN_3 on KF and are expected to show that FN_3 is unbound on both NaF and LiF, thereby revealing the mechanism by which FN_3 binds to surfaces. A knowledge of this mechanism will be useful in the development of energetically enhanced materials.

Fig. 3 gives preliminary results for the FN_3 triplet curve. Also shown in the figure is the FN_3 singlet curve, which was computed previously (March 1 - May 31, 1987 Quarterly Progress Report). Both the triplet and singlet curves were obtained by geometry optimizations at the MP2 6-31G* level. As shown by the figure, the triplet-singlet crossing occurs just inside the peak of the singlet curve.

II. Be_2B_2

Extensive calculations have been done on clusters of Be_2B_2 in order to determine if this molecule will form a stable molecular solid. The molecular geometry used for Be_2B_2, which is the tetrahedral configuration given in Fig. 4, was obtained from Koop Lammertsma, who employed Gaussian 82 and the 6-31G* basis set to perform geometry optimizations at the MP4 level. Dr. Lammertsma also considered a rhombic structure for Be_2B_2 and found it to be 61 kcal/mole higher in energy than the tetrahedral structure. Based on these results, we chose the tetrahedron for use in the cluster calculations, since it is unlikely that crystalline forces could overcome an energy difference of 61 kcal/mole.

Several solid state packing structures were considered for the Be_2B_2 tetrahedron, including the ones given in Figs. 5 and 6. For the structure of Fig. 5, cluster calculations on the dimer and trimer of the Be_2B_2 tetrahedron showed that the dimer is bound with respect to the monomer and that the trimer is bound with respect to the dimer. For the Fig. 6 structure, calculations on the dimer containing the center tetrahedron showed that this dimer is also bound with respect to the monomer. Calculations on trimers of the Fig. 6 structure are currently in progress. The calculations completed thus far have led to the following conclusions:

1) Since all of the dimers and trimers considered thus far have shown binding, there is a high probability that Be_2B_2 will form a stable solid.

2) A possible structure for the Be_2B_2 solid is a combination of the Fig. 4 and Fig. 5 structures, in which the tetrahedrons are stacked in a column in the z direction (Fig. 4) and are arranged in a pattern similar to Fig. 5 in the x and y directions.

A search of the literature has provided further indications that Be_2B_2 can be stabilized as a molecular solid. The literature search has revealed that the crystal structure is known for the following Be-B compounds[1-3]:

Be_6B

Be_3B

Be_2B

BeB_2

BeB_4

BeB_6

BeB_8

BeB_{10}

BeB_{12}

The above Be-B compounds have a range of crystal structures including cubic fluorite, hexagonal, and tetragonal. The important point is that no crystal structure has been reported in the literature for Be_2B_2. Thus in the case of Be_2B_2, there is no known crystal structure that would be preferred energetically over a molecular crystal. This fact suggests that Be_2B_2 could be maintained in the form of a molecular solid.

III. O_4

As in the case of Be_2B_2, cluster calculations have been done on O_4 to study the possibility of forming a molecular crystal of this material. The primary O_4 geometry used in the cluster calculations, which is the twisted square configuration shown in Fig. 7, was obtained from Fritz Schaefer and Chuck Dlahous. This geometry was optimized at the CISD level with a DZP basis set. A square configuration was also considered in the cluster studies since the square was found to be only slightly higher in energy than the twisted square.

Calculations were done on several dimers of the twisted square, including those shown in Figs. 8 and 9. Calculations were also done on the cube and rectangular solid shown in Figs. 10 and 11, which are dimers of the square. The Fig. 9 and Fig. 11 dimers were found to be bound with respect to the monomer (the twisted square), with the Fig. 9 dimer being the most strongly bound, while the other dimers considered were unbound. Thus the O_4 calculations completed so far show binding for several configurations, indicating the possibility that O_4 can be stabilized as a molecular solid. Further O_4 calculations are needed in order to draw definite conclusions regarding this material.

[1]D. E. Sands, C. F. Cline, A. Zalkin and C. L. Hoenig, Acta Cryst. 14, 309 (1961).

[2]M. B. Khusidman and V. S. Neshpor, Porosh. Met. 10, 67 (1970).

[3]J. Stecher and F. Aldinger, Z. Metallk. 64, 684 (1973).

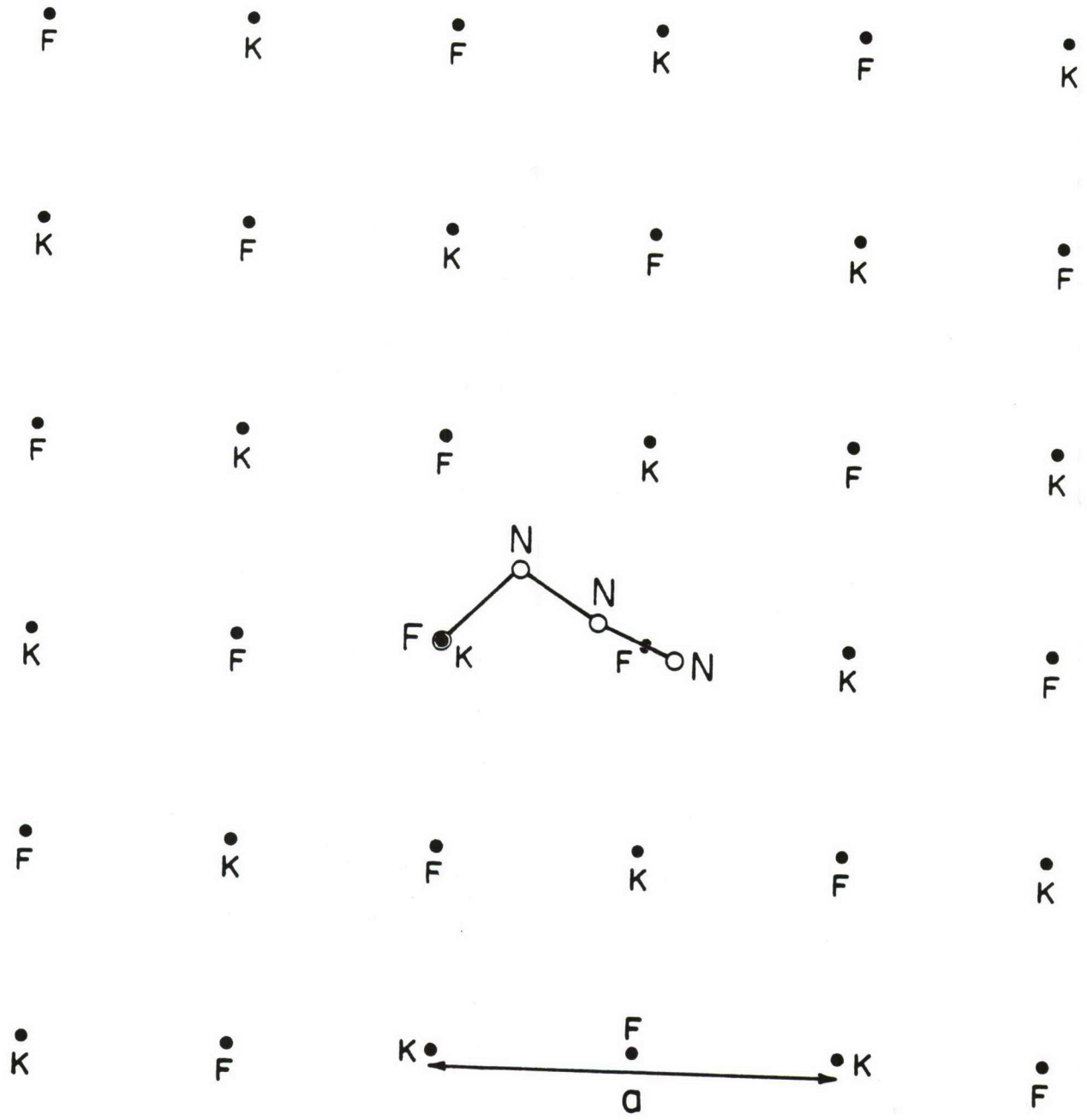

Figure 1. FN_3 molecule on a (100) KF surface. The lattice constant, a, of the KF surface is 5.347 Å. The FN_3 molecule is in the geometry of Fig. 2. Various distances from the surface and orientations of the FN_3 molecule are being considered in the calculations. The one shown in the figure is parallel to the surface, with the F in FN_3 being directly above a K atom.

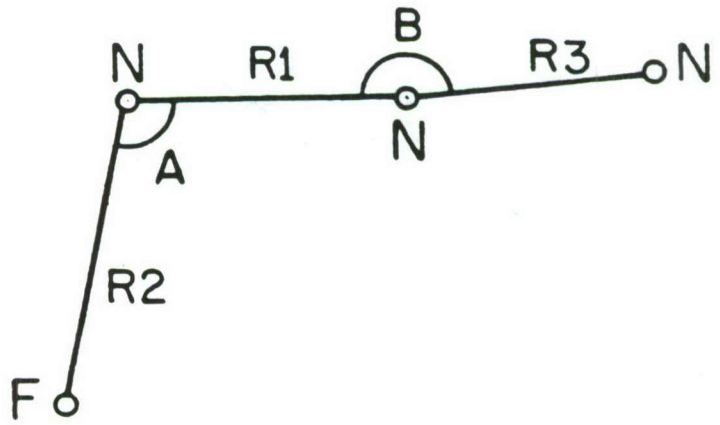

Figure 2. Ground state geometry of the FN_3 molecule. Geometry optimizations were done at the SCF 6-31G* level. The bond lengths (in Angstroms) and bond angles are given by

R1 = 1.2536
R2 = 1.3819
R3 = 1.0995
A = 104.33°
B = 173.99°

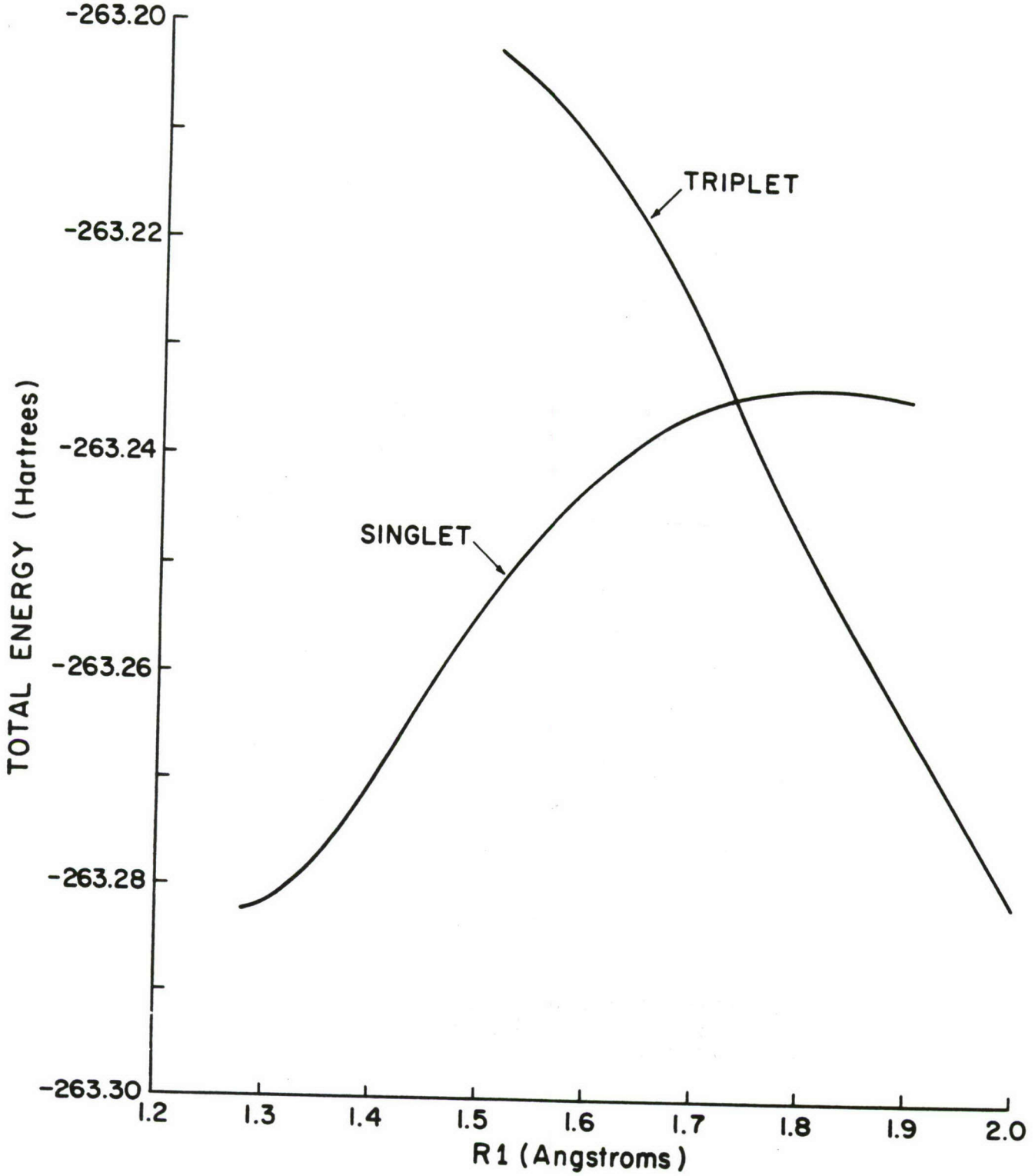

Figure 3. FN_3 singlet and triplet curves. Both curves were obtained by geometry optimizations at the MP2 6-31G* level. R1 is the central bond length, defined in Fig. 2. In the optimizations, R1 was held fixed while the rest of the geometrical parameters were optimized.

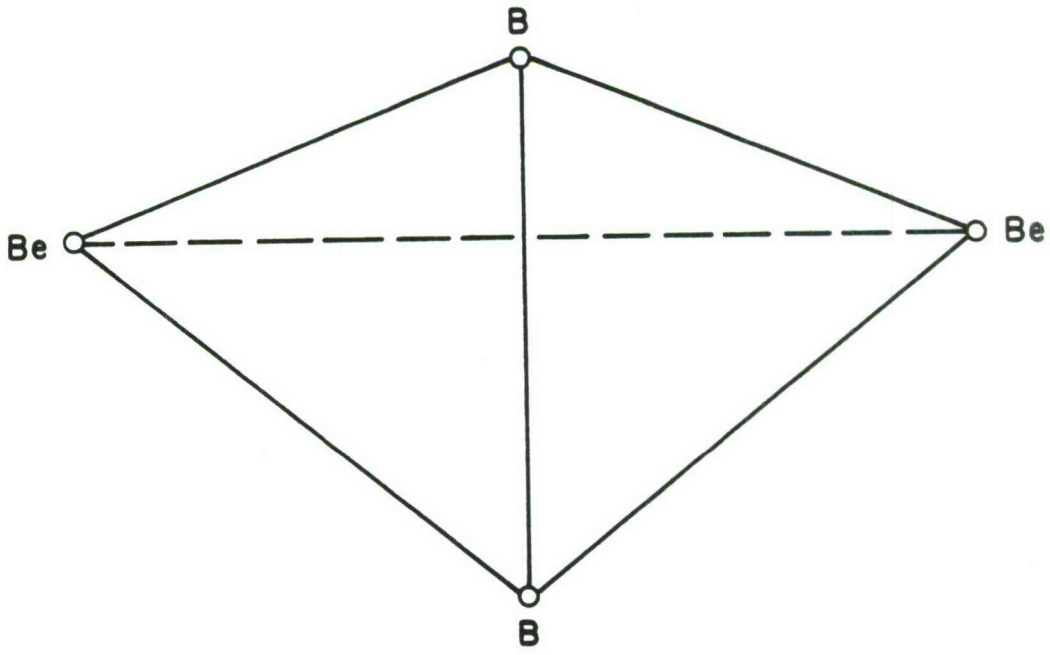

Figure 4. Be_2B_2 tetrahedron. This geometry was optimized at the MP4 6-31G* level. The Be-Be, B-B, and Be-B distances are 2.1565, 1.5478, and 1.7722 Å, respectively.

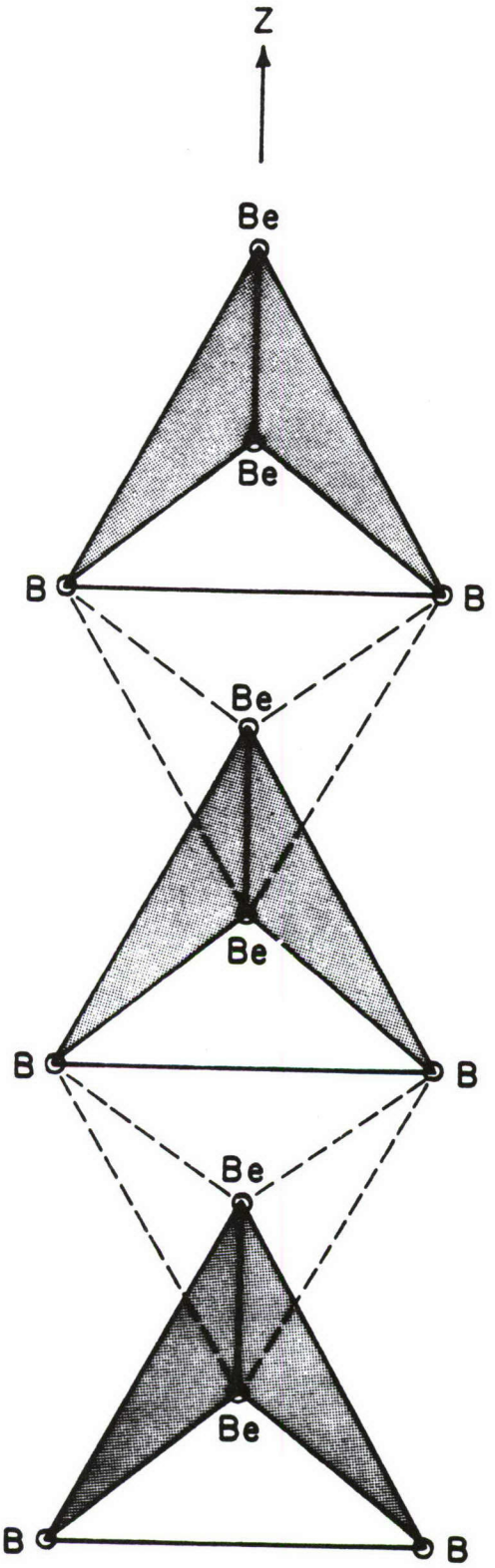

Figure 5. Packing structure for Be_2B_2 tetrahedrons in the z direction. The Be-Be lines at the top of the tetrahedrons are perpendicular to the z axis. The tetrahedrons are stacked in such a way that tetrahedrons with the Be-Be line at the bottom would fit between them, as indicated by the dashed lines.

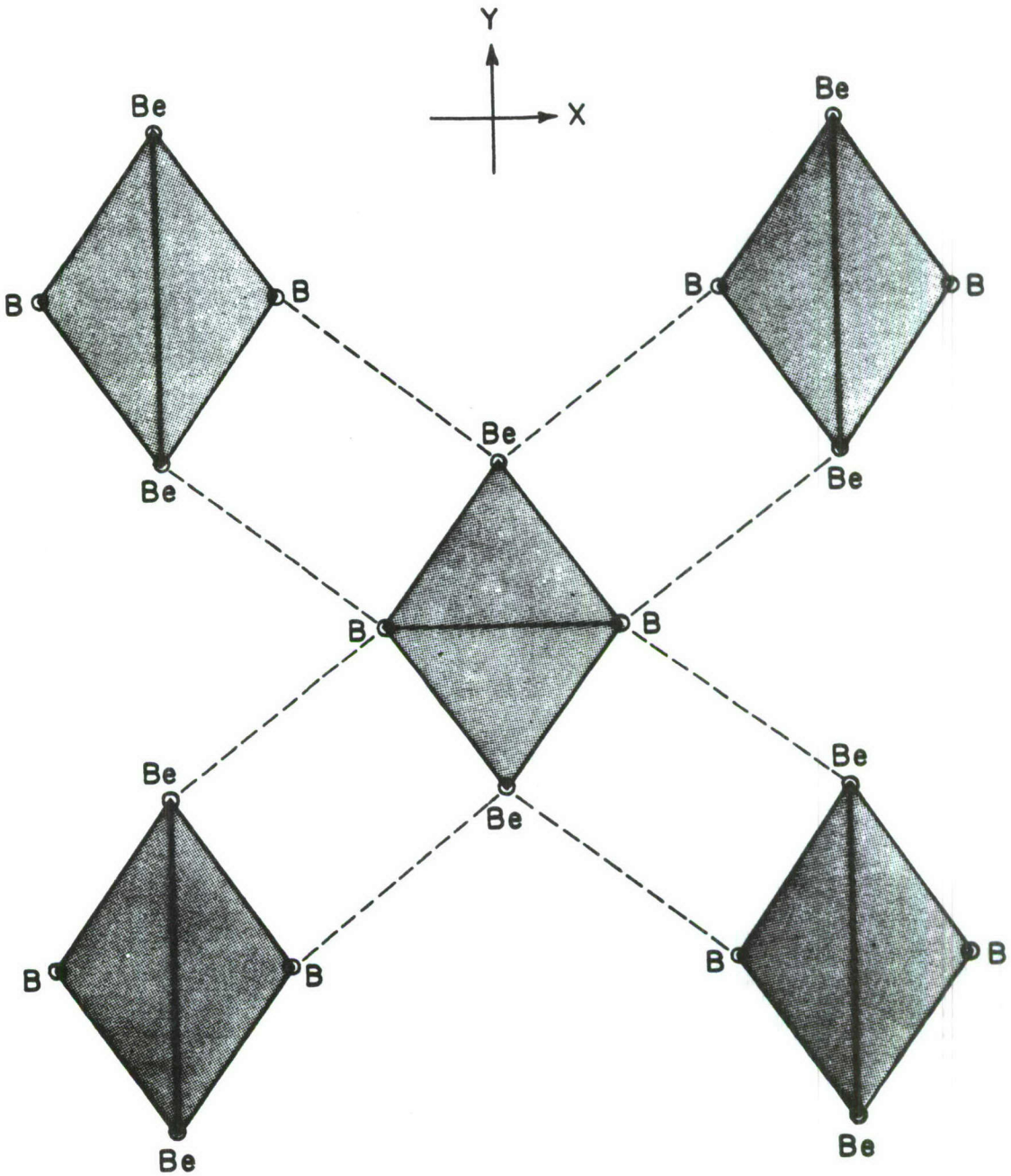

Figure 6. Packing structure for Be_2B_2 tetrahedrons in the x and y directions. The Be-Be and B-B lines are parallel to the x-y plane. In each of the tetrahedrons, the solid line (either a Be-Be or a B-B line) is at the top of the tetrahedron. These solid lines at the tops of the tetrahedrons are all in the same plane (which is perpendicular to the z axis). The tetrahedrons are packed such that the Be-B distance between neighboring tetrahedrons, indicated by the dashed lines, is the same as that for an individual tetrahedron (1.7722 Å). Also the Be-Be distance between the two tetrahedrons on the left and between the two tetrahedrons on the right is the same as that for an individual tetrahedron (2.1565 Å).

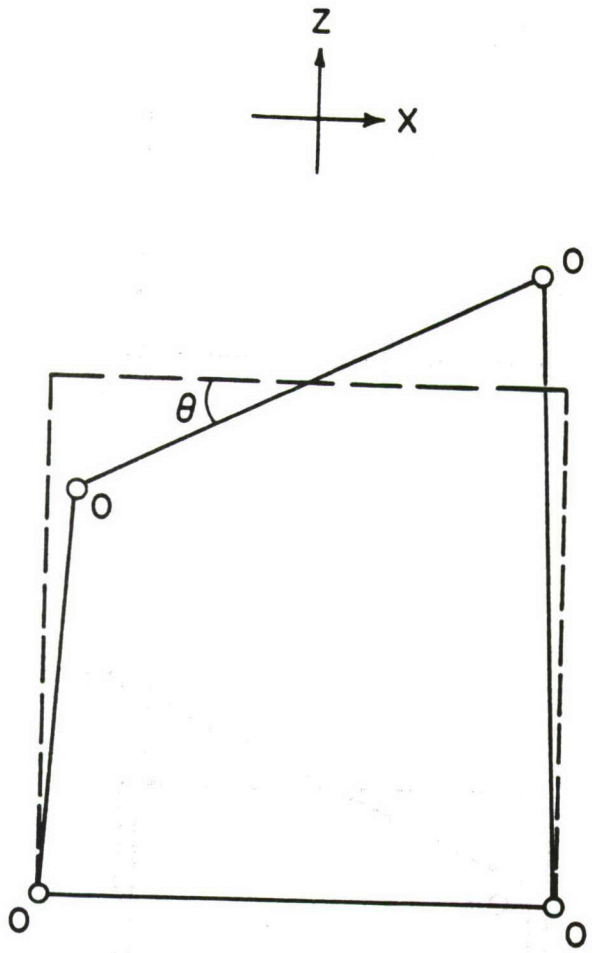

Figure 7. O_4 twisted square. This geometry was optimized at the CISD DZP level. The distance between neighboring O atoms is 1.4341 Å and the twist angle, θ, is 24.8°.

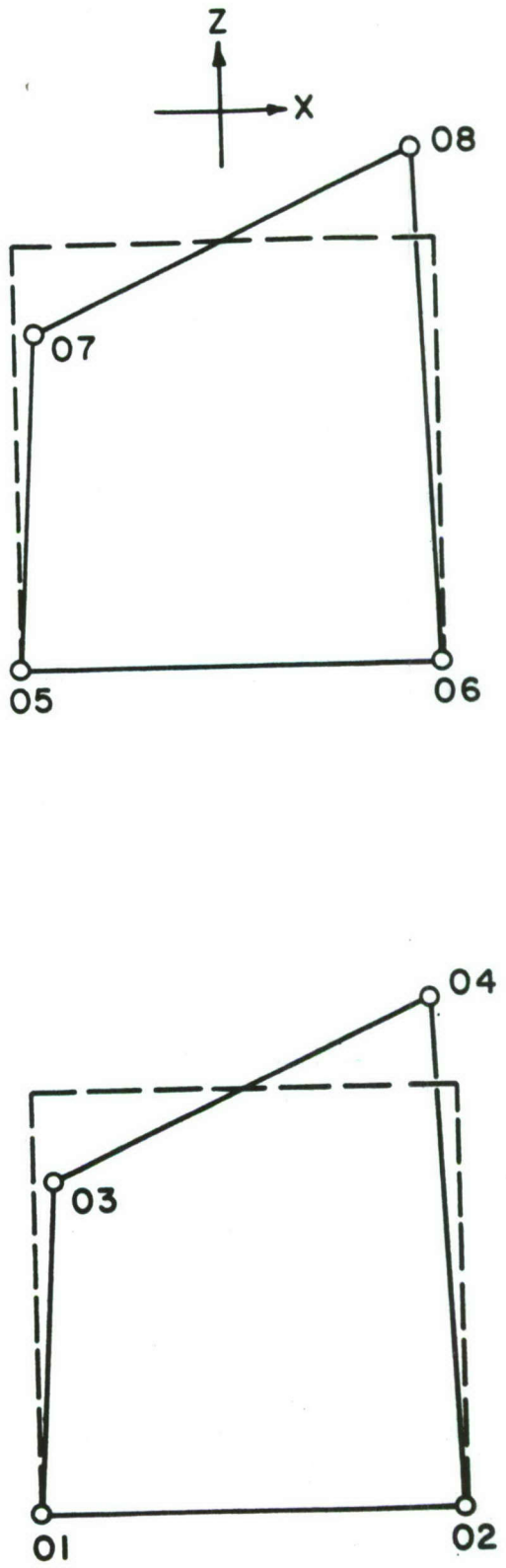

Figure 8a. Dimer of the O_4 twisted square. The two twisted squares are stacked in the z direction, with the rectangles, given by the dashed lines, being in the x-z plane. The distance between the twisted squares in the z direction is the same as the height (z dimension) of an individual twisted square.

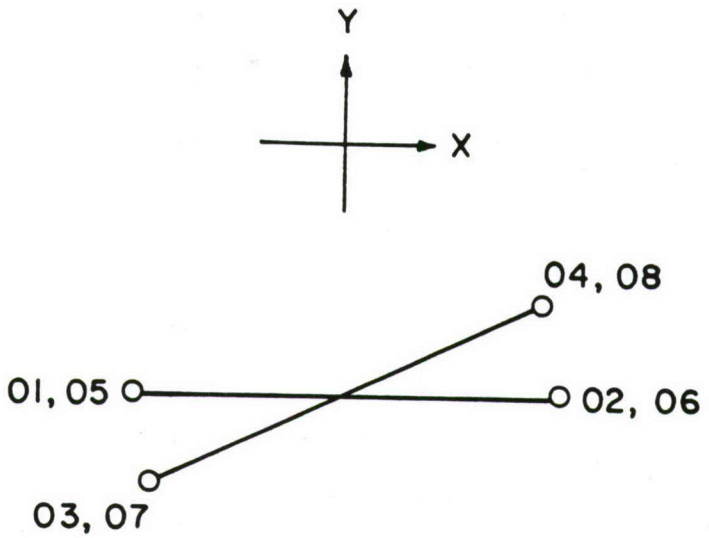

Figure 8b. View from above (from the positive z direction) of the Fig. 8a dimer.

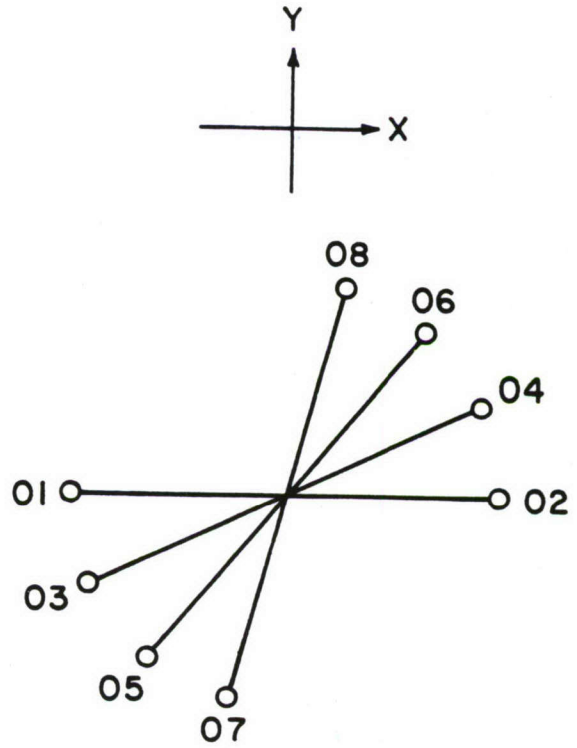

Figure 9. View from above (from the positive z direction) of another dimer of the O_4 twisted square. This dimer is the same as the Fig. 8 dimer except that in this case, the top twisted square is rotated counterclockwise about the z axis by an angle of 49.6°.

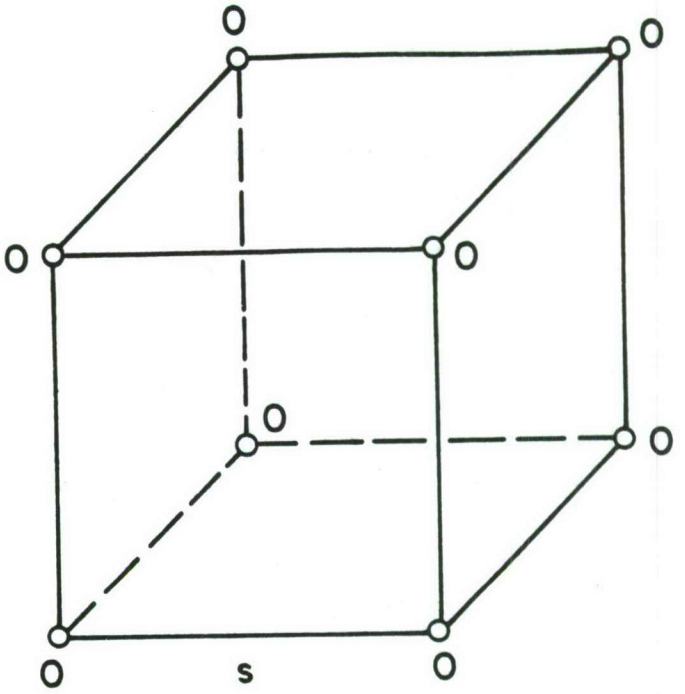

Figure 10. Oxygen cube (dimer of the O_4 square). The length of a side of the O_4 square, s, is 1.4341 Å.

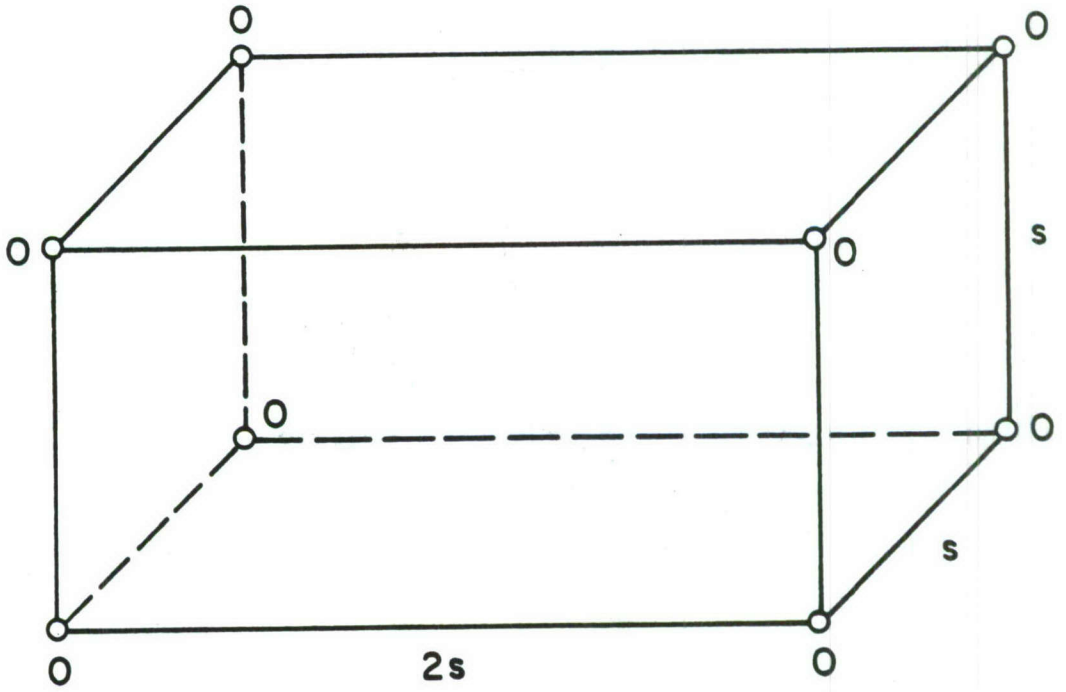

Figure 11. Oxygen rectangular solid (another dimer of the O_4 square). The distance s is given in the Fig. 10 caption.

COLLABORATIVE EXPERIMENTAL AND THEORETICAL STUDY OF THE PHOTODISSOCIATION AND REACTIONS OF THE AZIDE RADICAL

Millard H. Alexander, Department of Chemistry, University of Maryland, College Park, MD 20742

Paul J. Dagdigian, Department of Chemistry, The Johns Hopkins University, Baltimore, MD 21218

A. Theoretical Program

We have initiated a study of the single-collision dynamics of simple chemical reactions and photodissociation of the azide radical. As an initial theoretical project, we have carried out an investigation of the energetics and mechanism of the dissociation of ground state HN_3 ($\tilde{X}\ ^1A'$).

In many photodissociation reactions one or more of the diatomic fragments are formed in open-shell electronic states. The distribution of the products among the various possible fine-structure levels can, in principle, provide considerable insight into the photolytic mechanism. Much attention has been focussed on fragments in $^2\Pi$ electronic states, where each rotational level is split into a closely spaced Λ doublet. The preferential production of a given Λ-doublet level can be interpreted by analysis of the evolution of the molecular orbitals of the precursor species during the dissociation.

A similarly simple explanation is unfortunately not available for unequal populations in different spin-orbit manifolds, which have been observed in a number of photodissociation processes.[1,2] In principle, it is easier to understand spin selectivity in photodissociation leading to a molecule in a $^{2S+1}\Sigma$ state, since any complications arising from the presence of a non-zero orbital electronic orbital angular momentum are absent. In a molecule in a $^{2S+1}\Sigma$ electronic state the (2S+1) spin multiplets correspond to the allowed vector coupling of the spin (**S**) and nuclear rotational (**N**) angular momentum.[3] The origin of spin selectivity must be qualitatively different than that of the Λ doublet specificity discussed in the

---

1 F. Shokoohi, S. Hay, and C. Wittig, Chem. Phys. Lett. **110**, 1 (1984); I. Nadler, D. Mahgerefteh, H. Reisler, and C. Wittig, J. Chem. Phys. **82**, 3885 (1985).

2 H. Joswig, M. A. O'Halloran, R. N. Zare, and M. S. Child, Faraday Disc. Chem. Soc. **82**, 83 (1986).

3 G. Herzberg, *Molecular Spectra and Molecular Structure. I. Spectra of Diatomic Molecules* (D. Van Nostrand, Princeton, 1950).

preceding paragraph, since in the former case the selectivity corresponds to a preferential orientation of the electronic *spin* relative to some internal axis, rather than a preferential *spatial* orientation of the electronic wavefunction.[4]

Recently, Stephenson, Casassa, and King[5] have observed an intriguing spin-selectivity in the dissociation of deuterated hydrazoic acid (DN_3) to form ND molecules in the ground $^3\Sigma^-$ electronic state:

$$DN_3(\tilde{X}\,^1A') \xrightarrow{nh\nu} ND(X\,^3\Sigma^-) + N_2(X\,^1\Sigma_g^+)$$

This dissociation is induced by infrared multiphoton pumping and therefore takes place on the ground electronic surface. As illustrated schematically in Fig. 1, this is a spin-forbidden forbidden process; the

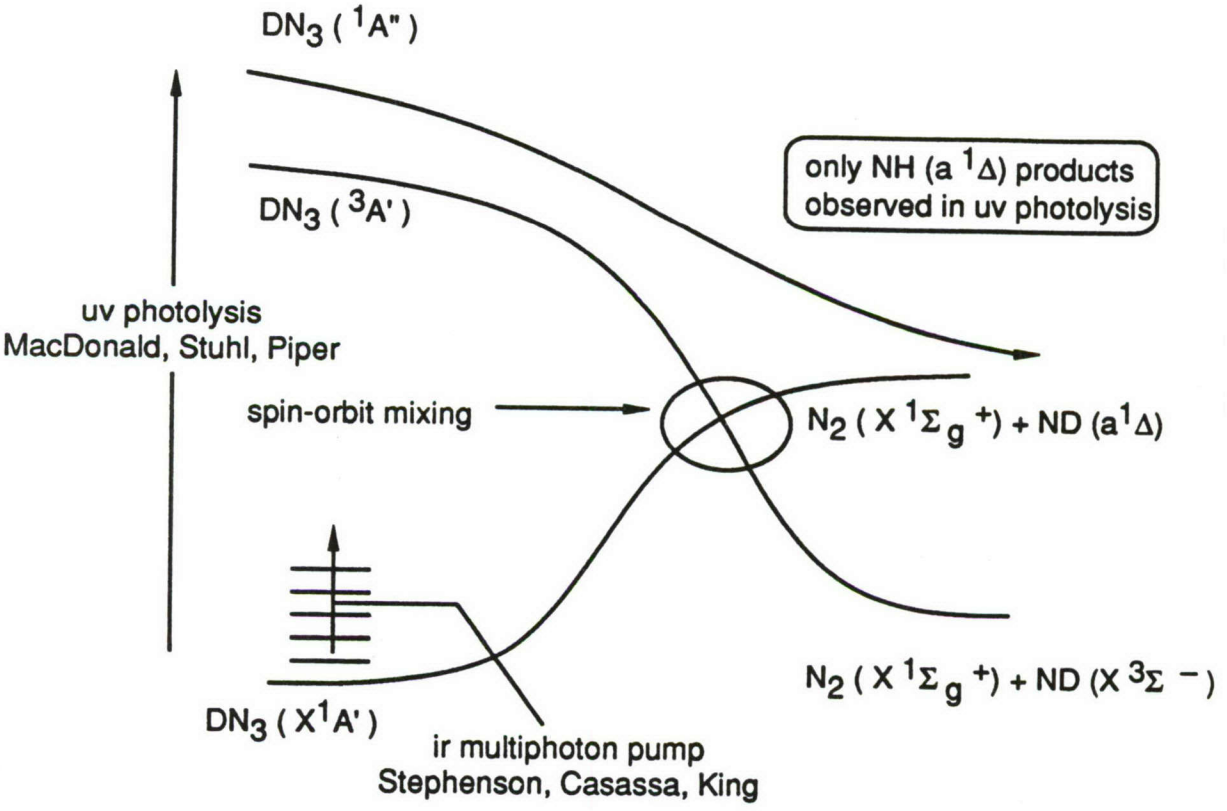

Fig. 1. Schematic reaction coordinate diagram for the energetics of the dissociation of DN_3 by multiphoton pumping on the ground electronic surface.

4 M. H. Alexander and P. J. Dagdigian, J. Chem. Phys. **80**, 4325 (1984); B. Pouilly, P. J. Dagdigian, and M. H. Alexander, *ibid.* **87**, 7118 (1987).

5 Abstract presented at this meeting, and J. Chem. Phys., submitted.

spin-allowed pathway would lead to the lowest electronically excited product channel of singlet multiplicity, namely ND ($a^1\Delta$). The spin-forbidden decomposition occurs by a spin-orbit induced crossing between singlet and triplet surfaces.The ND molecule is found to be produced preferentially in the F_1 and F_3 spin multiplet levels, with little population in the F_2 levels.

Three factors are essential to an understanding of the dynamics of the dissociation of hydrazoic acid studied by Stephenson, Casassa, and King.[5] The first is the location and height of the crossing between the lowest singlet and lowest triplet surfaces (Fig. 1), which is the activation barrier to the formation of spin-forbidden products. In addition the gradient of the triplet surface after the barrier will determine the degree to which the internal energy of the HN_3 molecule is transformed into internal or translational energy of the fragments.

The second crucial factor is the origin of the singlet-triplet coupling which leads to the formation of triplet NH from a singlet state of HN_3. The lowest spin-allowed channel is N_2 ($X^1\Sigma_g^+$) + NH ($a^1\Delta$), and the lowest triplet channel is N_2 ($X^1\Sigma_g^+$) + NH ($X^3\Sigma^-$). At first glance the singlet-triplet coupling would thus appear to arise from spin-orbit mixing in the NH molecule as it separates from the N_2 fragment. However, it is well-known that for the isolated NH molecule the spin-orbit Hamiltonian will *not* couple $^1\Delta$ and $^3\Sigma^-$ electronic states.[6]

Thirdly, it is important to understand the startling spin-state selectivity in the NH ($X^3\Sigma^-$) product.

We have carried out *ab initio* calculations on the HN_3 molecule to determine the location and height of the singlet-triplet crossing. It was necessary to use multiconfiguration self-consistent-field (MCSCF) and multireference configuration-interaction (MCSCF-CI) techniques to describe adequately the orbital distortion and changes in electron occupancies which accompany the bond breaking. Our calculations involved a large orbital basis consisting of 94 contracted Gaussian type orbitals and included >165,000 configurations. These calculations predict the singlet-triplet crossing to occur at the geometry shown in Fig. 2 (next page). The minimum singlet-triplet crossing lies 12300 cm^{-1} above the calculated energy of HN_3 ($\tilde{X}\ ^1A'$) at the experimental geometry. Without including any zero-point corrections, we observe that this theoretical estimate of this activation energy agrees well with the value estimated by

6 H. Lefebvre-Brion and R. W. Field, *Perturbations in the Spectra of Diatomic Molecules* (Academic, New York, 1986).

Kajimoto *et al.*[7] from thermal dissociation studies in a shock tube ($E_a \cong 36$ kcal/mol = 12,700 cm^{-1}).

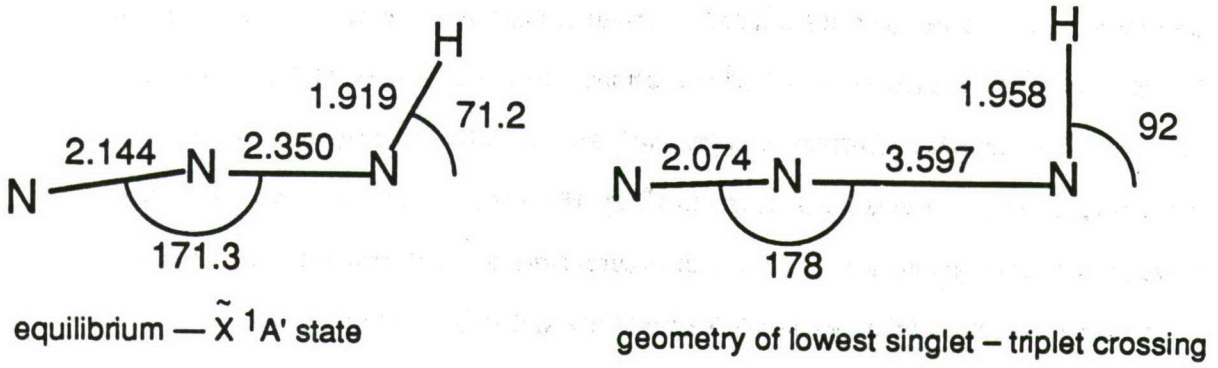

Fig. 2. Geometry of HN_3. The left diagram illustrates the geometry at the experimental minimum for the $\tilde{X}\,^1A'$ state. The right diagram illustrates the lowest point of crossing between the $^1A'$ and lowest $^3A''$ surface, predicted by MCSCF-CI calculations. This point corresponds to the curve crossing depicted in Fig. 1.

The product internal energy distributions of the fragment N_2 and NH molecules will be sensitive to the forces exerted on the nascent products as the system crosses over from the $^1A'$ to the $^3A''$ surface. Since the bond distances of the N_2 and NH fragments at the position of lowest singlet-triplet crossing are identical to those in the isolated N_2 and NH molecules,[8] we anticipate that the dissociation process will be vibrationally adiabatic. Our calculations indicate that the torques on the NH molecules in the dissociation channel are small, so that the energy release will be mainly translational, with little rotational excitation of the NH or N_2 fragments.

At equilibrium the HN_3 molecule in the ground $\tilde{X}\,^1A'$ electronic state is planar. Planarity of the molecule will persist during the dissociation process, since at the point of lowest singlet-triplet crossing the terminal N–N bond and the N–H bonds are nearly perpendicular (Fig. 2). For an exactly perpendicular

7 O. Kajimoto, T. Yamamoto, and T. Fueno, J. Phys. Chem. 83, 429 (1979).

8 K. P. Huber and G. Herzberg, *Molecular Spectra and Molecular Structure. IV. Constants of Diatomic Molecules* (Van Nostrand Reinhold, New York, 1979).

geometry the energy will be *independent* of the dihedral angle between the terminal N–N and the N–H bonds, so that there will be no torques causing a loss of planarity.

Our *ab initio* calculations were also used to unravel the mechanism whereby facile singlet-triplet transfer occurs, even though in the isolated NH molecule there exists no spin-orbit coupling between the lowest triplet ($X^3\Sigma^-$) and lowest singlet ($a^1\Delta$) electronic states. As the N–N···N–H distance becomes large, the molecular orbitals become associated with either the N_2 or NH fragment, the latter in either the lower or upper *singlet* valence states ($a^1\Delta$ and $b^1\Sigma^+$). However, as the N_2-NH distance decreases, the wavefunction of the ground state ($\tilde{X}\ ^1A'$) can be considered, to a first approximation, to be a linear combination of $N_2(X)$·NH($a^1\Delta$) and $N_2(X)$·NH($b^1\Sigma^+$), that is $\Psi(1^1A') \approx 2^{-1/2}[\Psi(^1\Delta) + \Psi(^1\Sigma^+)]$. It is the presence of $^1\Sigma^+$ character in the wavefunction that explains the facile spin-orbit mixing, since in the isolated NH molecule the $l_z s_z$ term in the spin-orbit Hamiltonian, where z designates the NH bond axis, *can* couple a $^1\Sigma^+$ state with a $^3\Sigma^-$ state.[6] From recent *ab initio* calculations on NH by Marian and Klotz[9] we estimate the magnitude of the $^1A' - {}^3A''$ matrix element to be ~ 45 cm^{-1}.

At the point of lowest singlet-triplet crossing the molecule will be planar, or nearly so, and there will be little or no dihedral torque as the N_2 and NH fragments separate. Thus the rotational motion of the nascent NH and N_2 molecules will be confined to the initial HN_3 plane; in other words both the N_2 and NH bond axes will lie in the plane of the initial HN_3 molecule. In the ground state ($\tilde{X}\ ^1A'$) the electronic wavefunction of HN_3 is symmetric with respect to reflection of the spin and space coordinates of the electrons in the molecular plane. Similarly, the $l_z s_z$ term in the spin-orbit Hamiltonian is symmetric with respect to reflection of the spin and space coordinates of the electrons in any plane containing the NH bond axis — here the HN_3 molecular plane. Since both the initial electronic state, as well as the coupling operator, are symmetric with respect to this operation, coupling will be possible only to final states which are also symmetric.

Since the wavefunction of the ground state of N_2 is symmetric with respect to reflection of the electronic coordinates in a plane containing the molecular axis, the wavefunction of the nascent NH molecules in the $X^3\Sigma^-$ state must also be symmetric with respect to this operation. This restriction will limit population to only the F_1 and F_3 spin multiplet levels — those in which the wavefunction is symmetric with

9 C. M. Marian and R. Klotz, Chem. Phys. **95**, 213 (1985).

respect to reflection of the electronic coordinates in the plane of the initial HN_3 molecule (the wavefunctions of the F_2 levels are antisymmetric). The relevant operators are those which correspond to reflection of the spatial *and* spin coordinates of all the electrons. One can extend this symmetry argument to predict that NH ($a^1\Delta$) products formed in the spin-allowed dissociation channel will be found predominantly in the e , or $\Delta(A')$, Λ-doublet levels, which are symmetric with respect to reflection of the electronic coordinates in the plane of rotation of the molecule. The absence of population in the F_2 levels of the NH ($X^3\Sigma^-$) products and the preferential production of NH ($a^1\Delta$) in the $\Delta(A')$ Λ-doublet levels have both been found experimentally by Stephenson, Casassa, and King.[5]

B. Experimental Program

Our experimental program will concentrate on the study of reactions of the azide radical with atoms, as exemplified by the reaction with hydrogen atoms:

$$H + N_3 \rightarrow NH(X^3\Sigma^-, a^1\Delta) + N_2.$$

This reaction can proceed through 4 different potential energy surfaces (2 of singlet and 2 of triplet spin multiplicity). If the reactive trajectories involve mainly the ground state ($\tilde{X}\ ^1A'$) HN_3 potential, then one would expect formation of the NH products predominantly in the $a^1\Delta$ state. The NH $X^3\Sigma^-$ to $a^1\Delta$ electronic state branching ratio will reflect the importance of singlet-triplet curve crossing, as in the IRMPD of HN_3, as well as the possible role of reactive trajectories along triplet surfaces.

We plan to carry out the study of the dynamics of these atom-azide radical reactions in a crossed molecular beam apparatus with laser fluorescence detection of the products. In preparation for these studies, we have succeeded in generating beams of N_3 through the thermal decomposition of lead azide, as currently been done in several flow experiments.[10,11] This technique for production of N_3 is several orders of magnitude more efficient than the thermal decomposition of sodium azide.[12] Production of N_3 was monitored by observation of NO chemiluminescence from the O + N_3 reaction in a crossed beam

10 W. J. Marinelli and L. G. Piper, private communication.

11 S. Rosenwaks, private communication.

12 L. G. Piper, R. H. Krech, and R. L. Taylor, J. Chem. Phys. **71**, 2099 (1979).

arrangement, which is illustrated in Fig. 3. The oxygen atoms were generated from a supersonic microwave discharge source. This source utilizes an extended[13] Evenson-Broida 2450 MHz cavity to allow the adjustment controls to be located outside the vacuum envelope. From the observed NO^* emission intensity, we estimate that 10-100% of the vapor from the decomposition of lead azide is in the form of the azide radical. This derived production efficiency is only good to an order of magnitude since the photomultiplier sensitivity and the absolute oxygen atom density have not been measured.

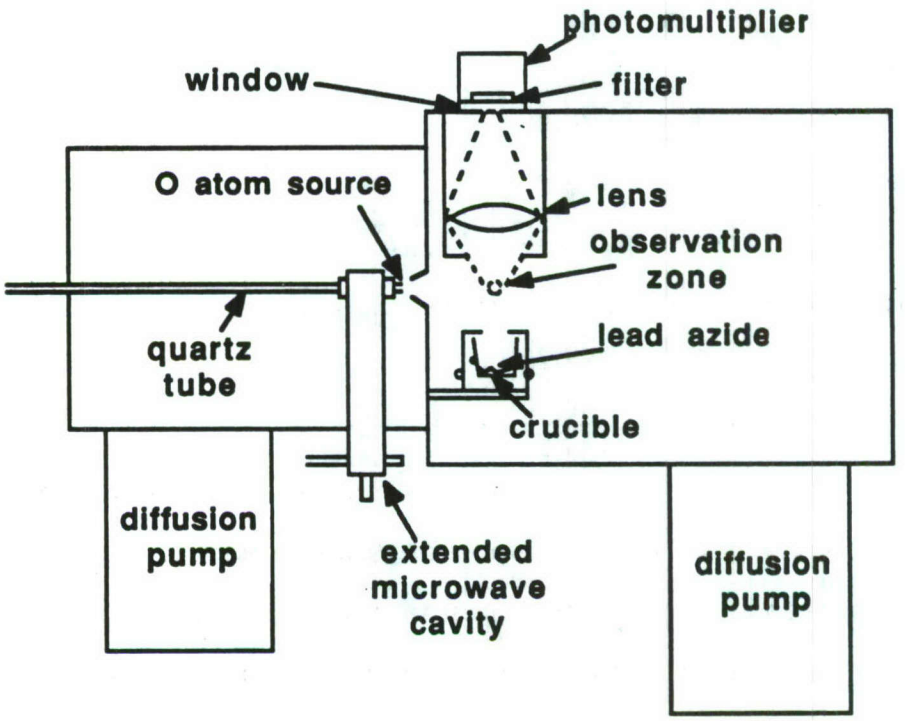

Fig. 3. Schematic of the experimental apparatus.

13 E. J. Murphy and J. H. Brophy, Rev. Sci. Instrum. 50, 635 (1979).

ENERGY FLOW AND DECOMPOSITION OF ENERGETIC MOLECULES FROM METASTABLE VIBRATIONAL STATES

B.R. Foy, M.P. Casassa, J.C. Stephenson, and D.S. King
National Bureau of Standards
Molecular Spectroscopy Division
Gaithersburg, Md 20899

We report the initial distribution of kinetic, vibrational, and rotational energy in the collision-free CO_2 laser induced IRMPD reactions:[1]

$$DN_3\ (X\ ^1A') \longrightarrow DN\ (X\ ^3\Sigma^-) + N_2\ (X) \qquad \Delta H = 15\ \text{kcal/mol},$$

$$\longrightarrow DN\ (a\ ^1\Delta) + N_2\ (X) \qquad \Delta H = 51\ \text{kcal/mol},$$

and measurements of the unimolecular vibrational predissociation lifetimes and $NH(X^3\Sigma^-)$ product state distributions following excitation of the 4th and 5th NH-stretching overtone transitions of HN_3. These state-to-state photodissociation experiments provide an exceptionally detailed view of the dynamics of rovibrationally excited HN_3 and complement high resolution spectra and linewidth data for assigned rovibrational levels of v_1 = 4, 5, and 6.[2,3] The results build upon previous overtone excitation experiments[4] on HOOH and tetramethyldioxetane, and theoretical calculations[5] on the energetics and product spin-selectivity of these reactions.[6] The dissociation is spin forbidden, and the large barrier corresponds to the minimum energy singlet-triplet crossing.[5]

The measurements were performed using low pressure, thermal (293 K) DN_3/HN_3 samples in a flow cell. The CO_2 laser which photolyzed the gaseous DN_3 produced temporal "square wave" pulses[7] of 50 ns duration at a repetition rate of 2Hz. Most product state data were obtained with the P(18) line at 946 cm^{-1}, pulse energy of 100 mJ focussed to a beam waist of w = .011 cm corresponding to I=10GW/cm^2. The overtone pump laser which photolyzed HN_3 operated at 575 (v_1=6←0) or 662 nm (v_1=5←0) with a spectral

bandwidth ≈0.4 cm^{-1} and energies 3 to 6 mJ. The DN/HN fragments were probed by laser-induced fluorescence of the $A^3\Pi$ - $X^3\Sigma^-$ or $c^1\Pi$ - $a^1\Delta$ transitions using a frequency-doubled dye laser with a bandwidth of 0.7 cm^{-1} and energy 5μJ (etalon-narrowed to 0.05 cm^{-1} for the measurement of Doppler profiles, energy ≈ 0.2 μJ). For lifetime measurements, the time delay between pump and probe was stepped electronically in 1 ns increments.

The experimental observations yield information about the distribution of energy in the reactant, the microscopic reaction rates, the location of barriers to dissociation, and the geometry of the transition states. Multiphoton vibrational excitation of DN_3 by a CO_2 laser led to dissociation forming DN in both $X^3\Sigma^-$ (spin forbidden) and $a^1\Delta$ (spin allowed) electronic states. Under collisionless conditions, the DN ($X\ ^3\Sigma^-$) molecules were formed predominantly in the symmetric F_1 and F_3 spin-rotation states with little population (≤6%) in the anti-symmetric F_2 levels. There was no significant population (<3%) in excited DN ($^3\Sigma^-$) vibrational levels. The distribution of rotational states was Boltzmann-like, characterized by a rotational "temperature" of about 920K for the F_1, F_3 states and 500K for F_2 levels. Doppler profiles showed a large kinetic energy release of about 10,100 cm^{-1} total in the triplet channel. The DN ($^1\Delta$) products were formed preferentially in the symmetric $\Delta(A')$, e-labeled lambda doublet levels: $\Delta(A')/\Delta(A") = 1.44$. The DN ($^1\Delta$) was formed with no vibrational excitation (<2%); the rotational state population distributions were Boltzmann-like with a rotational "temperature" of 425K. Doppler profiles gave a total kinetic energy of about 1500 cm^{-1} in this channel.

Excitation of the NH-stretch overtone transitions of HN_3 to $v_1 = 5$ and 6 resulted in predissociation to $HN(^3\Sigma^-X)$ and $N_2(X)$ with lifetimes of

80 $\pm^{60}_{30}$ and $\leq$ 3 ns, respectively. Following excitation of either overtone, the HN-fragments were formed predominantly in the symmetric F_1, F_3 spin-rotation states, with less than 4% population in the anti-symmetric F_2 levels. Fragment Doppler profiles confirmed that most of the available energy (>96%) went into translational motion.

Dramatic DN/HN spin selectivity, no fragment vibrational excitation, little rotational excitation and essentially total (>96%) kinetic energy release occurred in both the overtone pumping and IRMPD experiments. The large increase in unimolecular reaction rate with vibrational energy in the overtone experiments is inconsistent with the scaling of rate with state density ρ, $k_{uni}(E) \approx A\rho(E-E_a)/\rho(E)$, expected for statistical reactions,[8] which predicts $k_{uni}(6\nu_1)/k_{uni}(5\nu_1) \approx 3$. According to the calculations of Alexander and coworkers,[5] F_1 and F_3 spin selectivity arise from the symmetry of the spin-orbit operator matrix elements for a planar transition state. A similar argument pertains to the population of Λ-doublets in the spin-allowed channel. Little product vibrational and rotational excitation occur because the HN and NN bonds in the singlet-triplet crossing region have free-molecule lengths, the impact parameter is very small (linear NNN, $\theta_{HNN} \approx 90°$), and there is little anisotropy in the exit channel of the potential surface.[5]

The authors thank D. Halligan and M.J. Berry for communicating their HN_3 overtone results, M. Alexander for theoretical interpretation, and the Air Force Office of Scientific Research for supporting this work.

REFERENCES

1. The enthalpy of the DN ($^3\Sigma^-$) channel has been estimated in recent literature at various values from 11 to 17 kcal/mol. The

enthalpies shown were estimated by Carl Melius (private communication).

2. David T. Halligan, Ph.D. Thesis, Rice University (June 1988).

3. M. Carlotti, G. DiLonardo, G. Galloni, and A. Trombetti, Trans. Faraday Soc. 67, 2852 (1971).

4. F.F. Crim in Molecular Photodissociation Dynamics, M.N.R. Ashfold and J.E. Baggott eds., (Royal Society of Chemistry, London, 1987).

5. M.H. Alexander, H.-J. Werner, and P.J. Dagdigian, accompanying article.

6. O. Kajimoto, T. Yamamoto, T. Fueno, J. Chem. Phys. 83, 429 (1979).

7. J. C. Stephenson and D. S. King, J. Chem. Phys. 78, 1867 (1983); J. C. Stephenson, J. A. Blazy, C.-L. Lin, and D. S. King, J. Chem. Phys. 76, 5989 (1982).

8. W. Forst, J. Chem. Phys. 76, 342 (1972); "Theory of Unimolecular Reactions" (Academic Press, N.Y. 1973).

CHEMICALLY BOUND EXCITED CLUSTERS*

C.A.Nicolaides

Theoretical and Physical Chemistry Institute

National Hellenic Research Foundation

48,Vas.Constantinou Ave., Athens 116 35

Greece

Abstract

According to the conventional understanding of their electronic structure, polyatomic clusters of "nonreactive" closed shell molecular fragments, have been considered as undergoing exclusively van der Waals bonding, even when excited. Since 1983, new results and proposals have been presented regarding such clusters /1-8/. These refer to the existence of chemical bonding in excited states, caused by charge transfer and overlap effects in unusual geometries. Directly related to these developments is the study of $He+H_2^*$ collisions /1,9,10/ and of fluorescence quenching of the H_2 B $^1\Sigma_4^+$ state by the noble gases /1,2,11/. It is reasonable to expect that there exist a variety of such clusters and that they may play an important role in the storage and distribution of energy in the molecular, liquid or solid state.

In this short report, I review a portion of our published and unpublished work on the existence and properties of chemically bound excited clusters (CBEC).

---

*Lecture delivered at the second contractors Meeting on High Energy Density Materials, Newport Beach, California,Febr.28-March 2, 1988, sponsored by the AFOSR and AFAL and organized by the National Research Council.

I. CONCEPTS AND RESULTS

The CBEC are formed in geometries which can be predicted semiquantitatively according to the "maximum ionicity excited state" (MIES) theory of bonding /2-4/. This theory predicts chemical (e.g. larger than 1eV) minima in excited states of clusters of normally noninteracting species by relating the binding and the corresponding geometry to the strong charge transfer which occurs in one of the molecular constituents of the cluster, in its excited state. In its equilibrium configuration, this constituent is bonded mainly covalently. For example, in the case of H_2^* $B^1\Sigma_u^+$, the equilibrium geometry is at 2.4 a_o, whereas the geometry of the MIES is around 4.0 a_o /12/.

The quantitative understanding of excited states /13/, especially of those molecular states which give rise to avoided crossings, requires the application of elaborate, general and powerful methods for the reliable computation of wavefunctions and properties. Their hypersurfaces are much more complicated and challenging from the point of view of chemical physics than those of the ground state. For our study of diabatic and adiabatic hypersurfaces and of dissociation lifetimes of MIES clusters, we have used computer programs for open-shell SCF /14/, for "multireference singles and doubles configuration interaction" (MRDCI) /15/, for multiconfigurational SCF(MCSCF) /16/ and for full CI(FCI) and gradient optimized geometry /16/ computations.

The first numerical applications have dealt with the

high energy content clusters which are formed from reactions of the H_2^* $B\,^1\Sigma_u^+$ state (11.4eV above the $X\,^1\Sigma_g^+$ state) with closed shell species. These are noble gas dihydrides, HeH_2^* /1,3/, NeH_2^* /3/ and ArH_2^* /3/, tetrahydrogen, H_4^*, /2,4-6, 8/ and polyhydrogen /4/. Their energy minima occur at avoided crossings with repulsive surfaces of the same symmetry which correlate with products in their ground state. For example, in H_4^* of C_s symmetry, the lowest $^1A'$ surface correlates with $H_2(^1\Sigma_g^+)+H_2(^1\Sigma_g^+)$ whereas the first excited $^1A'$ surface, with which it avoids crossing at a geometry of trigonal pyramid, with an isosceles triangle base, correlates with $H_2^*(^1\Sigma_u^+) + H_2(^1\Sigma_g^+)$ /6,8/. Thus, the stability of these CBEC, as well as of similar ones that can be formed from all kinds of combinations of closed shell molecules, depends on the transition probability of two types of decay modes. The first is the radiative one. It is expected to be relatively slow since, on the one hand at the same geometry the energy diffence between the surfaces is very small (avoided crossing), while, on the other hand, at the dissociation limit of two ground state molecules the geometrical differences are large and yield a very small vibrational functions overlap. Of course, the determination of the exact magnitude of the radiative decay requires a complete calculation of the integrated emission transition probability.

The second decay mode is the radiationless fragmentation via the nonadiabatic vibronic coupling between the surfaces. It constitutes the physically important mechanism for the

release of the energy of the CBEC. Given the original work on the CBEC, understanding the dynamics of this mechanism and deducing the lifetime of H_4^* has been of considerable scientific and technological interest. Here we report for the first time that its lifetime is of the order of 10^{-11} sec. I also take the opportunity to propose and present the first results in a new area of chemical physics which I call "Fragmentation Lifetime Molecular Engineering". Its purpose is the quantitative understanding and manipulation of the wavefunctions and surfaces of specific molecular states by embedding them in solid media, so as to affect their degree of stability.

The following Tables and Figures have been selected from our published work. I then continue with recent results from our unpublished work.

II. EXCERPTS FROM PUBLISHED WORK

Tetrahydrogen

Polyhydrogen

J.Chem.Phys. 80 1705(1984)

81 748(1984)

J.Phys. B21, L77, (1988)

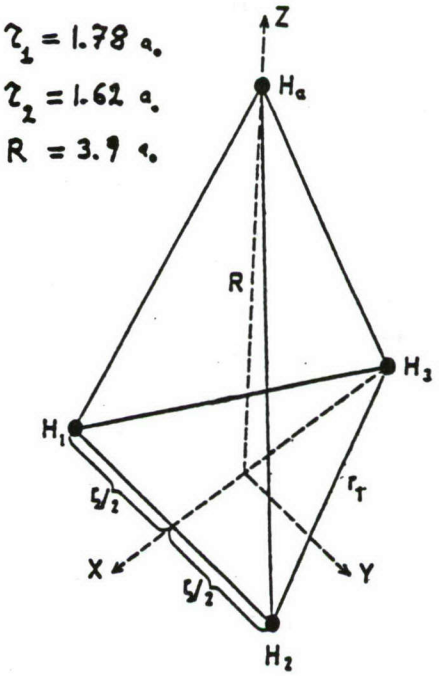

Fig. 1. Geometry of H_4^* at the minimum of the CBEC $^1A'$ surface

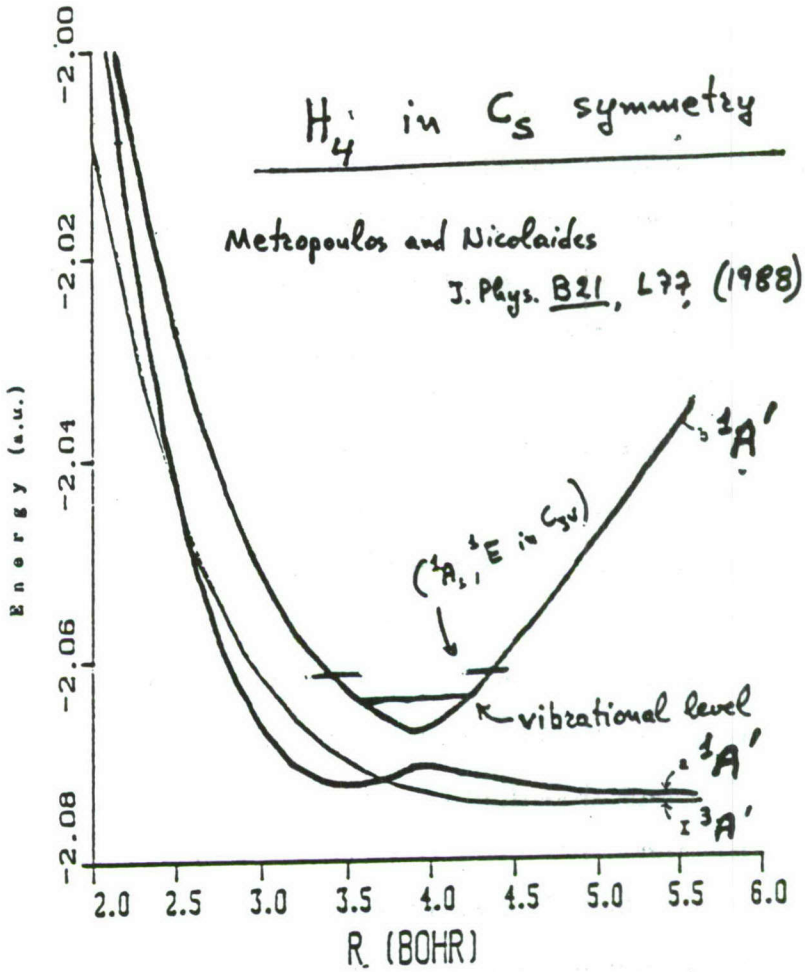

Fig. 2. The H_4 (C_s) lowest triplet and singlet A' states. The dissociation limit for both X $^3A'$ and a $^1A'$ is the $H(1s\ ^2S) + H_3(X\ ^2A_1)$ while for the b $^1A'$ it is the $H(1s\ ^2S) + H_3(A\ ^2A_1)$ system. The A $^3A'$ state lies above -1.97 a.u. and it is dissociative.

J. Chem. Phys. 81, 748, (1984)

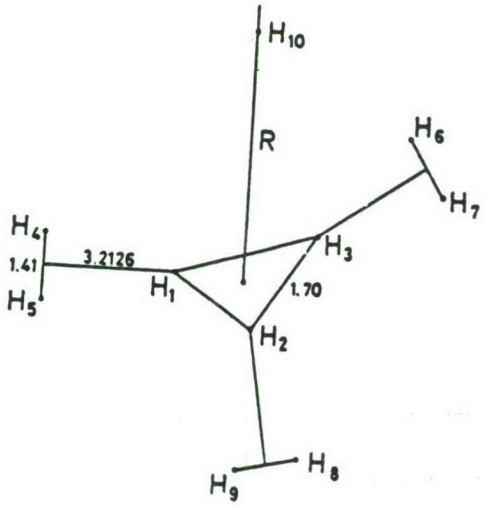

FIG. 3. The MIES (approximate) geometry of $(H_2)_5^*$

Table I. Total energies, in a.u., and the square of t coefficients of the most important configurations at avoided crossing, in C_s symmetry, for the $(H_2)_5$CBEC, according to MRD-CI calculations. The MIES (approxim geometry is given in Fig.3.

R_{1a}		Ground ($\tilde{X}\,^1A'$)	Excited ($2\,^1A'$)
5.0	E	− 5.503 265	− 5.483 400
$1a'^2 2a'^2 3a'^2 4a'^2 1a''^2$		0.730 6	0.000 4
$1a'^2 2a'^2 3a'^2 1a''^2 4a'5a'$		0.181 4	0.000 7
	$4a'6a'$	0.000 0	0.620 5
	$4a'10a'$	0.011 0	0.014 4
	$4a'11a'$	0.000 2	0.143 9
6.0	E	− 5.490 132	− 5.484 097
$1a'^2 2a'^2 3a'^2 4a'^2 1a''^2$		0.674 5	0.000 8
	$4a'5a'$	0.234 5	0.000 2
	$4a'6a'$	0.000 8	0.457 2
	$4a'10a'$	0.014 6	0.052 7
	$4a'11a'$	0.000 1	0.233 9
6.5	E	− 5.484 136	− 5.484 035
$1a'^2 2a'^2 3a'^2 4a'^2 1a''^2$		0.649 4	0.000 9
	$4a'5a'$	0.261 8	0.000 1
	$4a'6a'$	0.001 7	0.393 3
	$4a'10a'$	0.008 5	0.085 4
	$4a'11a'$	0.000 1	0.264 0
8.0	E	− 5.483 734	− 5.467 109
$1a'^2 2a'^2 3a'^2 4a'^2 1a''^2$		0.001 4	0.584 9
	$4a'5a'$	0.002 5	0.325 8
	$4a'6a'$	0.262 4	0.000 0
	$4a'10a'$	0.130 1	0.005 7
	$4a'11a'$	0.321 5	0.001 6

Noble Gas Dihydrides

Chem. Phys. Lett. 100, 263, (1983)

J. Chem. Phys. 80, 1900 (1984)

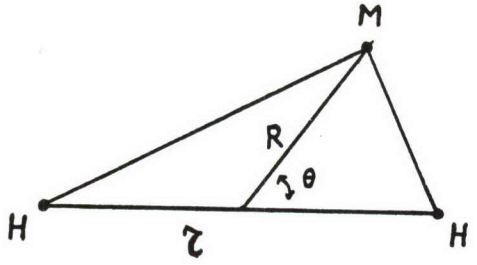

Fig. 4

TABLE II . Geometries of minimum energy of the $^1A'$ excited state of the noble gas dihydrides, according to the present state-specific SCF calculations. A detailed search of the hypersurface was outside the scope of this study

	r(a.u.)	R (a.u.)	ϑ (deg)	SCF Binding energy (eV) (with respect to $M(^1S) + H_2(B\,^1\Sigma_u^+)$
M = He	4.2	1.4	45	1.1
Ne	4.4	2.1	50	1.1
Ar	4.8	2.6	55	1.0

TABLE III Comparison between the present open-shell SCF results for the binding energy (in mhartree) of the $^1A'$ excited state of HeH_2 and those from the MRD-CI calculations. For fixed R (= 1.5a_0) and ϑ (= 45°).

r(a_0)	MRD-CI	Open-shell SCF
1.4	...	188.7
2.4	98.8	139.9
3.0	23.7	13.8
3.5	− 35.2	− 27.2
3.8	...	− 30.6
4.0	− 55.8	− 33.6
4.2	...	− 34.6
4.5	− 44.9	− 10.5
5.0	− 25.8	0.5
6.0	19.1	20.9

HeH_2

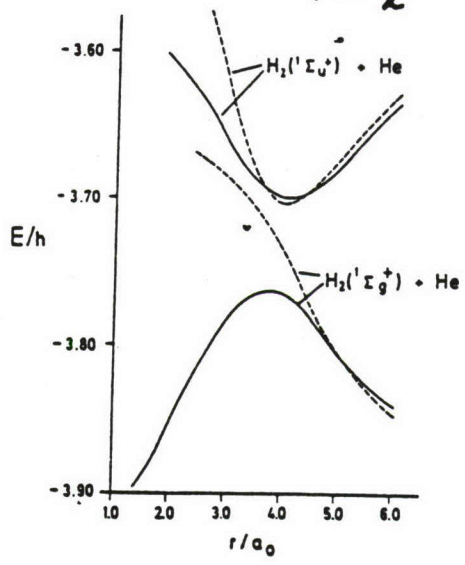

Fig. 5. The potentials of the ground and the first excited state ($^1A'$) as functions of the H–H distance. Solid lines correspond to $R = 2.0\,a_0$ and dashed lines to $R = 1.5\,a_0$.

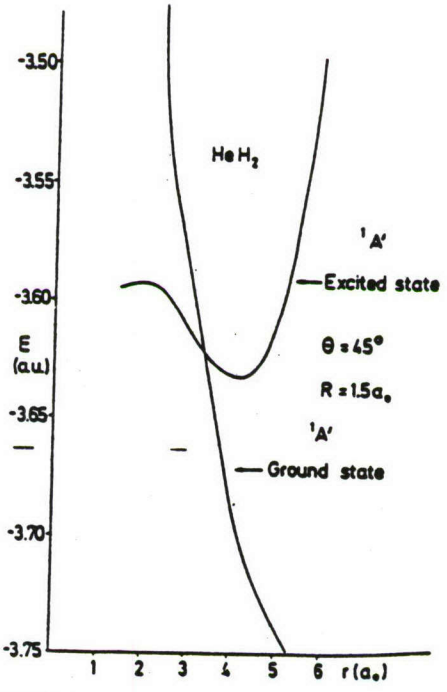

FIG. 6 Diabatic potential energy surfaces for the ground and first excited $^1A'$ states of HeH_2, as a function of the H–H internuclear distance r, from geometry optimized closed and open-shell SCF calculations. The excited state curve goes through the minimum (Table III).

III. UNPUBLISHED WORK (17)

The theoretical study of CBEC presents a number of conceptual and computational challenges. Essentially, it requires the accurate knowledge of the properties of hypersurfaces and the dynamics of formation and fragmentation.

Thus far, our unpublished work has gone into areas such as:

1) Appropriate methods of computation of wavefunctions and hypersurfaces of excited states of polyatomics, especially in regions of (avoided) crossings.

2) Evaluation of the lifetimes of CBEC, with first application to H_4^*.

3) Prediction and calculation of new CBEC, based on the MIES theory

4) Environmental effects on the CBEC.

Some of the results in each area are the following:

1') Full CI optimized geometry of H_4^*

Using the program GAMESSS /16/, we have confirmed and extended the results of /8/ for H_4^*, at the full CI level, with geometry optimization /18/. Fig.7 shows the two surfaces as a function of R. Given the heavy mixing around the avoided crossing region, we have also identified the closed or open-shell character of the roots, as revealed from a natural orbital transformation. Such information is useful when further analysis and use of these functions is required (E.g.fig.8,9)

2') Lifetime of H_4^*-

Using analytic vibronic functions for initial and final states, we have produced the first results for the predissociation lifetime of H_4^* along the R coordinate /19/. The sensitivity of this quantity to the type of calculation does not yet allow an accurate prediction. According to our semifinal results, the lifetime of the H_4^* CBEC is of the order of 10^{-11} sec.

3') Search for new CBEC: The excited water dimer, $(H_2O)_2^*$.

For obvious reasons, the water dimer has been attracting the interest of theoreticians and experimentalists alike. However, as with the other clusters of closed shell species, only the ground state properties have been examined.

As part of our search for new and more complex than the poly-hydrogen systems, we have been looking at $(H_2O)_2^*$ and its possible hypersurfaces and dissociation products. We have established /18/, that the protonated hydrogen peroxide, $(H_2O_2)H^+$ is stable, and have determined the corresponding geometry and vibrational frequencies at the SCF and MCSCF level.

4') Fragmentation lifetime Molecular Engineering.Clusters in solid media. Application to H_4

Given the practical aim of the study of CBEC, we have initiated a research program for the understanding of the behavior of such

H_4 in Solid Ionic Media

Fig. 7

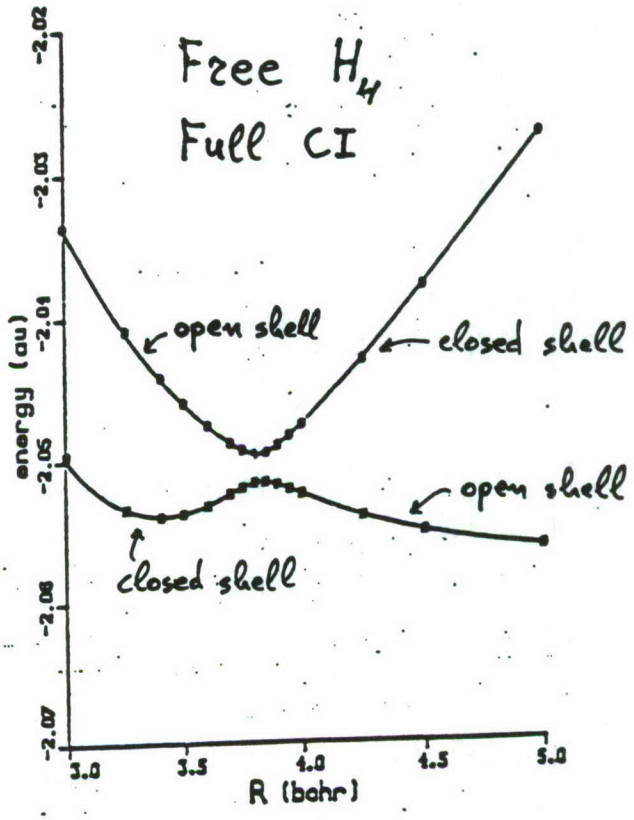

Fig. 8

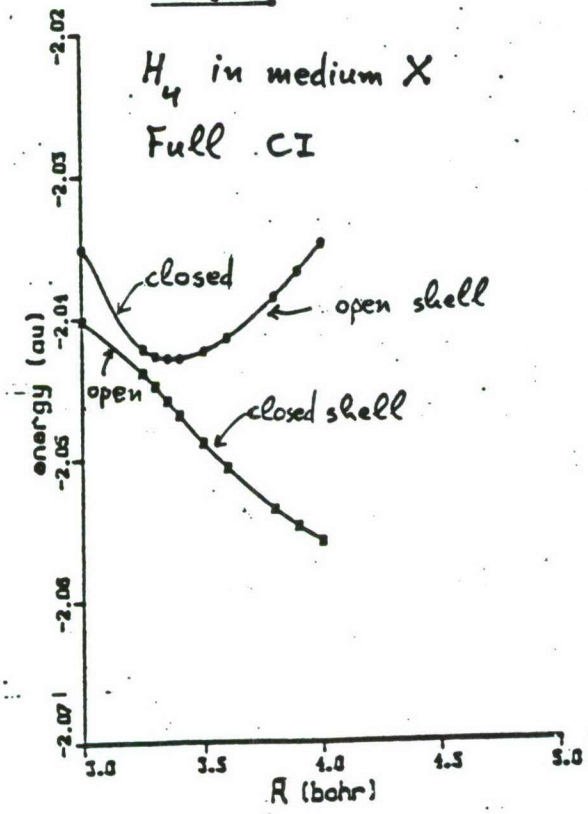

Fig. 9

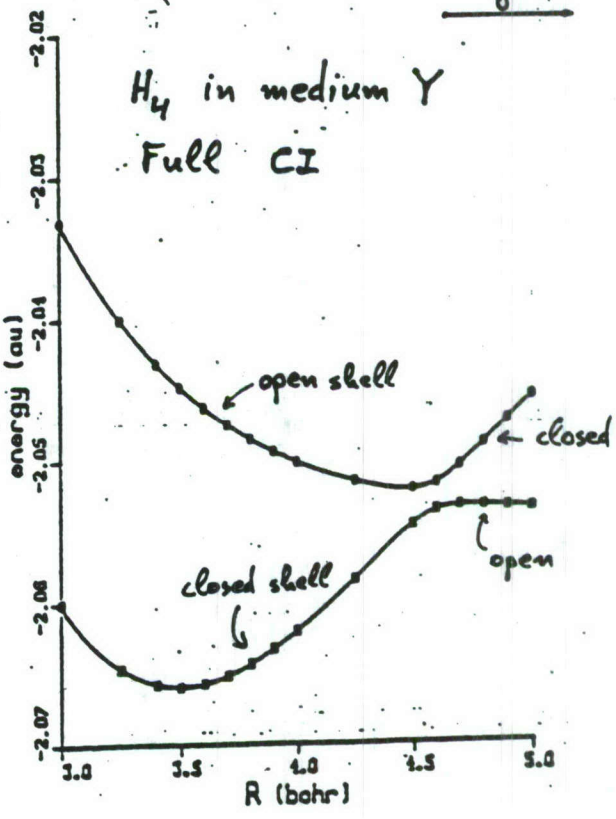

molecules when they are immersed in an environment which perturbs but does not destroy their molecular character /20/. What happens to the spectrum? What happens to the dynamics of energy absorption and dissipation? Can we manipulate the molecular states so as to alter the degree of stability of such systems?

The first choice of study along these lines was tetrahydrogen in realistic solid media of ionic character /21/. There is no previous information, even at the level of a simple model, about such problems. Our calculations have accounted for the self-consistent field as well as for the electron correlation effects. The results which have emerged are impressive. Indeed, the perturbation which is induced on the overall molecular spectrum is significant. This is demonstrated in Figures 8 and 9. Medium X of fig.8 induces an effect which brings the initially excited state below the initially ground state, while changing it into purely repulsive. We note that according to our calculations as well as of others'/7,22/, the surface corresponding to the free ground state wavefunctions does not have a stable minimum. On the other hand, medium Y of fig.9 keeps the initial spectral form but now the characteristics of the surfaces at the avoided crossing are different.

How these changes affect the fragmentation lifetime of H_4^* will be the subject of the next stage of our research in this area.

Acknowledgments

The development and implementation of computational software and the series of applications which are related to our published and unpublished work on CBEC, is a result of collaboration in our

institute among C.A.Nicolaides, R.J.Buenker, G.Theodorakopoulos, A.Metropoulos, I.Petsalakis, P.Valtazanos and M.Bacalis. Our current research in this area is partially supported by research grant AFOSR-87-0348.

REFERENCES

1. S.C.Farantos,G.Theodorakopoulos and C.A.Nicolaides, Chem.Phys.Lett.100, 263 (1983).
2. C.A.Nicolaides,G.Theodorakopoulos and I.D.Petsalakis, J.Chem.Phys.80,1705(1984)
3. C.A.Nicolaides and A.Zdetsis, J.Chem.Phys.80, 1900(1984)
4. C.A.Nicolaides,I.D.Petsalakis and G.Theodorakopoulos, J.Chem.Phys.81,748(1984)
5. G.Theodorakopoulos,I.D.Petsalakis and C.A.Nicolaides, J.Mol.Str.(Theochem.)149,23(1987)
6. A.Metropoulos and C.A.Nicolaides, Z.Phys.D5,175(1987)
7. S-Yu Huang, Z.Sun and W.A.Lester,Jr., in the Proceedings of the High energy density matter contractors conference (1987).
8. A.Metropoulos and C.A.Nicolaides, J.Phys.B21,L77(1988)
9. S.C.Farantos,Mol.Phys.54, 835(1985)
10. R.M.Grimes, W.A.Lester and M.Dupuis,J.Chem.Phys.84,5437(1986)
11. E.H.Fink,D.L.Akins and C.B.Moore, J.Chem.Phys.56,900(1972)
12. W.Kołos and L.Wolniewicz,J.Chem.Phys.48,3672(1968)
13. See C.A.Nicolaides in "Advanced Theories and Computational Approaches to the Electronic Structure of Molecules"ed.C.E.Dykstra,Reidel(1984)p.161
14. W.G.Hunt,T.H.Dunning and W.A.Goddard III,Chem.Phys.Lett., 3,606(1969)
15. R.J.Buenker and R.A.Phillips,J.Mol.Struct.(Theochem) 123 291(1985), and refs.therein.
16. M.Dupuis, D.Spangler and J.J.Wendoloski, Natl.Res.Comput. Chem. Software Catalogue 1, Prog.no QG01 (GAMESS)(1980); H.B.Schlegel, J.Comp.Chem.3, 214,(1982)

17. See the acknowledgments

18. P.Valtazanos and C.A.Nicolaides, unpublished

19. A.Metropoulos, I.Petsalakis and C.A.Nicolaides,unpublished

20. We have published on similar concepts and calculations of "dressed atoms in solids". C.A.Nicolaides, Chem.Phys.Lett.19, 69(1973); D.R.Beck and C.A.Nicolaides, Int.J.Qu.Chem.S14, 323(1980); C.A.Nicolaides and A.Zdetsis, Sol.St.Comm. 50, 857(1984); A.Andriotis and C.A.Nicolaides, Phys.Rev.B35, 2583(1987)

21. C.A.Nicolaides, P.Valtazanos and M.Bacalis, unpublished

22. J.A.Montgomery and H.H.Michels, J.Chem.Phys.86,5882(1987)

Photochemical Preparation and Spectroscopic Detection of H_4

A. H. Kung, Y. T. Lee, C. B. Moore

Extended Abstract

We report on two sets of experiments designed to obtain spectroscopic and dynamical information that would allow experimental testing of the possible existence of H_4. The first set of experiments studies the collision dynamics of $H_2(B) + H_2$ as a function of quantum state of the free molecules. The second set examines high Rydberg states of H_2 and of hydrogen dimers and higher clusters.

(1) Molecular collision dynamics of B-state hydrogen:

A. $D_2^* + 4He$

This system was studied because of its closeness to the $H_2^* + H_2$ system and the availability of high level ab initio potential surfaces. The cross sections for electronic quenching are determined by monitoring the total fluorescence from selectively excited ro-vibronic states of hydrogen. The products of the reaction are presumably He and ground state hydrogen molecules or atoms. The values for the cross sections are presented in Table I.

The effects that we see of initial vibrational or rotational quantum number of the excited deuterium may possibly be explained by the fact that there is a barrier on the potential before the bound, metastable HeD_2^* is reached. This could also explain the size of cross sections in relation to the cross sections for the $H_2^*-D_2$ system.

B. $H_2^* + D_2$

The cross sections for this system were determined in the same way, and the results are given in Table II. There does not appear to be any significant dependence of the cross section on increasing vibrational energy of the hydrogen, but there might be a slight decrease in the cross section in going from J=0 to J=1 in the ground vibrational state. However, the overall effect of initial rotation and vibration of the excited H_2 parent appears to be small. All of this is in good qualitative accord with the absence of a barrier along the reaction coordinate for $H_2(B) + H_2 \rightarrow H_4^*$ found in ab initio calculations by Lester's group.

(2) Rydberg spectroscopy of Van der Waals molecules of H_2:

Relaxation of Rydberg states of small hydrogen clusters, $(H_2)_n$, yield various ions containing the strongly bound H_3^+ moiety. Since the theoretically predicted metastable H_4 molecule is an $H_3^+.H^-$ structure and the Rydberg states of H_4 are likely to be $(H_3^+.H)^*$, intramolecular chemical relaxation of the highly excited clusters offers unique opportunities for the experimental investigation of the possible existence of a metastable H_4 molecule.

The Rydberg states of H_2 and its small clusters can only be reached from the ground state using vacuum ultraviolet (VUV) and extreme ultraviolet (XUV) radiation. A VUV-XUV laser source continuously tunable from 74nm to >120nm has been developed in our laboratory for these studies. This source is based on a pulse-amplified CW single-mode dye laser. Pulse power in the visible is >15 MW in a near-transform-limited and diffraction-limited beam. Consequently it provides up to ~10^{12} photons per pulse in the XUV for utilization.

Another important development in these studies is the construction of a liquid-nitrogen cooled pulsed molecular beam sourse. Cooling to 77 K is essential for the formation of dimers in a H_2 beam. This is achieved by modifying a pulsed nozzle so that the part of the gas reservoir adjacent to the nozzle is liquid-nitrogen cooled. Efficient dimer formation is achieved with a density of up to several percent of the total beam intensity (Figure 1).

By using these two sources we have recorded a laser ionization spectrum of H_2. Figure 2 shows a portion of the spectrum obtained. The peaks are assignable to known Rydberg series of H_2. The ionization threshold of H_2 is at ~80.4 nm. There is a red shift of the ionization threshold for the dimer to ~88 nm. Excitation of a LN_2-cooled beam of H_2 and its Van der Waals molecules at wavelengths greater than 80.4 nm would show resonances associated with the dimers. Excitation at wavelengths longer than 88 nm. would allow the identification of dimer Rydberg levels that correlate to tetrahydrogen. We have scanned several broad spectral regions around 80 nm., 84nm., 88 nm., and 90 nm., searching for resonances assignable to the dimer by monitoring H_3^+. No resonances are observed. It is thus evident that either the Rydberg levels of the dimer have very small cross sections ($< 10^{-18}$ cm^2), which is quite unlikely since perturbation of the H_2 resonances by the dimer is expected to be small, or the levels are strongly predissociative to yield $H_3^+ + 2H$, broadening the widths of the levels to >~10 cm^{-1}. This corresponds to predissociative lifetimes of a few picoseconds and shorter. More experiments are required to further understand the absence of Rydberg resonances.

Table I D_2^* - He Quenching Results

D_2 Quantum State $\|v',J'\rangle$	Quenching Cross Section ($Å^2$)	Line
$\|0,0\rangle$	1.4±0.4, 1.55±0.1	P(1)
$\|0,1\rangle$	3.1±0.2, 3.0±0.2	R(0)
$\|0,1\rangle$	2.3 ± 0.1	P(2)[a]
$\|0,2\rangle$	3.6 ± 0.5	R(1)
$\|0,3\rangle$	2.1±0.3, 2.5±0.1	R(2)
$\|0,4\rangle$	2.8 ± 0.2	R(3)[a]
$\|1,4\rangle$	4.6±0.4, 4.3± 0.2	P(5)
$\|3,2\rangle$	9.9 ± 1.3[b]	R(1)

[a] Overlapped bands.
[b] This value is for HD^* and is from Fink, Akins, and Moore, J. Chem. Phys. **56**, 900 (1972).

Table II H_2^* - D_2 Quenching Results

H_2 Quantum State $\|v',J'\rangle$	Quenching Cross Section ($Å^2$)	Line
$\|0,0\rangle$	105 ± 13	P(1)
$\|0,1\rangle$	69 ± 9	R(0)
$\|0,2\rangle$	68 ± 14	R(1)
$\|0,3\rangle$	76 ± 10	R(2)
$\|1,2\rangle$	84 ± 11	P(3)
$\|1,4\rangle$	77 ± 11	R(3)
$\|3,2\rangle$	79 ± 14[a]	R(1)

[a] This value is for HD^* self-quenching and is from Fink, Akins, and Moore, J. Chem. Phys. **56**, 900 (1972).

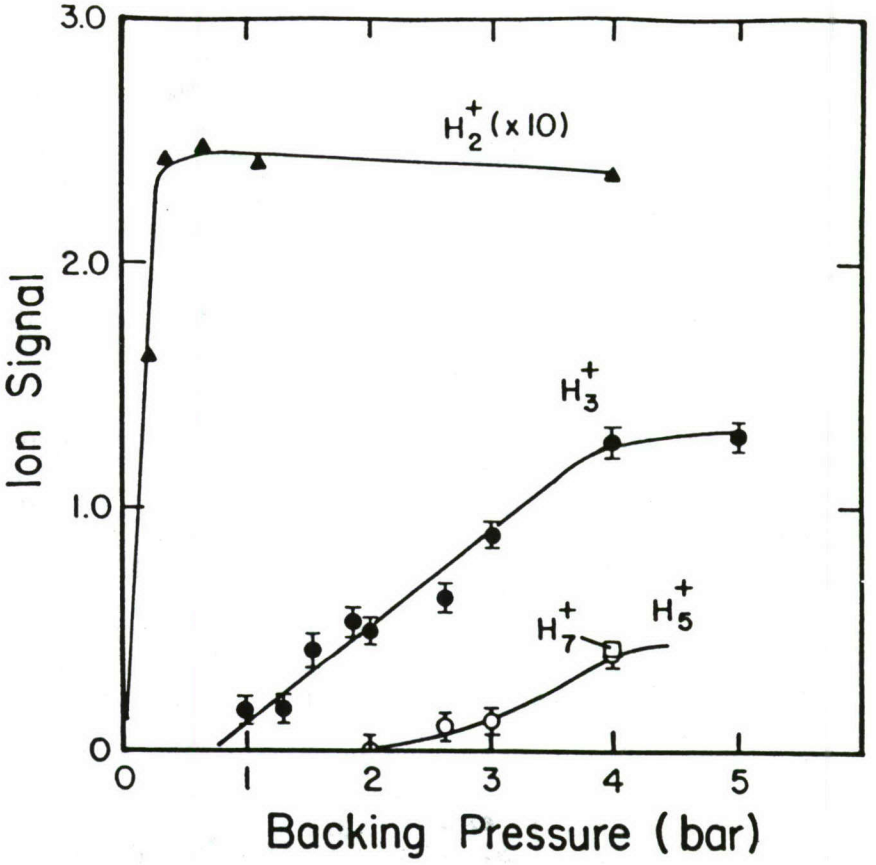

Figure 1.

H_2 cluster ion signal vs pressure of H_2 in pulsed valve reservoir. Reservoir temperature is 77 K.

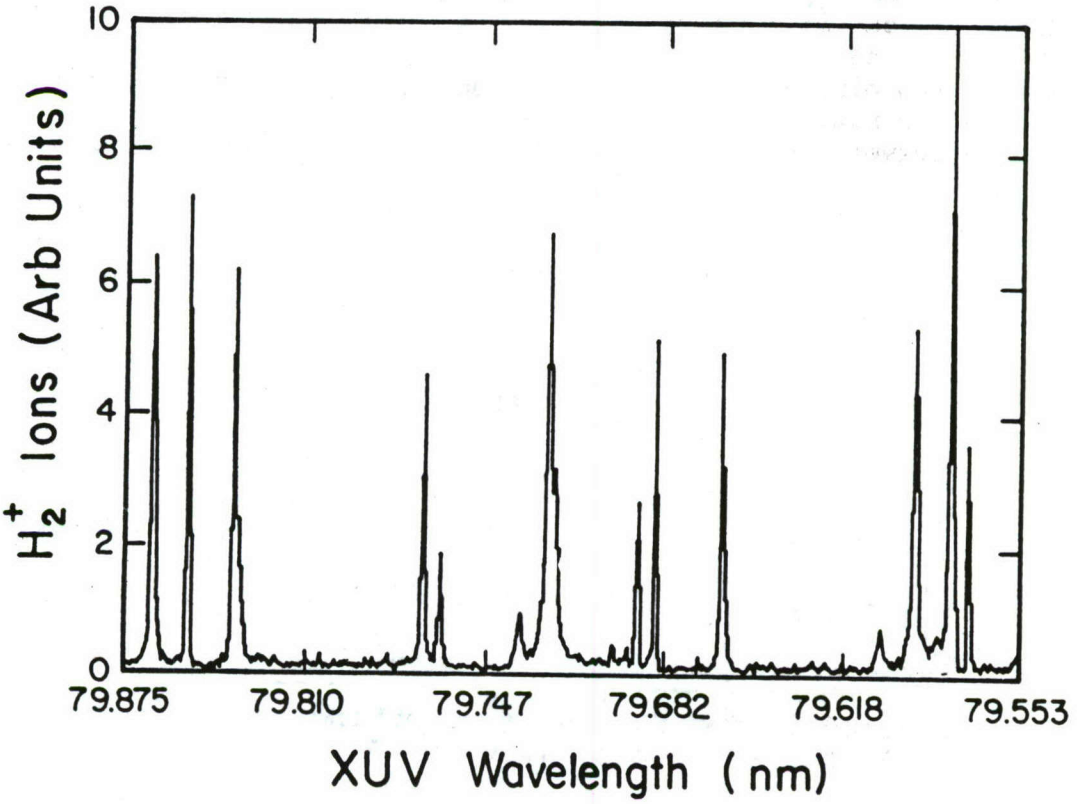

Figure 2. Direct laser photoionization spectrum of H_2 in a pulsed beam.

CHARACTERIZATION OF TETRAHYDROGEN VIA STATE-SELECTED EXCITATION OF H_2

W.J. Marinelli and A.M. Woodward

High Energy Density Matter Conference
Newport Beach, CA

29 February to 2 March 1988

The theoretical studies of Nicolaides et al.[1-3] predict that a bound "excimer state" of H_4 arises from the reaction of H_2 in its ground state with H_2 that has been excited to the $B^1\Sigma_u^+$ state:

$$H_2(B^1\Sigma_u^+) + H_2(X^1\Sigma_g^+) + M \rightarrow H_4^* + M \quad .$$

The goal of our program is to produce and characterize H_4^*. Our approach to producing H_4^* is to create $H_2(B)$ in a supersonic jet while providing a sufficient number of collisions with H_2 to produce H_4^* in the expansion.

In our initial experiments, $H_2(B)$ was formed by discharge excitation of H_2 or H_2/Ar mixtures. This was accomplished using the throat-discharge modifications to an NRC pulsed valve as described by Grant and coworkers[4] and further modified in our laboratory. These modifications are shown in Figure 1. The basic concept involves the passage of the expanding gas through a region between two biased plates. The two plates are separated by a ceramic insulator. When the nozzle is closed the pressure is sufficiently low that no discharge occurs between the plates. As the valve opens and gas fills the void between the plates, initially spark breakdown occurs between the plates

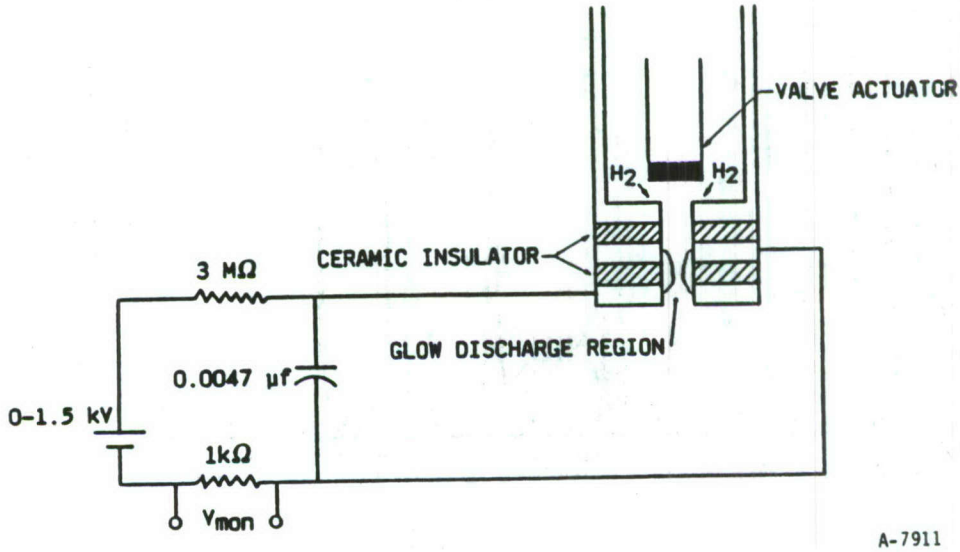

Figure 1. Schematic of Nozzle Discharge Source

and then, as the pressure increases, the transition to glow discharge conditions occurs. Under our operating conditions the discharge self-fires and has a 2 μs pulse duration.

A spectrum of the emission from the discharge region was obtained using a vacuum ultraviolet monochromator. A typical spectrum for a pure H_2 discharge is given in Figure 2 along with a computer generated spectral fit to the spectrum. The vibrational distribution peaks at $v'=3$.

After determining that $H_2(B)$ was formed in the discharge, an attempt was made to observe H_4^*. Detection of H_4^* may be via observation of passive emission from the radiating excimer or via photodissociation of H_4^* to produce $H_2(B)$, which may be observed in emission. Emission was detected with a broadband radiometer (130 to 190 nm) or a monochromator (190 to 540 nm). No passive emission from H_4^* was observed. A nitrogen laser was used for photolysis of H_4^* at 337 nm. The photolysis laser was delayed with respect to the discharge source. Delays of 0 to 30 μs were used, but no $H_2(B)$ emission was observed. To determine if H_4^* is photodissociating to form ions, a cleaner source of $H_2(B)$, such as direct laser excitation (our discharge source produces ions), would be required.

Nicolaides[5] predicts an H_4^* lifetime of 1 to 100 ps. If the excited state lifetime of H_4^* is 100 ps, we calculate the efficiency for producing H_4^* from quenching of $H_2(B)$ in ouor experiments is less than 0.02. From our calculations we should have been able to detect H_4^* if the lifetime is longer than 5 ps. Several problems with the discharge source exist. If the

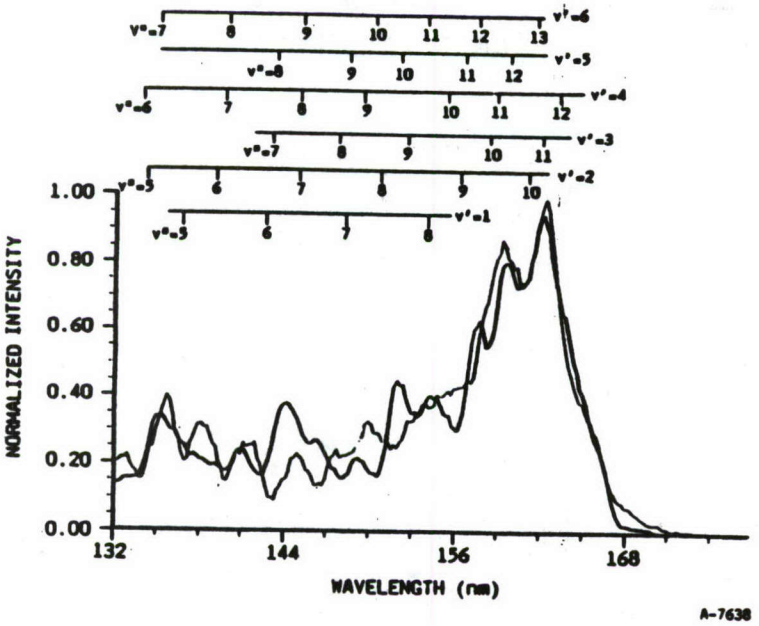

Figure 2. $H_2(B)$ Emission Spectrum. Thin line represents measured spectrum and thick line is the spectral fit.

discharge fires before the valve fully opens, then the H_2 concentration could be considerably less than the nozzle stagnation pressure. Hence, the question arises whether $H_2(B)$ is quenched. The discharge source also produces H-atoms which could quench $H_2(B)$ or possibly react with H_4^*. Finally, it is questionable as to whether the H_4^* complex can survive the hot plasma environment of the discharge. Hence, while our experiments are not conclusive, they do point towards a low efficiency for H_4 production.

In our studies we have also measured rovibronic quenching rate coefficients for $H_2(B)$ and examined the vibrational relaxation channel. In these experiments, $H_2(B)$ is formed by three-photon laser excitation of H_2. The fluorescence from $H_2(B)$ is then measured as a function of hydrogen pressure in a static cell. A three-photon excitation spectrum of hydrogen is obtained by scanning the laser and measuring the total $H_2(B)$ fluorescence signal. A typical excitation spectrum is given in Figure 3. Alternatively, one can set the laser wavelength to excite a single rotational transition and then scan the monochromator to obtain a resolved-fluorescence spectrum. The spectrum in Figure 4 was obtained by exciting $H_2(B, v'=3, J'=2)$ and resolving the fluorescence signal at a resolution of 40 Å.

Our computer spectral fitting codes were used to generate a fit to the experimental spectrum, which is also shown in Figure 4. All features in the spectrum could be assigned to $v'=3$, the vibrational state that was excited by the laser. No evidence for vibrational relaxation was found.

To determine quenching of $H_2(B)$ by H_2 the intensity of a single rotational transition was measured as a function of H_2 pressure in the cell. The

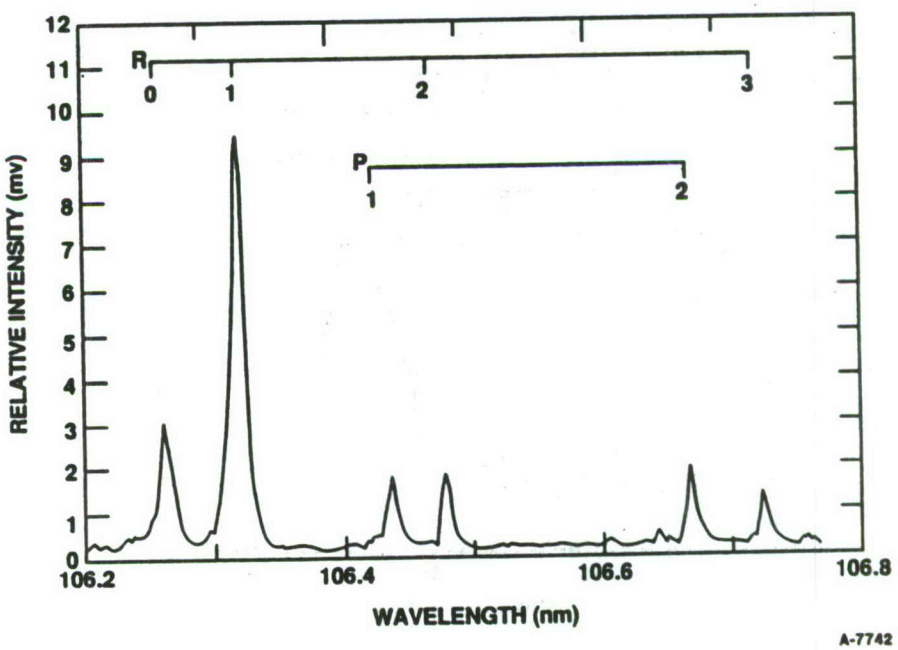

Figure 3. Three-Photon H_2 Excitation Spectrum. $H_2(B,v'=3)$ - $H_2(X,v=0)$, 80 torr of H_2

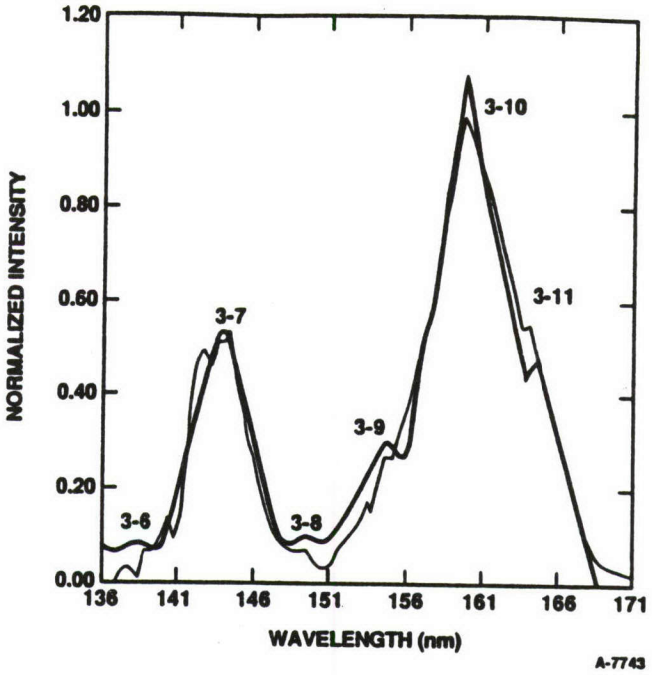

Figure 4. Excitation of v'=3, J'=2 Transition $H_2(B)$ Emission Spectrum. Spectrum taken with 40 Å resolution and 102 torr of H_2.

intensity was then determined by integrating the area under the peak. Use of peak height as an intensity measure was insufficient for two reasons. First, pressure broadening of the peak becomes appreciable as the pressure is increased. In addition, a second broadening mechanism, stark broadening from the laser field, was also observed.

A Stern-Volmer analysis of the data is used to determine the quenching rate coefficient. The production and depletion of $H_2(B)$ can be summarized in three equations:

$$H_2 + h\nu \text{ (3 photons)} \rightarrow H_2(B,V',J') \qquad k_1 \qquad (1)$$

$$H_2(B,V',J') \rightarrow H_2(X,V'',J'') + h\nu \text{ (Lyman Bands)} \qquad k_2 \qquad (2)$$

$$H_2(B,V',J') + H_2 \rightarrow \text{Products } (2H_2, \text{ H-Atoms, } H_4^*) \qquad k_3 \quad . \qquad (3)$$

The $[H_2(B)]$ is in steady state during the laser pulse since the radiative lifetime is ten times shorter than the laser pulse duration:

$$\frac{d[H_2(B)]}{dt} = k_1[H_2] - (k_2 + k_3[H_2])\,[H_2(B)] = 0 \quad . \qquad (4)$$

Substituting $[H_2(B)] = I^*/k_2$ and rearranging, one obtains the equation

$$\frac{[H_2]}{I^*} = \frac{1}{k_1} + \frac{k_3}{k_1 k_2}[H_2] \quad . \tag{5}$$

To obtain k_3, one plots $[H_2]/I^*$ versus $[H_2]$ where the slope/intercept ratio is k_3/k_2. A summary of all the quenching rate coefficients determined is given in Table 1. There does not appear to be any significant difference in quenching coefficients for the two vibrational levels for the same J level. There does appear to be some difference between different J levels but, because of the uncertainty in the measurements, it is difficult to determine if a true rotational dependence of the quenching rate coefficient exists.

Table 1. $H_2(B)$ Quenching Rate Coefficients

v	J′	Transition	$k_3(10^{-10}$ cm^3 molecule^{-1} s$^{-1})$
3	0	P(1)	8.4 ± 1.8
	1	P(2)	13 ± 3
	2	R(1)	15 ± 6
	3	R(2)	13 ± 3
	4	R(3)	5.5 ± 1.5
4	1	P(2)	6.6 ± 1.4
	2	R(1)	13 ± 4
	4	R(3)	4.5 ± 1.0

REFERENCES

1. Metropulos, A. and Nicolaides, C.A., "Towards Understanding the Stability of the $H_4^*(C_{3V})$ Cluster," Z. Phys. D., 5, 175 (1987).

2. Nicolaides, C.A., Theodorakopoulos, G., and Petsalakis, I.D., "Theory of Chemical Reactions of Vibrationally Excited $H_2(B^1\Sigma_u^+)$. I. Prediction of a Strongly Bound Excited State of H_4," J. Chem. Phys., 80, 1705 (1984).

3. Nicolaides, C.A., Petsalakis, I.D., and Theodorakpooulos, G., "Theory of Chemical Reactions of Vibronically Excited $H_2(B^1\Sigma_u^+)$. I. Prediction of a Strongly Bound Excited State of H_4," J. Chem. Phys., 80, 1705 (1984).

4. Grant, E.R., private communication.

5. Nicolaides, C.A., HEDM Conference, Newport Beach, CA, March 1988.

Spectroscopy of Polyatomic Hydrogenic Species

Takeshi Oka

Department of Chemistry and
Department of Astronomy and Astrophysics
The University of Chicago
Chicago, Illinois 60637

Several experiments have been conducted in order to observe and characterize novel spectra of polyatomic hydrogenic species in the infrared region using a laser spectrometer as well as a Fourier transform spectrometer. We report here on two of them which have produced definitive results.

(1) Observation of the $2\nu_2 \leftarrow \nu_2$ and the $\nu_1 + \nu_2 \leftarrow \nu_1$ Hot Band Spectra of H_3^+.

Moungi Bawendi and Brent Rehfuss.

Ever since the discovery of the infrared spectrum of the H_3^+ molecular ion (1), attempts to observe and characterize higher excited vibrational states of this fundamental molecular ion have been made. Using a high temperature high pressure hollow cathode plasma Majewsky, Marshall, McKellar, Johns and Watson (2) observed spectra starting from rotationally hot levels up to J=10. We have observed spectra of H_3^+ starting from the ν_1 and the ν_2 vibrationally excited states which are 3181 cm^{-1} and 2521 cm^{-1} above the ground state, respectively (see Fig. 1).

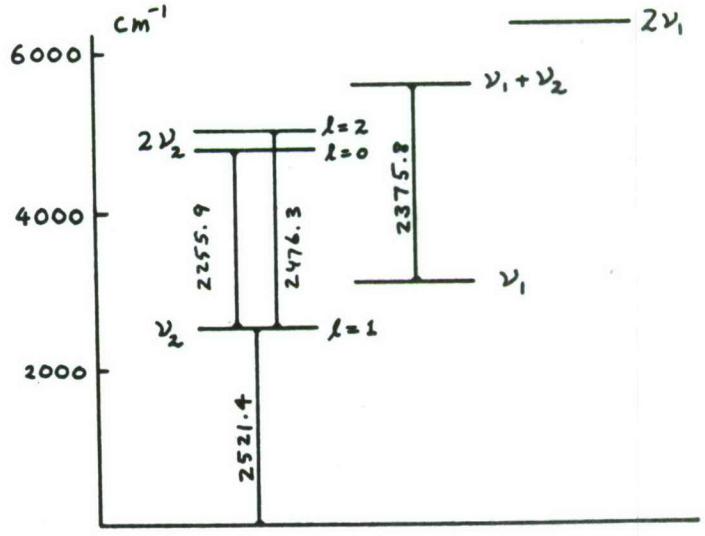

Figure 1

Two techniques previously not used for spectroscopy of H_3^+ were useful for the observation.

A. Liquid N_2 Cooled He:H_2 Plasmas.

In order to observe hot bands, we need to prepare H_3^+ in excited vibrational states but in relatively low rotational levels so that the rotational partition function is not large. In other words, we need a plasma with high vibrational temperature but low rotational temperature. This was done by using a liquid-N_2 cooled multiple inlet-outlet cell and a mixture of He and H_2 with the mixing ratio of ~10:1. The large ionization potential of He (24.6 eV versus 15.4 eV of H_2) increases the electron temperature of the plasma, while the low proton affinity of He (1.9 eV versus 4.4 eV of H_2) keeps the concentration of H_3^+ unreduced. In addition, the discharge characteristics of He which allows stable discharges at relatively high pressure (~10 torr) decreases the electron drift velocity in the plasma and thus increases the electron and ion concentration for a given discharge current. We thus produced plasmas with vibrational temperature of 1000 ~ 1500 K and rotational temperature of ~400 K.

B. $LiIO_3$ as the Non-Linear Optical Element.

In order to cover the hot band spectra, it was necessary to extend the coverage of the difference frequency laser system to longer wavelength regions. This was done by using $LiIO_3$ crystals as the non-linear optical element rather than the usual $LiNbO_3$ crystal. In addition the phase matching condition required an angle tuning instead of temperature tuning (3). The optical arrangement of the crystals is shown in Figure 2. Green (5145 Å) single moded radiation from an Ar ion laser with the power of ~1 Watt and yellow to red frequency tunable radiation from a ring dye laser with the power of ~800 mWatt are mixed in the $LiIO_3$ crystals to generate frequency tunable infrared radiation with the power of the order of ~5 μWatt. This device has enabled us to

cover from 5000 cm^{-1} to 1850 cm^{-1} so that the whole spectra of the three hot bands are covered.

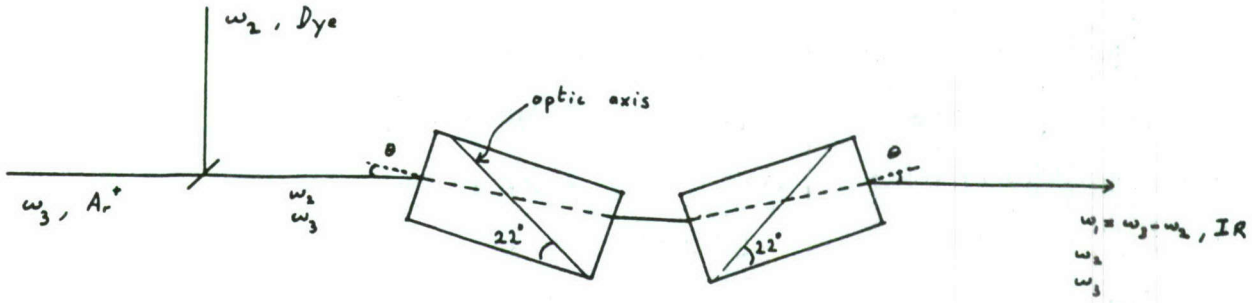

Figure 2

C. Observed Spectrum.

We have observed about 300 lines in the frequency region between 2950 and 2000 cm^{-1}. Many lines have been assigned to the $2\nu_2(\ell = 2) \leftarrow \nu_2(\ell = 1)$ and $\nu_1 + \nu_2 \leftarrow \nu_1$ hot bands. The theoretical ab-initio prediction by Miller and Tennyson (4) has been of great help. The $2\nu_2(\ell = 0) \leftarrow \nu_2(\ell = 1)$ band is yet to be assigned. There are many more lines observed than expected from the three hot bands. They suggest that we have higher hot bands and various forbidden transitions. The complete analysis of the spectrum will take some time.

Observation of the hot bands opens the possibility for the study of vibrational temperatures in the plasma. In particular, we should be able to study the dependence of temperature on the symmetry of the vibrational modes.

2. Observation of the Tetrahexacontapole (2^6)-Type Transitions in Solid Hydrogen.

Mitchio Okumura and Man-Chor Chan

Because of the relatively weak intermolecular interaction, molecular hydrogens are "freely" rotating even in solids and thus have discrete rotational levels. On the other hand the intermolecular interaction induces dipole moments

in H_2 and causes intense quadrupole-type transitions as initially studied by Welsh and his colleagues (5). Such interaction also causes higher multipole transitions and hexadecapole-type ($\Delta J=4$) vibration-rotation transitions (6) and pure rotational transitions (7) have been reported.

We have observed tetrahexacontapole (2^6)-type W($\Delta J=6$) rotational transitions and U($\Delta J=4$) + S($\Delta J=2$) double transitions in the infrared spectrum of solid hydrogen. Spectra from 1800 to 8000 cm^{-1} of polycrystalline hydrogen at 4K in a 115 mm cell were recorded with a Bomem FT-IR spectrometer.

References.

(1) T. Oka, Phys. Rev. Lett. 45, 531 (1980).

(2) W.A. Majewsky, M.D. Marshall, A.R.W. McKellar, J.W.C. Johns, and J.K.G. Watson, J. Mol. Spectrosc. 122, 341 (1987).

(3) S. Yu. Volkov, D.N. Kozlow, P.V. Nikles, A.M. Prokhorov, V.V. Smirnov, and S.M. Chuksin, Sov. J. Quantum Electron 11, 135 (1981).

(4) S. Miller and J. Tennyson, J. Mol. Spectrosc. 128, 530 (1988).

(5) H.P. Gush, W.J.J. Hare, E.J. Allin, and H.L. Welsh, Can. J. Phys. 38, 176 (1960).

(6) P.R.G. Prasad, M.J. Clouter and S.P. Reddy, Phys. Rev. A17, 169 (1978).

(7) T.K. Balasubramanian, C.-H. Lien, K.N. Rao, and J.R. Gaines, Phys. Rev. Lett. 47, 1277 (1981).

STABLE AND UNSTABLE ORBITS OF THREE PROTONS AND THREE ELECTRONS

H. Helm, P. C. Cosby and L. J. Lembo.
Molecular Physics Department,
SRI International

A detailed study on photoexcitation of long-lived H_3 species has been carried out. Four groups of experiments were performed.

1. Photodissociation of H_3

This study allows direct access into the ground state of H_3, under conditions where all good quantum numbers of the six-particle system, the total energy, the parity, and the geometry of the transition state are defined within the uncertainty-principle limit. The half-collision of the laser-selected transition state into the continuum is mapped out by measuring the translational energy and internal energy content of the dissociation products $H_2(v,J)$ + H(1s). First views of the triple-collision of the transition state into three separate atomic products, H(1s) + H(1(s) + H(1s) + E_{kin} are obtained also.

2. Two-Photon Ionization of H_3

In this experiment, one-photon-resonant two photon ionization is used to measure the energy separations between the lowest metastable species of H_3 and H_3 states built from H_3^+ cores in different state of vibrational excitation with either a 3s or 3d electron. The novel pieces of information obtained here are the bending and symmetric stretch vibrational frequencies of neutral H_3.

3. Field Ionization of High Rydberg States of H_3

Photoexcitation of the nd Rydberg states (n ranging from 26 to above n=100) is detected by field-ionization of the weakly bound electron. This study permits us to explore electron-core interactions. Specifically, we observe the mixing of cores with rotational quantum numbers N^+=3 and N^+=1 with d-electrons in different n-values. The analysis of the data obtained here will enable us to characterize the gradual uncoupling of the motion of the electron from the motion of the core. Theoretical models exist for this uncoupling in H_3. The fun here is that H_3 behaves in many respects like an atomic, one-electron system, where one knows the core structure and its orientation.

4. Vibrational Autoionization of H_3

Photoexcitation of vibrationally excited H_3 molecules permits us to populate Rydberg states that are bound to vibrationally excited cores, but that lie above the ionization threshold. Exchange of electron and core energy

allows vibrational autoionization. We have obtained first data on the rate of autoionization for symmetric stretch and bending mode excited cores. A first analysis points to the symmetric stretch mode having the faster autoionization rate; however, more detailed analysis is needed before general rules can be derived.

Details

The longevity of H_3 in the $2p^2A_2"$ state in the lowest rotational level, J=0 is by now experimentally well established.[1,2]. This species is built by adding a p-orbital perpendicular to the triangular H_3^+ ion in the lowest ortho (three parallel nuclear spins) state. The core is characterized by the quantum numbers $N^+ = 1$, $K^+ = 0$. This molecular frame tumbles end-over-end, the angular momentum of rotation being balanced by the p-orbital angular momentum to result in J = 0. The lifetime of this state with respect to predissociation appears to ultimately derive from the fact that rotational coupling to the ground-state H_3 surface is suppressed since the latter cannot exist in a J = 0 state of the same overall symmetry.[3]

We form the metastable molecule by adding an electron to a mass-selected beam of H_3^+ in a charge-transfer reaction with cesium. A new high-intensity source of H_3^+ has significantly enhanced the signal to noise level over what we had obtained previously. The neutral beam is either photoexcited in the coaxial laser-neutral beams spectrometer described in Reference 4 or in the photodissociation spectrometer described in Reference 5.

The following figures serve to illustrate some of the findings: in Figure 1 we show the nd Rydberg series converging to the lowest vibrational level of H_3^+ excited from the non-vibrating metastable state. The line positions of the series follow within 0.1 cm^{-1} the simple Rydberg formula

$$E = E_{lim} - Ry/(n-\delta)^2, \qquad (1)$$

where the ionization limit is found to be $E_{lim} = 29862.58\ cm^{-1}$, and the quantum defect $\delta = 0.0204$. The absorption intensity of the series shows a distinct modulation which results from the interaction of Rydberg states built on various cores, specifically the d-series on $(N^+, K^+) = (1,0)$ and $(3,0)$. A second perturbation appears to derive from the (3,3) core, but should not exist based on selection rules. We are currently struggling with an explanation.

Figure 2 shows the location of the field ionized series and the vibrationally autoionizing series members that we have observed to date. A sample of vibrationally autoionizing transitions is given in Figure 3. We suspect that the excessive width of the 6d peak may be a consequence of power broadening.

A photodissociation spectrum near 6000 Å is shown in Figure 4. The transitions shown are diagonal transitions from differing ν_1,ν_2 cores,

populating the 3s and 3d states. The 3s predissociates as a consequence of vibronic coupling to the ground-state surface; the 3d does so by rotational coupling. Predissociation is observed here by monitoring the appearance of the two neutral fragments H_2 and H using a position and time-sensitive detector. This permits a determination of the internal energy content of the H_2 photofragment. A typical example of such a distribution is given in Figure 5.

Several months of data-analysis lie ahead! We thank the Air Force Office of Scientific Research for financial support of this work. We also acknowledge support by NSF for the construction of the spectrometers and the initial photoionization work. It is a pleasure to thank Dr. D. L. Huestis and Dr. R. P. Saxon for many stimulating discussions.

1. G. I. Gellene and R. F. Porter, J. Chem. Phys. 79, 5976 (1983).
2. J. F. Garvey and A. Kuppermann, Chem. Phys. Lett. 107, 491 (1984).
3. D. L. Huestis, private communication.
4. H. Helm, Phys. Rev. Lett. 56, 42 (1985).
5. H. Helm and P. C. Cosby, J. Chem. Phys. 86, 6813 (1987).

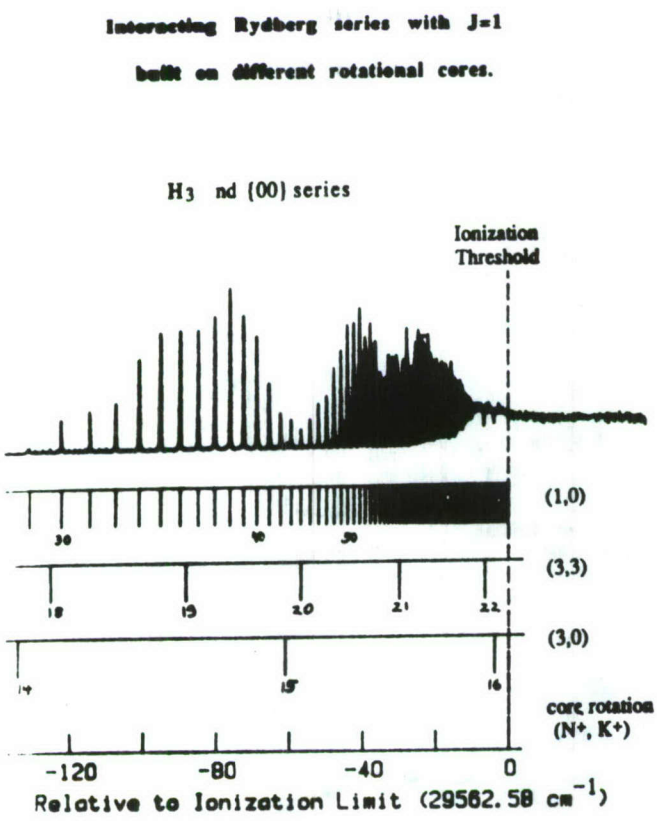

Figure 1

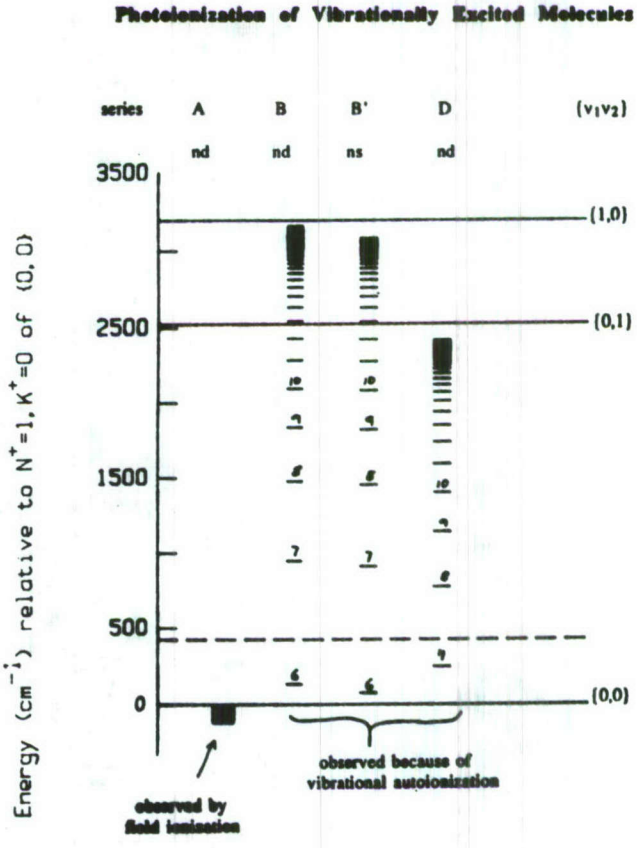

Figure 2

Vibrational Autoionization Lifetimes

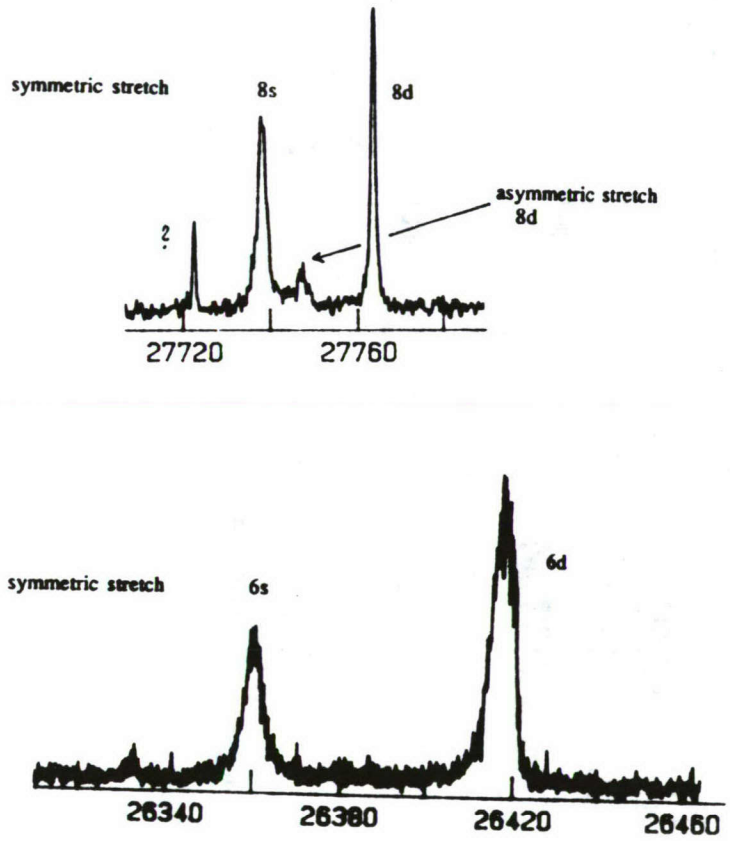

Figure 3

Photoabsorption of metastable H_3 $2pA_2''$ $(v_1\ v_2)$ detected by monitoring photodissociation

Atomic-like spectrum, since molecule is long lived only in the lowest rotational level.

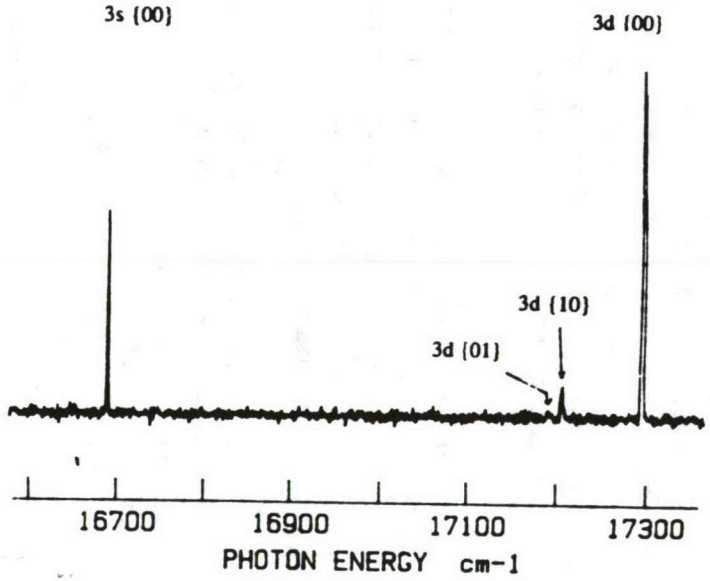

Figure 4

Predissociation of H_3 3s (0,0)

vibronic coupling to the H_3 ground state surface

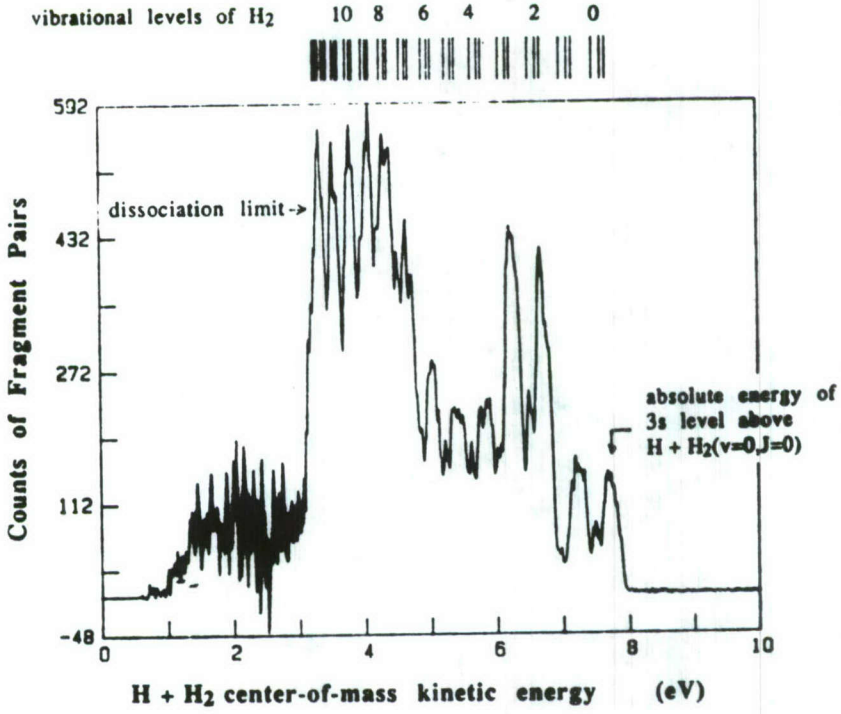

Figure 5

IONIC SOLID HYDROGEN FUEL: PRODUCTION AND PROPERTIES OF HYDROGEN CLUSTERS

Young K. Bae and Philip C. Cosby
Molecular Physics Department
SRI International

1. Introduction

One of the most attractive candidates for a new propellant might be the tetrahydrogen, H_4^* molecule. However, recent theoretical calculations indicate that the H_4^* might have a very short lifetime in gas phase. Although the H_4^* may have a short lifetime in gas phase, its essential components, H_3^+ and H^-, might be stably stored in solid of H_2. The solid hydrogen contains very high concentration of H_3^+ and H^-, and each ion is completely surrounded by H_2 which acts as a buffer against the direct reaction between ions. Figure 1a shows one possible example of such a hypothetical solid: ionic solid hydrogen whose specific impulse is greater than 1000 s. The solid becomes regular solid hydrogen with the hexagonal close-packed structure, if the ions are left out.

In the first order approximation, stability of this kind of solid can be estimated based on stability of positive and negative hydrogen cluster ions. In fact, the theoretically predicted[1,2] H_{13}^+ (H_3^+ completely surrounded by five H_2 molecules) shown in Figure 1b has a very similar arrangement of H_2 molecules to solid H_2. Thus, H_3^+ can be imbedded in the H_2 matrix without disturbing its lattice characteristics. On the other hand, the stability of H_{11}^- (H^- completely surrounded by H_2 molecules) shown in Figure 1c is not well understood,[2] and further experimental and theoretical studies on the negative hydrogen cluster ions will be very important. Perhaps, estimating the stability of the ionic solid based on gas phase negative cluster ions would be erroneous, because their binding energies are very small, and thus they can be strongly purturbed by surrounding molecules in the condensed phase unlike the positive cluster ions. In this case, direct studies of H^- in the H_2 matrix would be required.

We also proposed that one possible method of producing such solid would be codepositing positive and negative hydrogen cluster ions on a cryogenic surface. Therefore, studies of hydrogen cluster ions will lead to vital information on the properties as well as mass production methods of such high energy density ionic solid hydrogen fuel.

2. Production of intense positive hydrogen cluster ion beams

We have designed, built, and successfully tested an ion source to produce intense fast beams of "rotationally cold" hydrogen cluster ions. The schematic diagram of the experimental apparatus is shown in Figure 2. The positive hydrogen cluster ions are produced by the ion source which is composed of a pulsed supersonic expansion of ~5 atm H_2 gas through a

1-mm-diameter nozzle followed by intense electron beam bombardment (~ 1 mm from the exit of the nozzle) in the early stage of expansion. In this stage, abundant H_3^+ ions which are nucleation cores for the positive cluster ions are generated in the following reactions:

$$H_2 + e \rightarrow H_2^+ + 2e \quad (1)$$

$$H_2^+ + H_2 \rightarrow H_3^+ + H. \quad (2)$$

Subsequently, the rotationally cold cluster ions are produced by nucleating H_2 onto H_3^+ via three body clustering reactions occurring during the free-jet expansion. After formation, the cluster ions are accelerated to 3 keV, mass analyzed, and highly collimated by series of ion optics. Figure 3 shows the typical mass spectrum of hydrogen cluster ions produced by the source. The most abundant species is H_3^+ which is produced in the reaction (2). As the size of the clusters becomes large, the intensity of the clusters becomes progressively small. The peak currents of H_5^+ measured on a Faraday cup just prior to the laser ion beam interaction region was about 10 nA.

3. Preliminary photofragment study of H_5^+

We performed preliminary photofragment experiment of H_5^+ at single laser energy (3.50 eV, tripled YAG output). The mass selected and collimated ion beam is merged coaxially with a laser beam over a length of 60 cm using an electrostatic quadrupole, Q1. The fragment ions produced in the interaction region are separated from the primary ion beam by a second quadrupole, Q2 and then detected by a channel electron multiplier. With this arrangement, individual fragment channel can be clearly separated. The result is given in the table 1 in which each channel yield is normalized to the photofragment yield of H^+ from H_2^+. The most abundant channel of H_5^+ photofragmentation is $H_3^+ + H_2$. This observation agrees with the theoretical prediction[1,2] and the experimental observation[3] that the ground state of H_5^+ is composed of weakly bound H_3^+ and H_2. However, we could also observe weak channels that produce H^+ and H_2^+ as well as very weak H_4^+ channel.

With the above picture for H_5^+, the only way we can produce H^+ and H_2^+ channels is by breaking H_3^+. To tell whether H_3^+ can be broken into either H^+ or H_2^+ at this photon energy, 3.50 eV, we also have performed fragmentation of H_3^+ and observed both H^+ and H_2^+ channels. We have found that the channel for H^+ is a two photon process, but that for H_2^+ is a single photon process. Although the dissociation channels for H^+ and H_4^+ are not well understood at the present time, the channel for H_2^+ can be understood in the following explanation.

Very recently, Saxon and Talbi[4] have calculated the transition dipole moments connecting ground state ($1^1A'$), and first excited states of D_{3h} geometries ($1^1E'$) and C_s geometries ($2^1A'$). They have found that the transition dipole moment near the equilibrium geometry is substantial, but photodissociation of H_3^+ in its low vibrational state would require a very

high energy photon (>15 eV). Furthermore, they have predicted that there are C_s geometries, highly vibrationally excited state in the asymmetric stretch, where the transition moment is substantial and the excitation energy is 3-4 eV. These geometries in which the H^+ moves far away (4-5 a_o) from the H_2, can be described by a picture in which H_2^+ and H^+ are competing for an electron. In the $1^1A'$ state, H_2^+ wins, and the electron is localized around H_2^+. On the other hand, in the dissociative $2^1A'$ state, the electron is localized around H^+. Thus, strong dipole matrix elements connecting these states can be expected to produce H_2^+ fragments with single 3.5 eV photon.

H_3^+ generated in the reaction (1) and (2) can be both rotationally and vibrationally hot. Although in our supersonic source rotational energies are expected to be quenched by collisions in the expansion, vibrational energies which are very difficult to quench by collisions can survive. Thus, the observed dissociation channel for H_2^+ could well be originated from the highly vibrationally excited $1^1A'$ state (lies ~4 eV above the v=0 state). If the H_2^+ channel of H_5^+ is produced by breaking H_3^+, then, the present observation suggests that highly vibrationally excited states of H_3^+ lives extremlely long (> 1 μs) in the H_5^+. Considering that the binding energy between H_3^+ and H_2 (~ 0.25 eV) is much smaller than the expected vibrational energy, it is surprising that such highly vibrationally excited H_3^+ states can live so long in H_5^+. Further explanation will require more experimental investigation.

We thank the AFFTC for supporting this exciting research. We also wish to thank Drs. D. C. Lorents, R. P. Saxon, D. Talbi, and H. Helm for many useful suggestions and discussions.

1. Y. Yamaguchi, J. F. Gaw, and H. F. Schaefer III, J. Chem. Phys. 78, 4074 (1983).
2. K. Hirao and S. Yamabe, Chem. Phys. Lett. 80, 237 (1983).
3. M. Okumura, L. I. Yeh, and Y. T. Lee, J. Chem. Phys. 88 (1988).
4. R. P. Saxon and D. Talbi, SRI Final Report, MP 87-263 (1987).

Table 1

Photofragment at 354.7 nm (3.50 eV)

Primary Ion	Fragment	Relative Intensity
H_2^+	H^+	100
H_3^+	H^+	9.2
	H_2^+	3.6
H_5^+	H^+	2.3
	H_2^+	4.2
	H_3^+	360
	H_4^+	0.4

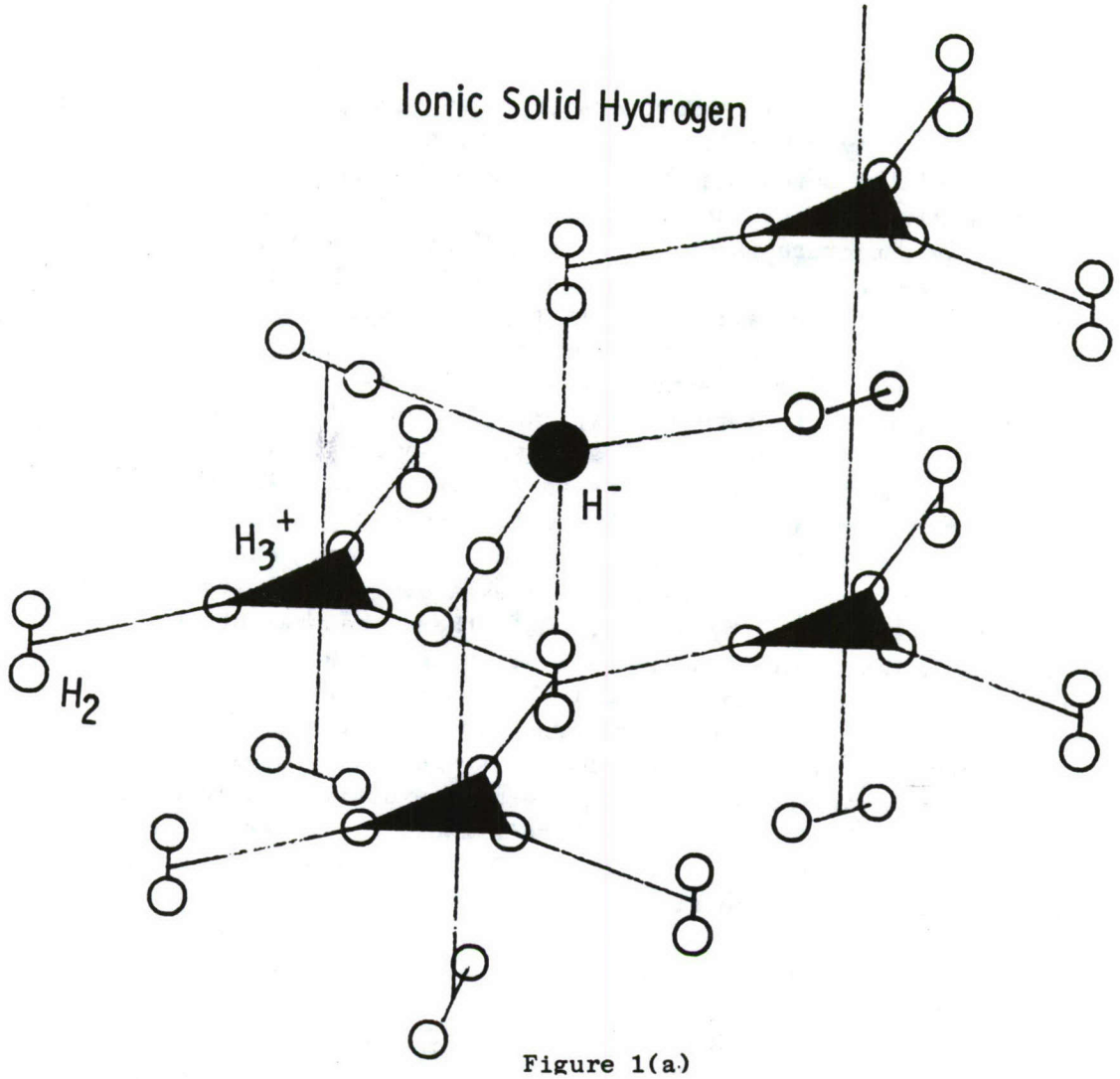

Figure 1(a)

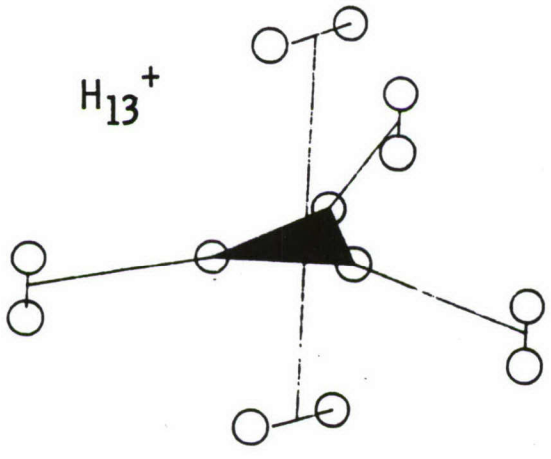

Figure 1(b)

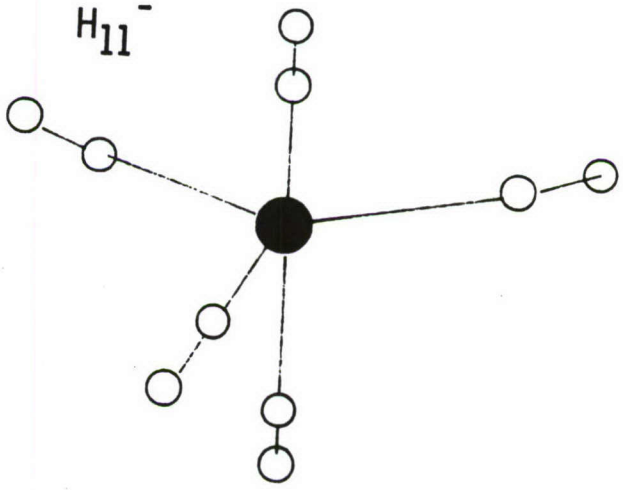

Figure 1(c)

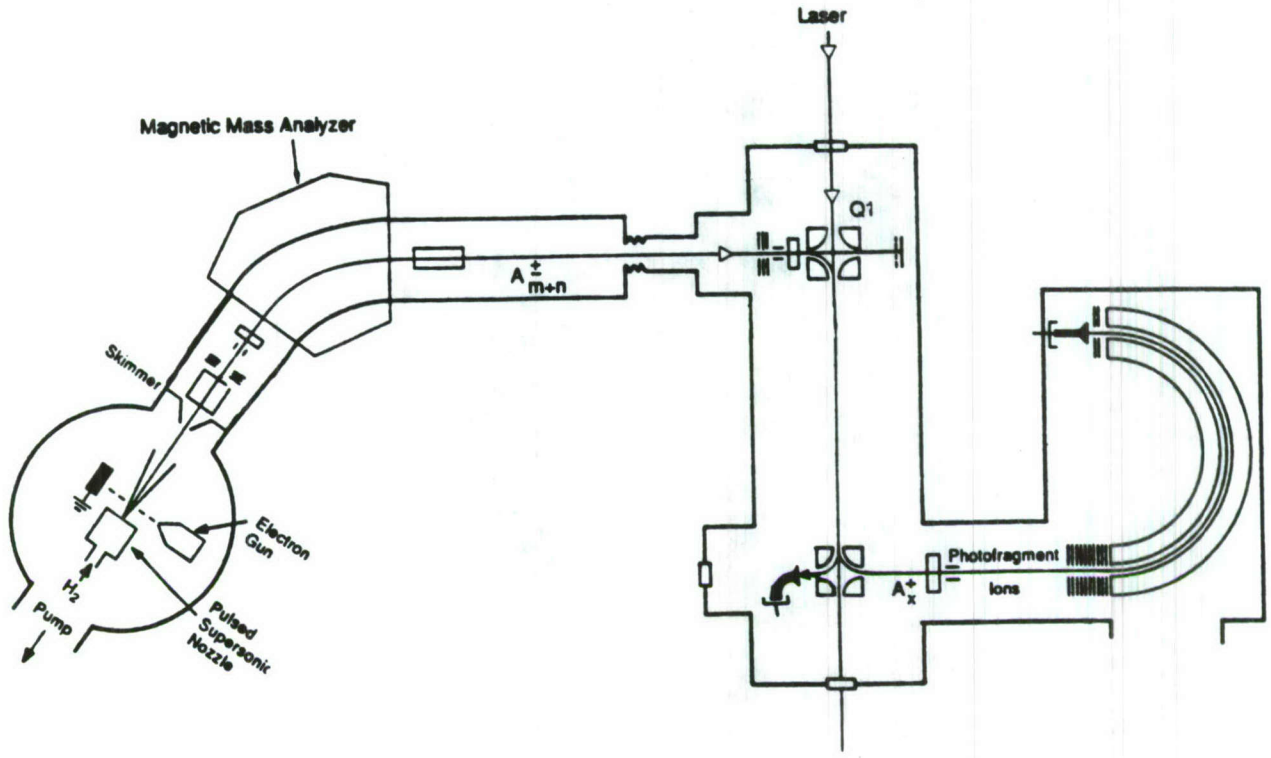

Figure 2

RA-m-330583-80

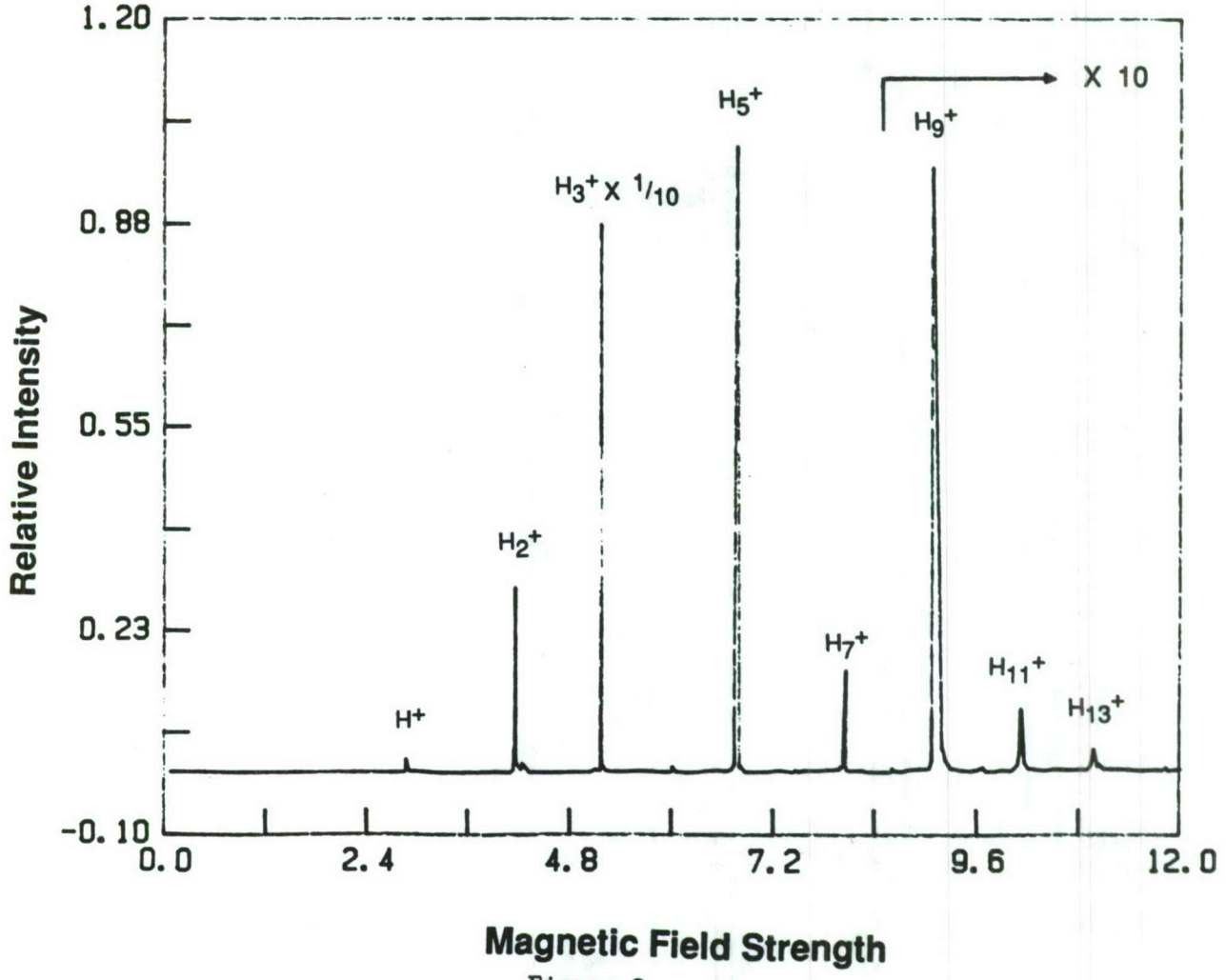

Figure 3

Quantum Monte Carlo Study of Decomposition Pathway of Tetrahydrogen

Sheng-yu Huang and William A. Lester, Jr.

Department of Chemistry

University of California, Berkeley and

Lawrence Berkeley Laboratory

Berkeley, CA 94720

ABSTRACT

The chemistry of molecules in excited electronic states can be very different from that of the corresponding ground-state species. The interaction of $H_2(X^1\sum_g^+)$ $\equiv$ $H_2(X)$ with $H_2(B^1\sum_u^+)$ $\equiv$ $H_2(B)$ has received considerable attention recently with the determination of a local minimum at a pyramidal nuclear arrangement.[1] The electronic distribution about the base was found to be electron deficient, resembling H_3^+, and the peak H was determined to be H^-.

Our recent efforts to extend understanding of the stability and energetics of this system have proceeded in two directions: (1) computation of nonadiabatic coupling matrix (NCM) elements over a range of geometries in 2 dimensions achieved by distorting the initial C_{3v} pyramidal geometry, and (2) calculation of the energetics of a T-approach pathway.

Calculations of NCM's in one dimension, the pyramid height R, have been carried by Nicolaides and coworkers[2] and by the present authors[3]. The interest here was to explore the crossing seam by including changes of the length of the pyramid base r. (For simplicity, all calculations were carried out in C_{3v} symmetry.) Full exploration of the NCM's for this system would require a 6-dimensional search.

As a first step towards the computation of NCM's in 2D, potential energies have been computed using MCSCF-CI methods at five geometries and are presented in

Fig. 1. The accompanying table lists the coordinates of the geometry number - the geometry number is simply an ordering scheme. A curve crossing is indicated between geometries 4 and 5. Note that further geometry variation would be necessary to fully delineate the crossing seam. Independent calculations that sample the seam had been presented previously by the Nicolaides group.

We have computed NCM's for the geometries considered in Fig. 1. The largest coupling is found for the dissociative doubly degenerate modes of C_{3v} symmetry. Fig. 2 shows the coupling strength vs. the inverse of the energy gap between the ground- and excited-state potential energy surfaces and confirms a linear dependence.

To complement out earlier study of the interaction energy for $H_2(B)$ approach to $H_2(X)$ in the perpendicular bisector plane, we have carried out calculations for a T-approach (both molecules lying in the same plane). These results show that collinear $H_3 + H$ can be formed without passing through the maximum ionicity excited state (MIES) pyramidal arrangement. The correlation diagram of Fig. 3 shows this finding schematically.

References

1. Nicolaides, C. A., Theodorakopouls, G., and Petsalakis, I. D., J. Chem. Phys. **80**, 1705 (1984).

2. Metropoulos, A. and Nicolaides, C. A., Z. Phys. D. **5**, 175 (1987).

3. Lester, W. A., Jr., *Quantum Monte Carlo Study of the MIES Associated with* $H_2(X^1\sum_g^+)$ *and* $H_2(B^1\sum_u^+)$, Final Report, Air Force Astronautics Laboratory, AFRPL 69022, October, 1987.

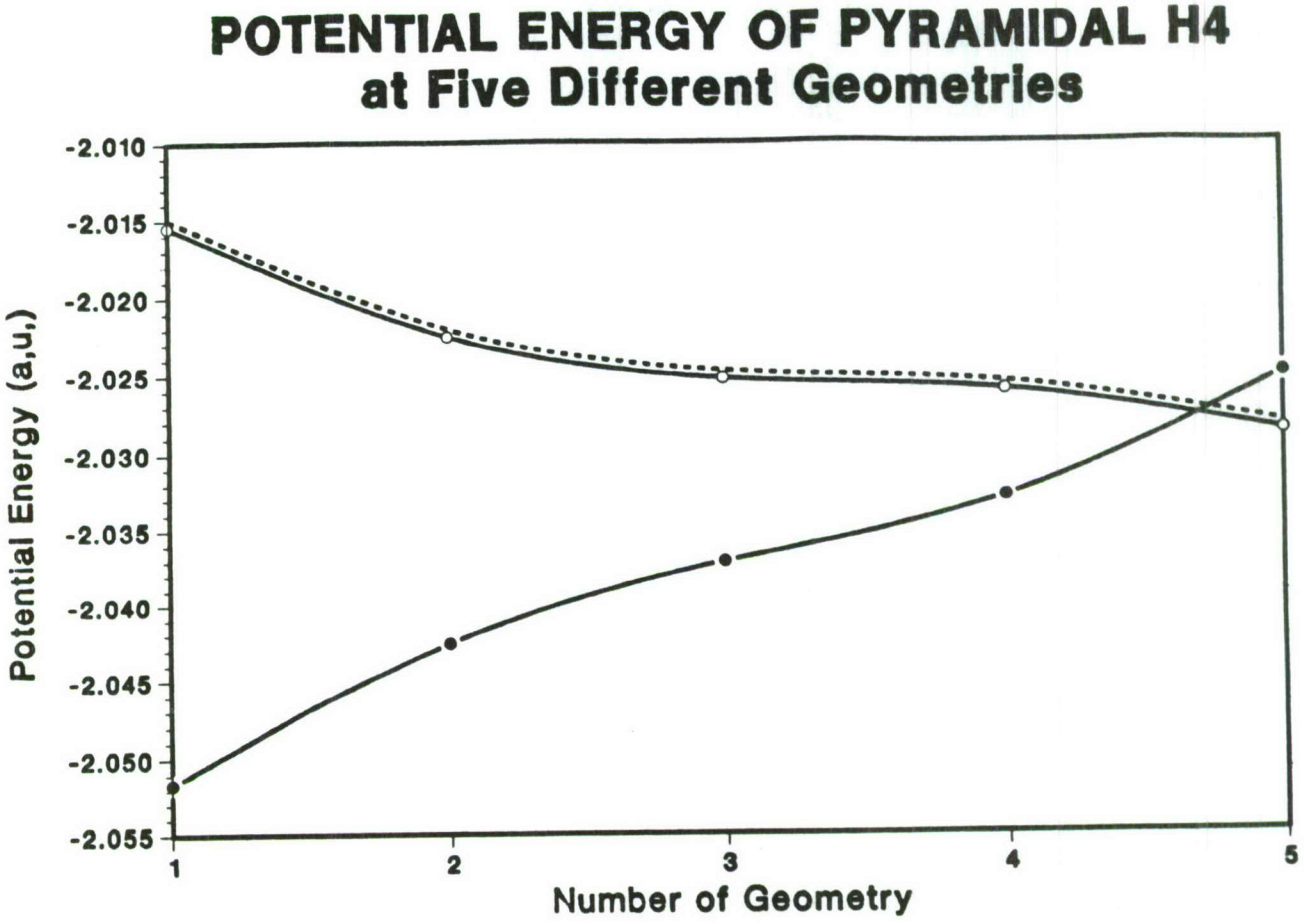

Table 1 Total Energies of Pyramidal H_4

#	r (a.u.)	R (a.u.)	E_1 (a.u.)	E_2 (a.u.)	E_3 (a.u.)
1	1.70	4.0	-2.05165	-2.01548	-2.01548[a]
2	1.80	4.22	-2.04257	-2.02251	-2.02251[a]
3	1.80	4.4	-2.03717	-2.02527	-2.02527[a]
4	1.80	4.6	-2.03294	-2.02607	-2.02607[a]
5	1.90	4.6	-2.02877	-2.02877	-2.02512[b]

[a] *Ground state is A and excited states are doubly degenerate E of C_{3v}.*

[b] *Ground state is doubly degenerate E and the excited state is A of C_{3v}.*

Fig. 1

COUPLING vs INVERSE OF ENERGY GAP

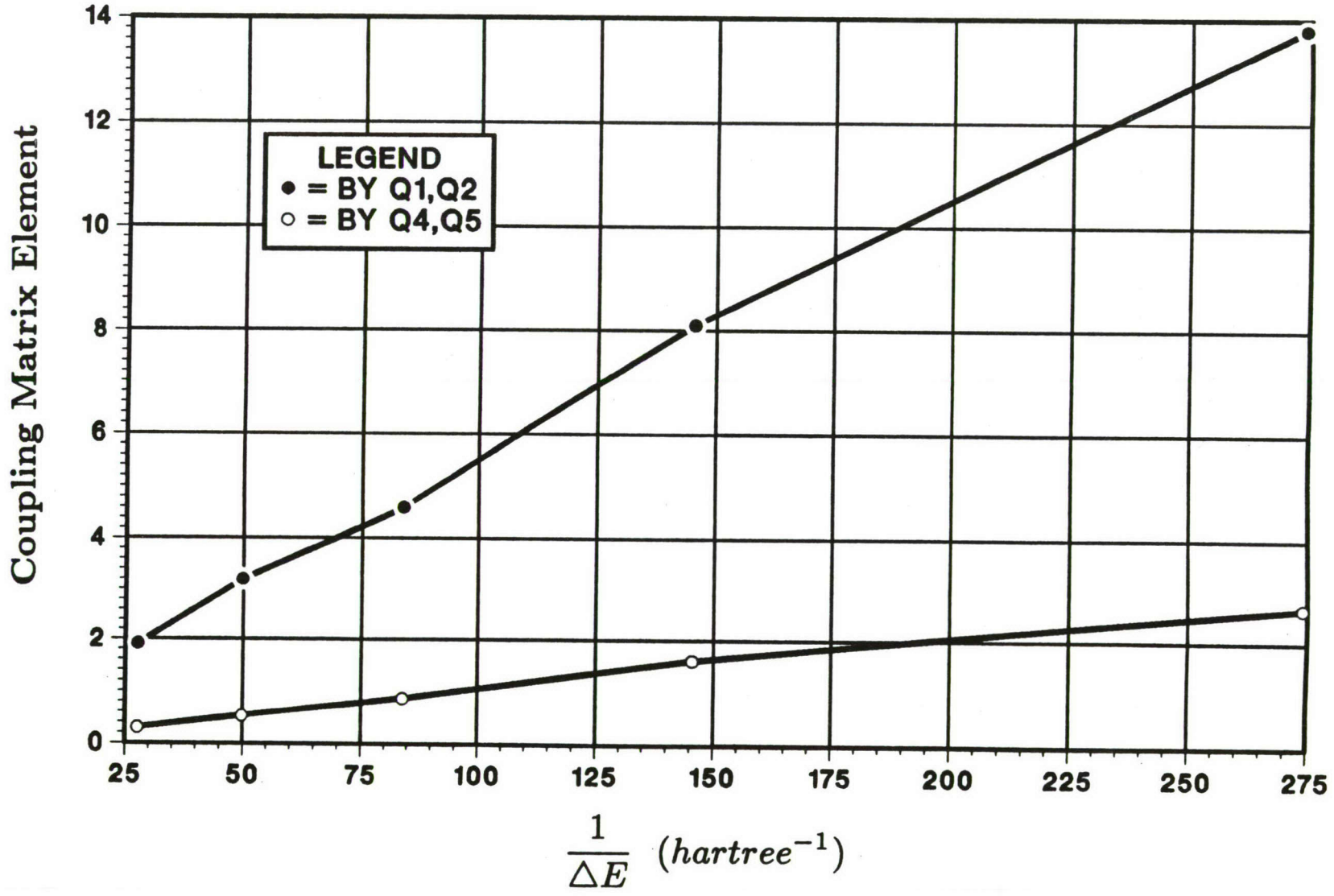

Fig. 2

Correlation Diagram

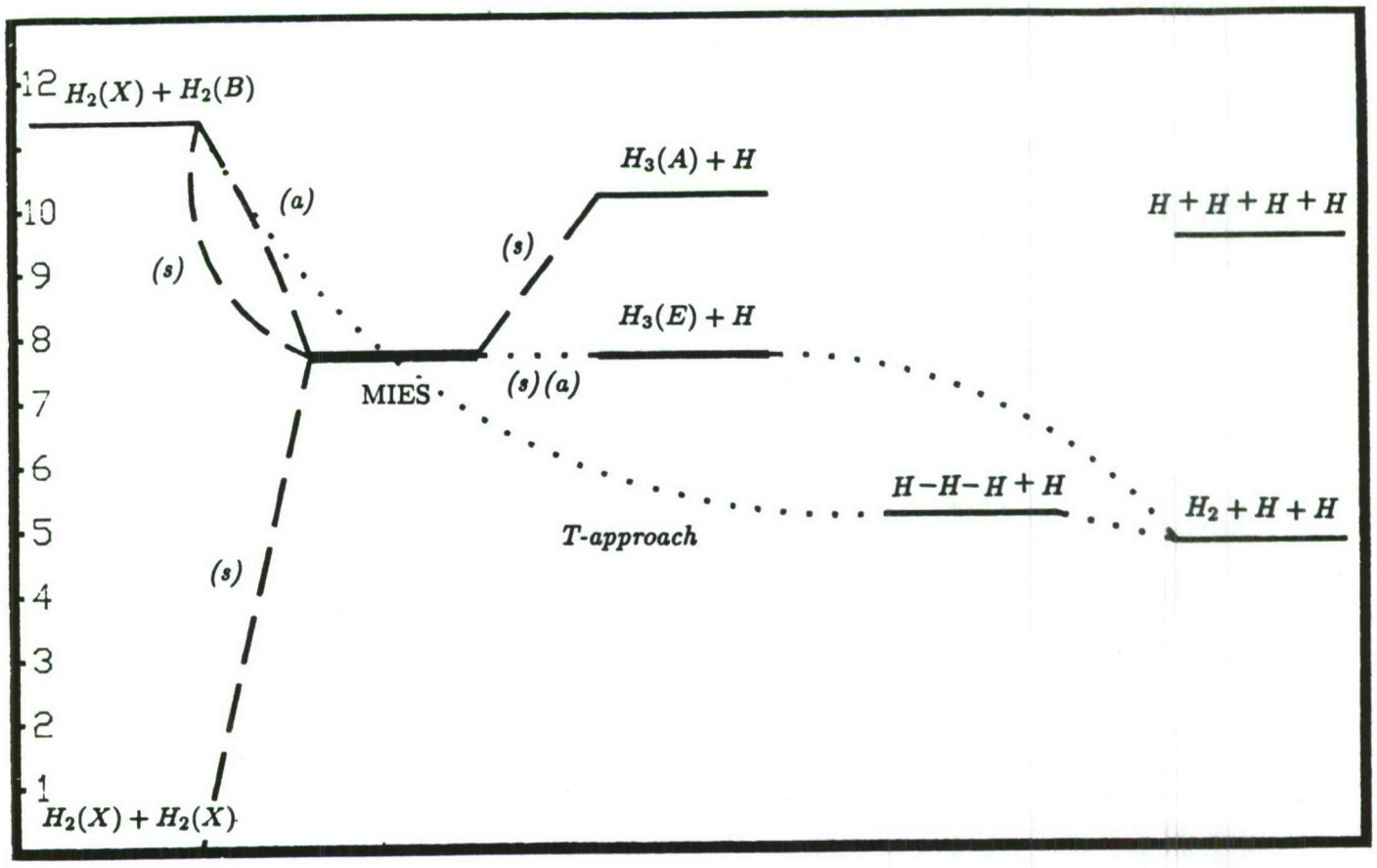

Theoretical Studies of the Radiative Lifetime for the Spin-Forbidden Transition $X^1\Sigma_g^+ <- a^3\Sigma_u^+$ in He_2^* Using Ab Initio State Averaged MCSCF + CI.

David R. Yarkony
Department of Chemistry
The Johns Hopkins University
Baltimore, MD 21218

James O. Jensen
CRDEC,
Aberdeen Proving Grounds, MD

Cary F Chabalowski and Byron H. Lengsfield III
Ballistic Research Laboratory,
Aberdeen Proving Ground, MD

The generation of neutral excited state atoms or molecules in a liquid helium bath via collisions with alpha particles was initially reported by Surko and Reif (1). Calvani et al. (2), generating the neutral entities from an alpha source, set a lower limit of 0.1 sec on it's natural lifetime (τ). A more recent experimental study by Mehrotra, et al. (3) concluded that the neutral excited species was the molecular a u state in He2. This is reported to be the lowest energy excited electronic state in He2 and the lowest bound state (the X Σg ground state is essentially repulsive). They predict from their data a lower bound on the natural lifetime of 10 sec's in the liquid medium.

There is interest in this laboratory in finding novel ways to store energy. One such approach might include storing energy in long-lived excited electronic states. The a Σu is such a state, since a Σu -> X Σg is a spin-forbidden transition and the spin-orbit interactions are expected to be small for such light atoms. And in view of the large difference (a factor of 100) predicted by the two experiments (3,4) for the lower limit in τ, the time seems right for estimating the lifetime through high quality ab initio calculations.

I. Methods

This study calculates τ for the spin-forbidden transition $a^3\Sigma_u^+ \rightarrow X^1\Sigma_g^+$ for He_2^* in the gas phase using state averaged MCSCF plus CI to generate the appropriate zeroth-order wavefunctions. In order to calculate this spin-forbidden process, spin-orbit (S-O) interactions are calculated with a manifold of exited states via matrix elements over configuration- state-functions (CSF's) using the microscopic Breit-Pauli Hamiltonian. This newly implemented method (4) incorporates the application of the symbolic matrix method of Liu and Yoshimine (5) into the formation of the SO matrix elements. In addition, the calculation is further simplified by solving directly for the first-order correction, Ψ^1, to the state wavefunction by obtaining directly Ψ^1 as an eigenvector that results from diagonalizing a set of linear equations which contain matrix elements over CSF's.

In contrast, the usual representation for the first-order correction $\Psi^1(I)$ due to S-O effects is

$$1. \quad \Psi^1(I) = \sum_L^{\infty} \frac{\langle \Psi_J^o | \tilde{H}^{so} | \Psi_I^o \rangle}{(E_J^o - E_I^o)} \Psi_J^o$$

The summation over the L electronic states is, in principle, infinite. One often used approach to solving for $\Psi^1(I)$ is to calculate explicitly the wavefunctions for a relatively small number of excited states thereby drastically truncating L. This might cause one to miss important contributions to $\Psi^1(I)$ from the omitted states.

This "omitted states" problem can be significantly reduced by the method used in this study wherein one solves for Ψ^1 directly from

$$2. \quad (\tilde{H}^o - E_I) \Psi_I^1 = -\tilde{H}^{so} \Psi_I^o$$

with $\tilde{H}^o$ being the nonrelativistic Hamiltonian. Eq. 2 can be transformed into matrix form as

$$3.\quad (\underset{\sim}{H}^o - E_I)\underset{\sim}{V}^I = -\underset{\sim}{H}^{so}\underset{\sim}{C}^I$$

where it must be emphasized that $\underset{\sim}{H}^o$ and $\underset{\sim}{H}^{so}$ are matrices with elements formed over CSF's, NOT over eigenstates. The vectors $\underset{\sim}{V}^I$ and $\underset{\sim}{C}^I$ are defined as the coefficients for the first- and zeroth-order parts of Ψ_I:

$$4a.\quad \Psi_I^o = \sum_i C_i\phi_i(\kappa)$$

$$4b.\quad \Psi_I^1 = \sum_j V_j\phi_j(\kappa').$$

The κ and κ' label the spatial symmetries to which the CSF's belong, and in general $\kappa \neq \kappa'$. Eq. 3 forms a large set of linear inhomogeneous equations which are solved to obtain V_j by a variant of the method suggested by Pople et al. (6).

The natural lifetime is then dependent upon the electric transition dipole moment for the electronic transition $X^1\Sigma_g^+ \leftarrow a^3\Sigma_u^+$. This is finally represented as the sum of singlet and triplet contributions:

$$5.\ \Sigma|Re| = \langle \Psi^o(a^3\Sigma_u^+)\ |\vec{\mu}|\ \Psi^1(^3\Pi_g)\rangle + \langle \Psi^1(^1\Pi_u)\ |\vec{\mu}|\ \Psi^o(X^1\Sigma_g^+)\rangle$$

which are matrix elements in terms of zeroth- and first-order corrections to the wavefunctions. The $\Sigma|Re|$ values were then used in a vibrational analysis to include the effects of nuclear motion which allows one to predict vibrational energy levels and make direct comparison with experimental values for lifetimes of the excited state vibrational levels.

II. Details of Calculations

The gaussian type basis set is essentially that used by Sunil, et al. (7) in an earlier theoretical study on excited states of He2 with two exceptions. A single primitive p function has been added with it's exponent optimized to give the lowest CI energy for the $F^1\Pi u$ at r= 2.00 au. In addition, the orbital exponent for the more diffuse d-function was changed to be consistent with a basis set used in an earlier study on He2 in this laboratory (8). The final basis set consists of (10s,6p,2d) primitives contracted to [7s,5p,2d] AO's, for a total of 34 basis functions per atom.

The spatial symmetry is chosen to be the D2h point group for all the calculations performed. The SAMCSCF is of the CAS type wherein the 4 electrons are distributed, in all possible ways amongst the lowest 3 MO's from IRREP's Ag(σg) and B1u(σu), and the lowest MO from B2u(πuy), B3u(πux), B2g(πgx), and B3g(πgy), consistent with space and spin symmetry restrictions. The state averaged energy is then optimized including the states $X^1\Sigma_g^+$, $a^3\Sigma_u^+$, $b^3\Pi$gx, $b^3\Pi$gy, $F^1\Pi$ux, and $F^1\Pi$uy. The MO's obtained from the SAMCSCF were then used as the basis set for the CI. The CSF's used in the SAMCSCF's were then used as reference CSF's in the CI, from which all single and double exicitations .ere performed.

III. Results

A. State properties

The main configuration for each of the four states as found in the CI at r=2.00 is $X^1\Sigma_g^+$: $1\sigma_g^2 1\sigma_u^2$, $a^3\Sigma_u^+$: $1\sigma_g^2 2\sigma_g 1\sigma_u$, $b^3\Pi$g: $1\sigma_g^2 1\sigma_u 1\pi_u$, $F^1\Pi$u: $1\sigma_g^2 1\sigma_u 1\pi_g$. And Table 1 compares the molecular constants for the four states of interest as predicted by a vibrational analysis on the PEC's from this study and experiment. The theoretical D_e values are calculated as the difference in energy $E(r_e)$ - E(r=40

bohr). As can be seen, the calculated r_e, w_e, T_e, and D_e for all four states vary from experiment by no more than 1%. These states seem well described.

Potential energy curves for the four states are shown in Fig. 1. The $a^3\Sigma_u^+$ and $F^1\Pi u$ are found to have local maxima in their PEC's as the molecule goes toward dissociation. Various experimental and theoretical estimates have been made on the height and location of these humps, and a summary of these predictions (including the results from this study) can be found in Table 2. These calculations give the barrier size (i.e. ΔE= E(max)- E(dissociation)) and location of the $a^3\Sigma_u^+$ to be ΔE=1.56 kcal/mol and r(He-He)=2.7 angs, respectively. And for the $F^1\Pi u$ state, the barrier height is ΔE=10.9 kcal/mol at the internuclear separation r(He-He)=1.79 angs. The $F^1\Pi u$ values vary somewhat from earlier estimates (see Table 1).

B. Spin-Orbit Interactions

The first-order S-O corrections to the $X^1\Sigma_g^+$ and $a^3\Sigma_u^+$ states arise from interactions of these zeroth-order wavefunctions with the $^3\Pi g$ and $^1\Pi u$ state manifolds (respectively) as defined by the CSF expansions for these Π spaces. The magnitude of the S-O perturbation of the $a^3\Sigma_u^+$ by the entire $^1\Pi u$ manifold (as spanned by this CSF space) is plotted in Figure 2a, and labeled Curve A. The Curve B in Figure 2a represents the first-order S-O interaction between the $a^3\Sigma_u^+$ zeroth-order wavefunction and only the lowest energy state of $^1\Pi u$ symmetry, i.e. the $F^1\Pi u$. This represents the first-order correction to $\Psi(a^3\Sigma_u^+)$ by setting L=1 in the summation of eq. 1. Therefore, the difference in magnitude between curves A and B should reflect the amount of first-order perturbation to $\Psi^1(a^3\Sigma_u^+)$ that is missed by truncating the summation in eq. 1 to simply L=1. The analogous information is plotted in Figure 2b for the $X^1\Sigma_g^+$ state perturbed by the $^3\Pi g$ manifold (Curve A) or only the $b^3\Pi g$ state (Curve B).

One can immediately see that much of the contribution to the total perturbation is excluded from the Ψ's if the only interaction allowed with $a^3\Sigma_u^+$ and $X^1\Sigma_g^+$ is with the lowest energy $^1\Pi u$ or $^3\Pi g$ state, respectively. This type of analysis highlights the importance of including higher lying excited states (a benefit of this method) and points to the possible danger of premature truncation which is an intrinsic problem when one tries to represent Ψ^1 as a sum of interactions over discreet eigenstates as represented by Eq. 1.

C. Electric Transition Dipole Moments and Lifetimes

The total electric transition dipole moment, as well as it's two components (see eq. 5) are plotted in Figure 3. It can be seen that the singlet component dominates over most of the a Σu bound potential, with the triplet component having comparable magnitude only at small internuclear separations. The two moments have opposite signs for values less than 2.0 bohr, and then remain the same sign up through r = 3.5, after which they are again opposites. The difference in signs at small internuclear separation causes a cancellation in forming the total transition moment, generating a near zero moment at r=1.50 bohr. From r=1.85 onward, the total transition dipole is essentially determined by the singlet component which has a maximum value of 6.0x10(-6) au at r=3.8.

If we wish to give an explanation for the shape of $\Sigma|Re|$, we need to look primarily at the singlet states, and in particular the Πu states. The hump in the F Πu occurs due to an avoided crossing of this state with higher lying Πu states. One theoretical study (9) reports substantial interactions of the F Πu with the Πu that dissociates to the 1s +1s3d limit. The location of the F Πu hump in the PEC at r=1.85 angs (in the current study) lies reasonably close to the maximum at r=2.1 angs in the singlet component of the transition moment (see Figure 3). The $a^3\Sigma_u^+$-$^1\Pi u$ S-O interaction also shows a maximum at r=2.1 angs (see Figure 2a, Curve A). It would appear therefore that the $\langle a^3\Sigma_u^+|H^{SO}|{}^1\Pi u\rangle$ S-O perturbation and the singlet contribution to $\Sigma|Re|$ (and hence the total $\Sigma|Re|$) depend not only upon interactions with the $F^1\Pi u$ but also with higher lying $^1\Pi u$ states.

The results of the vibrational analysis are given in Table 3, where one finds

the predicted lifetime of the v=0 level in $a^3\Sigma_u^+$ to be 18 sec.'s, which is consistent with the more current experimental prediction of 10 sec's for a lower bound (3). The lifetimes are seen to monotonically decrease with increasing vibrational quantum number, at least up to v=9. At v=5 the lifetime falls below the predicted lower bound of 10 secs, suggesting that the majority of excited He2 neutrals observed by Mehrotra et al. (3) in their experiment reside in the v=0 to v=4 or 5 levels.

1. C. M. Surko and F. Reif, Phys. Rev. Lett. 20, 582 (1968); Phys. Rev. 175, 229 (1968).
2. P. Calvani, B. Maraviglia, and C Messana, Phys. Lett. 39A, 123 (1972); P. Calvani, C. DeSimone, A. Giovannelli, and B. Maraviglia, Nuovo Cimento 19B, 271 (1974).
3. R. Mehrotra, E. K. Mann, and A. J. Dahm, J. Low Temp. Phys. 36, 47 (1979)
4. D. R. Yarkony, J. Chem. Phys. 86, 1642 (1987); 85, 7261 (1986), and references therein.
5. B. Liu adn M. Yoshimine, J. Chem. Phys. 74, 612 (1981).
6. J. A. Pople, R. Krishnan, H. B. Schlegel, and J. S. Binckley, Int. J. Quantum Chem. 13, 225 (1979).
7. K. K. Sunil, J. Lin, H. Siddiqui, P. E. Siska, K. D. Jordan, and R. Shepard, J. Chem. Phys. 78, 6190 (1983).
8. D. D. Konowalow and B. H. Lengsfield III, Chem. Phys. Lett. 139, 417 (1987).
9. B. K. Gupta and F. A. Matsen 50, 3797 (1969).
10. R. M. Jordan, H. R. Siddiqui, and P. E. Siska, J. Chem. Phys. 84, 6719 (1986).
11. G. Peach, J. Phys. B11, 2107 (1978).
12. B. Brutschy and H. Haberland, Phys. Rev. 19, 2232 (1979).
13. K. H. Lundlum, L. P. Larson, and J. M. Caffrey, J. Chem. Phys. 46, 127 (1967).
14. K. P. Huber and G. Herzberg, "Molecular Spectra and Molecular Structure", Van Nostrand-Rheinhold, New York, 1979.
15. G. Herzberg, "Spectra of Diatomic Molecules", Van Nostrand-Rheinhold, New York, 1950.
16. J. C. Browne, Phys. Rev. 1A 138, 9 (1965).

Table 1.
Molecular constants for the $a^3\Sigma_u^+$, $b^3\Pi_g$, and $F^1\Pi_u$ electronic states.(a)

Property		$a^3\Sigma_u^+$	$b^3\Pi_u$	$F^1\Pi_u$
r_e	Theo.	1.0493	1.0681	1.0869
	Exp.	1.0457	1.0635	1.0849
T_e(b)		143768.	148962.	165665.
		144048.	148835.	165971.
ω_e(c)		1807.	1752.	1670.
		1809.	1769.	1671.
D_e(d)		15636.	19942.	5293.
		15806.		

a. All distances in angstroms and energies in cm-1. Experimental data from reference 4.

b. The Te are with respect to the $X^1\Sigma_g^+$ at r=40 au.

c. Theoretical ω_e's from $\Delta G(2\text{-}1) - \Delta G(1\text{-}0) = -2\omega_e x_e$ and $\omega_e = G(1\text{-}0) + 2\omega_e x_e$. See reference 15, pg 95.

d. Determined from the energy difference between r_e and r=40 au.

Table 2. Barrier heights and locations for the $a^3\Sigma_u^+$ and $F^1\Pi_u$ states.

	This Study		Previous Theory		Experiment	
State	Height[a]	Position[b]	Height	Position	Height	Position
$a^3\Sigma_u^+$	1.56	2.70	2.7	2.9[c]	1.[illegible][f]	[illegible]
			1.85	2.68[d]	1.55[e]	2.77
					1.43±.05	2.72±.04[g]
$F^1\Pi_u$	10.9	1.79	13.5	1.73[h]		
			12.5[i]	1.78[i]		

a. Energies in kcal/mol. b. Distances in Angstroms. c. Reference 11.
d. Reference 7. MCSCF calculations. e. Reference 12. f. Reference 13.
g. Reference 10. h. Reference 9. Valence-bond calculations.
i. Reference 16. Browne did not report a barrier position from any fitting procedure, so these authors calculated the position and height by fitting the potential energy data in Table I of ref. 16 to a parabola giving these results.

Table 3. Results from vibrational analyses on the $a^3\Sigma_u^+$, $b^3\Pi_g$, and $F^1\Pi_u$ states with energies in cm^{-1} and lifetimes, τ, in seconds.

	$a^3\Sigma_u^+$		$b^3\Pi_g$	$F^1\Pi_u$
v	Energy	τ	Energy	Energy
0	915	18	893	795
1	2650	15	2587	2387
2	4313	13	4223	3901
3	5874	12	5776	5334
4	7358	11	7243	6664
5	8756	9.6	8641	7871
6	10063	8.4	9968	8874
7	11259	7.6	11226	
8	12371	7.0	12426	
9	13332	6.2	13516	

Figure 1. Potential Energy Curves for the $X^1\Sigma_g^+$, $a^3\Sigma_u^+$, $b^3\Pi_g$, and $F^1\Pi_u$ in He_2^*.

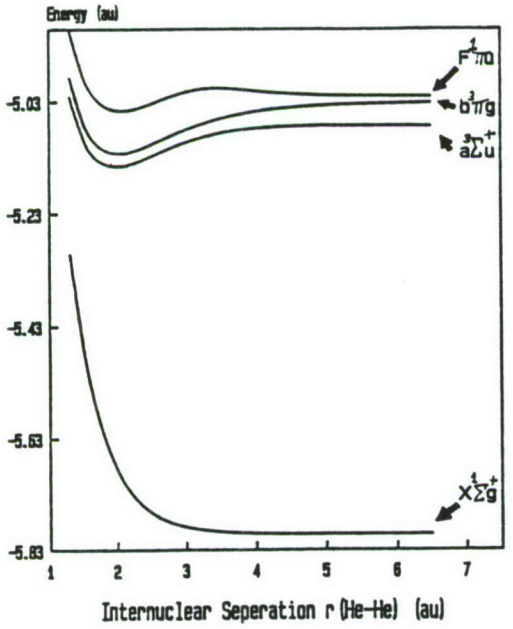

Figure 2a. First-order contribution to the Spin-Orbit perturbation of the $a^3\Sigma_u^+$ by the $^3\Pi_g$ state manifold (Curve A) and by the $F^1\Pi_u$ state (Curve B).

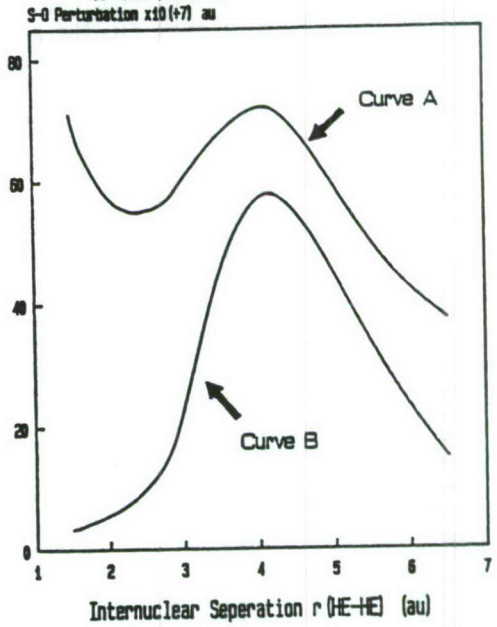

Figure 2b. First-order contribution to the Spin-Orbit perturbation of the $X^1\Sigma_g^+$ by the $^3\Pi_g$ state manifold (Curve A) and by the $b^3\Pi_g$ state (Curve B).

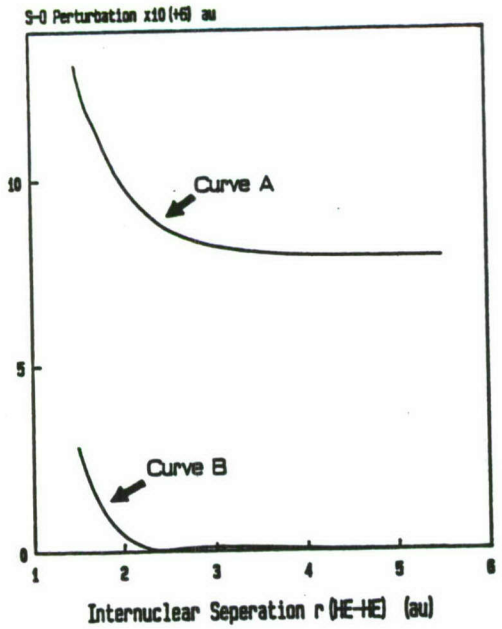

Figure 3. Total electric transition dipole moment with it's singlet and triplet components for the $X^1\Sigma_g^+$ - $^3\Sigma_u^+$ band system.

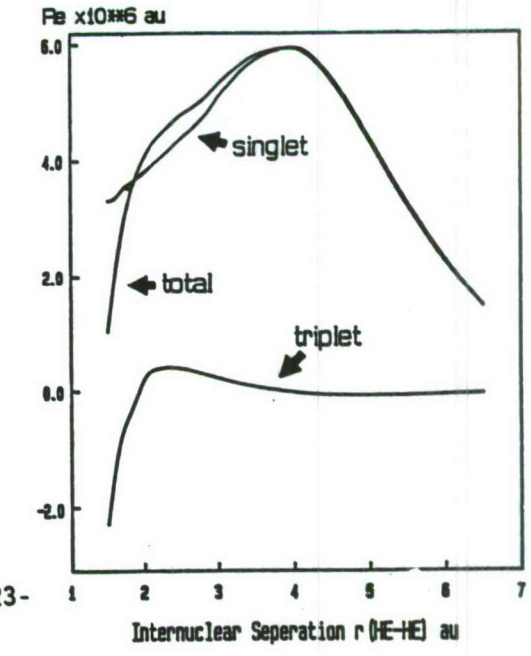

Abstract for
The Second Annual High Energy Density Matter (HEDM) Conference
February 28-March 2 1988
Newport Beach, CA

The Static and Dynamic Influence of Condensed Phase on Metastability*

by

P. K. Swaminathan*, B. C. Garrett, C. S. Murthy, M. J. Redmon, and B. M. Rice
Chemical Dynamics Corporation
9560 Pennsylvania Avenue #106
Upper Marlboro, MD 20772

HEDM's involve energetic species whose stability and reaction attributes are often dictated by electronically excited states of the constituent atoms or molecules. Condensed phase influence on HEDM candidates plays a critical role depending on storage conditions. Our research involves a comprehensive theoretical methodology including quantum chemistry input (from the Ballistics Research Laboratory), modern computer simulation techniques, and semiclassical eikonal description of electronic inelasticity.

We are studying factors important in determining HEDM stability in condensed phases that ultimately influence their practical usefulness. The chemistry and quenching mechanisms require treatment of electronically nonadiabatic collision dynamics in condensed phases. Our continued work on Helium metastables will be presented and will include:

- the validation of the eikonal method in gas phase quenching and excitation rate computations by comparison to exact quantal scattering results.
- the use of accurate electronic potentials and couplings from *ab initio* studies.
- the development of Monte Carlo and Molecular Dynamics methods for use in the presence of a reacting HEDM to characterize GLE heatbaths of bulk Helium for various pressures.
- the characterization of the Helium bubble around excited Helium HEDM for various electronic states.
- the comparison of gas phase and condensed phase radiative/nonradiative quenching of the HEDM.

Future work will (1) take up molecular candidates (He_n^* as well as any promising HEDM species) and examine the condensed phase influence and (2) examine trends in condensed phase energy transfer and reaction attributes in order to suggest criteria for chemical and physical requirements of HEDM candidates.

* Research Supported by AFAL Contract Number F04611-86-C-0068

Gas Phase

- A semiclassical theory using the Selfconsistent Eikonal Method (SCEM) (D. A. Micha, J. Chem. Phys. 78, 7138 (1983)) was validated by comparison of quenching cross sections to exact quantum results for a model (with accurate potentials and arbitrary electronic couplings) of B to c state $He^*(^1P)$-$He(^3S)$ quenching dynamics.

- Figure 1 shows the relevant potentials and couplings and figure 2 the total quenching cross sections from semiclassical and quantal routes. Figures 3-5 compare primitive eikonal and exact opacities. Figure 5 reveals the need for inclusion of quantal interference effects near an orbiting resonance. This is being done by employing semiclassical wavefunctions within SCEM.

He_2 Potentials and Couplings

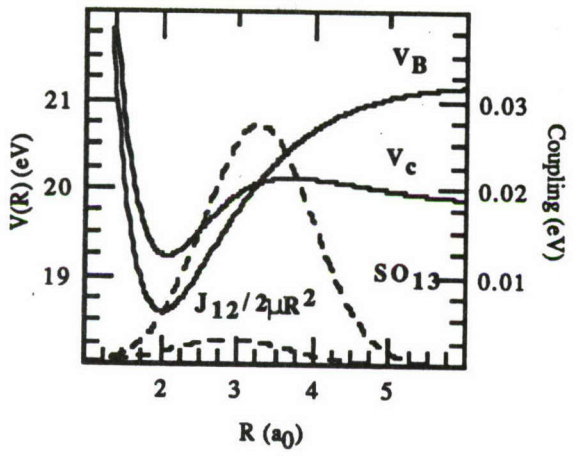

(1)

He (^1P) quenching to He(^3S): B->c

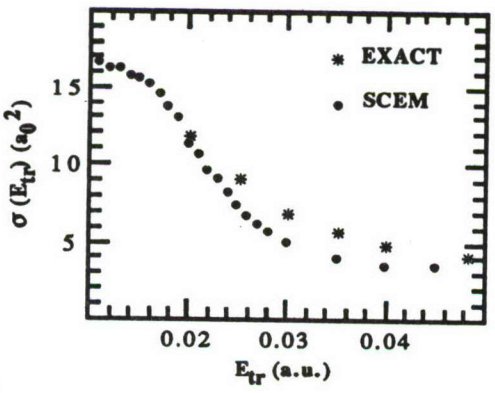

(2)

SCEM vs. EXACT opacities at E_{tr}=0.2eV

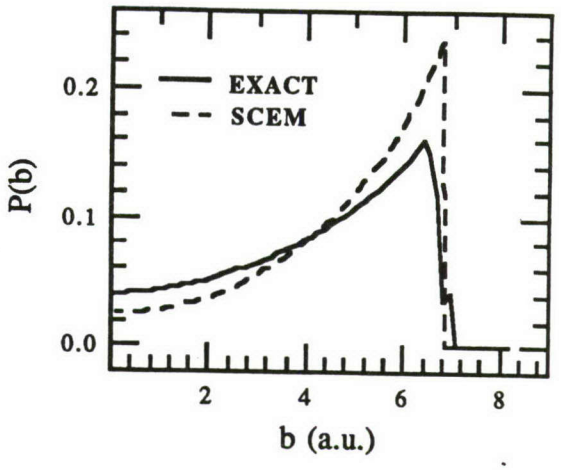

(3)

SCEM vs. EXACT opacities at E_{tr}=3.0eV

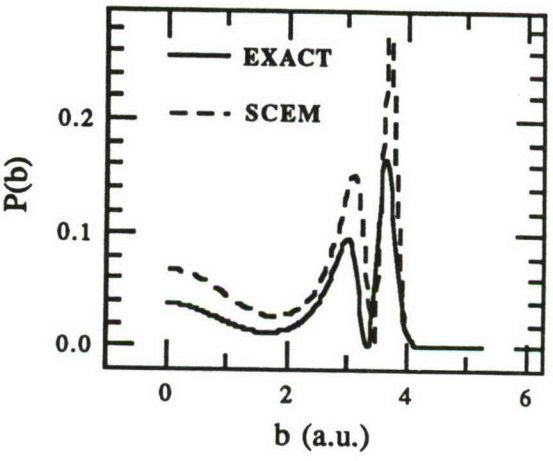

(4)

SCEM vs. EXACT opacities at Etr=0.5eV

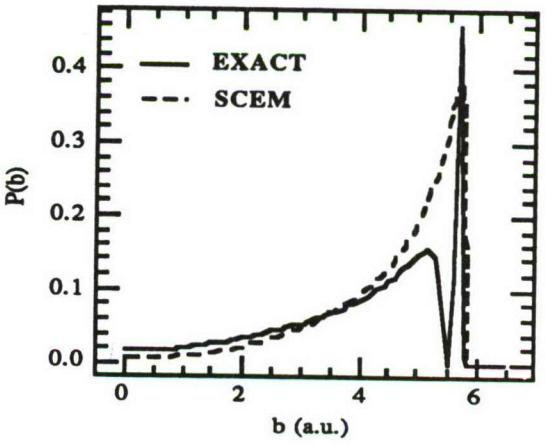

(5)

Gas/Surface

- Rotonically inelastic collisions of NO with Ag(111) surface were studied [with ARO/SDI support] and compared to previous quantal computations. Figure 6 compares accurate quantum mechanical (line: see J. E. Smedley, G. C. Corey and M. H. Alexander, J. Chem. Phys. **87**, 3218 (1987)) and self consistent eikonal method (•) distributions of final rotational states of NO in collisions of NO in its lowest rotonic state with a smooth rigid Ag surface. The line connects the quantum mechanical points at discrete J values. Both sets of calculations were performed for a 282-rotonic state model at a translational energy of 6700 cm^{-1}. The results indicate the accuracy of the methodology

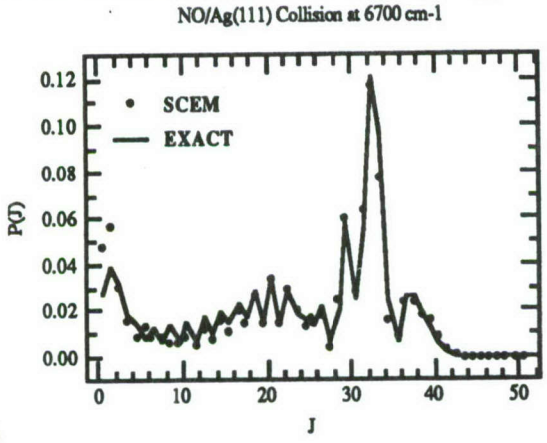

(6)

and demonstrate the value of semiclassical methods for the dynamics of complex systems. The main advantage of the present framework is that it is computationally feasible for polyatomic systems. Furthermore, the trajectories provide detailed dynamical insight into the rotonic inelasticity in this example at a level that cannot be readily obtained from quantal approaches.

Solvation Structure

- Solvation structure around an $He^*(^3S)$ in high pressure He liquid bath was studied via Monte Carlo/Molecular Dynamics techniques for various pressures. Figures 7-8 display the relevant potentials and key computer simulation results.

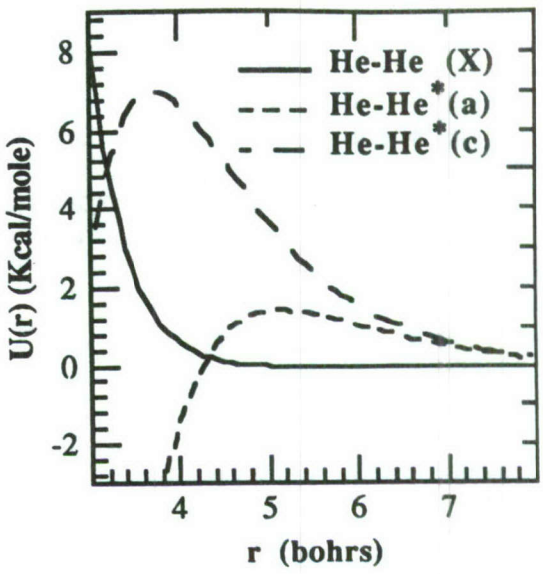

(7)

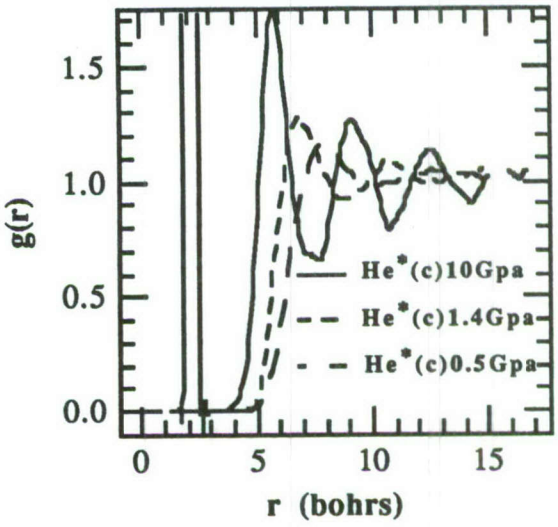

(8)

- Figure 8 displays appearance of a reactive participation by solvent, leading to the dimer (c-state) at high pressure (10 Gpa) whereas no reaction is evident at the lower pressures. Similarly, for a-bubble also, simulations were found to display the effects of dimer formation, but at even lower pressures (1.4 Gpa). The difference comes from the lower barier of a-bubble(fig. 7). The solvation is a nonequilibrium phenomenon and inherently dynamical for the smallest choice of primary zone (the single HEDM atom). Such simulations characterize Generalized Langevin heatbath model requirements in our work.

Solvated Dynamics

- Since the bubble is too large to explicitly include all the solvent He atoms of the first solvation shell, solvated dynamics was modelled by one solvent on either side of a collinear triatomic model with the central atom being an atomic HEDM, $He^*(^3S)$.

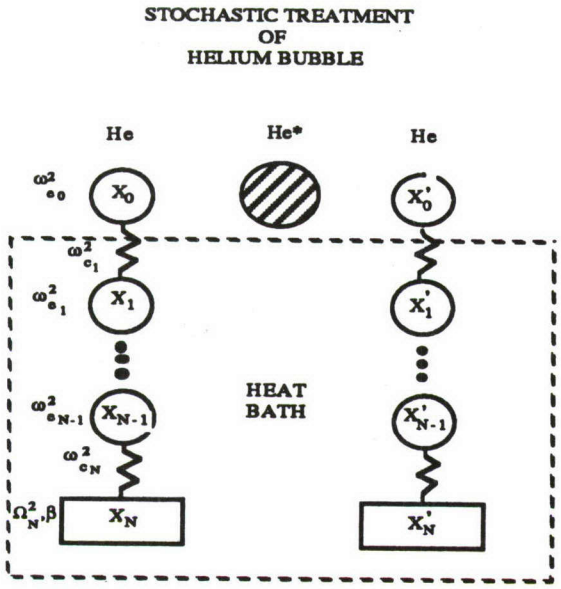

The collinear triatomic system modelling the He^* bubble in a high pressure He liquid matrix was studied using the semiclassical eikonal method for the primary zone and the generalized Langevin equation (GLE) to simulate heatbath effects. Probability fluctuation auto correlation functions (ACF's) for ^3S state of He^* are shown in figures 9 and 10 for 0.5Gpa and 1.4Gpa a-bubble in comparison to the displacement autocorrelations. The comparison of a variety of mode ACF's can yield information about the roles of various condensed phase modes of quenching in destabilizing the HEDM. The generalized Langevin approach correctly interpolates between the local and macroscopic mode participations in quenching dynamics.

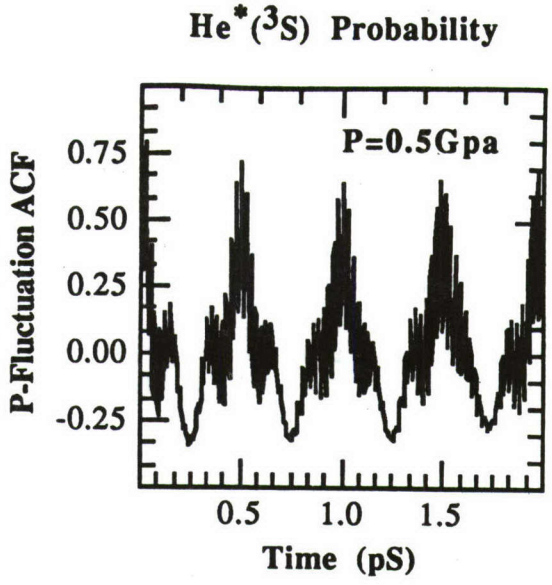

(9a)

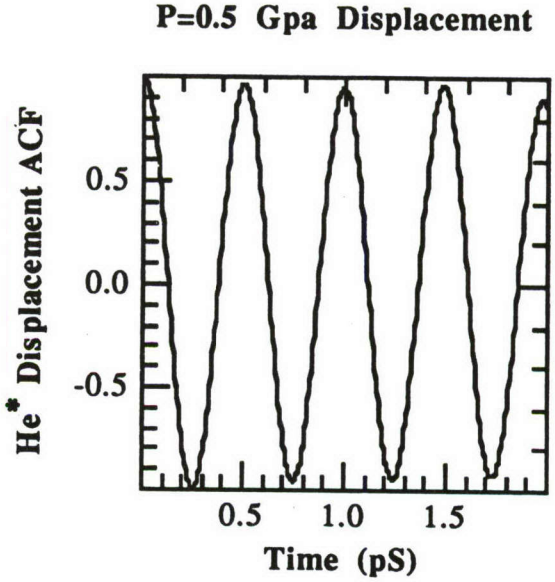

(9b)

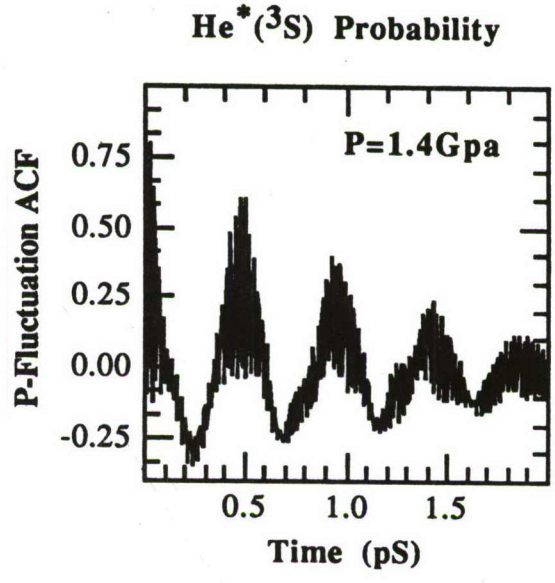

(10a)

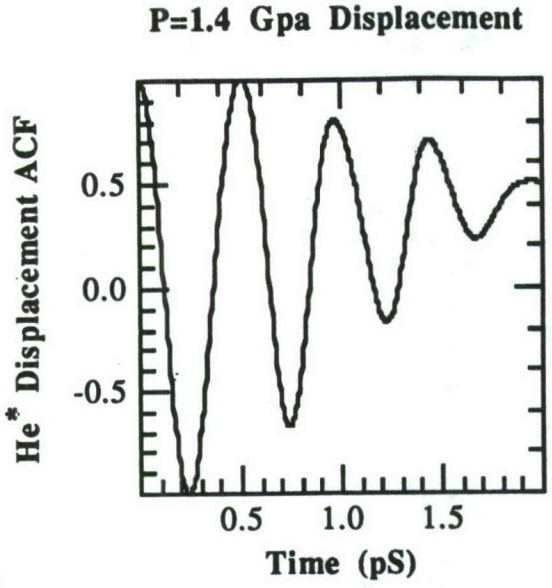

(10b)

The dynamics shown is for radiative quenching of $He^*(^3S)$ but we have employed arbitrarily increased electronic dipole couplings so as to obtain numerically facile rapid quenching behavior. Special dynamical methods will be developed for treating very long-lived HEDM species, otherwise requiring long trajectories.

Studies on the H_2 matrix

- An effective anisotropic pair potential is being devised for condensed phase simulations of molecular hydrogen. MD calculations have been carried out for liquid H_2 system of 108 molecules interacting through two Lennard-Jones centers (2LJC) coincident with the positions of the atomic masses. Figures 11-13 display the center of mass (COM) pair correlation functions (PCF's) for special configurations and the time correlation functions (TCF's) for 2LJC-model H_2 at 265K and 4 GPa.

- Figures 11-12 display COM PCF's for configurations which lie within $\pm 10^0$ of specific relative orientations: 'X'='crossed', 'P'='parallel adjacent', 'T'='T-geometry', and 'L"="linear, or parallel end to end'. The position of the maxima of these PCF's compare well with the position of the potential energy minima for two isolated molecules in the corresponding configuration.

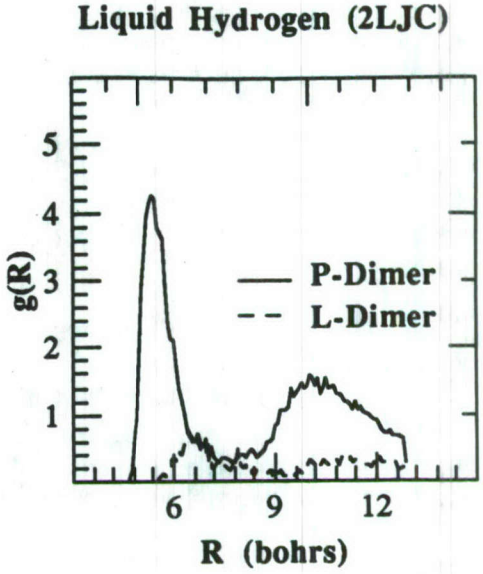

(11)

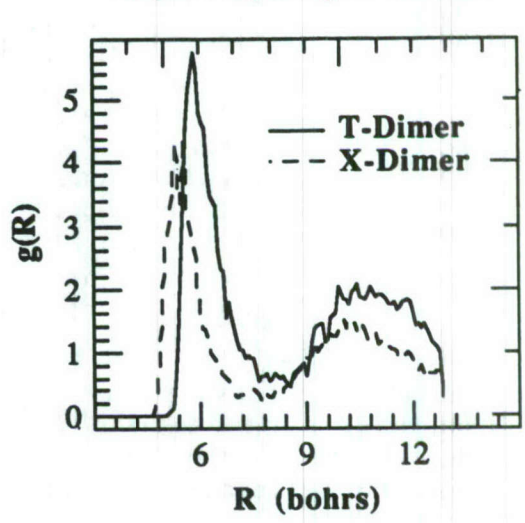

(12)

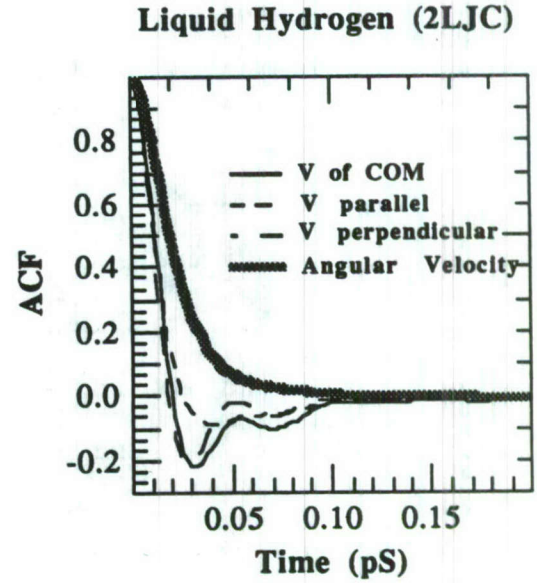

(13)

This indicates that the presence of other molecules in the dense liquid have little effect on the minimum of the potential field which acts on adjacent molecules. By contrast, for the models of other related linear molecules, (K. Singer, A. Taylor, and J. V. L. Singer Mol. Phys. 33, 1757 (1977)) the same arrangements have been found to be almost equally stable.

- Figure 13 displays the COM and angular velocity auto-correlation functions of the 2LJC-model H_2. In the liquid state, the VACF exhibits a negative minimum, which is interpreted as caused by back-scattering by nearest-neighbors, and a long negative tail, ascribed to a cooperative motion of the surrounding particles. The double minimum in the COM VACF can be interpreted (J. Barojas, D. Levesque, and B. Quentrec Phys. Rev. A2, 1092 (1973)) as arising from the different mobility of a linear molecule parallel and at right angles to its axis. This is clear from the COM VACF's of velocity components parallel and perpendicular to the molecular axis. The minimum of $VACF_{\perp}$ is deeper and occurs at earlier times than that of $VACF_{||}$. The presence of double minimum in $VACF_{\perp}$ was interpreted to be the result of successive negative impulses transmitted to the COM first by one and then by the other end of the molecule, as it encounters obstacles. The angular VACF would also exhibit negative minimum for more anisotropic systems (K. Singer, J. V. L. Singer, and A. J. Taylor, Mol. Phys. 37, 1239 (1979)).

SUMMARY

Overall, the above results offer a clear validaton for the new semiclassical dynamical methodology (based on the selfconsistent eikonal method (SCEM) in the gas phase, and combined with the generalized Langevin approach for the condensed phase, the latter based on direct computer simulations) for treating electronic plus nuclear dynamics, especially when it is noted that the results shown are all from what may be termed the selfconsistent classical-quantum (SCCQ) implementation of SCEM, employing classical trajectories for classical nuclear variables.

Nevertheless, quantitative agreement of the details of predictions can be improved by refinements of SCEM implementation, e.g., P(b) versus b results (figures 3-5) will improve upon treating quantal interference effects between trajectories (arising from nuclear semiclassical amplitudes, which may be called the selfconsistent semiclassical-quantum (SCSQ) implementation of SCEM, and which can yield P(J) versus J). Such work is in progress.

For the condensed phase lifetimes, long-lived species need special dynamical treatment to avoid unnecessarily long trajectories. This is also in progress.

Finally, vibrations of diatomic solvent molecules are yet to be included as are studies on the treatment of polyatomic HEDM species in gas and condensed phases.

Theoretical Studies of Spin-Forbidden and Electronically Nonadiabatic Processes Relevant to the Structure and Stability of Potential High Energy Density Materials

David R. Yarkony
Department of Chemistry
The Johns Hopkins University
Baltimore, MD 21218

Abstract:

We are concerned with the development and application of electronic structure techniques to study the structure and stability [decay processes] of potential high energy density materials. We will discuss radiative decay resulting from spin-forbidden dipole-allowed electronic transitions as well as radiationless decay, energy transfer, as a result of electronic nonadiabaticity.

A: The He + $H_2(B^1\Sigma_u^+)$ System

With: J. K. Perry

The captioned system has been suggested as a possible energy storage medium. It has been suggested that a locally stable ground state charge transfer structure of the form, $(HeH)^+-H^-$ accessible from the excited potential energy surface (PES) correlating with He + $H_2(B^1\Sigma_u^+)$ might be able to store a significant portion of the electronic energy, (more than 11 eV) in the B state of H_2. We have considered this possibility using ab initio techniques as follows:

The $1,2^1A'$ PES's of the He-H_2 system, which correlate asymptotically with $He(^1S)$ + $H_2(X^1\Sigma_g^+, B^1\Sigma_u^+)$ system states, were characterized using MCSCF/CI

wavefunctions. The existence of charge transfer structures of the form $(HeH)^+-H^-$ on the two PES's was considered as were the electronic structure aspects of the nonadiabatic quenching process $He + H_2(B^1\Sigma_u^+) \rightarrow He + H_2(X^1\Sigma_g^+)$. While this work builds on previously reported theoretical treatments of these PES's, both qualitative and quantitative differences are found. In particular, our predicted entrance channel saddle point corresponds to a barrier of 1.5 Kcal/mol on the $2^1A'$ PES which is significantly lower than previous work. More significantly an extended region of large nonadiabatic effect characterized by the near degeneracy of the $1^1A', 2^1A'$ PES's, $E(2^1A')-E(1^1A') < 0.5$ Kcal/mol, was located. This region, which is exothermic with respect to the $He + H_2(B^1\Sigma_u^+)$ asymptote, was not uncovered in previous studies. Using an analysis based on the evaluation of the nonadiabatic coupling matrix elements, $\langle \Psi(2^1A') \left| \frac{\partial}{\partial R_\alpha} \right| \Psi(1^1A') \rangle$ the breadth of this region was determined. A surface walking technique was used to consider the fate of the charge transfer structures resulting from the nonadiabatic transition $2^1A' \rightarrow 1^1A'$. No evidence for a stable charge transfer structure was found.

B: Stability With Respect to Spin-Forbidden Radiative Decay: Lifetimes for States which Undergo Spin-Forbidden Radiative Decay Originating in Coupling to Bound States Embedded in A Continuum. Application to CH^-.

With: B. H. Lengsfield and J. O. Jensen

One of the key aspects of our research program concerns the stability of energetic systems with respect to radiative and radiationless decay induced by the spin-orbit interaction. A potentially important and particularly challenging aspect of this problem is the characterization of a spin-forbidden radiative transition which borrows intensity from bound states embedded in a continuum. The difficulty associated with the characterization of such a

process is attributable to two interrelated problems arising from the need to characterize the first order spin-orbit induced perturbation (Ψ_I^1) to the zeroth order (nonrelativistic) wavefunction (Ψ_I^0). First a large number of eigenstates of the nonrelativistic Born-Oppenheimer (unperturbed) hamiltonian ($\hat{H}^0$) must be determined to describe the perturbed wavefunction. In addition the orbitals required to describe the configuration state function (CSF) space used to expand the perturbed wavefunction do not arise naturally from an SCF or multistate MCSCF calculation.

Our recently developed method for treating spin-forbidden electronic transitions within the Breit-Pauli approximation provides a means for characterizing such processes. The success of this approach is attributable principally to the need to specify only the configuration state function space, rather than its spectrum relative to $\hat{H}^0$, in order to obtain Ψ_I^1. This obtains since Ψ_I^1 is determined directly as the solution of $(\hat{H}^0 - E_I^0)\ \Psi_I^1 = -\hat{H}^{so}\ \Psi_I^0$ where $\hat{H}^{so}$ is the full microscopic spin-orbit portion of the Breit-Pauli interaction rather than using the traditional eigenstate expansion. To address the second point a method for obtaining the molecular orbital basis used to define Ψ_I^1 based on the iterative natural orbital (INO) procedure was developed.

The $a^1\Delta \rightarrow X^3\Sigma^-$ transition in CH^- was considered. Using the INO procedure it was found that the optimum orbital space for describing Ψ_I^1 includes a molecular orbital with character intermediate between the compact valence orbital and the diffuse orbital obtained from two alternative MCSCF procedures. Equivalent INO orbitals were obtained from these two distinctly different starting points. Using the INO orbital set a total radiative rate for the ground vibrational level of the $a^1\Delta$ state of $0.163s^{-1}$ was obtained which gives a lifetime, $T=6.14(\pm1.2)s$. This value is in excellent agreement

with the experimental value T=5.9(+0.8,-0.6)s reported by Okumura et al.

C: Description of Nonadiabatic Processes Using Adiabatic States: New Algorithms

With: J. O. Jensen

In an adiabatic states approach to an electronically nonadiabatic process nuclear motion on more than one Born-Oppenheimer PES results from dynamical couplings induced by the derivative coupling operators:

$$g_\alpha(J,I,\underset{\sim}{R}) = \langle \Psi_J(\underset{\sim}{r};\underset{\sim}{R}) \left| \frac{\partial}{\partial R_\alpha} \right. \Psi_I(\underset{\sim}{r};\underset{\sim}{R}) \rangle_{\underset{\sim}{r}}$$

and

$$h_{\alpha,\beta}(J,I,\underset{\sim}{R}) = \langle \Psi_J(\underset{\sim}{r};\underset{\sim}{R}) \left| \frac{\partial^2}{\partial R_\alpha \partial R_\beta} \right. \Psi_I(\underset{\sim}{r};\underset{\sim}{R}) \rangle_{\underset{\sim}{r}}$$

where Ψ_J are the Born-Oppenheimer adiabatic states (MCSCF/CI wavefunctions) and $\underset{\sim}{r}$, $\underset{\sim}{R}$ are the (space fixed) coordinates of electrons and nuclei respectively. Key to the description of such processes is the efficient calculation of the coupling of the coupling matrix elements $\underset{\sim}{g}$ and $\underset{\sim}{h}$ for large scale multireference CI wavefunctions. We have previously developed analytic gradient based techniques for evaluating, without approximation, $\underset{\sim}{g}$ and $\underset{\sim}{h}$ couplings. These methods, which are more efficient and more accurate than previous techniques based on numerical divided differences, were used in the characterization of the He + H_2 system discussed above. We have recently developed an improved approach for the evaluation of $h_{\alpha,\beta}(J,I,\underset{\sim}{R})$ for diatomic and triatomic systems. In particular the evaluation of the total second derivative nonadiabatic coupling matrix element, $H(J,I,\underset{\sim}{R}) = \langle \Psi_J(\underset{\sim}{r};\underset{\sim}{R}) \left| \sum_i \frac{-1}{2M_i} \frac{\partial^2}{\partial R_i^2} \right. \Psi_I(\underset{\sim}{r};\underset{\sim}{R}) \rangle_{\underset{\sim}{r}}$ has been considered. For diatomic and triatomic systems the computational effort associated with the evaluation of $H(J,I,\underset{\sim}{R})$ can be reduced considerably by the use of a body fixed frame approach. In this approach costly evaluation of the derivative wavefunction with respect to noninternal degrees of freedom

in the space fixed frame is replaced by the evaluation of matrix elements of many electron operators including the mass polarization operator (total electronic linear momentum squared) and the L^2 operator (total electronic orbital angular momentum squared). The equivalence of the body fixed frame and space fixed frame results leads to valuable diagnostic equations which provide stringent tests of the derivative methodology used to evaluate the remaining second derivatives with respect to internal coordinates.

The methods developed were applied to the benchmark systems BeH^+ and LiH. The Born-Oppenheimer diagonal correction or adiabatic correction (AC) was evaluated for the $X^1\Sigma^+$ state of these systems and used to consider the effect of isotopic substitution on equilibrium geometries. For the $X^1\Sigma^+$ state of LiH a troubling discrepancy exists between the AC determined by advanced theoretical and experimental techniques. For $R \lesssim R_e$ the AC determined directly with specialized CI wavefunctions and the experimental value inferred from a detailed spectroscopic analysis of the $A \rightarrow X$ emission agree. However for $R > R_e$ theory and experiment disagree qualitatively. For $R \lesssim R_e$ our results are consistent with the previous work. For $R > R_e$ our results are in accord with the experimentally derived AC thereby resolving the discrepancy!

*U.S. Government Printing Office 1988:522-348/00345